System Identification of Constructed Civil Engineering Structures and Uncertainty

A Thesis

Submitted to the Faculty

of

Drexel University

by

Qin Pan

in partial fulfillment of the

requirements for the degree

of

Doctor of Philosophy

Dec 2007

ACKNOWLEDGEMENT

I would like to express my sincere gratitude and appreciation to my advisor, Dr. A. Emin Aktan, for his guidance and support throughout the course of my research. His excellent mentorship and encouragement will continue to influence me in my career.

I would like to thank Dr. Franlin L. Moon for his comments and advise during my research. I am also thankful to all the other members of my dissertation committee, Drs. Patrick Gurian, Franco Motalto and Tein-Men Tan for their interest, participation and advice.

I would also like to thank the New York City Department of Transportation and Maria G. Bruschi and Serafim G. Arzoumanidis from Parsons Transportation Group for their guidance and support to the Henry Hudson Bridge project in the thesis.

I am also grateful to my dear friends and colleagues Korhan Ciloglu, Kirk Grimmelsman, John Prader and Hesham Sayed for their discussions, input and wonderful friendship.

Last but certainly not least, I would thank my parents for their countless love, sacrifice and support through all of the challenges I have faced.

Table of Contents

List of Tables

List of Figures

Abstract

System Identification of Constructed Civil Engineering Structures and Uncertainty

Qin Pan

A. Emin Aktan

Characterization of constructed civil engineering structures through system identification has gained increasing attention in recent years due to its tremendous potential for optimum infrastructure asset management and performance-based engineering. However, the lack of reliability in system identification, especially when applied to large-scale complex constructed systems, poses a major challenge for its widespread implementation. It is believed that this primarily stems from epistemic uncertainty associated with identification processes, due to unknown or less understood structural behaviors as well as the interaction of the system with its environment. The objective of this thesis is to investigate the effects of epistemic uncertainty on the reliability of identification and to develop solutions to recognize and mitigate these uncertainties. The research which was undertaken included laboratory and field investigation as the primary components. First, a cantilever beam with two test configurations was designed and constructed in the laboratory as a test bed. By comparing different identification scenarios, the impact of modeling uncertainty with epistemic mechanism on the field-calibrated analytical model was evaluated. Feasible techniques were developed to recognize and mitigate significant epistemic modeling uncertainty which controls the test-analysis discrepancy. In applications of system identification on real-life structural systems, the tempo, frequency and spatial incompatibility between detailed finite element model and information contained in test measurements often further complicates the identification process. It was demonstrated through the Henry Hudson Bridge that it was possible to characterize the fundamental behaviors of large-scale complex structures by integrating heuristics and conventional techniques. Measurements to assess the adequacy of the field-calibrated models were proposed to ensure that significant epistemic modeling uncertainty was efficiently reduced and critical physical mechanisms was properly conceptualized.

1 Introduction

1.1 Background

The characterization of constructed civil structures has gained increasing attentions in recent years and hundreds of investigation on real structures have been performed and reported in literature (Moon and Aktan 2006). One of primary motivating factors can be attributed to the high expense associated with the maintenance, retrofit and replacement of an increasing number of aged infrastructures. The main bridge building boom in the US were during the 1960s and most of the bridges are now reaching the end of their useful design life and need rehabilitation and replacement. The Federal Highway Administration reported that about 26.6% in the National Bridge Inventory (NBI) are deemed structurally deficient or functional obsolete (Chase 2003). Other countries around the world are facing the similar situation. The number of the aged bridges in Japan will constitute half of all road bridges by the year 2020 since most of them were constructed in the 1970s (Fujino and Abe 2002). Therefore there is an imperative demand for innovative approaches to efficiently and reliably screen a large population of bridges and obtain a sufficient understanding of their existing conditions so that optimum asset management decision could be made (Salawu and Williams 1995; Aktan et al. 1996; Alaylioglu and Alaylioglu 1999; Aktan et al. 2000; Feng et al. 2004). In addition, extreme loading events such as recent earthquakes which occurred in Turkey, Taiwan and Peru remind continuous need to facilitate the development of realistic, effective, comprehensive and reliable design techniques and procedures. As the state of the art of civil engineering is advancing from specification-based toward performance based engineering, better understanding of the in-service characteristics and performance of constructed systems at different stages of their life cycle can help to define metrics and establish standards in developing new performance criteria for design, which represent a prerequisite for a meaningful transition (Aktan et al. 2007).

Analytical and numerical tools have long been used in civil engineering to simulate and predict the physical behaviors of large-scale and complex structures. Since it was introduced by Clough after a sabbatical collaborating with the structural dynamics unit of Boeing Airplane Company (Turner, Clough, Martin and Topp 1956), finite element method (FEM) soon found extensive applications in structural and continuum analysis of mechanical and constructed systems (Clough and Wilson 1999). Recent advances in computation science and engineering has rendered finite element modeling of large structures for new design, or condition and vulnerability assessment, rehabilitation or retrofit commonplace (Abdel-Ghaffar and Scanlan 1985; Ventura et al. 1995; Xu et al. 1997; Harik et al. 1997; Shama et al. 2001; Ren et al. 2004).

In the meanwhile, growing interest in dynamic behaviors of aircrafts in 1930s initialized the development of modal testing techniques. The emergence of Fast Fourier Transform (FFT) algorithm (Cooley and Tukey 1965) and the advances in digital computer technology in 1970s formed a breakthrough in dynamic testing and experimental modal analysis of structures. Varney and Galambos (1966) presented an early summary of dynamic testing of highway bridges in the US performed between 1948 and 1965. A review of dynamic load testing of 226 beam and slab type highway bridges conducted in Switzerland between 1958 and 1981 was given by Cantieni (1984). Salawu and Williams (1995) summarized full-scale dynamic testing of bridge structures while Ivanovic et al. (2000) offered a detailed review on ambient vibration tests on different types of constructed systems with a significant emphasis on the history of its application to building structures.

For a long time finite element method and experimental modal analysis have evolved apart to enhance our knowledge of how real-life structures behave. However, it has been gradually realized that reliable simulation of the as-built characteristics of existing structural systems, either by a three dimensional microscopic FE model or by much simpler and greatly idealized macroscopic models, require calibration and validation based on actual observations and

measured experimental data. Meanwhile, the paradigm of making meaningful observations and taking reliable measurements from actual operating constructed systems in the field is still an emerging art. Until 1970s the concept of system identification, which originated in electrical engineering in relation to circuit and control theory, was introduced to civil engineering community by engineering mechanics researchers by Hart and Yao (1977) and to civil-structural engineering researchers by Liu and Yao (1978). Farrar et al (2001) further defined structural identification (St-Id), a subset of system identification as "the parametric correlation of structural response characteristics predicted by a mathematical model with analogous quantities derived from experimental measurements". These seminal papers continuously inspired many researchers to investigate various aspects of Sys-Id in order to establish better understanding of the intrinsic complex nature and wide range of demands on system performance of constructed structures. The best efforts include international research collaborations such as the Seymour Bridge (HAM-561-0683) project led by University of Cincinnati Infrastructure Institute (Catbas et al. 1998), the I-40 Bridge project led by Los Alamos National Laboratory (Farrar et al. 2000), and the Swiss Z24 Bridge project (ww.kuleuven.ac.be/bwm/SIMCES.htm). The benchmark study on a four-story two-by-two bay regular steel frame constructed at University of British Columbia which was initialized by the IASC-ASCE SHM task group using (Beck 2004), as well as the two-story "Steelquake" structure which was set up in Italy during the COST (Co-operation in the field of Scientific and Technical Research) Action 'F3' in Structural Dynamics initiated by the European Community (Worden 2003; Golinval and Link 2003) also shared the same goal.

1.2 Integrative Paradigm for System Identification (Sys-Id)

System identification is usually involved with six basic steps, as illustrated in Figure 1-1. A successful application may be accomplished by either linear progression or across, or in various combinations until convergence is achieved. In some cases, iterative cycles of investigation may

be required to accurately and completely capture the actual physical behaviors of the structure under study.

1.2.1 Utilization of Sys-Id Results

One cycle of integrative application of Sys-Id paradigm typically starts from establishment of utilization of models, which defines the investigation objectives. Real-life systems such as buildings and bridges generally can be represented by various models with different fidelity, depending on different investigation objectives. Thus the utilization of model should be unambiguously specified in order to determine the form, structure and level of accuracy of initial analytical model(s). Several scenarios are envisioned in which the resulting field-calibrated analytical model would be used and they are as follows:

(1) Design, verification, and construction planning in case of challenging and/or ground-breaking new designs;

(2) A means of measurement-based delivery of a design-build contract in a performance-based approach;

(3) Document as-is structural characteristics to serve as a baseline for assessing any future changes, due to aging and deterioration, following hazards, etc.;

(4) Load-capacity rating for inventory, operations or special permits;

(5) Evaluate possible causes of, and, mitigate and/or correct causes of deterioration, damage and/or other types of performance deficiencies (e.g. vibrations, cracking, settlement, etc.);

(6) Evaluate reliability and vulnerability (changes in live-load demands, threats, hazards, increased performance requirements);

(7) Designing structural modification, retrofit or hardening due to changes in use-modes, codes, aging, and/or for increasing system-reliability to more desirable levels ;

(8) Health and performance monitoring for operational and maintenance management;

(9) Asset management (based on lifecycle benefit/cost).

In addition to the above, many civil engineers are interested in advancing the professions' understanding of how actual structural systems are loaded (during construction and after commissioning), how they deform, i.e. their kinematics at supports, joints, connections, and how they transfer their forces through the members to foundations and to soil. There is sufficient evidence that the current knowledge base on the loading, behavior, and performance of constructed systems is greatly incomplete, especially when new construction materials and systems are considered.

1.2.2 Conceptualization & A-Priori Modeling

Once the investigation objectives are well defined, a-priori model(s) can be created on the basis of original drawings, available survey and material sampling test data, reports of earlier structural health monitoring applications as well as engineering heuristics of the analyst. The analytical prediction yielded from preliminary model(s) is often useful to determine optimal experimentation parameters such as critical sensor locations and frequency band of interest. However, initial FE models created on the basis of design drawings and idealizations are never free from modeling uncertainty. Potential uncertainty sources due to the shape functions and geometry of various finite elements, geometric errors, discretization errors and numerical computation errors were well recognized early in the development of finite element method. The misrepresentation or incomplete representation of a structural system during the mathematical modeling stage, in terms of geometry, kinematics of deformation, material properties and their

variation, any nonlinearities, boundary and continuity conditions, and, possible mechanisms leading to non-stationary structural properties and loads were also gradually recognized. Excellent review could be provided in these papers (Natke 1988; Imregun and Visser 1991; Mottershead and Friswell 1993; 1995).

1.2.3 Monitoring, Controlled Experimentation & Data Processing and Interpretation

Before controlled experimentation and/or monitoring program is carried out, test plan is often developed to observe and measure the performance of the constructed system under its normal operation or designed forced excitation, based on preliminary analysis and site visits. The critical test design parameters include type of excitation and transducers, the number and locations of sensors, measurement sampling frequency and the duration of measurement and so on. After test measurements become available, dynamic characteristics of the structure can be extracted through parameter estimation algorithms. Although recent advances in sensing and information technology greatly increases our capability of observing and measuring the structural responses under normal or extreme conditions, the reliability of identification results is often heavily influenced by unavoidable electrical and environmental noise and experimental uncertainty due to the nature of input, nonstationarity and nonlinearity of the structure as well as data pre- and post processing techniques. Related issues were discussed by some researchers (Peeters and De Roeck 1998; Peeters 2000; Ciloglu 2006; Grimmelsman 2006) but far from exhaustive.

1.2.4 Model Calibration

Model calibration is a restricted form of the inverse problem and it emerged in 1980s as finite element modeling capacities and modal testing has become more matured areas of structural dynamics (Natke 1988; Mottershead and Friswell 1993; 1995). During the calibration process, linearity is usually assumed and the finite element model is adjusted so that either analytically predicted time history responses, frequency response functions, or modal parameters ‘best’ match the corresponding quantities measured or identified from the test data. Commonly used methods

can be classified as direct method and iterative sensitivity-based method. Both of the two categories of methods assume that the structure is properly conceptualized in the a priori model and experimental measurements also accurately reflect actual structural properties of the system. However, detailed analytical model and limited information embedded in test data are usually high mismatched and this often produces ill-conditioning and non-uniqueness of model calibration. Currently there are no well-accepted solutions.

1.2.5 Model Completeness Check

Distinguished from model updating, model quality assessment exists as a separate procedure to validate the predictive capability of the updated candidate models through a comprehensive set of independent references. It is intended to evaluate the adequacy of calibrated analytical model. This is critical for engineering applications since any followed decision making is tightly linked with the predictive accuracy and robustness of updated analytical model.

Although each step of the paradigm has been researched to some extent, many challenges do remain. The primary challenge remaining is how the steps of the paradigm are integrated to achieve convergence. Some researchers and practitioners have a wrong impression that modeling, testing, parameter estimation, model calibration and validation are relatively independent on each other. In fact, high-fidelity characterization of a constructed civil structure requires effective integration of every individual step of the Sys-Id paradigm. Initial analytical models not only serve as the start point of our understanding about how the structure is functioning under normal operation or extreme loading circumstances, but also provide valuable information to guide experiment design and execution. The interpretation of test measurement often requires availability of analytical models, since the number of measurement degrees of freedom is usually very sparse compared with the large size of the structure. On the other hand, the quantity and quality of information contained in the test measurements have a substantial effect on the field-calibrated analytical model. It is essential that researchers have access to comprehensive

measurements from experiments, interpolated as necessary to collocate with discrete model locations (such as node points in a FEM model) as well as documentation and authentication of the testing and data processing method.

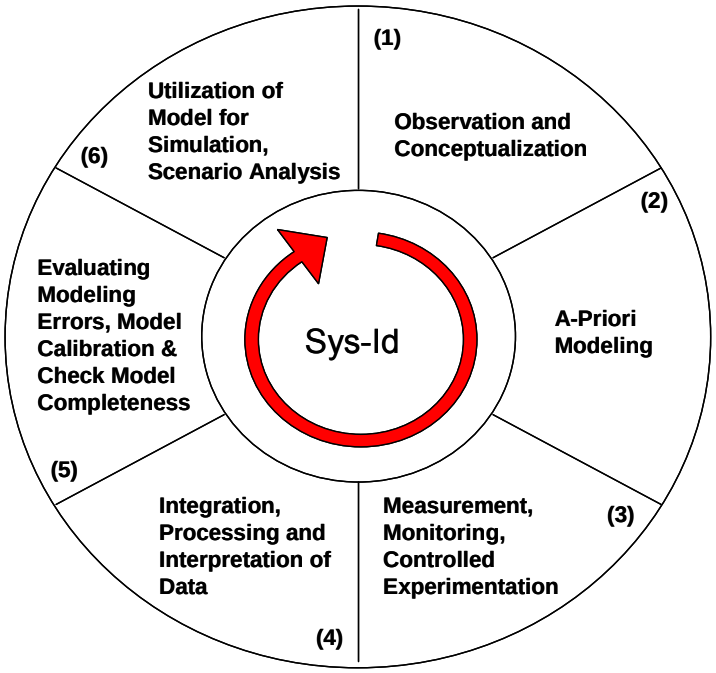

Figure 1-1 Diagram of the Structural Identification of Constructed Civil Structures

1.3 Previous Experience of System Identification of Constructed Systems

Although the concept of Sys-Id has gradually matured over the past decade, the use of Sys-Id in engineering practice remains in its infancy and has enjoyed only sparse implementation. This sharply contrasts with the cases of manufactured systems in which the model-based simulation and updating have become a routine practice for engineering design and product development of manufactured systems such as automotive and aerospace systems. While several researchers have argued it is primarily due to a lack of practical sensing and networking technology, recent advances in these areas have not been accompanied by widespread implementation of St-Id. The researchers in Drexel Infrastructure Institute have been conducting system identification research on operating and decommissioned constructed systems for many years, attempting to effectively incorporate analysis, laboratory testing of physical models, and controlled tests and long-term

monitoring of buildings and bridges in the field into a rational framework to reveal actual physical behaviors of constructed systems. The following observations from some recent experience are presented with the premise that it will serve to help advance understanding and appreciation of critical challenges imposed upon the Sys-Id of constructed civil structures.

1.3.1 Commodore Barry Bridge (CBB)

Since 1998, researchers of Drexel University Infrastructure Institute embarked on a long-term monitoring project on the three-mile long Commodore Barry Bridge (as shown in Figure 1-2). The Commodore Barry Bridge carries U.S. Route 322 across the Delaware River between Chester, Pennsylvania and Bridgeport, New Jersey and is owned and operated by the Delaware River Port Authority. The main span of the bridge is a cantilever through truss that consists of two anchor spans, two cantilever arms, and one suspended span. The total length of suspended span is 250 m. The suspended span is connected to the adjacent cantilever arms by four vertical pin and hanger members. By integrating 500 channels of acceleration, strain, rotation, displacement, temperature, wind speed/direction, and multiple video images (Aktan and Faust 2003), this monitor system was capable of providing multi-mode data which was spatially distributed over a wide area and captured at different frequency bandwidths, following various triggered and continuous data acquisition regimes commensurate with the bandwidth of data acquisition. This project was intended to demonstrate the feasibility of extending the concept of supervisory control and data acquisition system to a real-life structural health monitoring tool, with an ultimate goal to assist with lifecycle asset management by capturing actual physical behaviors of the bridge.

As the outcome of system identification, a mixed microscopic-structural element level three dimensional linear, deterministic finite element model was developed and calibrated to simulate the mechanical characteristics of the structure and its behaviors under realistic load effects and especially intrinsic force distribution (Catbas et al. 2007). The initial analytical model was first

globally calibrated with experimental modal properties established from ambient vibration testing. With assumptions that the movement systems of the bridge were fully restrained and the flexible length of the piers was equal to 62.5 percent of the total length, the model exhibits very good correlation with the test observations. The average percentage error between the predicted and the measured modal frequencies is around 2.3 percent. However, both the initial model and the globally calibrated one overestimated the stresses for all of the seven instrumented sections, compared with the measurements from local load testing. In addition, the predictions from the globally calibrated model were only slightly better than the simulated local responses from the initial model. The average error for stress prediction was around 55 and 48 percent before and after calibration respectively. This value could be reduced to 24 percent by further assuming a rigid body behavior between the deck, stringer and floor beam. It must be noted that the assumptions which led to the improvement of the analytical model after global and local calibration could not be justified. For example, many of the movement mechanisms were measured to intermittently experience slippage, which is obviously against one assumption made in the updated model. This example indicated the difficulty in accurate and complete conceptualization of the physical mechanisms embedded in a constructed system and it is especially true for large-scale complex structures.

Another unsolved puzzle related to the Commodore Barry Bridge occurred during its retrofit execution. An auxiliary support system which consisted of four vertical stainless steel rods at each hanger location was added to the bridge in order to provide redundancy to the pin and hanger connections between the suspended span and its adjacent cantilever arms. The rods were tensioned during their installation to remove a portion of the dead load acting on each hanger member. As displayed in Figure 1-3, each hanger member and added rods were instrumented with vibrating wire strain gages, and the members are continuously monitored before, during and after the rods were tensioned. The objectives of the monitoring were to characterize the installation of

the rods and the effects of this installation on the hanger and other truss members, and to monitor the performance of the auxiliary support system while in service. In conjunction with the nominal values of the modulus of elasticity for the steel of the hanger and the stainless steel of rods as well as the areas of their cross sections, these measurements are used to determine the axial force for each rod and the change in axial force for the hanger. It was observed that on average only three quarters of the total force generated on the rods were transferred to the hanger and another one quarter of force went into the bridge system with unknown force distribution mechanism. Given the fact that the rods and hangers are primarily axially loaded members, and that the distances between the hanger and the adjacent truss panel points were large, the difference between the sum of the rod forces and the change in hanger force at each location appeared too substantial to be completely accounted fro by 3D force transfer effects. Physically meaningful explanation could not be found for the observation.

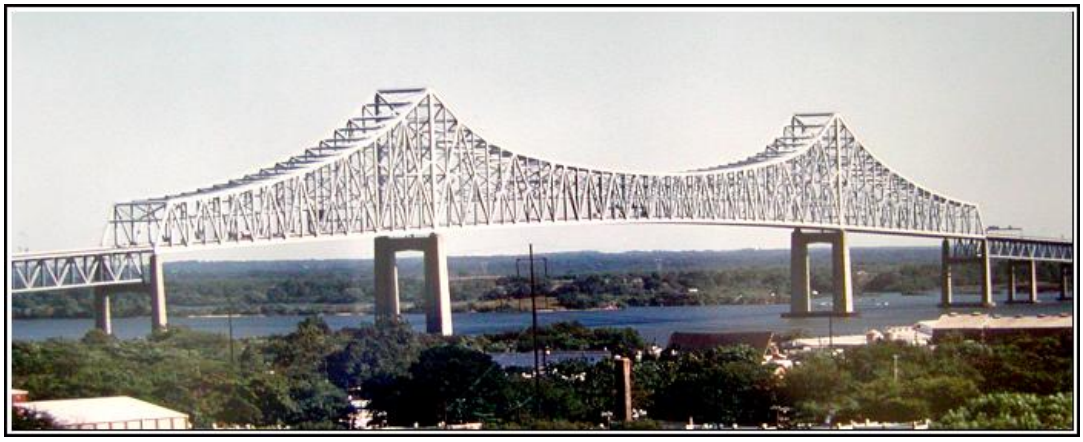

Figure 1-2 Commodore Barry Bridge

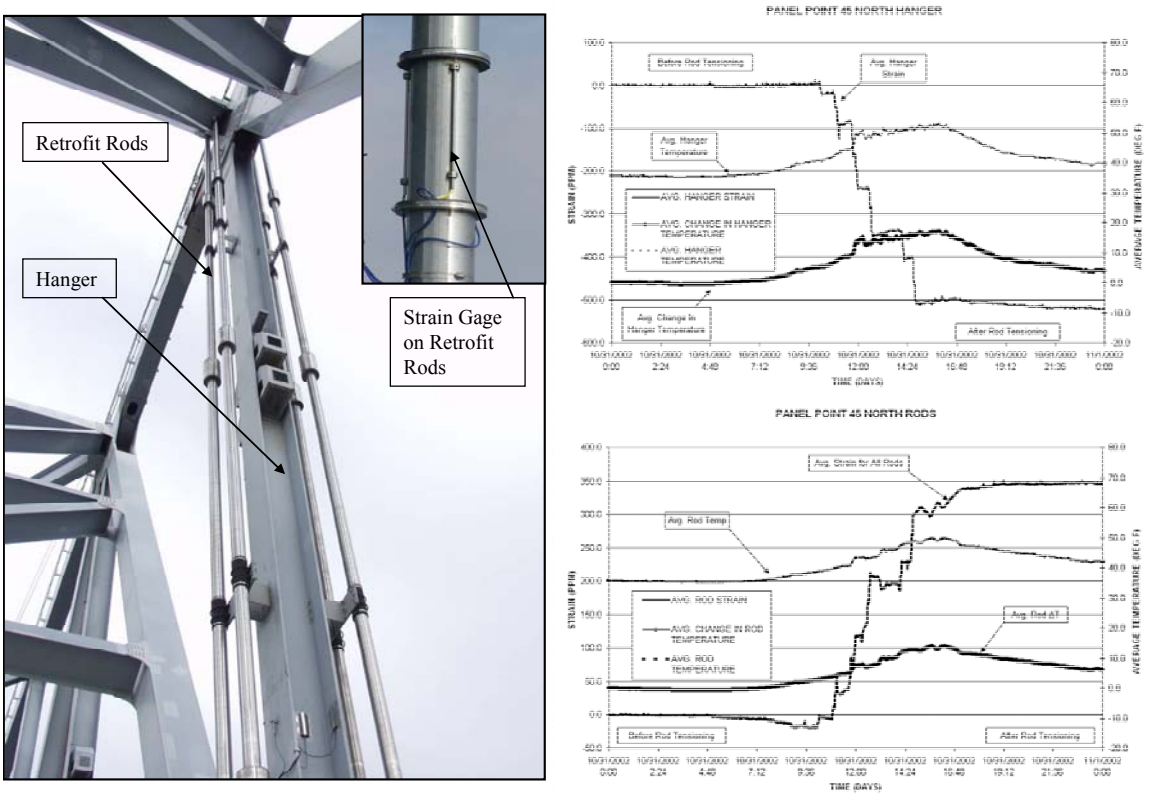

Figure 1-3 Auxiliary support system and average axial strain on the hanger and rods immediately before, during and immediately after tensioning

1.3.2 Brooklyn Bridge (BB)

In 2004 ambient vibration monitoring was conducted on the Brooklyn Bridge as a supplement to a seismic retrofit investigation in which the bridge owner desired to ensure safe and reliable long-term performance of this historic landmark suspension after its more than one-hundred-year service (Grimelsman and Aktan 2005; Grimmelsman 2006). Although many vibration investigations on large-scale cable-supported bridges were reported in literature, critical knowledge gap remained in the responses of bridge towers as well as their interactions with bridge spans. The primary challenge encountered in the identification was related to fundamental dynamic characteristics of masonry towers of cable-stayed bridges. Were there pure tower modes distinct in the global structural system – the same modes that exist for the free-standing towers can be identified in the dynamic response of the global structure? It was observed from the measured acceleration spectra of the Brooklyn tower that a large number of peaks showed up in

the frequency band of interest and many of them even demonstrated similar unit normalized deflection shapes. Was it possible to differentiate meaningful tower dynamic properties from spurious and less relevant results and how? Before these puzzles could be solved, a high-level of uncertainty would be associated with identification results. Therefore an idealized analytical model of the suspension bridge was developed and the analytical simulation revealed that dramatic difference in mass and stiffness of the masonry towers and suspended spans of the Brooklyn Bridge formed a special weakly-coupled system and resonant modes associated with the tower remained distinct when the tower was integrated with the rest of the structure. Meanwhile, a laboratory investigation explored the influences of the nature of excitation on the identified modal parameters as well as the effectiveness of a multiple-reference modal identification approach. The additional information obtained from the analytical and experimental components of the research made it possible to improve the understanding of the physical behaviors of the global system. As a result, the most likely dynamic properties of the bridge tower were identified.

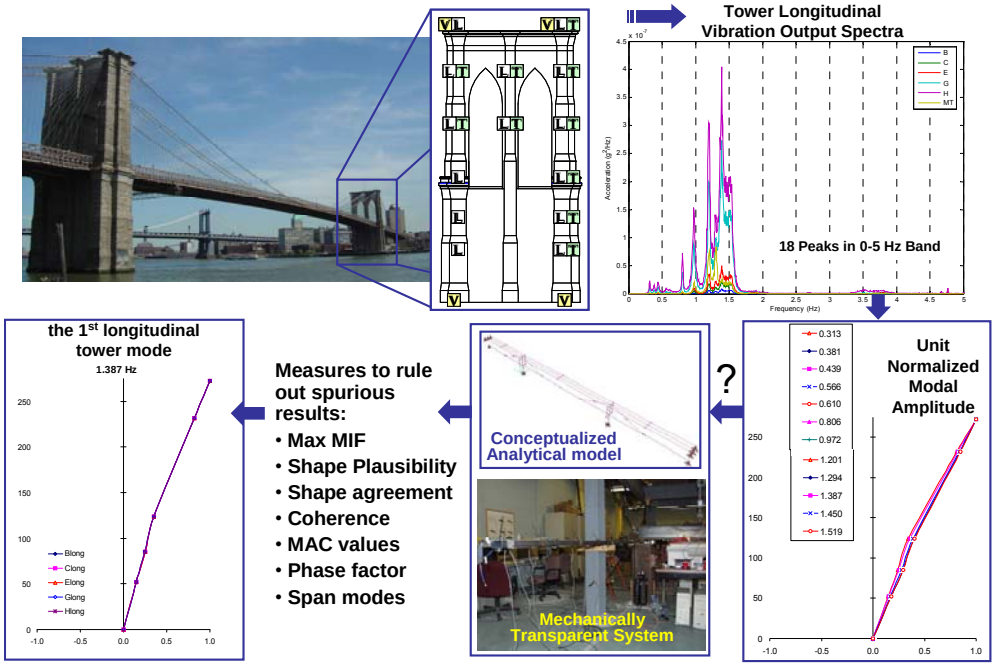

Figure 1-4 Characterization of the motions of the Brooklyn tower

1.3.3 Deck-on-Beam Bridge Model

In many current applications of system identification on constructed systems, models are usually identified through matching measurement data with analytical model predictions. This strategy is based on the assumption that that test measurements reflect the actual physical behaviors of constructed structures. In recent years, however, it has been accepted that experimentally obtained structural properties are also unavoidably exposed to various source of uncertainty. Except electronic and environmental noise inherent in experimentation, the spectral and spatial nature of input (Farrar et al 2000; Wenzel and Pichler 2005), and varying environmental effects such as temperature, humidity and wind speed (Farrar et al 1997; Peeters and De Roeck 1998; Fujino et al 2000) were gradually recognized as primary contributors of the experiment uncertainty. By taking advantage of a reduced-scaled deck-on-beam bridge model in DI3 lab, a systematic investigation of various aspects of operational modal analysis was carried out Ciloglu (2006), as shown in Figure 1-5. It was revealed that in ambient vibration testing the spectral and spatial nature of excitation, pre-processing techniques (averaging, filtering and windowing and etc) and modal parameter estimation algorithm could, individually or together, lead to different estimated modal properties (modal frequency, damping ratio and mode shape). In some identification cases, one or several modes may be completely absent from the obtained test results (Figure 1-6). This was further complicated by structural complexity such as indefinable boundary and continuity conditions.

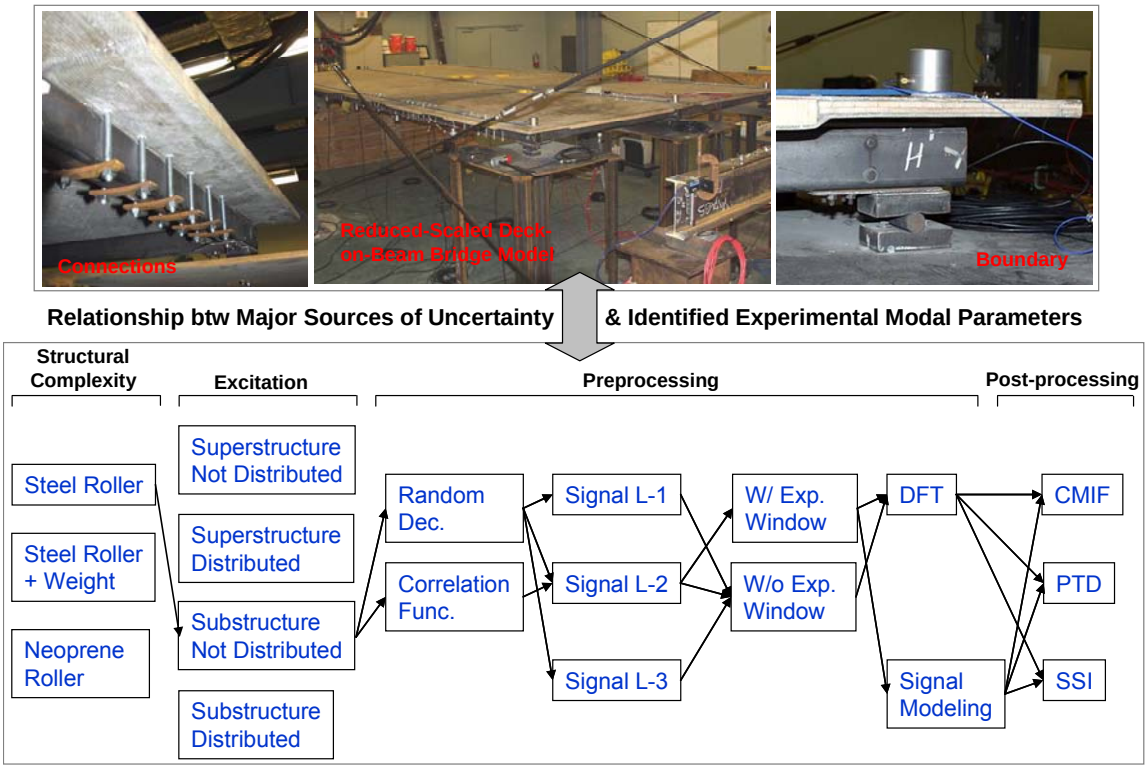

Figure 1-5 Major sources of uncertainty associated with the deck-on-beam bridge model

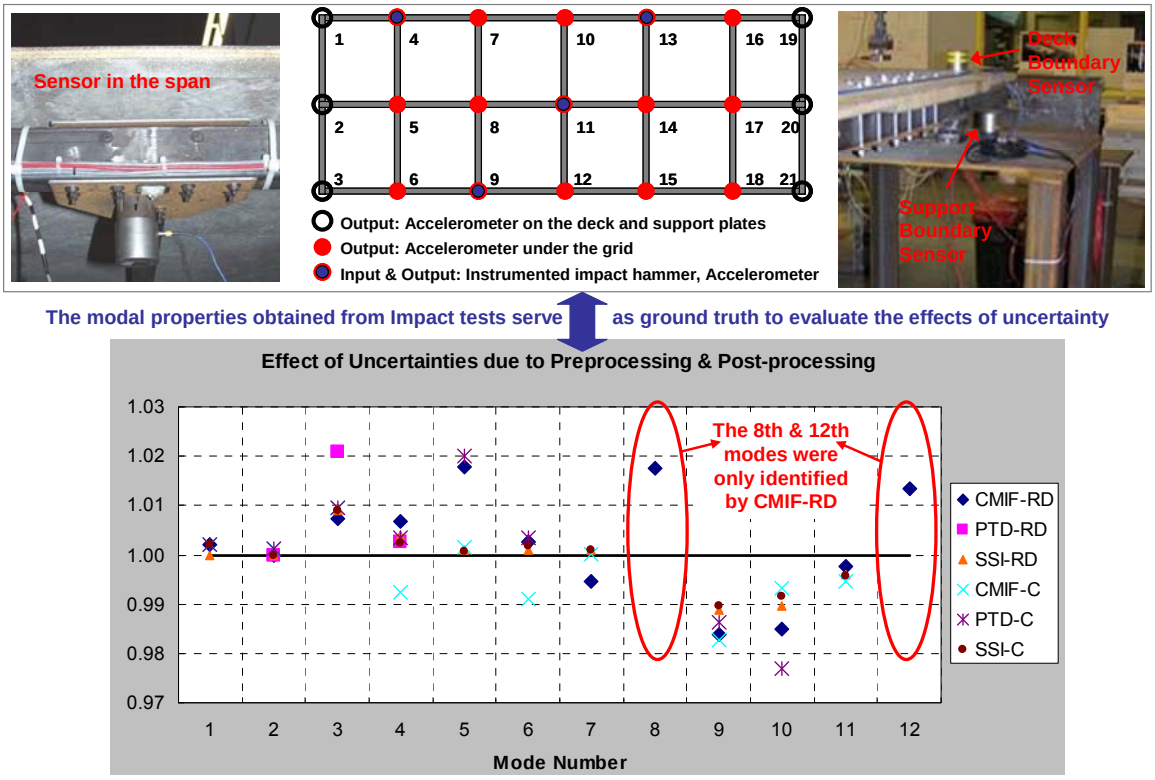

Figure 1-6 the effects of uncertainty on identified modal parameters

1.4 Motivation – Lessons Leant from Previous Experience

It becomes increasingly evident that in addition to technological barriers, significant obstacles for more widespread implementations of system identification in engineering practice stems from the skepticism towards the reliability of identification results held by owners/stewards of constructed systems. This is further compounded by the reality that in many cases irrelevant and unreliable data, especially erroneous identification of deterioration or damage, become a liability for managers. Therefore a critical and pervasive challenge facing civil engineering today is to realize the weakness of system identification which may potentially hamper the credibility of identification results.

The aforementioned examples revealed limitations of system identification when applied to large-scale complex constructed civil engineering structure. These limitations arise due to those unknown or less understood structural behaviors as well as their interactions with surrounding environments which lead to various forms of loads and intrinsic actions, vibrations, weathering, aging and deterioration mechanisms that impact operations, serviceability and durability of constructed systems. Sparse resolution of measurement grid, compared with the large size of civil structures, often further complicates the identification. As a consequence, various sources of uncertainty smear into each identification step through the choice of model structure, idealization of boundary and continuity conditions as well as the design, execution and interpretation of field testing and monitoring program, casting a shadow on the final outcome of system identification.

In spite of the fact that these uncertainties persist decades after early field testing applications (Hudson 1971 Ibanez 1972), very few research efforts were invested to improve our understanding of uncertainty mechanisms and their impact on the credibility of identification. Typically, uncertainty associated with system identification is often acknowledged as a small number of uncertain model parameters in the a priori analytical model, which are adjusted at the model calibration stage to be consistent with the structural responses measured in field test (Chen

and Garba 1980; Torkamani and Ahmadi 1988; Natke 1988; Imregun and Visser 1991; Fritzen and Zhu 1991; Hjelmstad et al. 1992; Mottershead and Friswell 1993; 1995). In some most recent system identification attempts made on real-life structures, it is still commonly assumed that the idealization of the structure in the a priori model is sufficiently complete and accurate and that experiment results also accurately reflect the actual state of the structure (Zhang et al. 2001; Brownjohn et al. 2003 Teughels and De Roeck 2004; Jaishi and Ren 2005). In late 1990's, some researches developed a Bayesian statistical framework for model updating, attempting to provide a more accurate prediction of structural response to prescribed dynamic loading and a quantitative assessment of this accuracy (Beck and Katafygiotis 1998; Vanik, Beck and Au 2000). The effects of uncertainty associated with modeling and experimentation are combined and addressed as random variables with their underlying probability distribution. It can be concluded that the art-of-the-state of system identification is either totally ignoring the uncertainties associated or a lack of distinction of different types of uncertainty.

In fact, uncertainties contained in a system can generally be classified as epistemic uncertainty and aleatory uncertainty (Oberkampf and Helton 2001; Ang and De Leon 2005). Aleatory uncertainty typically arises from the randomness of nature and is irreducible. Epistemic uncertainty is due to a lack of knowledge of a system but usually can be reduced given additional information. The distinction between them can be significant and should be clearly delineated. While it may be proper to describe aleatory uncertainty as random variables with prescribed probability models, epistemic uncertainty due to imperfect knowledge of the structure may be difficult if not impossible to be sufficiently represented with probability theory. Figure 1-7 illustrates how potential uncertainties may affect the six steps of Sys-Id, by a partial listing of uncertainty mechanisms. As indicated, steps of a-priori modeling and experimentation are often governed by challenging epistemic uncertainty, due to fundamental gaps in our knowledge of how a constructed system behave especially the soil-foundation surface, sub-and-super-structure

interfaces as well as the nonlinearity and nonstationarity of intrinsic forces. In order to ensure a reasonable level of reliability of the field-calibrated model, therefore, it is essential to also incorporate uncertainty analysis, especially uncertainty with epistemic mechanisms into the integrative paradigm of system identification of constructed civil structure.

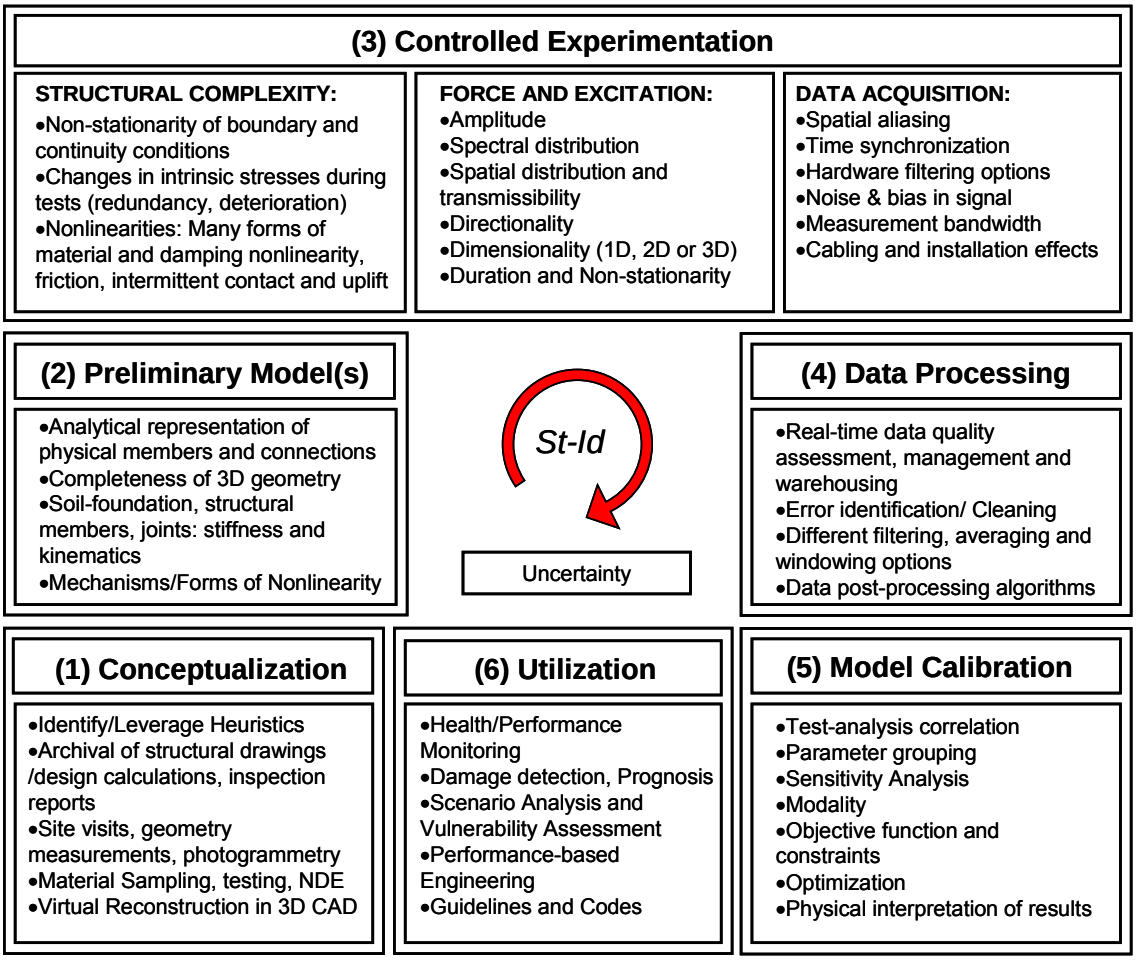

Figure 1-7 Aleatory and epistemic uncertainties governing Sys-Id

1.5 Objectives and Scope of the Research

The principle objective of this thesis is to establish a good understanding of uncertainty associated with system identification of constructed civil structures and to develop feasible techniques to recognize and mitigate it. In particular the focus is placed on epistemic uncertainties which are commonly encountered in the process of constructing analytical models. Different topics related to preparatory and actual model calibration, such as test-analysis correlation,

sensitivity analysis, error localization techniques, parameter updating algorithms and optimization techniques, are extensively discussed. However, the research described herein is not intended to confine itself within analytical aspects, since it is manifested from previous discussions that system identification is actually an integrative framework of conceptualization and simulation, test designing and execution, data processing and parameter estimation as well as model calibration and validation. The research contains experimental and analytical components, including a beam test specimen in the laboratory and a real-life long-span bridge structure. The ultimate goal is intended to provide some outlines for complete and accurate characterization of large-scale complex constructed systems. The objectives and scope of the thesis is further described as follows:

(1) Investigate the influence of modeling uncertainty with epistemic mechanism on the reliability of field-calibrated analytical model of a constructed system. As opposed to mass-produced manufactured mechanical systems, civil structures are generally constructed as one of a kind. Each individual structure distinguishes itself by the unique attributes such as the as-built material and geometry properties, intrinsic force distribution, and soil-foundation characteristics and so on. Incomplete and inaccurate knowledge of these unique attributes could introduce modeling uncertainty to the analytical representation of the structure, in addition to widely recognized uncertainties due to discretization and uncertain model parameters. However, the consequent epistemic modeling uncertainty has rarely been examined, in many cases because they are difficult to be parameterized and thus can not be incorporated in the updating procedure. The impact of unacknowledged epistemic modeling uncertainty on the quality of identification outcome is systematically investigated through comparison between various identification cases on the same lab specimen with different test configurations.

(2) Develop feasible techniques to recognize and mitigate significant epistemic modeling uncertainties inherent in a-priori simulation of a constructed system. Generating a priori

simulation model for a constructed system usually represents a delicate balancing act. The model must be able to capture the essential physics of the system while deliberately ignoring the aspects irrelevant to the ultimate utilization of the calibrated model. Most conventional model updating techniques, assuming that simplification and idealization in a prior model is complete and accurate, are developed to correct erroneous model parameters. The objective is intended to provide a feasible tool to examine if such an assumption is valid when the a priori model is calibrated with experimental data. Otherwise, measures to mitigate significant epistemic modeling uncertainty which controls the test-analysis discrepancy should be taken. These measures are often involved with carefully designed supplementary tests in order to obtain additional information about the areas of the structure where the recognized epistemic uncertainty is associated with.

(3) Investigate feasible tools to evaluate the adequacy of the field-calibrated model. In model calibration, the immense space and frequency incompatibility between analytical predictions and test observations often leads to non-unique identification results. In many cases, the same structure can be simulated and calibrated with more than one analytical model, which belong to either the same class of models with different parameterization or different classes of models. The objective is to evaluate whether the essential physics of the structure is adequately represented in one specific choice of modeling, attempting to reduce epistemic uncertainty and the degree of non-uniqueness. A real-life application of system identification on a long-span bridge structure, the Henry Hudson Bridge, is utilized to demonstrate the value of model adequacy check. However, the model adequacy check can not ensure that the resulting model is unique and fully converged to the real state of the constructed system. Instead, it can be considered as the most admissible one with given information and additional tests are otherwise required for improved accuracy and reliability, although such requirements may not be impractical in engineering practice.

(4) Several different preparatory model updating procedures are extensively discussed for their applicability and accuracy, including test-analysis correlation, error localization, sensitivity analysis, and test data informativeness quantification. They are considered as an essential component for the model calibration step in the complete process of system identification. This is not only because successful implementation of these procedures play an important role in the actual model calibration but also because they are often applied in conjunction with engineering heuristics to determine in some degree the reliability of the final outcome of identification. Their applications are to be extensively demonstrated and compared in the cases of lab cantilever beam setups and the Henry Hudson Bridge.

1.6 Structure of the Thesis

The thesis is organized as follows:

Chapter 1 introduces the background of the system identification and challenges in its applications on constructed civil structures. Under the framework of proposed integrative Sys-Id paradigm, the objective and scope of the thesis are situated. The organization of the text of the thesis is also clarified.

Chapter 2 provides a comprehensive summary of various sources of uncertainty encountered in real-life applications of system identification on constructed systems. The state-of-the-art of recognition and mitigation of epistemic modeling uncertainty is also discussed.

Chapter 3 addressed the preparatory procedures which should be carefully examined before model calibration, including model correlation, error localization, sensitivity analysis and test data informativeness evaluation. This chapter also presented the two groups of commonly used model updating algorithms, and the theoretical exposition on the sensitivity-based approach is provided.

Chapter 4 presents the investigation of modeling uncertainty with epistemic mechanism. A test bed of a cantilever beam with different test configurations were designed to examine the fundamental impacts of epistemic uncertainty inherent in a-priori models of a constructed system. Techniques to recognize and mitigate the existence of epistemic modeling uncertainty are proposed and demonstrated in the identification process of the beam system.

Chapter 5 presented a real-life application of the integrative system identification paradigm on a long-span steel arch bridge. The experimental uncertainty associated with data measurement and processing as well as modeling uncertainty embedded in preliminary FE model of the bridge is examined. Technique to evaluate model adequacy is proposed to ensure no significant epistemic uncertainty remained in the calibrated model – critical physical mechanisms of the constructed system under study are completely and accurately conceptualized.

Chapter 6 provides a summary and conclusion of the research work presented in the thesis and gives some suggestions for future work.

2 Uncertainty Associated with System Identification

2.1 Introduction

In recent years, the need for an appropriate uncertainty analysis as part of Sys-Id of constructed civil structures that support the following decision making such as maintenance, retrofit and management of infrastructure systems has attained wide recognition. The concept of uncertainty is, in fact, not new for civil engineers and structural engineers in particularly, and has already been applied in subjects such as structural safety and reliability analysis for many years. The appreciation of the effects of uncertainties which arise from imperfection in modeling and prediction of reality has led to the development of more consistent criteria for design of engineered structural systems. However, the challenges which stem from the incomplete knowledge of the actual loading mechanisms, intrinsic force distributions, kinematics, failure modes and capacities of existing constructed systems have not yet well understood.

As illustrated in Table 1-2, the Sys-Id process of constructed systems usually has various sources and levels of uncertainties embedded at each stage. It is important for engineers to distinguish the difference between randomness and knowledge based uncertainty. Table 2-1 presents eight pairs of alternate terminologies proposed in the literature to describe the dual meaning of uncertainty over the years. It is summarized by researchers Baecher and Christian, based on a table compiled for analysis of flood risk (National Research Council 1995), and is slightly revised when cited. Following the nomenclature of Ang and De Leon (2005), this thesis uses the terminologies ‘aleatory uncertainty’ and ‘epistemic uncertainty’. This is done not only because they have achieved wide circulation and application but also because the names precisely describe the key characteristics of the two types of uncertainty.

The designator aleatory is after the Latin word for gambler or dice thrower and is used to describe the inherent (natural) variation associated with the system and environment under consideration. The fundamental feature of aleatory uncertainty is randomness and its significance requires description in

terms of probability. Thus aleatory uncertainty is generally modeled with probability theory by probability distribution established through data analysis or through subjective judgment. Although aleatory uncertainty is irreducible, more information may help to estimate more precisely the parameters governing that uncertainty.

The designator epistemic is used to define potential inaccuracy due to lack of knowledge. Generally more information tends to reduce epistemic uncertainty although sometimes the cost of reducing it may not be worth it. The features associated with epistemic uncertainty are as follows: (1) 'potential' means that the inaccuracy may or may not exist. We may happen to model the phenomena correctly even though there is a lack of knowledge; (2) the fundamental cause of epistemic uncertainty is incomplete information. The incomplete information can be resulted from vagueness, nonspecificity or dissonance. Vagueness characterizes information that is imprecisely defined, unclear or indistinct. Nonspecificity refers to the variety of alternatives in a given situation that are all possible. And dissonance means the existence of totally or partially conflicting evidence.

In this chapter a brief review of the state-of-the-art of recent advances in Sys-Id and applications on laboratory specimen and real-life structures will be provided, which shows that there is yet no systematic investigation on uncertainty associated with Sys-Id, although a lot of research efforts have been invested on each stage of it in the past decades. Hence various forms and levels of uncertainty that may be encountered in modeling, experimentation and data processing are summarized. Some of them are well accepted sources such as environmental noise and temperature bias and their influences as well as possible treatment have been extensively investigated. Some of them, especially the epistemic modeling errors which were recognized and extracted from Sys-Id applications on real structures, are put together for the first time to provide insight on is versatile forms and to demonstrate its fundamental effects on our understanding of actual performances of constructed structures.

For clarity, various sources of uncertainty are grouped as experiment uncertainty and modeling uncertainty. The first category includes all which take place during field testing and modal analysis, while the second category is used to refer the ones which are introduced during the model construction.

Table 2-1 Terms used in literature to describe dual meaning of uncertainty (adapted from Christian 2004)

Uncertainty due to naturally variable phenomena in time or space	Uncertainty due to lack of knowledge or understanding of nature	Reference citation
Aleatory uncertainty	Epistemic uncertainty	Hacking 1975; McCann 1999; Ang and De Leon 2005
Natural variability	Knowledge uncertainty	NRC 2000
Random or stochastic variability	Functional uncertainty	Stedinger et al. 1996
Objective uncertainty	Subjective uncertainty	Chow et al. 1988
External uncertainty	Internal uncertainty	Chow et al. 1988
Statistical uncertainty	Inductive probability	Carnap 1936
Irreducible uncertainty	Reducible uncertainty	
Chance	Probability	Poisson, Cournot (Hacking 1975)

2.2 Applications of Sys-Id

Early developments on vibration-based structural identification of constructed engineering systems stemmed from studies conducted by oil industry in the 1970s and early 1980s, which were aimed to detect possible damages of offshore facilities. In the past several decades, active engagements of engineers and scientists from various disciplines have fostered innovations in technologies of sensing, computation and signal processing. This leads to great advances in the applications of system identification in engineering practice. Intermittent or long-term vibration monitoring techniques have been extensively applied on an increasing number of civil engineering structures to improve the understanding of actual structural behaviors and augment traditional assessment. The utilizations of system identification based structural health monitoring (SHM) on infrastructure systems also make it possible to evaluate the real-time structural condition and detect the onset of damage or deterioration at the earliest stage and thus optimal operational and maintenance management of entire infrastructure system can be achieved.

Los Alamos National Laboratory (LANL) researchers presented two extensive literature reviews on laboratory and field investigations on damage detection and structural health monitoring (1996; 2003). Salawu and Williams (1995) summarized full-scale dynamic testing of bridge structures. Ivanovic et al. (2000) offered a detailed review on ambient vibration tests on different types of constructed systems with a significant emphasis on the history of its application to building structures. These previous literature reviews are useful for tracing the history of development and applications of structural identification and understanding some generic issues to any class of constructed systems.

A wealth of sensing and testing techniques as well as parameter identification and damage detection algorithms emerged with the advances of technology. In order to investigate and assess the performances of various techniques for realistic conditions, IASC-ASCE SHM task group constructed a four-story two-by-two bay regular steel frame at University of British Columbia (Beck 2004) as well-defined benchmark problems. Besides, a two-story "Steelquake" structure was set up in Italy during the COST (Co-operation in the field of Scientific and Technical Research) Action 'F3' in Structural Dynamics initiated by the European Community (Worden 2003; Golinval and Link 2003) for similar purpose. The structure can be interpreted as a module of a high-rise building, which has been loaded via shakers to simulate an earthquake-like loading. Several other benchmark projects were conducted on decommissioned highway bridges with progressively introduced damages, including the Brite Euram project BE96-3157 system identification to monitor civil engineering structures (SIMCES) based on the Swiss Z24 Bridge (ww.kuleuven.ac.be/bwm/SIMCES.htm), the I-40 Bridge project led by Los Alamos National Laboratory (Farrar et al. 2000) as well as Seymour Bridge (HAM-561-0683) project conducted by University of Cincinnati Infrastructure Institute (Catbas et al. 1998). These benchmark studies also stimulate further evolution of recent advances for manufactured systems in the context of civil engineering applications.

Additionally, the as-situ physical behaviors of constructed structural systems under normal operation and extreme loading events keep fascinating researchers and professional engineers and

hundreds of investigations on existing civil structures have been reported in literature. Listed below are the ones with real-life implementations of the integrative Sys-Id paradigm in either linear progression or various combinations. Since the objective varies case by case, each individual investigation may have a distinct focus and thus reveals potential strength and challenges in different aspects of identification. But they include early examples of recognition and discussion of measurement or modeling uncertainty encountered in an implicit way. And it is good to have them to serve as the context in which the research presented in this thesis is conducted.

McLamore, Hart and Stubbs (1971) described one of the earliest identification efforts on two suspension bridges using ambient vibration test method, in order to investigate the structural responses to wind. Buckland et al (1979) presented their effort to reveal vibration characteristics of a suspension bridge by combining analytical and experimental tools. Abdel-Ghaffar and Scanlan (1984) attempted to characterize the dynamic behaviors of the span and tower components of the Golden Gate Bridge by short-term vibration monitoring.

Brownjohn et al. (1987) investigated the Humber Bridge with an aim to verify their numerical studies on the dynamic characteristics of the bridge. Both the suspension span and concrete towers were instrumented during the test. Brownjohn et al. (1989) and Brownjohn, Dumanoglu and Severn (1992) presented their St-Id applications on the Bosporus Suspension Bridge and the Fatih Sultan Mehmet (Second Bosporus) suspension bridge respectively. The scope for the studies was to validate finite element models in order to conduct seismic evaluation. Lateral vibration modes were found difficult to be accurately identified due to the low excitation in lateral direction under ambient conditions. By modifying uncertain structural parameters such as Young's modulus of concrete and structural geometry, Brownjohn and Xia (2000) investigated the application of model updating technology to the dynamic assessment of the Safti Link Bridge, a curved cable-stayed bridge in Singapore. Significant improvement in the simulated dynamic properties obtained after updating. In 2003, Brownjohn et al. presented the dynamic testing and modal analysis used to identify the

vibration properties of a highway bridge, and the effectiveness of the upgrading was quantified through a subsequent model updating.

Harik et al. (1997) presented the study on the double-deck through-truss Brent-Spence Bridge with structural identification approach to assess the structural integrity under a seismic event. Ren et al (2004) provided their analytical and experimental investigations of the Roebling Suspension Bridge over the Ohio River with an ultimate goal to assess the bridge's load-carrying capacity. The vibration properties of the bridge were evaluated on the basis of finite element model calibrated by ambient vibration test data. Jaishi and Ren (2005) demonstrated utilization of ambient testing and model updating to identify structural dynamic characteristics through a case study on the Beichuan River Bridge in China. Ren, Peng and Lin (2005) presented an analytical and experimental modal analysis conducted on the cable-stayed Qingzhou Bridge in China. The validated finite element model was then used as the baseline for long-term health monitoring of the bridge.

Field ambient vibration monitoring (Chang 1998) as well as finite element simulation was conducted the Kap Shui Mun Bridge in Hong Kong in order to better understand dynamic response of the double-deck cable-stayed bridge. Model updating technique was utilized to correlate the findings of analytical and experimental aspects (Zhang et al 2001). St-Id was performed on two cable-stayed bridges, the Alamillo Bridge in Spain and the General Belgrano Bridge in Argentina. The former one was tested just after the completion of construction and test results were used to justify the scaled model used in the wind tunnel tests. And the latter bridge was investigated for a most effective retrofit design (Casas 1998). Cunha et al (1999) presented their effort to develop reliable analytical models in terms of the study of the dynamic response and health condition of long-span bridges under traffic, wind or seismic loads. They investigation was based on the cable-stayed Vasco da Gama Bridge.

With the application of Sys-Id on a lively footbridge in Montenegro, Zivanovic et al (2005; 2006; 2007) demonstrated the strength and challenges of applications of integrative Sys-Id on constructed structures. Pavic and Reynolds (2003) presented the results of a combined analytical and

experimental investigation on modal properties of a full-scale prototype high-strength concrete floor system before and after considerable deflection and serviceability cracking.

Ventura, Felber and Stiemer (1995) presented the ambient vibration testing on the Queensborogh Bridge in Vancouver area of Canada. Ventura, Brincker, Dascotte and Andersen (2001) describes results of a model updating study conducted on a 15-story reinforced concrete shear core building and provides an assessment of the usefulness of using model updating. In order to precisely evaluate the dynamic responses of the Nanjing TV tower, finite element model was constructed and validated with experimental results from ambient vibration testing (Wu and Li 2004).

Robert-Nicoud et al (2005) proposed an approach to make use of measurement data to perform diagnostic assessment of structures with a set of initial models. By updating candidate models the cause of observed behaviors can be identified and the one which produces predictions agree best with test measurement and also has physical significance is considered as a best representation of the structure.

Based on their experiences on the Commodore Barry Bridge, Catbas et al (2007) discussed limitations and challenges of Sys-Id, which is especially true for large structures, since the resolutions of the dynamic test grids are often quite sparse.

2.3 Experimental Uncertainty

In many current applications of system identification on constructed systems, models are usually identified through matching measurement data with analytical model predictions. This strategy is based on the assumption that that test measurements reflect the actual physical behaviors of constructed structures and that the best match between test and analysis is obtained only when correct values of model parameter are identified. However, this assumption is flawed because neither the analytical prediction nor the test results are free of errors. Since experimentally obtained dynamic characteristics of a structure usually serve as a baseline in model updating, their variability will

definitely cast a shadow on the confidence in the updated model and any engineering decisions followed.

The following section present a wide survey on errors/uncertainties induced to test data during recording and processing. The concentration is placed on vibration-based Sys-Id approach, while there are isolated reports of work involving static measurements such as deflections and strains to interpret the structure state.

Except unavoidable electronic noise and environmental noise inherent in experimentation, uncertainties due to the nature of input, nonstationarity and nonlinearity of the structure as well as data processing are primary concerns which may have detriment impact on the accuracy and reliability of identification. In reality, the contributions of the aforementioned experimental uncertainties are often combined up and their influences may either accumulate or cancel out in the estimated modal parameters. Consequently they are difficult to be differentiated from each other and hence impair the accuracy and reliability of system identification results.

2.3.1 Excitation

Difficulties associated with excitation of large structures adequately to overcome ambient vibration were discussed by Wenzel and Pichler (2005). Therefore, ambient vibration test using primarily traffic for excitation is becoming a widely used experiment tool for large scale structures such as long-span bridges in recent years, instead of shaker vibration or impulse hammer which are common techniques in dynamic testing of mechanical systems. Additionally, ambient vibration test are usually conducted under normal operational condition and neither the cost for excitation instrumentation nor that for lane closure is required. However, since no input information is available in ambient vibration test, the reliability of obtained modal properties sometimes can be questionable.

If there is no enough input energy distributed over the frequency band of interest, some modes of the structure may not be well excited. Their corresponding modal properties will thus be buried by

test noise and can not be accurately identified from test measurements. Brownjohn et al. (1989 and 1992) found that no reasonable lateral mode shapes were identified from ambient test measurements from the first and second Bosphorus Bridges in Turkey due to the low amplitude to excitation in lateral direction.

Farrar et al. (2000) found significant changes in the estimates of damping ratios of the Alamosa Canyon Bridge in New Mexico when different excitation techniques, including multiple impact, single impact, ambient traffic from adjacent bridge and test vehicle, were applied. The authors attributed it to different levels of excitation amplitude. The authors pointed out that some of the modes identified by impact testing could not be identified by ambient vibration testing.

Kramer, de Smet and Peeters (1999) compared the advantages and disadvantages of forced vibration testing and ambient vibration testing when applied on the Z24 Bridge in Switzerland.

For forced vibration test, accidental placement of excitation source (hammer impact or shaker) on nodal point of expected mode shapes usually leads to the failure to identify these modes. Catbas et al (1998) reported that locating the linear-mass shaker near a nodal point of the bridge resulted in several poor-excited modes during the shaker test on the Seymour Bridge, Ohio.

Wilson and Liu (1991) noted the difficulty in determining the damping ratios of a cable-stayed bridge using ambient vibration test because of the non-stationary nature of the input.

Variations in natural frequencies identified with wind velocity during the construction and with traffic load after the completion of the Second Severn Crossing cable-stayed cantilever (Macdonaldand and Daniell 2005).

2.3.2 Environmental Effects

Non-stationarity in the structural modal properties due to varying environmental effects is frequently reported in literature recently. Since constructed civil structures are always exposed to its environments, changes in temperature and humidity may have some fundamental impacts on the

internal redundancy mechanism (Catbas and Aktan 2002), load path, temperature gradients (Cornwell et. al. 1999) as well as mass and stiffness distribution (stiffening of expansion bearings, Fu and DeWolf 2001). Besides, boundary conditions of large-scale constructed structures are not always well defined and they usually highly depend on temperature and seasonal variations. Structures thus display non-stationary behaviors during a long-term observation. Some investigators declared that the changes of modal properties due to varying environmental and operational conditions produce changes in structural dynamic response that can be easily mistaken for damage.

Askegaard and Mossing (1988) investigated seasonal changes of modal parameters of a RC footbridge over a period of three-year. They observed about 10% changes in frequency and concluded that this was mainly due to variation of ambient temperature.

Farrar et al (1997) found that the first eigen-frequency of the Alamosa Canyon Bridge was subjected to changes of approximately 5% during a 24 hour time period. They also attributed it to the variation of temperature.

Peeters and De Roeck (1998) reported changes in the first four eigenfrequencies of the Z24 Bridge are in the range of 14-18%. These changes were mainly due to the increased elastic modulus of the asphalt at temperatures below 0 Celsius degrees. Peeters, Maeck and De Roeck (2001) demonstrated the effect of temperature on measured eigenfrequencies on the Z-24 Bridge and they proposed a ARX model to distinguish the temperature effects from real damage events.

Alampalli (1998) reported that the second and third eigenfrequencies of a small bridge were subjected to an increase of 40-50% due to freezing of the supports.

Fujino et al (2000) identified that the natural frequency of the first vertical bending mode decreased noticeably as the wind speed increased, from their observations from forced and ambient vibration tests on the Hakucho Bridge. The corresponding mode shape at the nodes near the towers

also slightly changed with the speed of wind. The authors associated the changes with the friction in the bearings at the bridge.

The long term variation of eigenfrequencies were found to correlate well with long term variations of temperature in half-year ambient vibration monitoring on a three span concrete highway bridge, the Romeo Bridge of the Obkirchen Viaduct (Feltrin 2001). The results showed that the frequency changes in the first three bending modes due to environmental effects are generally larger than that due to severe damage of the bridge while the changes due to small or moderate damage are similar in magnitude to the daily changes of frequencies.

In conjunction with temperature changes, other ambient conditions such as cloud cover, humidity, direction of temperature change, etc. were observed to affect bridge boundary conditions significantly (Aktan el al 1997).

2.3.3 Boundary & Continuity Conditions

It is well accepted that large constructed systems seldom display well-defined boundary and continuity conditions.

Brownjohn et al (2003) observed that the modal frequencies of a highway bridge in Singapore changed dramatically (up to 50%) before and after upgrading. The identification revealed that one of the causes for the significantly increased natural frequencies is the rotational restraint at the abutment.

Identification results from forced vibration tests on the Millikan Library Building in CalTech campus indicated that the modal parameters of structure-foundation and soil system varied considerably for the isolated base condition from the fixed based conditions (Luco et al 1988).

Catbas et al. (1998) reported the St-Id of a deteriorated steel-stringer concrete slab bridge using impact and crawl-speed truck testing procedures. Results indicated that although no shear connections were present between the slab and stringers the bridge was behaving in a composite manner due to chemical bond.

In the application of Sys-Id on a long-span steel truss bridge presented by Catbas et al (2007), an assumption that the piers are entirely rigid and that the movement systems of the bridge are fully restrained has to be made to yield the closest agreement with the experimental data from vibration monitoring.

2.3.4 Data Processing

As Farrar and Doebling pointed out, standard modal properties represent a form of data compression. Hundreds of thousands of data points in time history are reduced to several modal frequencies, mode shapes and damping ratios through system identification. Thus the uncertainties/errors in the data compression process (i.e. data analysis and parameter identification methods applied to the measured data) are unavoidable and the identified modal parameters may be not as representative of the true dynamic properties of the structure as expected. Over ten parameter identification algorithms were proposed after more than thirty years development in modal analysis. Performance of different algorithms were widely compared and evaluated.

Masri et al represented the main features and system architecture of optimized SHM system for the continuous real-time monitoring of Vincent Thomas Bridge, located in San Pedro, California. The identified modal parameters from 2003 big bear earthquake data as well as the results from ambient vibration tests conducted respectively by several other researchers, Abdel-Ghaffar and Housner (1977), and Lin and Betti (2003) were summarized by the writers. The range of frequencies from ambient and earthquake-induced motions reasonably agrees with each other but a significant difference in the absolute values was found for the indexed modes. Although the indexes of modes utilized by different researchers may not necessarily correspond to each other and significant retrofit performed in 2000 can lead to the difference, errors in not accounting for missing excitations in ambient testing, errors in different data analysis and parameter identification methods used, and uncertainties from changing environmental conditions, are all contributors of the observed discrepancies.

Anderson et al (1999) utilized the operational data obtained from an ambient testing from the Z-24 Bridge as a test bed to examine four popular parameter identification algorithms. They are frequency domain based peak picking method, polyreference LSCE method, stochastic subspace identification method and the prediction error method with ARMAV model.

Ren et al (2004) reported ambient vibration testing, using traffic and wind excitation, of a steel-girder arch bridge. The authors noted good agreement between frequencies identified by peak picking and Stochastic Subspace Identification (SSI) methods; however the SSI method provided superior mode shapes.

A systematic investigation (Ciloglu 2006) on a reduced-scale deck-on-girder bridge model in laboratory revealed that various sources of uncertainty associated with ambient vibration testing and data processing lead to difference in the resulting modal properties of the same structure. The uncertainty may originate from spatial and frequency nature of excitation, averaging, windowing and spectral estimation approaches used in pre-processing of the test measurements and different parameter estimation algorithms. Additionally, the series of tests showed that the change in boundary condition may be subtle and yet alter the dynamic test results.

2.4 Modeling Uncertainty

Civil engineers have been engaged in modeling and simulating physical behaviors of proposed or constructed structural systems for decades. Generally existing analytical methods can be broadly classified as two categories, physics-based models and non-physics-based models, as shown in Table 2-2. In recent years, a lot of research works on non-physics-based models emerged by taking advantage of fuzzy logic, probabilistic reasoning, artificial neural networks, and genetic algorithm. However, physics-based models are often preferred because most of the associated model parameters always have a clear physical meaning behind them.

Table 2-2 Classification of analytical modeling forms for structural systems

Physics-Based (PB) Models	Non-Physics-Based (NPB) Models
Laws of Mechanics • Newton's Laws of Motion • Hooke's Law *Continua Models* • Theory of Elasticity • Idealized Differential Equations (e.g. Beam theories of Bernoulli, Timoshenko, Vlasov) *Discrete Geometric Models* • Idealized macro or element level models (e.g. idealized grillage models) • FEM for solids and field problems • Modal models o Modal parameters (i.e. natural frequency, mode shape, damping) o Ritz vectors	*Semantic Models* • Ontologies • Semiotic Models *Meta Models* • Input-Output models • Rule-based meta models • Mathematical (e.g. Ramberg-Osgood representation of stress and strain near the yield region) *Numerical Models* • Statistical Data-Driven Models o ARMA modeling o Wavelets o Empirical Mode Decomposition o Artificial Neural Networks • Probabilistic Models o Histograms, probability and frequency distributions o Markov modeling o Agent-based models

Finite element method (FEM) was introduced to civil engineering by Clough after a sabbatical collaborating with the structural dynamics unit of Boeing Airplane Company (Turner, Clough, Martin and Topp 1956). Although the original concept of FEM was motivated for vibration and flutter analysis of aircrafts, FEM soon found extensive applications in structural and continuum analysis of mechanical and constructed systems (Clough and Wilson 1999). FEM has also been adopted and generalized by mathematicians and engineers for simulating field, and/or, multi-scale physics problems in geotechnical and environmental engineering, heat transfer, fluid mechanics, climatology, material science and biomedical engineering. With the growing capacities of computing technologies, FEM has become a powerful tool to simulate and predict the dynamic properties of various systems. For current applications of Sys-Id on constructed civil engineering structures, linear, stationary and deterministic finite element model is currently the most common analytical modeling form.

Owing to the process of discretization and idealization, it is inevitable that errors will be introduced in the presentation of continuous systems by finite element models. When the initial

analytical model(s) fail to accurately and completely conceptualize actual loading mechanisms, intrinsic force distributions, kinematics capacities of existing constructed systems, the analytical predictions on the basis of the model may be far away from the reality. It is important in the process of Sys-Id that every effort should be made to understand the causes of observed structural behaviors and thus to eliminate modeling errors embedded in initial FE model.

The following section provides an overview of finite element modeling and possible sources of modeling error with examples summarized from reported real-life applications of Sys-Id.

2.4.1 Conceptualization of Constructed Civil Structures

Unlike a non-existing structure for new design, modeling a constructed facility is a process to completely and accurately conceptualize the characteristics of a structural system. The preliminary analytical models are usually generated by taking advantage of the geometric material properties from documentations of original design drawings, available site inspection and material sampling test data, reports of earlier SHM applications on the structure as well as experiences from similar type of structures. Therefore construction tolerance or errors that can make as-built characteristics are different from designed values can hardly be taken into account in the initial FE models. Furthermore, existing civil structures distinguish themselves from manufactured mechanical engineering systems such as machinery and automobiles due to the following facts: (1) Each of civil structures is unique and exposed to different environments; (2) They are generally of large scale and comprised of a large number of structural and non-structural members; (3) The boundary and connectivity conditions between members are may change with the different environments and operation conditions. Due to incomplete knowledge of the actual structural state, a series of assumptions often have to be made to idealize the interactions between structure and soil and between different parts of sup-structure. As a result initial finite element models are not necessarily good representations of the real-life structure of interest, before any validation measures are taken to justify its reliability.

Although the general goal to construct finite element model is intended to enhance our ability to understand, predict and possibly control the behaviors of the system, the utility of ultimate identification results should always be unambiguously specified as they focus the modeling process on problem-specific issues. And depending on the objectives of St-Id investigation, the same real-world system may be idealized with sufficient accuracy by models of different fidelity. Additionally, the choice of model structure and model order also rely on available analytical and experiment resources, compatibility with experimental measurement degrees of freedom (for future test-analysis correlation) as well as the analyst's engineering judgment. For instance, the available computational software may set limits on selection of element type, mass formulation approach (lumped-mass or consistent mass) and accommodation of non-linearity and non-stationarity. Microscopic models may not be necessary if dynamic-based condition evaluation is the goal of system identification.

Satisfactory preliminary models of constructed facilities are expected to be capable of accurately and completely simulating:

(1) Geometry (dimensionality 2D, 3D, pseudo-3D etc);

(2) Stiffness and inertia distribution;

(3) Boundary and connectivity conditions and movement systems;

(4) Critical mechanisms of external and intrinsic loading path/distribution;

(5) Kinematics of deformation/displacement.

As opposed to modeling non-existing structures for design purposes, the models are also required to be such that modeling inaccuracy/uncertainty can be easily parameterized as far as possible. This is vital for subsequent model updating process. During the construction of models, software such as AutoCAD may be used to assist human eyes in fully conceptualizing complex geometric details. The structural degradation due to aging, local defects and other factors should be accommodated to reflect the direct exposure to the environment over the long life-cycles. The effects of changes in boundary

and connectivity conditions should be carefully investigated in order to properly simulate the interfaces of sub- and super-structure and connections between components. Aktan et al. (1997; 1998) provided excellent guidelines for the experimental and analytical aspects of structural identification respectively.

2.4.2 Possible Sources of Modeling Errors

The seventies witnessed a noticeable development for dynamic modeling due to the growing space and aeronautical programs. Finite element method has since then matured to be a capable tool and is being utilized by civil engineering consultants for practical applications. Despite of high sophistications of modern modeling and computation techniques, transforming a real world civil structure and its working environment into an idealized computer model with finite element method is always challenging. Considerable discrepancies can usually be expected when comparing analytically predicted dynamic properties with test measurements. Some of the discrepancy stems from uncertainty associated with experimentation, as discussed in previous section, and some can be attributed to modeling error inherent in finite element model(s) of the structure. The errors associated with modeling process are traditionally termed as modeling errors. Recognition of sources and locations of modeling errors in preliminary models can help analysts effectively implement experimental validation and objectively assess the reliability of structural predictions from refined models.

Commonly encountered modeling error in St-Id applications are including discretization errors, parameter errors and conceptualization errors. Discretization errors often result from mesh coarseness and improper shape functions and can be traced to the root of finite element methods. Since a FE model is a discrete numerical model of a continuous structural system, the existence of discretiztion errors is unavoidable and it may consequently make the eigen-solution deviate from its true value because the eigenvalues in the frequency range of interest are not fully converged. Sometimes, the convergence problem induced by discretization error is further complicated by coupling with

numerical errors. If an initial FE model with large discretization error is subjected to model updating, the embedded discretization errors may lead to divergence of the updating process or result in distorted updated parameters physically meaningless because the updating procedure is trying to compensate for the discretization errors (Chen 2001). Even if the discrepancies caused by the discretization errors of the FE model might be small, they will definitely affect the results with the final values of the updating parameters. Thus the compensation due to the discretization should be taken into account. Mottershead et al. (1995) presented a possible solution to mitigate the effects of discretization error in design process. Link and Conic (2000) incorporated finite element mesh density parameters allowing to refine the mesh within conventional iterative updating algorithms while Chen (2001) discussed the recognition of discretization error by comparing eigen-solution from different mass distribution approaches.

The as-built characteristics of constructed civil structures such as geometry and material properties are usually not straightforward. The construction tolerance and degradation due to aging, local defects and environmental actions are the main causes to deviate the actual property values from their designed values. Parameter errors are used to denote this type uncertainty. Due to their direct linkage with FE model parameters, parameter errors have been extensively investigated already. Almost all of current model updating applied for Sys-Id is aimed to correct erroneous parameter values assumed in the initial analytical model to better reflect the actual physical state of the structure. A series of parameter error localization methods were proposed in the 1990s and they includes best subspace method (Lallement and Piranda 1990; Link 1991; Maia et al 1994), force balance method (Fissette and Ibrahim 1988; Lallement and Piranda 1990; Baker and Marsh 1996), substructure energy function method (Link 1991 and Fritzen and Kiefer 1992) and etc.

The last but also the most important type of modeling errors is conceptualization errors. Due to epistemic mechanisms associated with this type of modeling errors, they are also referred to as epistemic modeling error in this thesis. Constructed civil engineering structures are usually highly

redundant system with the large number of structural members and non-structural members and the loading mechanisms, intrinsic force distributions, kinematics, boundary and joint connectivity conditions as well as failure modes are rarely well understood. As a consequence, the derivation of an appropriate finite element model to represent a real-life system usually employs physical laws, mathematical manipulation and behavioral assumptions through which conceptualization errors are often ejected into the resulting analytical model. For instance, unsuitable element types (e.g. missing shear deformation capability) and unsuitable boundary and connectivity condition are all potential sources of epistemic modeling error. More specifically, inappropriate conceptualization used in FE model construction results in a loss of some physical features and makes the model incapable of predicting the required dynamic properties accurately. However, epistemic errors are often neglected in most of the reported Sys-Id utilizations, although their profound influence on the analytical predictions of the structural performances as well as the following model updating have been mentioned (Friswell and Mottershead 1993; 1995; Sanayei et al 2001; Chen and Ewins 2004). This lies in the difficulty in proper recognition, characterization and parameterization of errors related with modeling idealization and assumptions.

Since FE modeling process is always involved with a large number of simplifications and assumptions, the resulting epistemic modeling errors may appear in various forms. In most analyses the model is limited to a portion of the total structure. This happens because part of the structure may be covered by non-structural members or buried under soil, or because the massive scale of the structure prohibits full coverage of measurement. Under these circumstances, boundary conditions are then explicitly applied at the interface with the rest of the structure. Sometimes, however, such simplification may lead to erroneous results by ignoring the inertial and stiffness contributions of the eliminated portion of the structure. Similarly, Geometric simplification when modeling components with complicated geometry can lead to modeling errors.

Another major potential source of conceptualization error is from dimensional reduction. By neglecting coupled responses in multiple dimensions, simplified 1D or 2D models may make it difficult to differentiate some higher order of modes and thus lead to more uncertainty in the evaluation and prediction of structural behaviors. The lack of knowledge of some critical mechanisms inherited in constructed systems may also lead to significant modeling errors. For instance, the energy dissipation mechanism in a specific structure is almost impossible to accurately simulate.

Boundary and connectivity between different components are always regions which can not be modeled with confidence. This situation can be further compounded by the non-stationarity and nonlinearity caused by environmental effects such as temperature and humidity. Lenett (1998) reported that several bearings of the Seymour Bridge displayed only intermittent contact at the operating limit state. Only after the supports were idealized to incorporate this phenomenon, the identification was successful.

Human errors which produced by human cognitive processes are often caused by inattention or thoughtlessness, inexperience, omission or commission. In creating a computer model involving thousands of degrees of freedom, even a minuscule error may result in disaster.

Table 2-3 Summary of Modeling Errors in Preliminary Analytical Models

Sources of Modeling errors	Explanation / Examples
Geometrical incompleteness / Geometrical simplification	Only a portion of the total structure is included in the model because the rest of the structure is ▪ Of massive scale; ▪ Covered by non-structural members; ▪ Buried by soil/water;
	Geometric details is ignored or simplified by smearing their inertia or stiffness contribution into adjacent components.
	The interaction of modeled portion of the structure with its surroundings is required to adequately represent through a set boundary conditions.
Dimensional Reduction	Coupled structural responses in multiple directions are neglected by reducing the 3D real structure into 2D plane-grid model or even 1D beam model.
Lack of knowledge of real world structure and its working environment	The ignorance of energy dissipation of a constructed civil structure makes it difficult to accurately simulate the damping of the system.
	Bridge bearings may display only intermittent contacts during operating limit state (Lenett 1998).
Uncertainty in as-built properties and environmental effects	The fabricated-constructed-erected nature of a system may be far different from what shown in the original design drawings.
	Direct exposure to the environment over long life-cycle makes it necessary to properly incorporate the effects of aging, local defects and etc on the geometry and material model used in the model
	Connectivity and boundary conditions may change with the temperature, humidity and etc.
Discretization error	The eigenvalues in the frequency range of interest can not be fully converged due to coarse mesh and shape function utilized in the model.
Blatant errors	Inattention or thoughtlessness, inexperience, omission or commission may lead to significant errors.

2.4.3 Epistemic Modeling Uncertainties Encountered in Real-Life Applications of St-Id

As stated in its definition, epistemic uncertainty is reducible when more information is available. Therefore the first step for a systematic investigation on modeling errors with epistemic mechanisms is to obtain more information about the source and form of appearance in the Sys-Id process of constructed civil structures. A wide literature survey is conducted to collect examples of epistemic modeling errors reported by researchers around the world. These structural attributes hidden in constructed systems, either in common with similar structure or unique for the specific system, dominate the observed structural behaviors but are absent from the preliminary FE simulations. It often takes experts one or more cycles of rigorous system identification to reveal them.

Ventura, Felber and Stiemer (1995) presented in this paper the ambient vibration testing on the Queensborogh Bridge in Vancouver area, Canada. The experimental dynamic properties obtained from the test were going to be used to refine linear elastic dynamic models in seismic retrofit studies. As a complementary test to the measurements on the deck level, lateral acceleration at selected piers was collected in order to obtain reliable lateral modes of vibration. The additional tests unexpectedly discovered that the fixity of the pier foundations varies greatly across the site. And the findings of soil-structure interaction at different locations along the bridge presented valuable information for the refinement of linear elastic dynamic models in retrofit studies and seismic assessment.

A significant difference in frequency of 1st mode was found btw experimental results and preliminary analytical modes. The author thought that the most plausible explanation for it may lie in the modeling of the boundary condition. The actual support conditions may have been more flexible than assumed. Adjusting the support flexibility through model updating was thus needed (Wang, Heo and Satipathi, 1998).

In order to assess current modeling techniques for bridge structures to predict actual field condition, ambient vibration tests were conducted on the University Drive/Crowchild Trail Bridge in Calgary, Alberta, Canada and four types of analytical models were built up to simulate the dynamic characteristics of the three span bridge with different assumptions and simplifications (Black and Ventura 1999). The four types of models are (a) distributed-parameter beam; (b) 2D uniform beam FE model; (c) 2D plane grid model; (d) 3D space frame FE model. Comparison between the identified modal properties from the ambient tests and the predicted values from various analytical models showed the strength and limitations of each of options considered.

Ren, Zhao and Harik (2004) performed a system identification investigation on the Tennessee River Bridge, a steel-girder arch bridge. Ambient vibration testing was carried out to validate two preliminary analytical models, one three-dimensional detailed model with the slab deck components simulated with shell elements and one simplified model by treating the deck as an equivalent beam

element. Although both models yielded comparable vertical and longitudinal frequencies which agree quite well with the test results, considerable discrepancy existed in transverse modes and the simplified model with joint lumped mass gave closer prediction than the detailed one. The writers found that the vertical and longitudinal modes simulated from both models agree well with the field test results but rather big difference existed in the transverse modes. The difference in the predicted transverse behaviors can be attributed to the different modeling method for the deck system.

In 2004 ambient vibration test was conducted on the Brooklyn Bridge as a supplement to analytical simulation for a seismic retrofit investigation (Grimelsman and Aktan 2005; Grimmelsman 2006). The instrumentation plan focused on the masonry bridge tower, since an extensive long-term and intermittent monitoring on the suspension span had been completed earlier by Lehigh University and a full instrumentation including both the span and tower was declined by the owner of the bridge. One major challenge emerged during the process of St-Id is that excitation sources of the tower under operational condition was comprised of not only ambient vibrations induced by wind and minor ground tremors but also transmitted motions from the suspension span which was directly subjected to traffic loads. The resulting filtered input would demonstrate harmonic characteristics and thus violated the general assumption for ambient vibration testing that the structure was excited by unknown random excitation. Additionally dramatic difference in mass and stiffness characteristics of the suspension span and bridge tower caused loose interaction between the different components of the bridge. As a result, repeated modal vectors were identified from measured frequency band – some of them were dominated by tower motion while the others were just reflections of span modes. This poses tremendous difficulty in reliably differentiating tower modes to characterize dynamic properties of the bridge towers, which is essential for seismic retrofit investigation because the bridge towers would be directly excited by ground motions during seismic events.

Researchers of Drexel Infrastructure Institute embarked on a long-term ambient monitoring on the Commodore Barry Bridge since 1998. The St-Id application was intended to obtain physical

properties of the bridge with an ultimate goal to develop a field-calibrated FE model for lifecycle asset management. An extensive monitoring system comprised of various types of transducers (accelerometers, strain gages, temperature transducers, wind sensors and etc) as well as video cameras formed to capture global and local responses of the bridge under its normal operation condition and controlled loading patterns. The global calibration of FE model with vibration test measurements was achieved by assuming the rigidity of the support and movement system of the bridge. And the predictions for the strain responses yielded from the globally validated model still demonstrated considerable discrepancy with the local responses obtained from load test measurements. It was concluded that the confidence in simulated global characteristics such as frequency and deflection is around 75-90% while the confidence in simulated local characteristics such as strains is around 50-75% (Catbas et al. 2007).

2.4.4 The State-of-the-Art of Recognition & Mitigation of Modeling Uncertainties with Epistemic Mechanism

Current applications of model updating on constructed systems are mainly limited to correct erroneous model parameters of initial analytical model, assuming that the conceptualization is adequate and that the experimentally obtained dynamic properties are accurate. This is usually not the case. In fact, finite element model construction for an existing structure is often involved with a compression process for all tempo and spatial information embedded in the system and the influences from aging, deterioration, mass and stiffness re-distribution, and many other factors may cast a shadow over a thorough understanding and conceptualization of its critical physical mechanisms under different loading patterns. Without appropriately acknowledging them in system identification, the credibility of identification results will be significantly impaired.

Sanayei et al (2001) approached this problem by presenting modeling errors with uncertain parameters which are assumed known and not to be estimated in the updating procedure. The rest of model parameters are either unknown parameter to be estimated or known parameters assumed to be

accurate. Through numerical simulations, the writers are able to investigate the influence of modeling errors with respect to excitation and measurement type and locations, type of error function and the location of uncertain parameters and etc through numerical simulations. However, the problem how to recognize and mitigate of modeling error remain unsolved.

Chen and Ewins (2004) proposed a vector projection method to check the existence of idealization errors in nominal models. The successful applications of the proposed approach on numerical examples and an aero-engine component demonstrated some promises to be utilized on constructed systems. However, large difference of analytical and measurement degrees of freedom in the cases of civil engineering applications may disable its capability to correctly localize the conceptualization modeling errors, since it is often impractical to instrument a long-span bridge or a high-rise building with a dense array of transducers.

Mottershead et al (2006) presented the study of a stochastic model updating technique using Monte-Carlo inverse propagation and multivariate multiple regression. The method allowed for manufacturing variability and modeling uncertainty so that a set of analytical models with randomized parameters are corrected by converging them upon a set of experimental results from a collection of nominal identical test pieces.

In the application of system identification on a highway bridge, Robert-Nicoud et al. (2005) made use of a set of analytical models in search for the causes of observed physical behaviors. In such a way, they attempted to progressively recognize the controlling modeling errors.

One problem coupled with the influence of epistemic modeling uncertainty is the un-uniqueness of identification results. Vibration-based system identification is actually a highly under-determined inverse problem with imprecise and incomplete information in both the measurements and initial simulation. Under many circumstances a large number of physically reasonable and significantly different models are capable of correctly predicting the behavior of the structure under a certain loading pattern. The non-uniqueness of the identification results poses great challenge to evaluate and

interpret the findings from Sys-Id and also brings difficulties in the following decision making. This problem was also pointed out by Avitabile (2000) by demonstrating the sensitivity of the updated model to parameters selected in the updating process with simulated test data. The same need was addressed to examine and evaluate the resulting candidate models which were all successfully updated to match with static test data to similar level (Berman 1998).

2.5 Conclusions

In order to better understand the challenges associated with Sys-Id on constructed civil structural systems, this chapter reviewed the state-of-the-art of theoretical developments and applications. It manifested an urgent need for a thorough investigation of the sources, characteristics and propagation of various uncertainties inherent at each stage of Sys-Id. Under such context, a comprehensive summary of uncertainty which may be encountered during the model construction, field testing and data processing was presented.

Difference between randomness and knowledge based uncertainties was carefully distinguished. And particular focus was placed on epistemic modeling uncertainty in this thesis. In utilizations of Sys-Id, modeling uncertainty with epistemic mechanism had profound influence on the reliability of identification results but they were often not properly acknowledged. This was further proved with examples extracted from the real-life applications, in which it took tremendous efforts of researchers to capture the linkage between dominant physical mechanisms of the structure and observed behaviors. Therefore a systematic study on modeling uncertainty with epistemic mechanism would benefit for the more widespread applications of Sys-Id in the near future.

3 Finite Element Model Updating

3.1 Introduction

Model updating, as one critical step in the flowchart of integrative Sys-Id, emerged in 1990s as a subject of immense importance to the design, construction and maintenance of mechanical engineering systems. With recent rapid growth in computation and information technology, model updating has already become part of the routine practice to replace repeated expensive prototype experimentation by experimentally validated analytical models in order to speed the design process and control design costs. The basic idea behind model updating is to utilize regression algorithms to identify system parameters when the form of relationship between system parameters and observed system outputs are known. Excellent reviews were provided by Friswell and Mottershead (1993; 1995), Lin and Ewins (1994), Natke (1998) and Sinha and Friswell (2003) and they comprehensively covered various aspects of model updating such as model preparation, updating methods, formulation of objective function, optimization algorithms, and techniques to improve numerical stability and so on.

In this chapter, model updating algorithms as well as preparatory procedures which are essential ahead of actual updating computation are presented. The preparatory steps include test-analysis correlation, error localization (parameter selection), sensitivity analysis and test data informativeness and etc. Although a good number of error localization indexes are available in literature (Fissette and Ibrahim 1988; Lallement and Prianda 1990; Link 1991; Zhang and Luo 1991; Fritzen and Kiefer 1992; Maia et al. 1994; Friswell and Mottershead 1995; Baker and Marsh 1996; Yang and Brown 1997; Mayes 1997; Larsson now Linderholt and Abrahamsson 1999), most of them were developed on the basis of theoretical derivation and verified with simulated test data, with an aim to serve for more ideally manufactured system. Their validity for constructed systems will be checked in the next chapters.

The model updating techniques can be broadly classified as direct method and iterative method. The inverse eigensensitivity approach, which belongs to iterative method, is one of the most commonly applied updating techniques in the real-life applications. In an iterative manner, the discrepancy between predicted and measured modal data of the structure is to be minimized with proper optimization techniques. The preference of iterative method over direct method lies in the fact that any adjustment made in updating is corresponding to changes in some structural properties and the physical significance of model can thus be preserved. Iterative approach can be further categorized as the method using modal data such as frequencies and mode shapes and etc. and the method directly using frequency response functions (Sestieri and D'Amrogio 1989; Friswell and Penny 1992; Imregun et al 1995).

3.2 Test-Analysis Correlation

Test-Analysis correlation is often considered as an essential step before any updating procedure can be conducted. If a satisfactory degree of correlation between initial analytical predictions and experimental observations can be achieved, it is extremely unlikely that any form of updating will succeed. In most of practical cases of St-Id applications on constructed civil structures, the analytical degrees of freedom defining finite element models are much greater than the measurement degrees of freedom. This incompatibility gives rise to a number of difficulties in correlating the analytical and experimental results. To resolve this problem, model expansion or reduction must be employed to either expanding the measured mode shapes to the size of their analytical counterparts or reduce the predicted mode shapes to the size of measured ones. For the purpose of model updating, model expansion is preferred because the following reasons: (1) measurement co-ordinates are unlikely to be the best master co-ordinates from a reduction point of view; (2) reduction process would inevitably damage the connectivity of the original finite element model; (3) potential modeling error would spread out and smear into all elements of the reduced matrices.

Comparison between analytical prediction and experimental modes is a common and effective tool to increase our understanding of the actual structural behaviors. Different methods are available for comparison of experiment and analysis. According to different domains in which the dynamic properties of a system are expressed, the methods to make comparison can be loosely classified as comparison of modal properties, comparison of frequency responses and etc. When the comparison is conducted in modal space, numerical comparison of natural frequencies and graphic comparison of mode shapes are the most obvious and popular way. In addition, numerical correlation indexes are proposed to quantify the difference between paired mode shapes between experiment and analysis. When the comparison is conducted in frequency domain, individual or complete set of frequency response functions is usually plotted out for evaluation.

3.2.1 Mode Shape Expansion

Mode shape expansion techniques were extensively investigated in 1990s. Many researchers (Gysin 1990; Imregun and Ewins 1993; Hemez and Farhat 1994; Gloth 2000) provided excellent overviews on various expansion methods. Generally the mode shape expansion methods can be grouped into three categories. The first approach is involved with pure geometric calculation and the shapes are expanded by interpolation or extrapolation of the measured co-ordinates to those of the full model. They had relative few applications. The second approach takes advantage of theoretical mass and stiffness matrices of the FE model to obtain information missing for the unmeasured degrees of freedom. The third alternative relies on the assumption that the measured mode shapes at full degrees of freedom can be expressed as linear combination of the analytical shapes. Comparative studies indicated that it is difficult to determine which method is the best since the quality of expanded mode shapes by different approaches seems to be case-dependent.

3.2.1.1 Expansion Using Analytical Mass and Stiffness Matrices

Suppose that ω_{EXPj} and ϕ_{EXPj} represent the jth measured natural frequency and the corresponding mode shape at the measured co-ordinates. Partitioning the mass and stiffness

matrix from the finite element model into measured and unmeasured co-ordinates, and substituting the measured natural frequency and mode shape, means that the equation of motion may be written as

$$\left(-\omega_{EXPj}^2 \begin{bmatrix} M_{mm} & M_{ms} \\ M_{sm} & M_{ss} \end{bmatrix} + \begin{bmatrix} K_{mm} & K_{ms} \\ K_{sm} & K_{ss} \end{bmatrix} \right) \begin{Bmatrix} \phi_{EXPj} \\ \phi_{sj} \end{Bmatrix} = \begin{Bmatrix} 0 \\ 0 \end{Bmatrix}$$

where ϕ_{sj} represents the estimated mode shape at the unmeasured degrees of freedom which also called the slave degrees of freedom. Rearranging the lower part of the matrix equation produces a solution for the unknown part of the measured mode shape vector. Thus,

$$\phi_{sj} = -\left(\omega_{EXPj}^2 M_{ss} + K_{ss}\right)^{-1} \left(-\omega_{EXPj}^2 M_{sm} + K_{sm}\right) \phi_{EXPj}$$

Other estimates of the unmeasured degrees of freedom of freedom may be obtained from the upper part of the equation, or form a combination of the two. Notice that the calculation will involve a pseudo inverse; using the upper part of the equation is really satisfactory only if the number of measured degrees of freedom exceeds the number of unmeasured degrees of freedom. Furthermore, from a practical viewpoint, this method may be difficult to implement if the finite element package does not store all the matrix elements in the model matrices.

3.2.1.2 Expansion Using Analytical Modal Data

This expansion method is based on the assumption that measured mode shape vector can be expressed as a linear combination of the analytically predicted ones.

$$\begin{Bmatrix} \phi_{EXPj} \\ \phi_{sj} \end{Bmatrix} = \begin{bmatrix} \Phi_{ANAm1} & \Phi_{ANAm2} \\ \Phi_{ANAs1} & \Phi_{ANAs2} \end{bmatrix} \begin{Bmatrix} \gamma_1 \\ \gamma_2 \end{Bmatrix}$$

where γ s denote the unknown linear expansion coefficients and the analytical mode shape matrix is split into master (measured) degrees of freedom and slave (unmeasured) degrees of freedom. If

it is further assumed that higher modes are expected to have a small influence on the lower measured modes, one can write

$$\{\gamma_2\} = \{0\}$$

Using the above equation will lead to a solution for the original problem, which can be approximated to

$$\begin{Bmatrix} \phi_{EXPj} \\ \phi_{sj} \end{Bmatrix} = \begin{bmatrix} \Phi_{ANAm1} \\ \Phi_{ANAs1} \end{bmatrix} \left[\Phi_{ANAm1}\right]^{-1} \{\phi_{EXPj}\}$$

The sub-matrix $\left[\Phi_{ANAm1}\right]$, in general case, is not a square matrix and hence its inversion is not straightforward. It is customary to invert it via the use of singular value decomposition or of a weighted least-squares algorithm. In any case, care must be taken not to include linear-dependent modal vectors as this will tend to make the matrix singular.

3.2.2 Correlation Index

Various indexes were developed in order to quantify the consistency between two modal vectors from finite element model and test observation, although they can also be utilized to compare modal vectors determined from different experimental or parameter estimation methods.

3.2.2.1 Modal Assurance Criterion (MAC)

Among them the most widely used one is the modal assurance criterion (MAC) which was proposed by Allemang and Brown (1982). It is often utilized to pair mode shapes derived from analytical models and test measurements. The MAC value between a measured mode and an analytical mode is defined as a scalar constant and provides a measure of the least squares deviation or ‘scatter’ of the points from the straight line correlation. MAC values can not discriminate between random scatter being responsible for the deviations or systematic deviations. The MAC is generally expressed as follows:

$$MAC(ANA, EXP) = \frac{\left|\sum_{i=1}^{n} (\phi_{EXP})_i (\phi_{ANA})_i^*\right|^2}{\left(\sum_{i=1}^{n} (\phi_{EXP})_i (\phi_{EXP})_i^* \cdot \sum_{i=1}^{n} (\phi_{ANA})_i (\phi_{ANA})_i^*\right)}$$

$$\text{Or } MAC(ANA, EXP) = \frac{\left|\{\phi_{EXP}\}^T \{\phi_{ANA}\}\right|^2}{\left(\{\phi_{EXP}\}^T \{\phi_{EXP}\}\right) \cdot \left(\{\phi_{ANA}\}^T \{\phi_{ANA}\}\right)}$$

in which ϕ_{EXP} and ϕ_{ANA} are the experimental and analysis mode shape vectors, respectively. n denotes the total number of degree of freedom included in comparison and i means the ith degree of freedom. The MAC values always lie between 0 and 1. When it is close to 1, it indicates a good correlation while a value close to 0 represents no consistent correspondence. However cautions should be paid when using MAC values to assess correlations of two modal vectors because they can also take on a value close to unity for the following reasons that the measurement degrees of freedom are insufficient to distinguish between independent mode shapes or that the mode shapes are primarily coherent noise. Similarly, a value close to zero of MAC index could be attributed to the facts: (1) the system is non-stationary; (2) the system is nonlinear; (3) parameter estimation algorithm is invalid for the measured test data; and (4) There is noise on the reference mode shape.

In practical applications, it is recommended that the correlation between a pair of mode shapes with MAC less than 0.6 is considered to be questionable. However, the modal assurance criterion can only indicate consistency, not validity. If the same errors, random or bias, exist in all modal vector estimates, this is not delineated by the modal assurance criterion.

3.2.2.2 Coordinate Modal Assurance Criterion (COMAC)

In the calculation of MAC value, a summation is made over all the degrees of freedom (DOFs) which are included in the paired modal vectors. However, there is spatial dependence of the correlation parameters. This becomes obvious when comparing the two MAC values produced by

using different selection of DOFs. The index Coordinate MAC or COMAC arises therefore to present the dependence directly. The COMAC is similar to MAC but determines the correlation between individual locations for all paired mode shapes (Ewins 2000). The COMAC index is generally expressed as:

$$COMAC(ANA_i, EXP_i) = \sum_{l=1}^{L} \frac{\left|(\phi_{EXP})_{il}(\phi_{ANA})_{il}\right|^2}{\left(\sum_{l=1}^{L}(\phi_{EXP})_{il}^2 \cdot \sum_{l=1}^{L}(\phi_{ANA})_{il}^2\right)}$$

in which ϕ_{EXP} and ϕ_{ANA} are the experimental and analysis mode shape vectors, respectively. L denotes the total number of paired modal vectors in comparison and l stands for the lth pair of modes, while i denotes the ith degree of freedom.

Although one is always tempted to conclude that the regions of the structure which have low COMAC values are those regions which contain significant discrepancy between analysis and experiments, it is seldom the case. However, the existence of systematic patterns of COMAC values almost always indicate systematic sources of discrepancy between test and analysis, even they are not immediately located.

3.2.2.3 Modal Scale Factor (MSF)

The quantity referred to as the Modal Scale Factor (MSF) represents the 'slope' of the best straight line through the points. It should be noted that this index gives no indication as the quality of the fit of points to the straight line but simply identifies its slope.

$$MSF(X, A) = \frac{\sum_{j=1}^{n}(\phi_X)_j(\phi_A)_j^*}{\sum_{j=1}^{n}(\phi_A)_j(\phi_A)_j^*}$$

$$MSF(A,X) = \frac{\sum_{j=1}^{n} (\phi_A)_j (\phi_X)_j^*}{\sum_{j=1}^{n} (\phi_X)_j (\phi_X)_j^*}$$

3.3 Error Location Index / Parameter Selection

For preliminary finite element models of civil structural systems, there are always a large multitude of parameters which may be prone to errors. The selection of parameters to update plays a crucial role in the success of identification. Firstly, it is impractical to include all candidates in model updating. Due to a limited amount of experimental results, the optimization process tends to appear underdetermined when involving with excessive updating parameters. Secondly, the level of sensitivity of each parameter to the change in modal data obtained from vibration tests is different. The insensitive parameters may lead to ill-conditioned sensitivity matrix for the updating algorithms. Furthermore, the selected parameters should reflect the actual modeling error associated with the initial models. Before model updating is conducted, therefore, the updating parameters should be carefully selected. The number of parameters should be kept as small as possible, and they should the ones which are sensitive to variation of experimental observations and have a controlling impact on the test-analysis discrepancies.

Numerous error indicator functions were proposed to localize potential modeling errors in model parameters (material or geometric properties) or mis-modeled areas (degree(s) of freedom, element(s) and/or substructure) associated with initial finite element model of the structure under consideration (Fissette and Ibrahim 1988; Lallement and Prianda 1990; Link 1991; Zhang and Luo 1991; Fritzen and Kiefer 1992; Maia et al. 1994; Friswell and Mottershead 1995; Baker and Marsh 1996; Yang and Brown 1997; Mayes 1997; Larsson now Linderholt and Abrahamsson 1999). These index functions were mainly developed based on simulated experiments with the aim to be applied on mechanical and aerospace systems and thus care must be taken when adapted to constructed civil engineering structures. Furthermore, the fact that these indexes are

only capable of dealing with parameter errors prevent them from recognizing more fundamental modeling error sources which could not be properly parameterized. As a result, the parameters selected for modification are not the primary source of test-analysis discrepancy. In these cases, it is correlation tools as well as good engineering judgment that an analyst must scrutinize the model to achieve its full potential as a predictive tool.

3.3.1 Balancing the Eigenvalue Equation

Balancing the Eigenvalue Equation method is also referred as Force Balance Method, Dynamic Reaction Method and Dynamic Force Residue Method and etc. in literature. Its early application can be traced back to Fissette and Ibrahim (1988). Lallement and Piranda (IMAC 1990) further formulated it and obtained the localization matrix. And Berger et al. (1990) developed similar indicator named as dynamic reaction Approach and Maia et al. (1994) summarized this method. Baker and Marsh (1996) referred to it as force balance method and compared it with other error localization methods. Friswell and Mottershead (1995) summarized it as balancing the eigenvalue equation Method.

The basic idea of this approach is to use measured eigenvalues and eigenvectors together with the analytical mass and stiffness matrices. This yields the following equation:

$$\left[K_{ANA} + \Delta K\right]\Phi_{EXP} - \left[M_{ANA} + \Delta M\right]\Phi_{EXP}\Lambda_{EXP} = 0$$

The matrix increments ΔK and ΔM are needed in order to keep the eigen-equation in balance after replacing analytical modal data by their experimental counterparts. By combining the effects of the increments, the localization matrix L can be obtained:

$$L = \Delta M\Phi_{EXP}\Lambda_{EXP} - \Delta K\Phi_{EXP} = K_{ANA}\Phi_{EXP} - M_{ANA}\Phi_{EXP}\Lambda_{EXP}$$

where the experimental modal matrix is a n-by-N matrix and contains N mode shapes corresponding to N measured frequencies. Since the number of measurement degrees of freedom

is far less than those of analysis, the measured mode shapes have to be expanded through the techniques discussed previously.

The dominant modeling errors are selected from examination of a location vector expressed below

$$q_i = \sum_{r=1}^{N} \rho_r L_{ir}^2, \qquad i = 1, \cdots, n$$

where the weighting scales, ρ_r, reflect the agreement (or otherwise) between the measured and analytical data for the *rth* mode. The uncertain regions in the model are given by those degrees of freedom associated with high values of q_i.

3.3.2 Substructure Energy Functions

Link and Santiago (1991) proposed an error localization method with the use of energy functions based upon the substructures M_j and K_j. Thus a strain energy function can be expressed as

$$\Delta\Pi_j^s = \sum_{r=1}^{N} \left(\phi_{ANAr} - \phi_{EX\,\mathrm{Pr}}\right)^T K_j \left(\phi_{ANAr} - \phi_{EX\,\mathrm{Pr}}\right)$$

and a kinetic energy function as

$$\Delta\Pi_j^K = \sum_{r=1}^{N} \left(\phi_{ANAr} - \phi_{EX\,\mathrm{Pr}}\right)^T M_j \left(\phi_{ANAr} - \phi_{EX\,\mathrm{Pr}}\right)\omega_{EX\,\mathrm{Pr}}^2$$

where M_j, K_j are the mass and stiffness matrices of the *jth* element substrucgure (i.e. individual or groups of elements). An Energy function which takes a large value is an indicator of an erroneous substructure. A small value indicates either a small error or that the data is insensitive to changes in the substructure. However, what is vital to the success of this method is the correct

normalization of the parameters. One way to ensure satisfactory normalization is to use a parameterization where the initial parameter estimates are all unity.

3.3.3 Best Subspace Method

Lallement and Piranda (1990) presented an error indicator which was called Best subspace method. Later Fritzen and Kiefer (1992) and Maia et al. (1994) referred to it as sensitivity method. It was developed from the Taylor expansion of the difference between analytical and experimental modal data (frequencies and mode shapes), which can be generally expressed as follows if ignoring the high-order terms:

$$S \cdot \Delta\Theta = b$$

in which *S* denotes Jocabian matrices (first derivatives) of the modal data with respective to *p* candidate updating parameters Θ , $\Delta\Theta$ and *b* represent the change of parameters and the difference of analytical and experimental modal responses respectively. The principle is the following: Among the columns of S matrix, the single column is sought which best represents the vector b. And then the combination of two and more columns constitutes the best sub-basis for the representation of the vector *b*. Let b^p denote the best representation of b in the sub-basis of dimension of *p*, the relative distance between *b* and b^p can be utilized as scalar error index.

$$e^p = \frac{\left\| b - b^p \right\|}{\left\| b \right\|} \times 100\%$$

An analysis of the errors e^p obtained with subspace of increasing dimension ($p = 1,2,3...$) permits the selection of the most probable combination of dominant modeling errors. For $p > 1$, an iterative approach is most efficient for the generation of the best subspace. The iteration starts with $p = 1$ the single parameter that is best able to represent the data is selected and the

following steps will keep adding more parameters so that the resulting group of parameters will better present the data.

3.4 Sensitivity Analysis

In addition to the error localization algorithms discussed in previous section, sensitivity analysis is also a convenient tool to assist the analyst to identify the most sensitive parameters from a pool of candidates with respect to the available structural responses. Generally the selected updating parameters are required not only to reflect the uncertainties due to actual modeling errors, but also to be sensitive to changes in test data. This is especially important to sensitivity-based optimization algorithms because incorporating insensitive parameters in updating procedure may lead to ill-conditioned sensitivity matrix and thus have detriment impact on the stability and accuracy of optimization process. As a result, the updating would either diverge or converge to erroneous values. It should be noted that low sensitivity of one parameter with respect to the available structural responses implies that the information content of the measurement is insufficient to estimate the parameter but the reverse is however invalid.

Most reported parameter sensitivity analyses were either performed by optimized proprietary software such as FEMtools (Brownjohn et al. 2000) or manually (Catbas et al. 2007). One common point for these applications is that they are based on the ‘change one factor at a time’ philosophy. In this section, an improved scheme adapted from experiment design is introduced to conduct sensitivity analysis. By simultaneously evaluate all parameters, this new scheme can provide a clear picture of how these candidate parameters behave separately and together. And therefore the selected parameters will either independently affect one modal response significantly (for example, the natural frequency of the first mode) or interact with other ones in their huge influence on a different modal response.

3.4.1 Two-level Factorial Orthogonal Design of Experiment

Factorial design is one of statistical test design method. To perform a factorial design, a fixed number of 'levels' of each of a number of factors are selected and experiments of all possible combinations are conducted. If only two levels are specified for each factor, it is often referred as two-level factorial design and the two levels of each factor are denoted as plus and minus levels. A full two-level factorial design will always result in 2^n experiments where n stands for the number of factors of interest. Thus the total number of experiments required for a full factorial design will increase exponentially as more possible updating parameters are to be taken into account. In such a case, fractional factorial design which employs some (such as an half or a quarter) of experiment runs can be constructed. And the resulting experiment data will then be analyzed to provide insight into 'which factors do what to which response' (Box, Hunter and Hunter 2005). It should be emphasized that interactions of all orders can be uniquely estimated with full factorial designs while only some (or no) interactions can be uniquely estimated with fraction factorial designs. While the main effects of each factor may compound with that of high-order interactions, carefully designed fractional factorial experiments will still be helpful to obtain better understanding the relative importance of each parameter.

Frequently the factor activity in factorial experiments is described with a 'main effect – interaction' model, in which the main effect of individual factor and coupling effect between factors are to be obtained from experimental data. The following two-level 2^3-run example helps to explain the calculation of main effects and high-order interactions. Assume that three factors A, B and C are studied in order to maximize a response y. Each of the factors is studied at it minus and plus levels and the resulting eight runs for a two-level full factorial test design can be formulated as shown in Table 3-1. The main effect of factor A is defined as the difference between the average of all four responses in which the factor is set as its plus level and the average of the other four responses in which the factor is at its minus level (as illustrated in Table

3-2). The main effects of factor B and C can be generated in a similar way. It should be noticed that all the eight observations are used to estimate the main effect of each factor. If a one-factor-at-a-time approach is applied, eight experiment runs are required in order to obtain equal precision.

Besides the information about the individual effects of the factors, factorial experiment design will also provide insight of the influence of factor interactions on the system response data. Generally, for an n-factor experiment, the total number of possible interactions of all orders is $2^k - 1 - n$. In practice, the most important interactions are likely to be 2-factor interactions and the total number of possible 2-factor interactions is $\frac{n(n-1)}{2}$. For example, if n = 3, the total number of possible interactions is 4 and that of 2-factor interactions is 3. In general interactions are not the same as the usual (multiplicative) cross-product. However, it is the case for the special case of 2-level designs, as shown in

Table 3-3. Using the same two-level 2^3-run example, the interaction between factors A and B (A*B) is defined as the difference between the average of all four responses in which the A*B interaction is set as its plus level and the average of the rest four responses in which the interaction is at its minus level. The other two 2-factor interactions B*C, A*C can be formulated in the same way.

Table 3-1 2-level 8-run full factorial design

Run Number	Factor 1: A	Factor 2: B	Factor 3: C	Response
1	+	+	+	y1
2	+	+	-	y2
3	+	-	+	y3
4	+	-	-	y4
5	-	+	+	y5
6	-	+	-	y6
7	-	-	+	y7
8	-	-	-	y8

Table 3-2 Main effect of factor A

Factor 2: B	Factor 3: C	Effects of Changing Factor A from
+	+	y1 - y5
+	-	y2 - y6
-	+	y3 - y7
-	-	y4 - y8
		Main effect of A: average of the above four items

Table 3-3 the Setting for A*B interaction

Factor 1: A	Factor 2: B	Interaction of Factors 1 & 2: A*B
+	+	+
+	-	-
-	+	-
-	-	+

3.4.2 Sensitivity Analysis Based on Exploratory Data Analysis (EDA)

The two-level factorial design has been used to design physical experiments for years (Box, Hunter and Hunter 2005). And the idea behind it is equally applicable to evaluate the sensitivity of updating parameters with respect to the response data. For model updating procedure, the most crucial information expected from sensitivity analysis is the importance rank list of all candidate parameters with respective to the responses of interest. In the traditional one-factor-at-a-time method, this is accomplished by having a single factor vary with the remaining factors held constant. For such an estimate, it is necessary to assume that the effect of individual factor was the same at all the other settings of the remaining factors. The two-level factorial design based sensitivity analysis will not only provide the main effects of individual factor more easily and accurately, but also yield high-order interaction effects between factors.

The 10-step exploratory data analysis (EDA) proposed by NIST is an approach to analyze the data obtained from 2^n full or 2^{n-p} fractional factorial designs. It aims to bring out all aspects of experimental data and to extract useful information on the relative importance of involved parameters through different plots with different basis and focus. In engineering applications, a factor can be important if it leads to a significant shift in the location of the response variable as the setting of the factor changes from minus level to plus level or vise versa.

The ten steps comprised of EDA includes: (1) Ordered data plot; (2) Dex (Design of experiments) scatter plot; (3) Dex mean plot; (4) Interaction effects matrix plot; (5) Block plot; (6) Dex Youden plot; (7) |Effects| plot; (8) Half-normal probability plot; (9) Cumulative residual standard deviation plot; (10) Dex contour plot. The purpose, output, definition and motivation of each plot are intensively presented in the Engineering Statistics Handbook of NIST.

3.5 Quantification of the Informativeness of Test Data

At the model updating stage of St-Id diagrams, modal data (modal frequencies, shape vectors, damping ratios or frequency response functions) extracted from test measurements are often used to validate initial analytical models in stead of the recorded time-domain responses. This is done because modal quantities are easier visualize, physically interpret and interpret in terms of standard mathematical modeling of vibrating systems than are the actual time-history measurements. A typical time-history collected on a real-life structure may contain 3,600,000 data points (30 measurement points, 200 Hz sampling frequency and 10-minute duration). If 20 modes are identified from the data, the original measurement is reduced to 640pieces of information, including 20 modal frequencies, 20 damping ratios and 20 shape vectors each of which contains 30 relative amplitude values. If frequency response functions (FRFs) are utilized, a typical FRF at one measurement location may contain 4096 frequency points and hence the 3,600,000 time data will still be reduced to 122,880 pieces of information. Therefore, standard modal parameter estimation can be considered as a form of data compression and information about the current state of the structure will be unavoidably lost during the compression.

This will naturally lead to the question – is there adequate information contained in the test data to correct the localized modeling errors inherent in initial FE model? Since the updating procedure generally makes use of experimental results as the reference, the amount and quality of information will thus be another key factor to the success of updating. Inadequate experimental measurements with respect to the localized modeling errors may fail to correct the initial model.

The concept of test data informativeness emerged in recent years and it is used to quantify the information carried by test data under a specific test configuration. Linderholt and Abrahamsson (1999) introduced an index called Data Information Richness (DIR) to help quantifying the data informativeness in the frequency band of interest. However, this index is based on nominal FE model and its theoretical validity has not been proved. Another informativeness index was proposed by the same researchers recently is related to the Fisher Information Matrix (Linderholt and Abrahamsson 2005). Due to the tight linkage to sensor positioning on the structure, researches on test data informativeness evaluation share

In the following section focus would be placed on the quantification of data informativeness. The assessment of information contained in test data is usually compounded with issues of identifiability, test design and optimal sensor placement and so on. This seems reasonable since the lack of information with respective to one specific parameter may lead to re-parameterization of updating parameters or new test design.

The researchers proposed another informativeness index which is shown to relate to Since test data informativeness is heavily influenced by sensor positioning on the structure, researches on optimal sensor placement algorithms which are intended to maximize the information to be obtained from vibration tests also serve as a good resource for the development of possible tools for test data evaluation (Brillhart and Kammer 1994; Kammer and Yao 1994; Udwadia 1994; Larson et al. 1995; Beck et al. 1998; Ibrahim 2000; Meo and Zumpano 2005).

3.5.1 Fisher Information Matrix

The Fisher Information matrix (FIM) was proposed as an important statistical measure to quantify the amount of information present in a noisy measurement with respect to unknown model parameters. The concept of FIM closely ties with the Maximum Likelihood (ML) theory. Let

$p = n \times 1$ dimensional state or parameter vector;

$y = m \times 1$ dimensional measurement vector;

$y_m = m \times 1$ dimensional system output;

$v = m \times 1$ dimensional noise vector;

$R = m \times m$ dimensional measurement covariance matrix,

the obtained test measurements can generally expressed as

$$y(t_i) = y_m(t_i, p^*) + v(t_i)$$

where $y_m(t_i, p^*)$ is the output of a deterministic structural model, p^* is the true value of the parameter vector. The type of probability density for the measurement noise will dictate the type of function of the output error to be employed. Among the broad families of distributions that can be considered, Gaussian (or normal) distributions are of special importance. One justification for this phenomenon lies in the central limit theorem, which states that the measurement noise tends to be normally distributed if its results from the summation of a large number of i.i.d. errors with finite variance. Here the noise contribution to the test observations is assumed as an m-dimensional independent Gaussian process with zero mean and covariance matrix $R(t_i)$.

The above observation equation of the structure thus implies that the measured system output is Gaussian once assuming the noise is Gaussian, since $y_m(t_i, p^*)$ is the output of a deterministic model. The conditional distribution density (also called likelihood function) of the observation of the output at time t_i can then be given as

$$f_y(y(t_i)|p) = \left((2\pi)^m \cdot det(R)\right)^{\frac{1}{2}} \cdot exp\left\{-\frac{1}{2}\left[y(t_i) - E_{y|p}\{y(t_i)|p\}\right]^T \cdot R^{-1} \cdot \left[y(t_i) - E_{y|p}\{y(t_i)|p\}\right]\right\}$$

where E denotes the expectation.

The likelihood function of the n_t observations of the output is

$$f_y(y|p)=\prod_{i=1}^{n_t}\left((2\pi)^m\cdot det(R)\right)^{-\frac{1}{2}}\cdot exp\left\{-\frac{1}{2}\left[y(t_i)-E_{y|p}\{y(t_i)|p\}\right]^T\cdot R^{-1}\cdot\left[y(t_i)-E_{y|p}\{y(t_i)|p\}\right]\right\}$$

$$ln\, f_y(y|p)=-\frac{m\cdot n_t}{2}ln(2\pi)-\frac{n_t}{2}ln\, det(R)$$
$$-\frac{1}{2}\sum_{i=1}^{n_t}\left[y(t_i)-E_{y|p}\{y(t_i)|p\}\right]^T\cdot R^{-1}\cdot\left[y(t_i)-E_{y|p}\{y(t_i)|p\}\right]$$

$$\frac{\partial}{\partial p}ln\, f_y(y|p)=-\frac{1}{2}\cdot 2\cdot\sum_{i=1}^{n_t}\left[\frac{\partial}{\partial p}E_{y|p}\{y(t_i)|p\}\right]^T\cdot(-1)\cdot R^{-1}\cdot\left[y(t_i)-E_{y|p}\{y(t_i)|p\}\right]$$
$$=\sum_{i=1}^{n_t}\left[\frac{\partial}{\partial p}E_{y|p}\{y(t_i)|p\}\right]^T\cdot R^{-1}\cdot\left[y(t_i)-E_{y|p}\{y(t_i)|p\}\right]$$

According to the definition of Fisher Information matrix, it can be written as

$$F=\underset{y|p}{E}\left\{\left[\frac{\partial}{\partial p}ln\, f_y(y|p)\right]\left[\frac{\partial}{\partial p}ln\, f_y(y|p)\right]^T\right\}$$
$$=\underset{y|p}{E}\left(\sum_{i=1}^{n_t}\left[\frac{\partial}{\partial p}E_{y|p}\{y(t_i)|p\}\right]^T\cdot R^{-1}\cdot\left[y(t_i)-E_{y|p}\{y(t_i)|p\}\right]\right)\cdot$$
$$\left(\sum_{i=1}^{n_t}\left[\frac{\partial}{\partial p}E_{y|p}\{y(t_i)|p\}\right]^T\cdot R^{-1}\cdot\left[y(t_i)-E_{y|p}\{y(t_i)|p\}\right]\right)^T$$

$$=\underset{y|p}{E}\sum_{i=1}^{n_t}\left[\frac{\partial}{\partial p}E_{y|p}\{y(t_i)|p\}\right]^T\cdot R^{-1}\cdot\left[y(t_i)-E_{y|p}\{y(t_i)|p\}\right]\cdot\left[y(t_i)-E_{y|p}\{y(t_i)|p\}\right]^T\cdot R^{-T}\cdot$$
$$\left[\frac{\partial}{\partial p}E_{y|p}\{y(t_i)|p\}\right]$$

$$= \sum_{i=1}^{n_t} \left[\frac{\partial}{\partial p} E_{y|p} \{ y(t_i) | p \} \right]^T \cdot R^{-1} \cdot \underset{y|p}{E} \left(\left[y(t_i) - E_{y|p} \{ y(t_i) | p \} \right] \cdot \left[y(t_i) - E_{y|p} \{ y(t_i) | p \} \right]^T \right) \cdot R^{-T} \cdot \left[\frac{\partial}{\partial p} E_{y|p} \{ y(t_i) | p \} \right]$$

Since R is symmetric, $R = R^T$

$$F = \sum_{i=1}^{n_t} \left[\frac{\partial}{\partial p} E_{y|p} \{ y(t_i) | p \} \right]^T \cdot R^{-1} \cdot R \cdot R^{-1} \cdot \left[\frac{\partial}{\partial p} E_{y|p} \{ y(t_i) | p \} \right]$$

$$= \sum_{i=1}^{n_t} \left[\frac{\partial}{\partial p} E_{y|p} \{ y(t_i) | p \} \right]^T \cdot R^{-1} \cdot \left[\frac{\partial}{\partial p} E_{y|p} \{ y(t_i) | p \} \right]$$

This is Fisher's information matrix about the parameter p based on the measured output y for a Gaussian conditional distribution density. Strictly, the FIM corresponds to the expected value. If no expectation is taken, we obtain a data-dependent quantity, which is often referred to as the observed FIM.

In the case of a linear system,

$$y_m(t_i, p^*) = C(t_i) \cdot p^*$$

$$\frac{\partial}{\partial p} E_{y|p} \{ y(t_i) | p \} = \frac{\partial}{\partial p} C(t_i) \cdot p = C(t_i)$$

And the FIM is simplified as

$$F = \sum_{i=1}^{n_t} C^T(t_i) \cdot R(t_i)^{-1} \cdot C(t_i)$$

In the case of a nonlinear system,

$$\underset{y|p}{E} \{ y | p \} = \underset{y|p}{E} \{ y_m(t_i, p^*) + v(t_i) | p \}$$

The linearization of the nonlinear system can be achieved by a Taylor series expansion at the initial parameter value,

$$y_m(t_i, p) = y_m(t_i, p)\Big|_{p=p^0} + \frac{\partial y_m(t_i, p)}{\partial p}\Big|_{p=p^0} \cdot (p - p^0) + h.o.t.$$

If neglecting the higher order terms,

$$F = \sum_{i=1}^{n_t} \left(\left[\frac{\partial y_m(t_i, p)}{\partial p} \right]\Big|_{p=p^0} \right)^T \cdot R(t_i)^{-1} \cdot \left(\left[\frac{\partial y_m(t_i, p)}{\partial p} \right]\Big|_{p=p^0} \right)$$

3.5.2 Quantifying Information Contained in Test Data

Utilization of the Fisher Information matrix could be found in previous work conducted by Shah and Udwadia (1978), Udawadia (1994), Kammer (1991; 1994) and Papadimitriou (2000; 2004) and so on. Udwadia (1994) developed a statistical-based approach to determine optimum sensor number and locations for test instrumentation by maximizing the trace of the Fisher Information matrix. Taking advantage of $y(t_i) = \phi_A \cdot q(t_i) + v(t_i)$, Krammer and Yao (1991; 1994) came up with an effective iterative algorithm to sequentially eliminate sensor location with the lowest reduction in the determinant of the Fisher Information matrix. Recently Papadimitriou et al (2000) introduced the information entropy as the measure to select optimal sensor configuration which minimizes the uncertainty in model parameter estimation. It was shown that minimization of the proposed information entropy was equivalent to the maximization of the determinant of the FIM. Linderholt and Abrahamsson (2005) proposed a data informativeness index, which shared resemblance with Fisher Information matrix, to optimize the test design for the purpose of model updating. Fritzen and Bohle (2001) introduced similar FIM-related measure to improve the model-based damage detection.

All the aforementioned investigations could be considered as extended applications of the Fisher Information matrix. Tracking back to the origin of the FIM, it could be found that the

inverse of Fisher Information matrix, also known as Cramer-Rao bound, defined the fundamental limits to the variance and covariance of any unbiased estimators. Irrespective of the methods used to extract parameters from the data, Cramer-Rao bound set up the limit to the estimation precision for given test data and noise properties. For error localization for model updating purpose, test data must contain sufficient information about the uncertain parameters of model. Otherwise, the identification may lead to erroneous results, if one particular parameter of which the given measurements have low information was chosen to be included in the updating procedure. Therefore it is advantageous to be able to evaluate and quantify the informativeness of the available data. Since the diagonal element of the Fisher Information matrix represent the degree of identifiability of each parameter of interest, it makes sense to use it as a measure of informativeness for the given test data with respective to corresponding parameter.

In the previous formula, the entries of the FIM are expressed in terms of partial derivatives of the system output with regards to model parameters and they are evaluating at the optimum parameter estimates. When measured data do not contain any information about certain parameters, those parameters can vary without changing the measured transfer functions of the system (Linderholt and Ambasson 2005). This implies that local non-informativity will lead to singularity of the FIM. Since the optimum parameter estimates are not available at this stage and the calculated FIM is only reliable if the parameter values are not deviating too much from their true values, it is necessary to assume that the parameter values in the initial FE models are reasonably close to the true values.

3.6 Finite Element Model Updating Algorithms

After all the preparatory updating procedures have been undertaken, the following step is the actual computation of updating corrections. The existing updating algorithms can generally be classified into two major types, direct method and iterative method. Direct method includes those methods in which individual elements of the system matrices of the initial FE model are adjusted

to reproduce the test data. With iterative method, the test-analysis discrepancy is minimized by searching for an adjustment of a selected set of physical or elemental properties in the model. Excellent reviews of various updating methods can be found in Imregun and Visser (1991), Mottershead and Friswell (1993), and Friswell and Mottershead (1995).

It should also be pointed out that successful updating can only be achieved with well prepared finite element model. This means that all key physical mechanisms of the structure are accurately and completely idealized, and that uncertainties associated with modeling are appropriately parameterized and included as updating parameters in the updating procedure.

3.6.1 Direct Method

Direct methods appeared in the late 1970s and early 1980s and they were widely utilized in the early applications of model updating. Nowadays they are still used and improved. Direct methods include direct matrix updating, reference basis method, matrix mixing method and eigenstructure assignment method and etc (Baruch and Bar-Itzhack 1978; Thoren and Ross; Minas and Inman). Direct methods usually involve the adjustment of parameters in mass matrix and/or stiffness matrix of the structure with imposed constraints such as symmetry, sparsity (model connectivity), orthogonality and definiteness. Without iteration, closed-form solutions can be derived in direct methods. The most important feature of direct methods is that the updated analytical model is capable of reproducing the given experimental data exactly. And since no iteration is involved, less computation cost is required in direct methods and problems related to numerical stability and convergence do not exist. However, the resulting model may lose its physical significance because changes in system matrices can not be related to physical changes in the original model. Besides, measurement errors can easily be propagated to the updated parameters by forcing the modal output of the updated model to be exact to the measured data. Direct methods are often highly sensitive to measurement noise.

Direct method usually requires the measured mode shapes for the full set of degrees of freedom. Therefore mode shape expansion techniques would normally used to expand the experimental modal vectors for the application of this method. This poses a challenge to the applications of direct method on large scale civil engineering structures because the measurement degrees of freedom during vibration monitoring are often sparse. Furthermore, non-uniqueness of updating results is inevitable, considering that the number of constraints imposed by conditions such as symmetry and orthogonality and etc is far less than the number of analytical degrees of freedom.

For example, the formula of direct matrix method for the updating is simply defined as follows (Ewins 2001?):

$$[\Delta M] = [M_A][\Phi_X][m_A]^{-1}([I] - [m_A])[m_A]^{-1}[\Phi_X]^T[M_A]$$

where

$$[m_A] = [\Phi_X]^T[M_A][\Phi_X]$$

followed by

$$[\Delta K] = [M_A][\Phi_X][\Phi_X]^T[K_A][\Phi_X][\Phi_X]^T[M_A] + [M_A][\Phi_X][\Lambda_X][\Phi_X]^T[M_A] - [K_A][\Phi_X][\Phi_X]^T[M_A] - [M_A][\Phi_X][\Phi_X]^T[K_A]$$

where the M_A and K_A stand for analytical mass and stiffness matrices respectively and Φ_X denotes the experimental mode shape matrix.

3.6.2 Iterative Method

Iterative model updating methods are currently the most popular model updating approaches and it is also referred to as sensitivity-based method. Iterative methods overcome the drawbacks of direct methods by improving the correlation between experimental results and analytical model in an iterative way. The discrepancy in the two sets of data are expressed in an objective function

in which different weighting factor can be assigned to each term according to different reliability level of available modal data. Modeling errors associated with initial analytical model are parameterized into updating terms and these pre-selected parameters are then tuned during an optimization process to minimize the objective function. Because the objective function is usually a nonlinear function of updating parameters, iterative procedure is required to obtain an optimum result.

The iterative method usually includes four main aspects – objective functions, selection of updating parameters, sensitivity derivative approximations and optimization techniques. According to the type of reference data used in the updating procedure, two different iterative updating methods exist – one is inverse eigensensitivity method using modal data and the other is response function method using FRFs. The large number of parameters available in the FE model of constructed systems often makes the choice of updating parameters extremely difficult. Candidates of updating parameters may include substructure parameters or physical quantities and etc. The number of updating parameters, the sensitivity of each parameter with respect to responses as well as the relatively independence between parameters are often the controlling factors for the numerical conditioning of sensitivity matrix. The calculation of sensitivity matrix is computationally intensive especially when the size of the problem is large. Close or repeated eigenvalues can cause ill-conditioning or slow convergence. Mode shapes are more difficult to be used in the update procedure than natural frequencies. The reasons are that mode shape often contains significant measurement errors and that it has to be normalized for consistency with the analytical model. Weighting matrix is often used in updating process reflect the relative confidence of the analyst on different physical responses. Usually the weighting matrix is set as the estimated variance of the measured data. However, this technique requires the variance of both the measured data and the initial analytical parameters to be specified.

3.6.2.1 Formulation of Inverse Eigensensitivity Updating Method

Let z_M represent the measured modal output of the system (frequencies, mode shapes, modal curvature, modal flexibility and etc.) and z_j represent their counterpart predicted by the initial FE model based on the parameter estimate in iteration j. Both z_M and z_j are considered to be a function of a set of pre-selected updating parameters θ. The difference between the measured and analytical results can be expressed as

$$\delta z_j = z_M - z_j$$

This difference vector is often called residual. An objective function in an ordinary least squares problem can then be defined as a sum of the squared residual vector. Minimization of the objective function will lead to maximization of the correlation between measured and analytical model.

$$J = \left(\delta z_j\right)^T \left(\delta z_j\right)$$

In order to account for the relative importance and reliability of each individual term in the residual vector δz_j, a weighting matrix W is often utilized to multiply with the residual vector. The objective function can rewritten as

$$J = \left(\delta z_j\right)^T W \left(\delta z_j\right)$$

Since the model vector z_j is generally a nonlinear function of the updating parameters θ, the minimization of objective function is a nonlinear optimization problem. One of the techniques to solve this problem is to expand the analytical modal vector into a truncated Taylor series. Omitting the higher order terms, the model vector is

$$z_j(\theta) = z_{j0} + \left.\frac{\partial z_j}{\partial \theta}\right|_{\theta=\theta_{j0}} \left(\theta_j - \theta_{j0}\right) = z_{j0} + S_j \cdot \delta\theta_j$$

where $z_{j0} = z_j\left(\theta = \theta_{j0}\right)$represents the analytical modal vector at the linearization point $\theta = \theta_{j0}$. S_j denotes the sensitivity matrix of the structure and contains the derivatives of the modal properties z_j with respect to the updating parameters θ, evaluated at $\theta = \theta_{j0}$. $\delta\theta_j$ represents the change of the parameter vector. Similar expression can be obtained at each iteration step.

Substituting the linearized expression of analytical modal data into the residual vector yields a linear residual. And the weighted objective function can also be rewritten as follows.

$$\delta z_j = z_M - z_j = z_M - z_{j0} - S_j \cdot \delta\theta_j = r_j - S_j \cdot \delta\theta_j$$

$$J = \left(r_j - S_j \cdot \delta\theta_j\right)^T W \left(r_j - S_j \cdot \delta\theta_j\right)$$

where $r_j = z_M - z_j$ contains the residual at the linearization point.

At each iteration step, the minimum of the objective function with respect to the updated parameters is achieved by setting the first-order derivative of the objective function as zero.

$$\delta\theta_j = \left(S_j^T \cdot S_j\right)^{-1} S \cdot_j^T r_j$$

or

$$\delta\theta_j = \left(S_j^T \cdot W \cdot S_j\right)^{-1} S_j^T \cdot W \cdot r_j$$

The above equation can then be explicitly written as

$$\theta_j = \theta_{j0} + \left(S_j^T \cdot S_j\right)^{-1} S \cdot_j^T r_j$$

or

$$\theta_j = \theta_{j0} + \left(S_j^T \cdot W \cdot S_j\right)^{-1} S_j^T \cdot W \cdot r_j$$

3.6.2.2 Objective Function

The objective function contains the discrepancies between analytical predictions and experimental observations which are to be minimized by the updating process. For inverse eigensensitivity method, typical data used to form the objective function are the modal properties extracted from recorded test data, such as frequencies, mode shapes, MAC values and combinations of these modal properties such as modal curvature, modal strain energy, modal flexibility and etc.

The functional relationship between the measured and the initial analytical eigen-properties can be approximated by a first-order Taylor series expansion with respect to the structural parameters:

$$r_j = S_j \cdot \delta\theta_j$$

where r_j, S_j and $\delta\theta_j$ are the same as defined as in previous section and they denote the residual at linearization point, sensitivity matrix and the adjustment of parameter vector respectively.

The above inverse problem can be equivalently solved by minimizing a least-squared error function with the form of

$$\min_{\theta} \left\| r_j - S_j \cdot \delta\theta_j \right\|^2$$

i.e. $J_1 = \left(r_j - S_j \cdot \delta\theta_j\right)^T W_E \left(r_j - S_j \cdot \delta\theta_j\right)$

where W_E is the positive-definite weighting matrix, reflecting the relative confidence in the accuracy of various measured modes.

When the number of structural parameters to be updated is greater than that of the measured modal properties (reference responses, or state variables), the inverse problem can be re-constructed as a constrained optimization problem taking the form of

$$\min \quad J_2 = \delta\theta_j^{\,T} \cdot W_\theta \cdot \delta\theta_j$$

$$\textit{subject} \quad \textit{to} \quad S_j \cdot \delta\theta_j = r_j$$

By adjusting the element of this weighting matrix, it is possible to limit the perturbation of these structural parameters separately so that it can be better reflect the fact that some parameters might be more precisely known than the others. Mathematically, the optimal solution from this constrained optimization problem gives the smallest weighted norm of the parameter perturbation.

Combining the two objective function can lead to a new one if the two weighting matrices are properly chosen.

$$J_3 = \delta\theta_j^{\,T} \cdot W_\theta \cdot \delta\theta_j + \left(S_j \cdot \delta\theta_j - r_j\right)^T W_E \left(S_j \cdot \delta\theta_j - r_j\right)$$

The first term in the new objective function acts not only as a regulator to eliminate the possible ill-conditioning associated with the second term but also as a perturbation monitor to provide proper constraints to the updated parameters.

The condition of the sensitivity matrix S_j plays an important role in the accuracy and uniqueness of the solution. In order to obtain meaningful updating results, the number of measurements is required no less than the number parameters. This will lead to over-determined equation system and unique results can be achieved. In engineering practice, the number of measurements is often confined by the available instrumentation, the scale of the structure and etc. It is recommended to reduce the number of updating parameters to retain only the most erroneous and sensitive ones. The inevitable noise in the measured data is another cause of ill-conditioning of sensitivity matrix. The deficient rank of sensitivity matrix usually leads to the divergence of optimization process.

In order to improve the numerical conditioning of the updating procedure, the weighted objective function is sometimes extended with the requirement that the parameter changes

$\delta\theta$ shall be kept small. Besides the norm of the weighted modal data residuals, a weighted norm of the changes in the updating terms is included in a new objective function. When $W_\theta = 0$, the new objective function represent the standard weighted least squares formulation. Otherwise, the solution to minimize the new objective function is affected by the choice of weighting matrix. If the W_θ is too small, the problem will still be close to the original ill-posed problem and the optimization process will be highly oscillatory due to noise amplification; if W_θ is set too large the solution will be too smooth and have little relation to the original problem.

Equivalently the above expression can be written in the form of norms of the residual vector and parameter vector,

$$J_4 = \frac{1}{2}\left\| r_j + S_j \cdot \delta\theta_j \right\|^2 + \beta \left\| B \cdot \delta\theta_j \right\|$$

where β is the regulation parameter and *B* is a user defined weighting matrix for the updating variables. The second term represents the perturbation in the design variables and relaxes the strict least squares criterion in favor of a nearby solution. This approach corresponds to the regulation techniques which originally developed in linear algebra to solve ill-conditioned systems of equations and was introduced by Tikhonov with Tikhonov regulation. The difficulty of this class of techniques is to choose a proper regularization parameter β such that it yields a suitable balance between the residual norm and the perturbation norm. If β is too small, the problem will be too close to the original ill-posed problem and the solution process will be highly oscillatory due to noise amplification; if β is too large then the solution will be too smooth and have little connection with the original problem.

The existing methods to determine the regulation parameter can usually be classified according to the availability of the measurement noise. However, this class of objective functions is a little bit cumbersome to manipulate and are lack of physical meaning. Teughels (2003)

proposed a damage function approach in order to provide an effective, physically meaningful tool for condition improvement.

3.6.2.3 Sensitivity Matrix

Since the minimization process is formulated in an iterative way, the sensitivity matrix (or the Jacobian matrix) needs to be calculated in each iteration. The matrix containing the first-order derivative of each element of the residual vector with respect to each updating parameter can be expressed as

$$S_j = \begin{bmatrix} \vdots & \\ \cdots & \dfrac{\partial r_j}{\partial \theta_i} \quad \cdots \\ \vdots & \end{bmatrix}_{m \times n}$$

in which m is the total number of residual terms and n is the number of updating parameters.

For modal data (eigenvalues and modal vectors), the methods for calculating eigen-derivatives include the modal method, Nelson's method and an improved modal method. The modal method is straightforward in theory but requires all the modes of system which is sometimes computationally expensive especially when systems with large dimensions are considered. Nelson's method attempts to calculate the eigen-derivatives of the rth mode by just using the modal parameters of that mode but matrix inverse of the system dimension (in fact of dimension N-1)is required for each mode in order to solve the linear algebraic equations involved.

Fox and Kapoor (1968) first proposed the close-formed solution to first-order derivatives of eigenvalue and eigen-vectors and the derivation was based on an undamped eigenvalue system. The derivation was outlined as follows. Assuming that no damping is considered, a vibration system in modal space can be expressed as:

$$K\phi_i - \lambda_i M\phi_i = 0$$

Differentiating the system eigen-equation with respect to the rth updating parameter θ_r,

$$\left(K-\lambda_i M\right)\frac{\partial \phi_i}{\partial \theta_r}+\left(\frac{\partial K}{\partial \theta_r}-\lambda_i \cdot \frac{\partial M}{\partial \theta_r}-\frac{\partial \lambda_i}{\partial \theta_r}\cdot M\right)\cdot \phi_i = 0$$

Assume that ϕ_i is normalized such that

$$\phi_i^T \cdot M \cdot \phi_i = 1$$

Multiply both sides by ϕ_i^T

$$\phi_i^T \cdot \left(K-\lambda_i M\right)\cdot \frac{\partial \phi_i}{\partial \theta_r}+\phi_i^T \cdot \left(\frac{\partial K}{\partial \theta_r}-\lambda_i \cdot \frac{\partial M}{\partial \theta_r}-\frac{\partial \lambda_i}{\partial \theta_r}\cdot M\right)\cdot \phi_i = 0$$

Because the first term of the equation is equal to zero and the orthogonality condition for mass matrix,

$$\phi_i^T \cdot \frac{\partial K}{\partial \theta_r}\cdot \phi_i - \phi_i^T \cdot \lambda_i \cdot \frac{\partial M}{\partial \theta_r}\cdot \phi_i - \frac{\partial \lambda_i}{\partial \theta_r} = 0$$

$$\frac{\partial \lambda_i}{\partial \theta_r} = \phi_i^T \cdot \left(\frac{\partial K}{\partial \theta_r}-\lambda_i \cdot \frac{\partial M}{\partial \theta_r}\right)\cdot \phi_i$$

The sensitivity of each mode shape vector with respect to updating parameter θ_r is sought as a linear combination of the mode shape vectors themselves.

$$\frac{\partial \phi_i}{\partial \theta_r} = \sum_{k=1}^{N} \beta_{ik}\phi_k$$

In order to calculate the coefficients β_{ij}, substitute the above equation into equation,

$$\phi_j^T \cdot \left(K-\lambda_i M\right)\cdot \sum_{k=1}^{N} \beta_{ik}\phi_k + \phi_j^T \cdot \left(\frac{\partial K}{\partial \theta_r}-\lambda_i \cdot \frac{\partial M}{\partial \theta_r}-\frac{\partial \lambda_i}{\partial \theta_r}\cdot M\right)\cdot \phi_i = 0$$

In the case $j \neq i$

$$\left(\lambda_j - \lambda_i\right)\beta_{ij} + \phi_j^T \cdot \left(\frac{\partial K}{\partial \theta_r} - \lambda_i \cdot \frac{\partial M}{\partial \theta_r}\right) \cdot \phi_i = 0$$

$$\beta_{ij} = \frac{\phi_j^T \cdot \left(\frac{\partial K}{\partial \theta_r} - \lambda_i \cdot \frac{\partial M}{\partial \theta_r}\right) \cdot \phi_i}{\lambda_i - \lambda_j}$$

When $j = i$, β_{ii} can be computed from the mass-normalization condition.

$$\phi_i^T \cdot \frac{\partial M}{\partial \theta_r} \cdot \phi_i + 2\phi_i^T \cdot M \cdot \frac{\partial \phi_i}{\partial \theta_r} = 0$$

Substituting

$$\beta_{ii} = -\frac{1}{2}\phi_i^T \cdot \frac{\partial M}{\partial \theta_r} \cdot \phi_i$$

Therefore the final expression for sensitivity of mode shape vector with respect to the updating parameter is

$$\frac{\partial \phi_i}{\partial \theta_r} = \sum_{j=1; j\neq i}^{N} \left(\frac{\phi_j^T \cdot \left(\frac{\partial K}{\partial \theta_r} - \lambda_i \cdot \frac{\partial M}{\partial \theta_r}\right) \cdot \phi_i}{\lambda_i - \lambda_j} \right) \cdot \phi_j - \frac{1}{2}\phi_i^T \cdot \frac{\partial M}{\partial \theta_r} \cdot \phi_i \cdot \phi_i$$

A truncated modal basis is often used in practice, which means that the summation in the equation extends to the number of modes available. This formula of the mode shape sensitivity provides a way to calculate the sensitivity analytically, avoiding the need to compute it with finite differences.

3.6.2.4 Numerical Optimization

The numerical optimization techniques are the core part of model updating and they are utilized to minimize the discrepancy between analytical and measured data. Teughels (2003) summarized existing local and global optimization methods with a particular focus on the ones for the least squares problem because the objective functions of inverse eigensensitivity algorithms are often in a form of the norm of residual vector. A brief review of commonly used local and global optimization methods are given below.

The local optimization methods generally start from one initial point and move toward to minimum point iteratively. The optimization procedure is often involved with the derivatives of the objective function. Typical method includes Newton method, quasi-Newton method, sequential quadratic programming and etc. the line search and trust region strategy are available in order to enhance convergence. For least squares problems, specific algorithms such as the Guass-Newton method and Levenberg-Marquardt have been developed based on the general local optimization methods, assuming that the Hessian can be approximated by the first-order derivative information only. The local optimization methods usually are effective and have a fast convergence but they may be trapped in a local minimum.

As opposed to the local methods, the global optimization approaches are generally more robust and more likely to converge to the global minimum. Global methods such as genetic algorithm (GA) and simulated annealing (SA) and etc usually require a large number of function evaluations because they are based on probabilistic searching without the use of gradient information. A recently proposed global optimization method is coupled local minimizations (CLM), which simultaneously uses multiple local optimization runs to find the global minimum. Since the CLM is based on the function derivatives, a relative fast convergence is maintained.

3.6.2.5 Response Function Method

The formulation of response function method is very similar to that of the inverse eigensensitivity method. For response function method, however, the residual vector is comprised of the difference between measured FRFs and their analytical counterparts. The basic equation for response function method can be expressed as

$$\delta H = R \cdot \delta\theta$$

where δH denotes the residual vector between measured FRFs and their analytical counterparts. R represents a matrix containing FRF data derived from the measured data set and from theoretical predictions and $\delta\theta$ is a vector of updating parameters. Again a number of variations exist for this method. The main features of response function method are as follows:

(1) There are large number of data available, compared with modal data;

(2) The characteristics of the damping of the system are automatically included;

(3) No test-analysis correlation is required ahead of updating;

(4) Information about higher modes is also included.

3.7 Conclusions

This chapter reviewed some essential preparatory updating procedures such as correlation analysis, error localization index, sensitivity analysis and test data informativeness quantification. In the meanwhile, an overview on the basics of finite element model updating was also covered.

It became obvious that correlation analysis, sensitivity analysis and error localization were actually intertwined with each other to provide insight on the similarity and difference between test and analysis as well as possible causes to the test-analysis difference. The informativeness of test data was a recently developed concept which reminded us that poor performance of model updating could be attributed to the limited information contained in the test data. The main

components of the inverse eigensensitivity method were also discussed in this chapter and its application would be demonstrated in the following chapter.

4 Cantilever Study

4.1 Introduction

The discussion in Chapter 2 manifests the uncertainties entailed in integrative paradigm of Sys-Id may arise from a good number of sources. The idealization process of a constructed structure is often governed by challenging conceptualization errors with epistemic mechanism, due to size, complexity and a lack of observability at especially soil-foundation as well as sub-and-super-structure interfaces, and the magnitude and nonstationarity of intrinsic forces of different components of the system. Existing model updating algorithms, through modifying a selected set of parameters either in direct method or iterative method, can only eliminate the test-analysis discrepancy caused by parameter errors. They are generally incapable of recognizing and mitigating any conceptualization error embedded in initial FE model, if this type of modeling error can not be properly parameterized and incorporated in the updating process, for instance, the uncertainty which stems from the selection of a particular model for a physical process.

Sanayei et al (2001) approached this problem by presenting modeling errors with uncertain parameters which are assumed known and not to be estimated in the updating procedure. The rest of model parameters are either unknown parameter to be estimated or known parameters assumed to be accurate. Through numerical simulations, the writers are able to investigate the influence of modeling errors with respect to excitation and measurement type and locations, type of error function and the location of uncertain parameters and etc through numerical simulations. However, the problem how to recognize and mitigate of modeling error remain unsolved. Chen and Ewins (2004) proposed a vector projection method to check the existence of idealization errors in nominal models. The successful applications of the proposed approach on numerical examples and an aero-engine component demonstrated some promises to be utilized on constructed systems. However, large difference of analytical and measurement degrees of freedom in the cases of civil engineering applications may disable its capability to correctly

localize the conceptualization modeling errors, since it is often impractical to instrument a long-span bridge or a high-rise building with a dense array of transducers.

One of the main objectives of this chapter is hence to investigate the impact of modeling uncertainty with epistemic mechanism introduced during the model creation of constructed systems to the reliability of the identification results, by taking advantage of a cantilever beam system in the DI3 lab. Solutions to recognize and mitigate them are to be examined as well. The idea to use a cantilever beam is justified by the fact that the physical simplicity in dynamic behaviors of cantilever beam will render the effects of modeling and experimental uncertainty transparent. The theory behind the dynamics of cantilever beams has been well established since the 1960s (Timoshenko 1960?) and this knowledge will serve as a baseline to guide analytical simulation, test design and execution as well as uncertainty investigation. Any deviation of the simulated or observed structural properties from their baseline values may indicate that some uncertainty mechanisms, either in modeling or experimentation, have not properly acknowledged yet.

Additionally, lab experimental conditions are usually much advantageous than field testing. Experimental uncertainty with random sources such as environmental noise, although will never be completely eliminated, can be effectively deactivated. Systematic experimental errors induced by fluctuation of temperature and/or change of humidity can be excluded. Careful calibration of data acquisition and sensor system will eliminate any blatant errors such as sensor positioning and wrong cabling. The resulting high signal-to-noise ratio test data will then make it possible to isolate modeling uncertainty in the system identification, which is the main interest of this research.

The only concern may then be whether a simple cantilever beam is adequately representative to the intrinsically complicated large-scale constructed systems such as long-span bridges and high-rise buildings. It is clear that conceptualization errors with epistemic mechanism may

originate from various sources and can appear in different forms, and many of them are highly structure specific. Hence it is neither possible nor necessary to simulate all of them experimentally (Actually even ‘simulating epistemic uncertainty’ may be inappropriate because the epistemic uncertainty is defined to describe uncertainty that arise due to the lack of information). The test specimen set up in two configurations – one to approximate ideally fixed boundary condition with clamps and hydrostone and the other to simulate partial flexibility with a designed boundary assembly which inevitably introduces more ambiguity to the whole system – provides a platform not only to evaluate the impact of epistemic modeling errors but also to discover feasible approaches to recognize and mitigate them. The attained understanding will benefit more widespread utilization of Sys-Id in the near future.

4.2 Initial Modeling of Cantilever Beam

4.2.1 Description of Test Specimen

The test specimen used for this study is a steel beam with a thin-walled rectangular tube section 3x1.5x1/8 in. The beam was oriented on a steel pedestal so that it has a clear length of 117.5 inches and would bend about its weak-axis direction. The pedestal is made of I-shape column and a cover plate. The relevant material and section properties for the beam are listed in the following table.

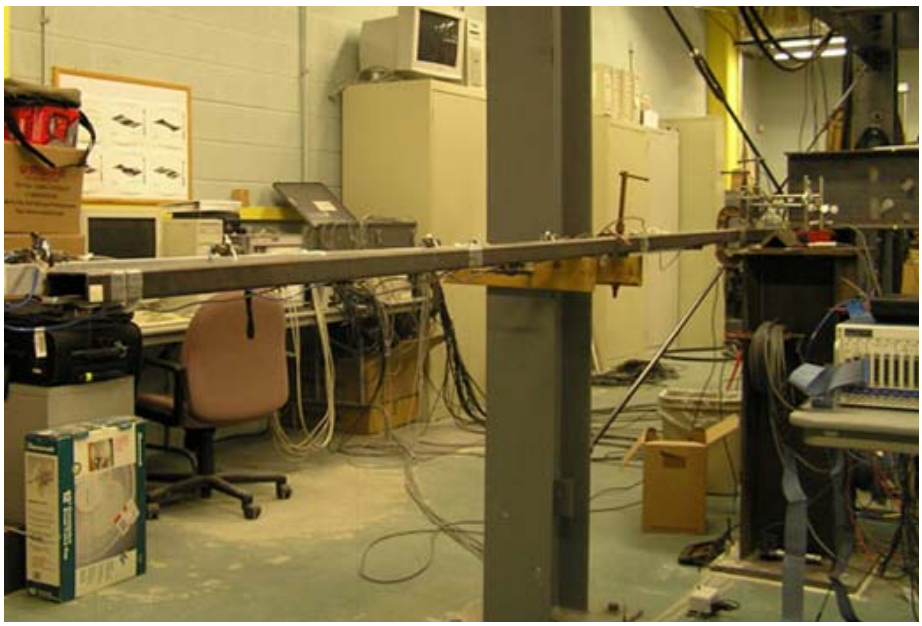

Figure 4-1the beam specimen in DI^3 Lab

Table 4-1 Mechanical and material properties of the beam

Property	Value
Density ρ	0.284 lb-f/in^3
Young's Modulus E	29x10^6 lb-f/in^2
Cross Section Area A	0.954 in^2
Moment of Inertia I about weak axis	0.355 in^4

4.2.2 Theoretical Solution to the Cantilever Beam

The theoretical dynamic properties of the beam were determined ahead of modal test to assist the experimentation design. The first five frequencies and mode shapes were calculated based on the theory of continuous systems. This information was utilized not only to guide the experimental program, but also to serve as a consistent baseline for future comparisons between test and finite element analysis.

Several assumptions were made prior to formulating the theoretical solution of the beam system:

(1) The boundary condition between the beam and pedestal is close to ideally fixed support;

(2) The mass contribution of the installed accelerometers was not taken into account because it is negligible relative to the self weight of the beam;

(3) Due to the small ratio of the beam depth and span length, the effects of shear deformation and rotational inertia are excluded from the analysis;

(4) Damping ratio of the steel structure is usually under 2% and its effect is not considered at this point.

With the assumptions mentioned above, the governing equations of motion for an Euler-Bernoulli beam system under free vibration can be expressed as

$$m(x)\frac{\partial^2 u}{\partial t^2}+\frac{\partial^2}{\partial x^2}\left[EI(x)\frac{\partial^2 u}{\partial x^2}\right]=0 \tag{4.1}$$

Assuming the solution has a form of

$$u(x,t)=\phi(x)q(t) \tag{4.2}$$

the above governing equation can be written as

$$m(x)\phi(x)\ddot{q}(t)+q(t)\left[EI(x)\phi''(x)\right]''=0 \tag{4.3}$$

Separating the two variables in the above partial differential equation will lend to two ordinary different equations

$$\ddot{q}(t)+\omega^2 q(t)=0 \tag{4.4}$$

$$\left[EI(x)\phi''(x)\right]''-\omega^2 m(x)\phi(x)=0 \tag{4.5}$$

One governing the time function $q(t)$ which has the same form as the equation governing free vibration of an SDF system with natural frequency ω, and the other equation defines the eigenvalue problem together with the boundary conditions of the beam.

For a beam with uniform mass and stiffness is (Chopra 1995), the second equation can be simplified as

$$\frac{d^4\phi(x)}{dx^4} - \beta^4\phi(x) = 0 \tag{4.6}$$

where

$$\beta^4 = \frac{\omega^2 m}{EI} \tag{4.7}$$

and m = mass per unit length, ω = natural frequency (rad/s), E = Young's modulus and I = moment of inertia of the beam cross section.

The general solution of the aforementioned partial differential equation can be expressed as

$$\phi(x) = C_1 \sin\beta x + C_2 \cos\beta x + C_3 \sinh\beta x + C_4 \cosh\beta x \tag{4.8}$$

where C1, C2, C3 and C4 are four constants to be determined.

In the case of a cantilever beam, the known boundary conditions at the fixed support and the free end can provide the following four extra equations,

$$\begin{cases} \phi(x) = 0 \\ \dfrac{d\phi(x)}{dx} = 0 \end{cases} \quad \text{when x = 0} \tag{4.9}$$

$$\begin{cases} EI\dfrac{d^2\phi(x)}{dx^2} = 0 \\ EI\dfrac{d^3\phi(x)}{dx} = 0 \end{cases} \quad \text{when x = L, L = the length of the beam} \tag{4.10}$$

Substituting the general solution into the boundary condition equations, the following equations can be obtained,

$$C_4 = -C_2 \tag{4.11}$$

$$C_3 = -C_1 \tag{4.12}$$

$$C_1(\sin\beta L + \sinh\beta L) + C_2(\cos\beta L + \cosh\beta L) = 0 \tag{4.13}$$

$$C_1(\cos\beta L + \cosh\beta L) + C_2(-\sin\beta L + \sinh\beta L) = 0 \tag{4.14}$$

Equations (1.8) and (1.9) can be further transformed into a matrix form,

$$\begin{bmatrix} \sin\beta L + \sinh\beta L & \cos\beta L + \cosh\beta L \\ \cos\beta L + \cosh\beta L & -\sin\beta L + \sinh\beta L \end{bmatrix} \begin{bmatrix} C_1 \\ C_2 \end{bmatrix} = \begin{bmatrix} 0 \\ 0 \end{bmatrix} \tag{4.15}$$

For a non-trivial solution, the determinate of the coefficient matrix must be zero. This leads to

$$1 + \cos\beta L \cdot \cosh\beta L = 0 \tag{4.16}$$

The numerical solutions which satisfy the equation (1.9) are as follows:

$$\beta_n L = 1.8751,\ 4.6941,\ 7.8548,\ \text{and } 10.9960,\ \text{for n =1, 2, 3, 4 respectively} \tag{4.17}$$

$$\beta_n L \approx (2n-1)\frac{\pi}{2},\ \text{for}\ n \geq 5 \tag{4.18}$$

And then by substituting equations (4.17) and (4.18) into equation (4.7), the first five natural frequencies of a cantilever beam with uniform mass and stiffness distribution can be obtained.

$$\omega_n = \frac{(\beta_n L)^2}{L^2}\sqrt{\frac{EI}{m}}, n = 1,2,3\ldots \tag{4.19}$$

The expression (4.20) of mode shape corresponding to each natural frequency can also be developed by combining equations (4.8) and (4.11) – (4.14).

$$\phi_n(x) = C_1\left[\cosh\beta_n x - \cos\beta_n x - \frac{\cosh\beta_n L + \cos\beta_n L}{\sinh\beta_n L + \sin\beta_n L}(\sinh\beta_n x - \sin\beta_n x)\right] \tag{4.20}$$

If ideal fixed support can be achieved, the two spans of the beam will vibrate as two independent cantilevers. As indicated in equation (4.19), the natural frequency of each mode is proportional to the inverse of the squares of the length of the cantilever beam. Therefore the first six natural frequencies for the 117.5 in span and the first two for the 28 in span were computed and the results were summarized in Table 4-2.

Table 4-2 Theoretical natural frequencies for the beam

Mode #	Vertical Mode Frequency (Hz)	Lateral Mode Frequency (Hz)
1	4.9099	8.481
2	30.7699	53.147
3	86.1571	148.813
4	168.8459	291.613
5	279.0910	482.055
6	416.9174	

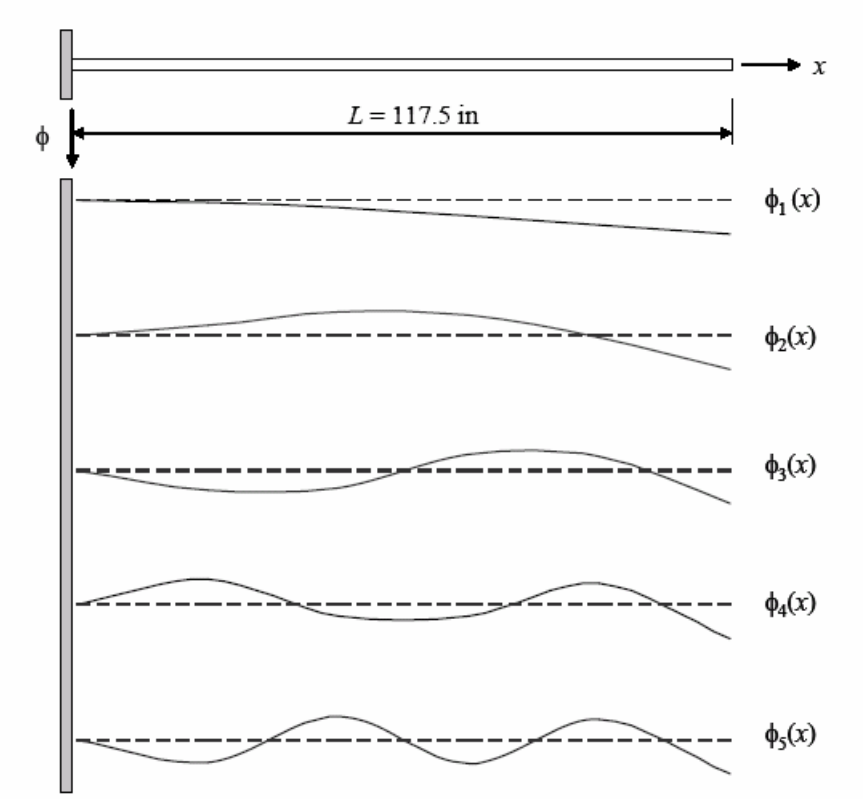

Figure 4-2 Theoretical mode shapes for the beam

4.2.3 Initial Finite Element Modeling of Cantilever Beam

A preliminary modal analysis was conducted using a commercial program SAP2000 with beam elements. The purpose is to find an optimal mesh size which not only yields a converged eigen-solution in the frequency band of interest but also keeps the size the model as small as possible. Models with five different mesh scales were examined one by one. The model with mesh scale 1 had the coarsest mesh size and the whole span of the beam was represented with 5

elements. As the mesh scale increased, the number of beam elements used was doubled. In the model with mesh scale 5, a total of 80 beam elements were utilized to simulate the beam.

Although the first two frequencies predicted by the model with mesh scale 1 were quite close to the closed-form solution, the fifth frequency differed by 25% from its theoretical counterpart. It was also observed that even the frequencies predicted by the finest mesh (mesh scale 5) didn't line up exactly with the theoretical results. Part of the discrepancy could be attributed to the fact that SAP2000 formulates the mass matrix by assuming the mass was lumped at each beam joint.

The vibration shapes of the first and fifth mode from the initial model were displayed in Figure 4-3 and Figure 4-4. Although the FE models with five mesh scales yielded almost exact the same mode shape for the first mode, the fifth mode shape from mesh scale 1 dramatically deviated from the others. The models with mesh scales 3 through 5 produced very close vibration shape for the fifth mode.

The convergence test illustrated that the model with mesh scale 3 was able to yield reasonably good eigenvalues and eigenvectors with a relatively small number of elements. For the following study, an initial FE model with 20 elements was constructed in Matlab to simulate the cantilever beam. Consistent mass was used instead of lumped mass.

Table 4-3 Frequency summary from FE model with different mesh scale

Mode No.	Theory	Mesh Scale 1 (5 elements)	Mesh Scale 2 (10 elements)	Mesh Scale 3 (20 elements)	Mesh Scale 4 (40 elements)	Mesh Scale 5 (80 elements)
1	4.9099	4.8174	4.8833	4.9001	4.9043	4.9054
2	30.7699	28.8560	30.1840	30.5410	30.6320	30.6540
3	86.1571	77.5130	83.3110	84.9340	85.3500	85.4540
4	168.8459	143.5000	160.5000	164.9700	166.1100	166.4000
5	279.0910	208.3200	259.9600	269.7600	272.2300	272.8500

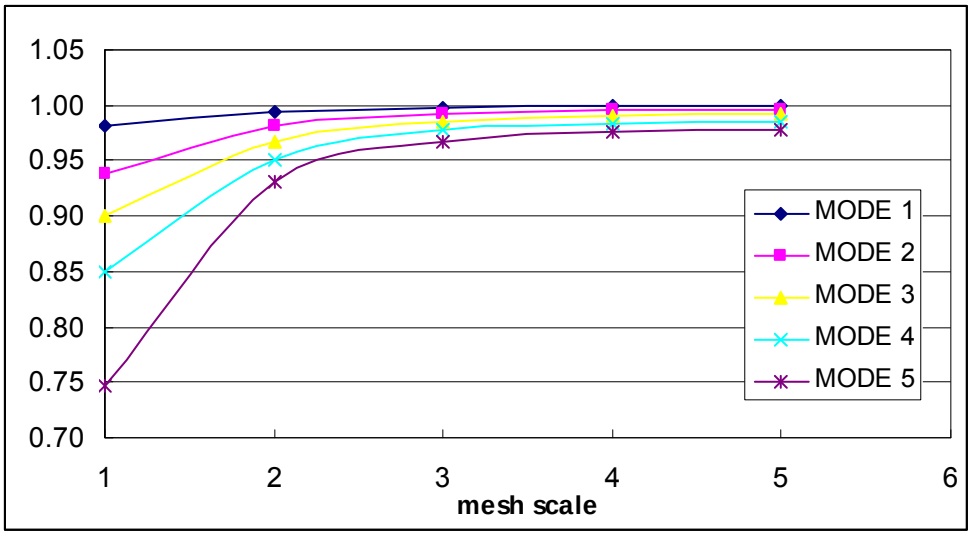

Figure 4-3 Grid Convergence Test

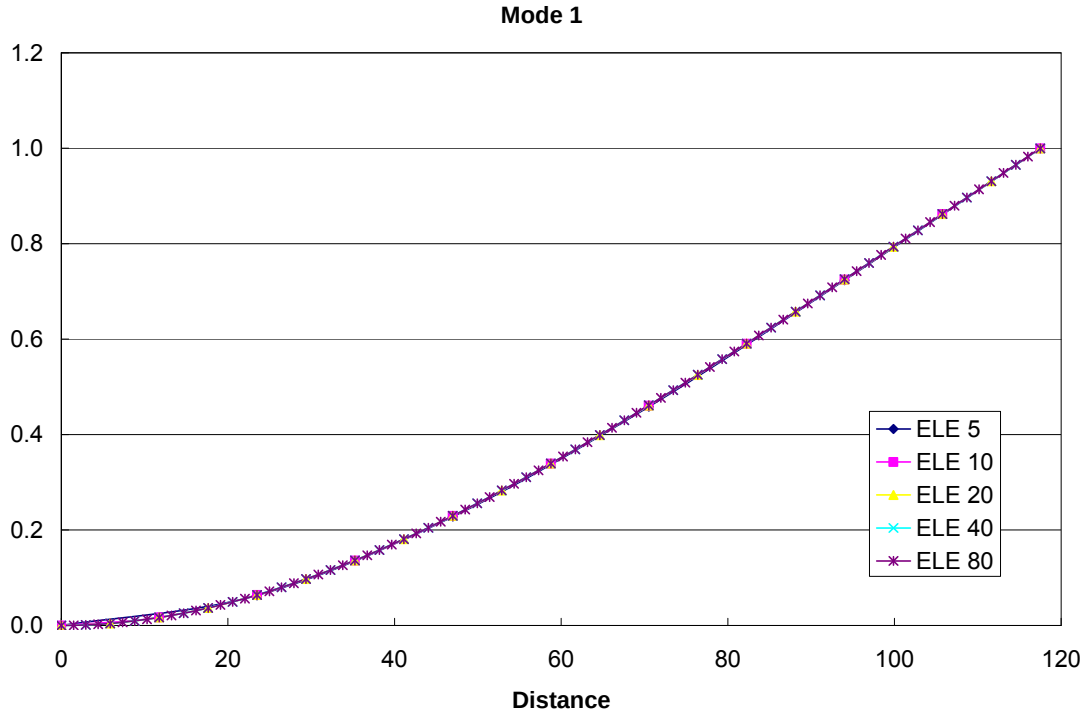

Figure 4-4 the First mode shape

4.2.4 Simulation of Impact Test on Cantilever Beam

An impact test on the cantilever beam was simulated with Duhamel's integral. Assume that five input-output stations were equally spaced along the beam, as shown in Figure 4-5. When an impulse was applied at station 1, theoretically the energy would spread over an infinite broad

band of frequency and all resonant modes of the structure would be excited. And the impulse responses predicted at each output station would be attributed to the summation of all resonant modes. If only considering the first five modes, the contribution of each mode to the responses at points 1 through 5 could be simulated as follows (Figure 4-6). The frequency domain counterpart of the impulse response functions, i.e., frequency response functions (FRF) would be as shown in Figure 4-7.

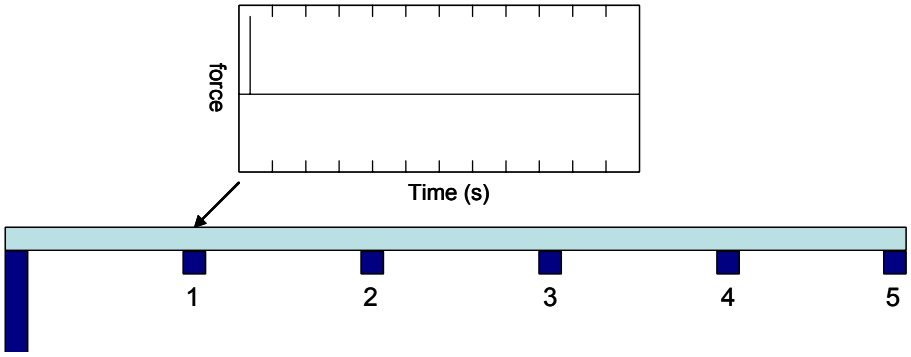

Figure 4-5 Simulation of impact test on cantilever beam

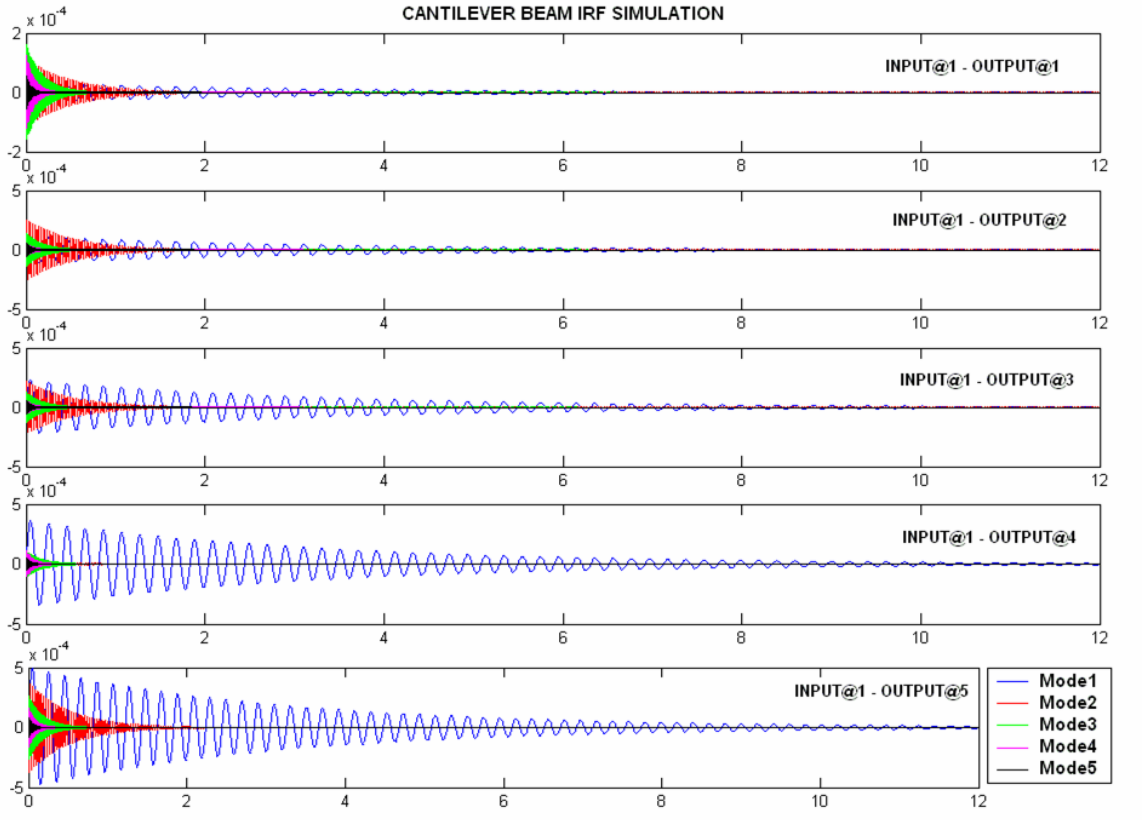

Figure 4-6 Contribution of each mode to the impulse response function at each measurement dof

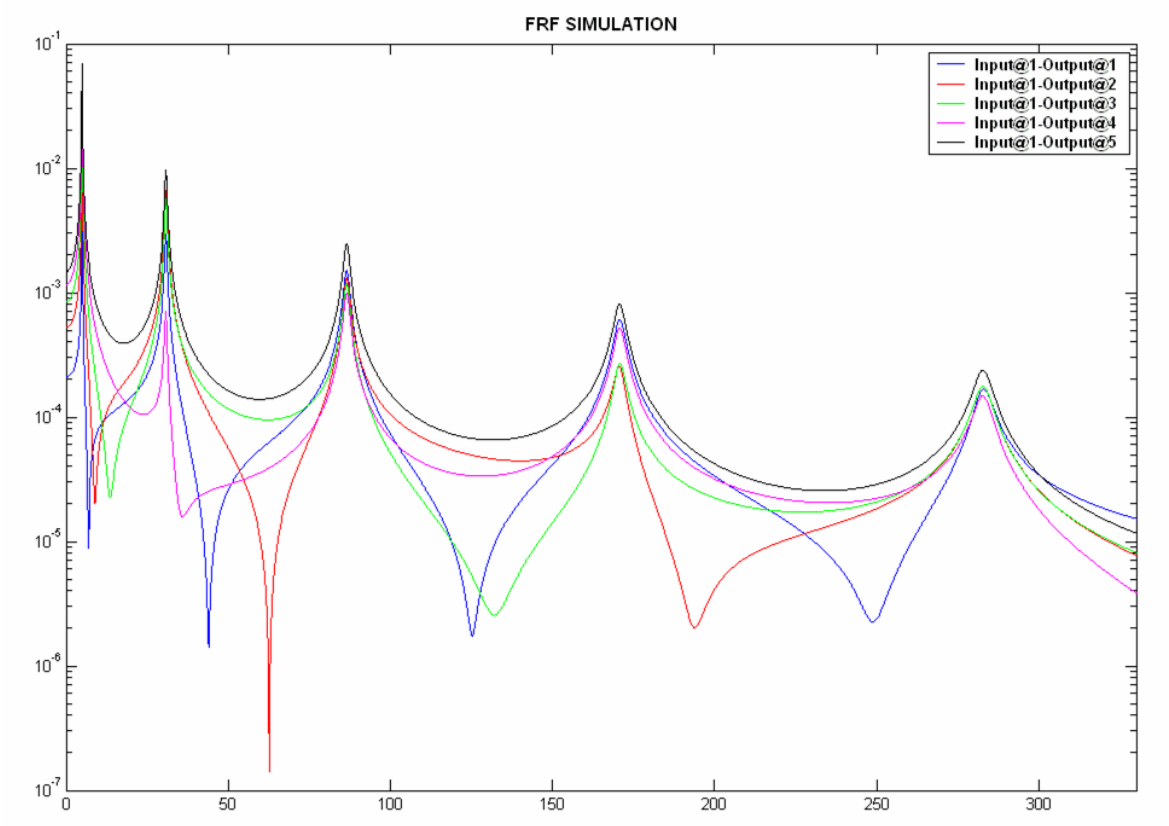

Figure 4-7 Frequency response function at each measurement dof when input at station 1

4.3 Experiments on the Test Specimen

In the DI3 laboratory, the test specimen was oriented on a steel pedestal so that it would bend about its weak axis under vertical loads. An advantage of this orientation was that quite a few modes will be present within a measurable frequency interval, e.g. 0-800 Hz. Although the existing data acquisition system was capable of recording dynamic signals over 1000 Hz, the demands on the measurement duration, data storage and processing would increased with the sampling frequency, for a reasonably good quality and resolution in the following modal estimation. Besides, the basic frequency band for most real-life civil engineering structures like bridges was usually below 100 Hz. The clear length of the beam is 117.5 inches, which prevent significant deformation under its self-weight. Additionally, the different dimension in height and width of the beam avoid unnecessary coupling effect between horizontal and vertical bending modes.

Earlier test programs in the DI3 Lab revealed the difficulty of obtaining ideal conditions for dynamic test: ambient vibration interferes with the artificial force input (vibrations caused by passing trains); finite rigidity of supports can affect frequencies and mode shapes; excitation from shaker located at the base of the support would induce inference from the vibrations of the floor system. In order to avoid aforementioned situations, the beam was set up a very stiff steel pedestal support and impact test scheme was implemented instead of ambient vibration test and shaker test.

The same beam is set up with two test configurations. The first configuration is aimed to approximate fixed support condition while the second one allows partial rotation at the support and therefore introduce more complexity and uncertainty in the whole system.

4.3.1 Test Setup

4.3.1.1 Configuration 1: Approximately Fixed Condition

In this configuration, the beam was clamped on the pedestal with five C-clamps and the fixity was improved by a layer of hydro-stone between the pedestal and the beam, thereby approximating ideally fixed boundary. The beam setup is illustrated in Figure 4-8 with the support condition at the boundary shown in Figure 4-9.

Figure 4-8 Test beam setup 1 with fixed support

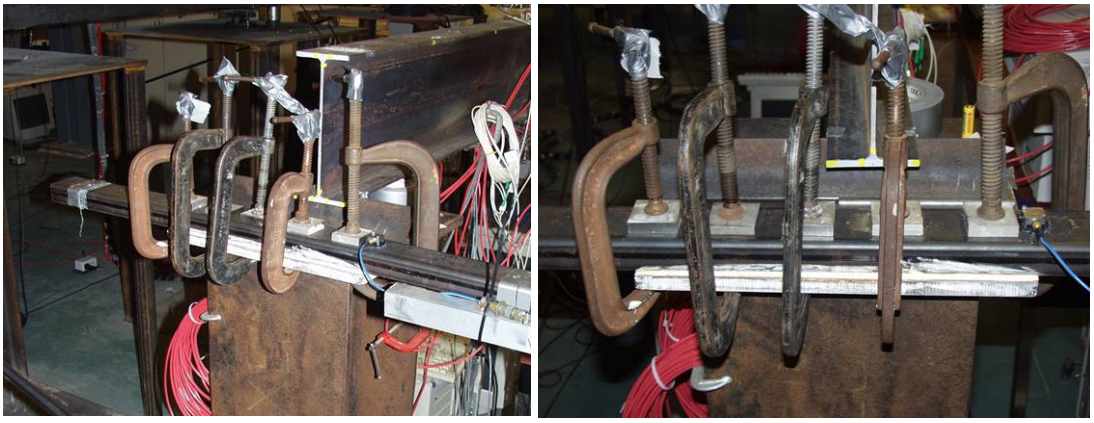

Figure 4-9 Boundary condition of test configuration 1

4.3.1.2 Configuration 2: Boundary Assembly Allowing Partial Rotation

In the second configuration, the beam is mounted on the knife edge of a stiff steel angle member, which is secured at the center of the pedestal, with a carefully designed boundary assembly (see Figures 4.10 through 4.12). The assembly was comprised of four 4-inch long aluminum angle parts with a cross section as 4x4x1/2in, two 24-inch long 3x3/4in steel plates and four high-strength steel rods with a diameter of 3/8 inch. The two steel plates perpendicularly sit

on the top of the beam, crossing over it with a distance of 4 inch between their center line and the beam support. Each end of the plates is respectively connected through the steel rod with one leg of the alumni angle. The assembly is then fixed to the flanges of I-shape columns of the pedestal through the other leg of the angle by C-clamps. The vertical distance between the angles and the top plates were kept as small as possible in order to prevent any instability of the rods due to their slenderness. When the beam tended to bend, the top plates would restrain its rotation by deforming themselves. In the meanwhile, the rods would experience compression or tension and the overhang leg of each of the angles would also bend. The relative smaller value of the Young's modulus of alumni provides partial flexibility of the support. The connection between the rod and angles and plates were achieved by high-strength steel nuts and washers. The composite assembly was oriented such that it was symmetric about the centerline of the beam in horizontal plane. Therefore any torsion mode of the whole structure would not be excited by vertical impacts on the beam.

The beam was tightened down to the pedestal by pre-stressing the assembly. A thin layer of hydro-stone was applied between the steel plates and the top surface of the beam and this would help to eliminate any possible relative movement between them. The complexity of the composite assembly unavoidably introduced some ambiguities at the beam support and therefore made the boundary conditions in configuration 2 not as well defined as the previous one. This somehow represents a similar level of uncertainty which may be encountered in real-life applications.

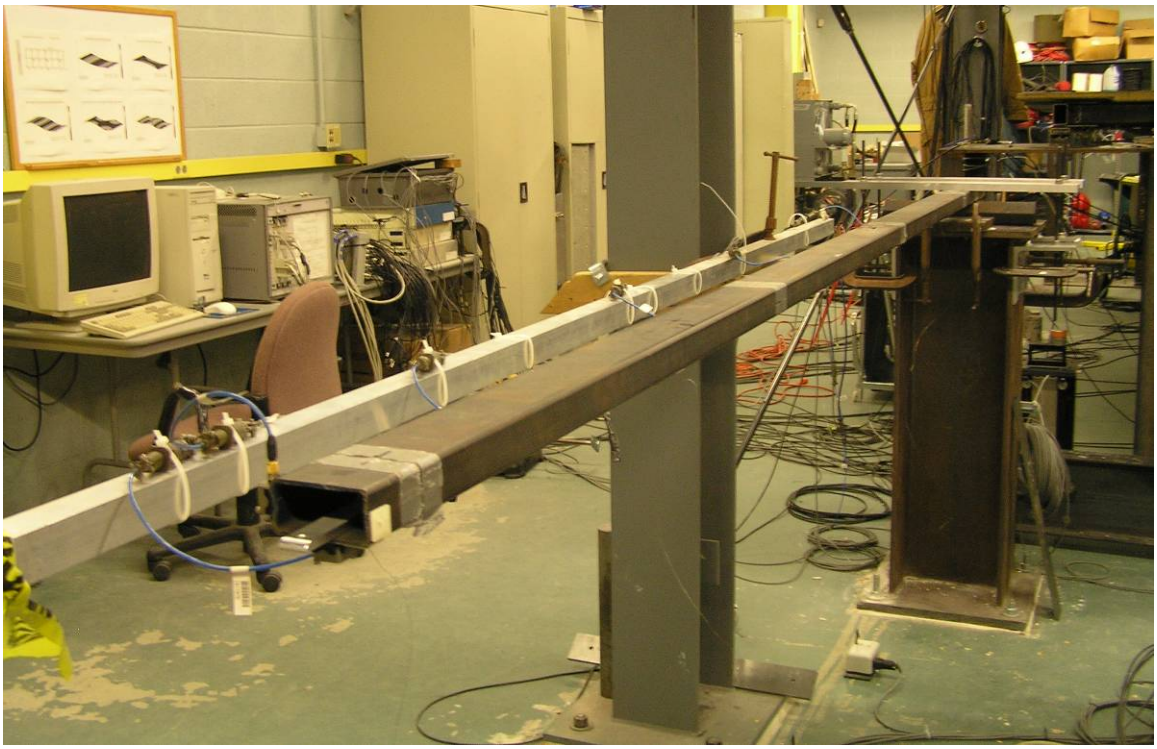

Figure 4-10 Beam with boundary assembly

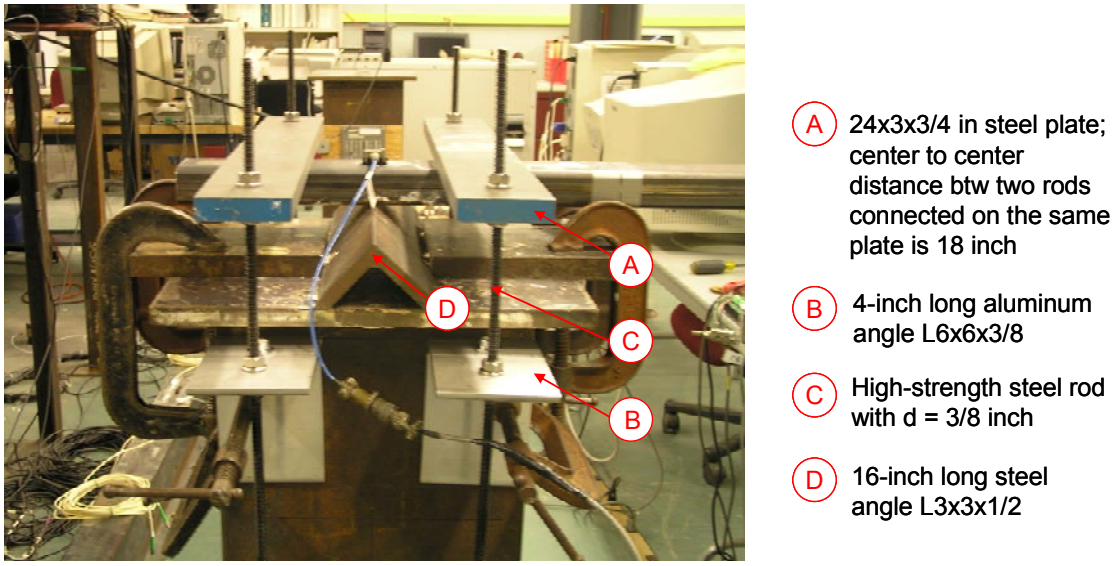

Figure 4-11 Components of the boundary assembly

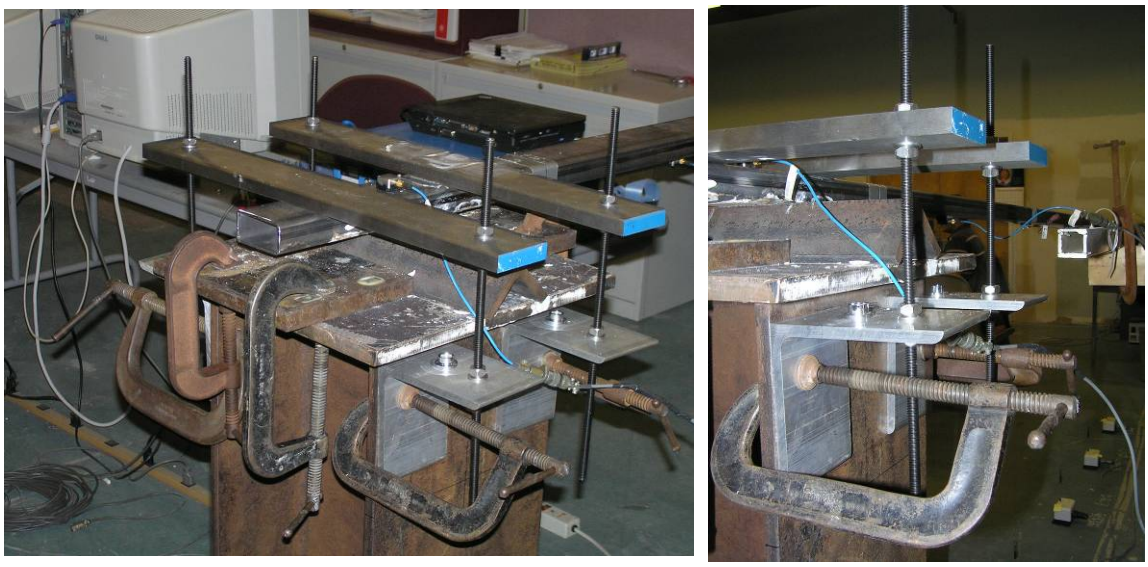

Figure 4-12 Details of the boundary assembly

4.3.2 Impact Test

The test specimen was instrumented with six uniaxial capacitive accelerometers (Model 3701G3FA3G from PCB Piezoelectronics Inc., as shown in Figure 4-13). This model of accelerometer has a measurement range of ± 3g, with a sensitivity of around 1 V/g and a broadband resolution of 30 μg rms. The self- weight of each sensor is only 0.62 ounces and thus its effect on the dynamic properties of the beam can be ignored. Five of them were on the centerline of the bottom surface and the one at the support were installed on the top surface with its center located at the edge of the pedestal. The boundary sensor was also used to check if there was any vertical movement at the support. Therefore the sensors were equally spaced by 23.5 inch between.

Forced vibration test scheme was applied to ensure the quality of test data. The dynamic force was generated by impacting the beam vertically at different measurement stations with an impulse-force hammer (Model 086C02 from PCB Piezoelectronics Inc., see Figure 4-13), accelerometer locations 2 through 6 as shown in Figure 4-16.

Shaker test was dismissed to avoid interference from vibrations of the floor system. With a sensitivity of 52.6mV/lb, the hammer can provide up to around 100 lb impact force and it is appropriate for small scale specimen like the beam of interest.

The data acquisition system consisted of three components: (1) multi-channel signal conditioner from PCB, (2) a Model E8401A HP VXI data acquisition mainframe with Model E1432A input modules from Agilent Technologies, and (3) a desktop computer with the X-Acquisition software which was developed by the Structural Dynamics Research Lab at University of Cincinnati (UC-SDRL). X-Acquisition provides a number of advantages for impact test data acquisition such as auto-ranging the voltage ranges of the sensors before each hit location and enabling the user to reject unwanted hits during data collection. Once an impact was stimulated, load cell at the hammer tip would pick up the force signal and in the meanwhile the recording of the accelerometer measurements would be triggered. All these signals went through the signal conditioner first and then into VXI unit which was connected with the desk computer.

A single-Input-Multiple-Output (SIMO) test scheme was employed in the dynamic testing. When the impact hammer hits at a specific test node, all the accelerometers will record the responses of the structure simultaneously. At each input node, the impact is repeated five times so that the frequency response functions are calculated as a result of averaging the five measurements. In this way random noise in the measurements can effectively be cancelled out. By roving the input locations along the beam, an equivalent Multiple-Input-Multiple-Output (MIMO) impact test was achieved. If all input and output degrees of freedom were taken into account in the subsequent parameter estimation algorithms, a five (no impact at the support) by six frequency response function (FRF) matrix can be formed at every frequency line.

Sampling is the process of recording the independent variable of analog signals and sampling frequency set in modal testing determines the success of digitizing analog signals and recovering valid frequency information. According to Shannon's Sampling Theorem, Nyquist frequency is

the theoretical limit for the maximum frequency and is defined to be one half of the sampling frequency. Due to the practical limitation about the analog filters, the sampling frequency is normally chosen to be greater than two times the maximum frequency of interest. According to preliminary modal analysis discussed in last section, as well as the capacity of the available hardware in DI^3 lab, the sampling rate of data acquisition was set to 800 Hz. This means that the vibration modes under 400 Hz can be accurately captured and therefore the first five frequencies of the beam would fall in the effective frequency band.

The same instrumentation was used for all impact tests of the beam under different configurations. All data acquisition parameters remain unchanged except that the voltage ranges for the accelerometers due to the difference in excitation levels between the two tests may vary.

Figure 4-13 PCB capacitive accelerometer model 3701G3FA3G (left) and PCB impulse-force test hammer model 086C02 (right)

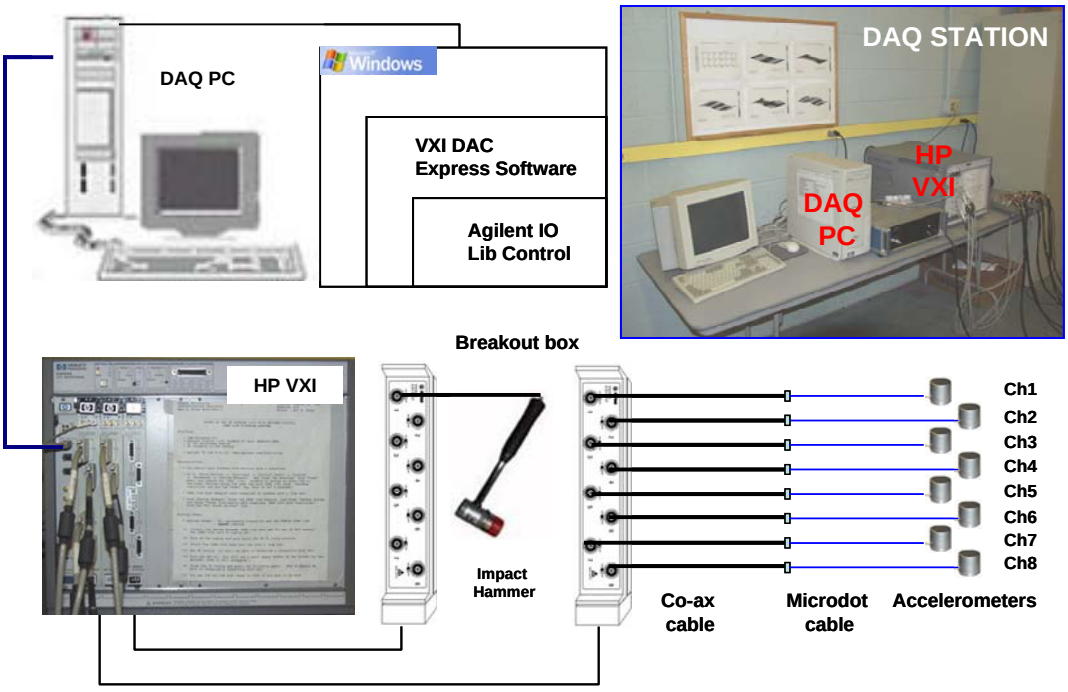

Figure 4-14 Data acquisition system

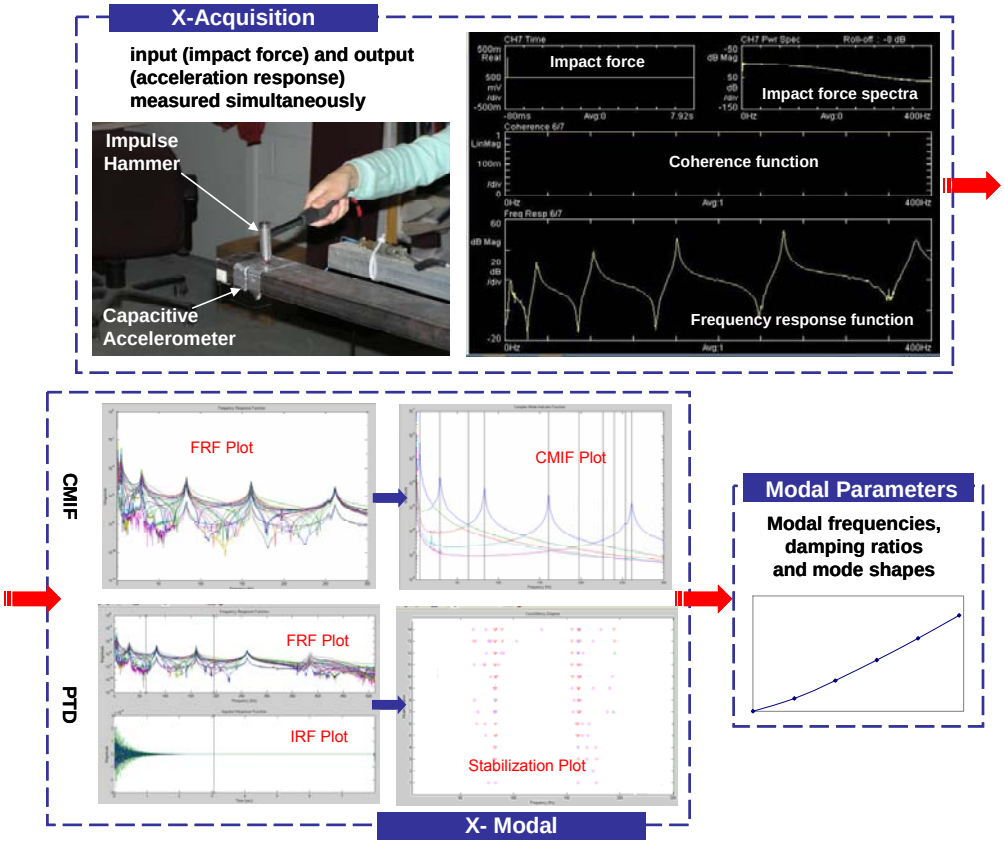

Figure 4-15 Flowchart of data acquisition and processing

As opposed to ambient vibration test, the simultaneous measurements of impulse force and acceleration responses in impact tests enable the experimenters to obtain the mode scaling information which was crucial to derive modal flexibility matrix of the beam. In each test configuration, the complete set of impact test (hit at five different input points) is repeated multiple times. This is done for the following reasons. First of all, modal testing generally assumed that the structure under consideration was linear and stationary when experiencing small-magnitude vibrations. The repeatability demonstrated in the estimated modal parameters would be the best proof for the conformance of such assumptions. Furthermore, in lab experiments, the equipments were usually well calibrated, the testing environments were also under control and therefore most sources of systematic error inherited in measurement were carefully deactivated. Multiple independent samples of data would enable us to assess the randomness of estimated modal parameters.

Five modes are expected in the frequency range of interest 0 – 400Hz, as predicted by the initial finite element analysis results. Two widely used modal parameter estimation algorithms, the polyreference time domain (PTD) method and complex mode indicator function (CMIF) method, were applied to each measured sample of impact test data. The resulting estimates could then be checked against each other. Another advantage of using more than one identification techniques on the same pieces of data laid in the fact that the difference in the modal properties extracted from the two approaches would be a reflection of algorithm dependent measurement errors. The flowchart of impact testing and the following data processing can be found in Figure 4-15.

Mean value and estimated standard deviation of modal parameters would be calculated from the all the estimation results. From the mean value $\bar{x}$ and estimated standard deviation $\hat{\sigma}_x$ of a stochastic variable x, the (100-α)% confidence interval on the true value of x usually could be expressed as

$$\left[\bar{x} - t_{\alpha/2,\nu}\hat{\sigma}_x, \bar{x} + t_{\alpha/2,\nu}\hat{\sigma}_x\right]$$

where $t_{\alpha/2,\nu}$ was found from a statistical table of Student's distribution. ν denoted the number of degrees of freedom, which was one less than the number of samples N, $\nu = N - 1$. In the case of the 95% confidence interval, $\alpha = 0.05$, $\nu = 2$ and $t_{\alpha/2,\nu} = 4.3$. Thus the 95% confidence interval of resonant frequency and damping ratio for all the five identified modes could be computed.

4.3.3 Dynamic Test Results from Test Configuration 1

The instrumentation plan of the beam in test configuration 1 is illustrated in Figure 4-16. Three independent impact tests were conducted and they were processed by CMIF and PTD methods respectively.

Typical test data collected by X-Acquisition from configuration 1 can be found in the top right corner of Figure 4-15. The screen-shot picture showed the impact force function and its frequency spectra in the upper half. The force spectra, which theoretically would be spread evenly over all the frequencies, dropped as the frequency increased. The lower half of the figure showed the magnitude plot of the driving point FRF when the impulse force was excited at the free end of the beam, i.e., the output station 6.

Five peaks clearly showed up in the plotted magnitude of frequency response functions (FRFs), which very much resembled the simulated FRFs in Figure 4-7.

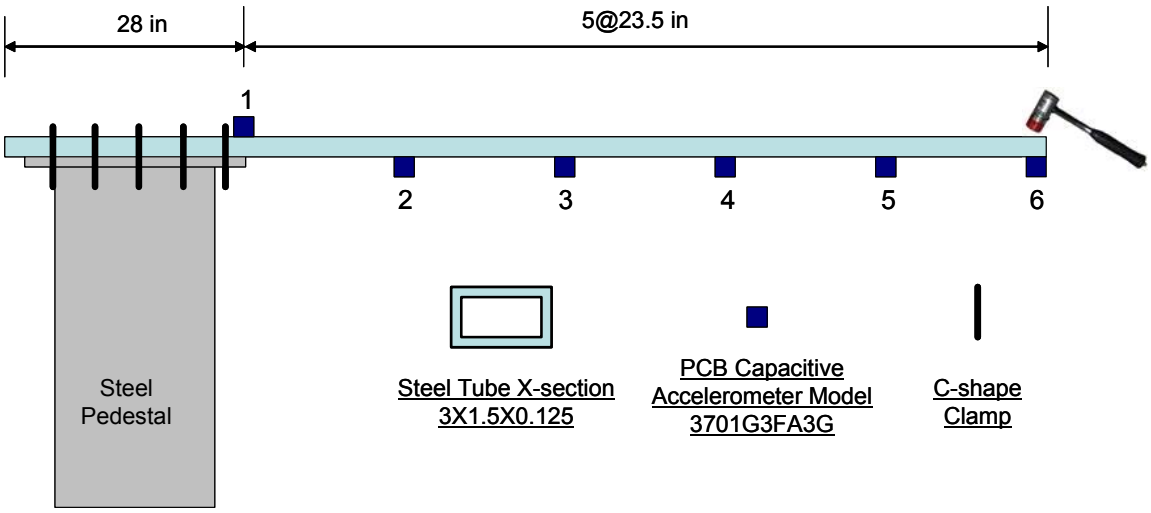

Figure 4-16 Dynamic test instrumentation

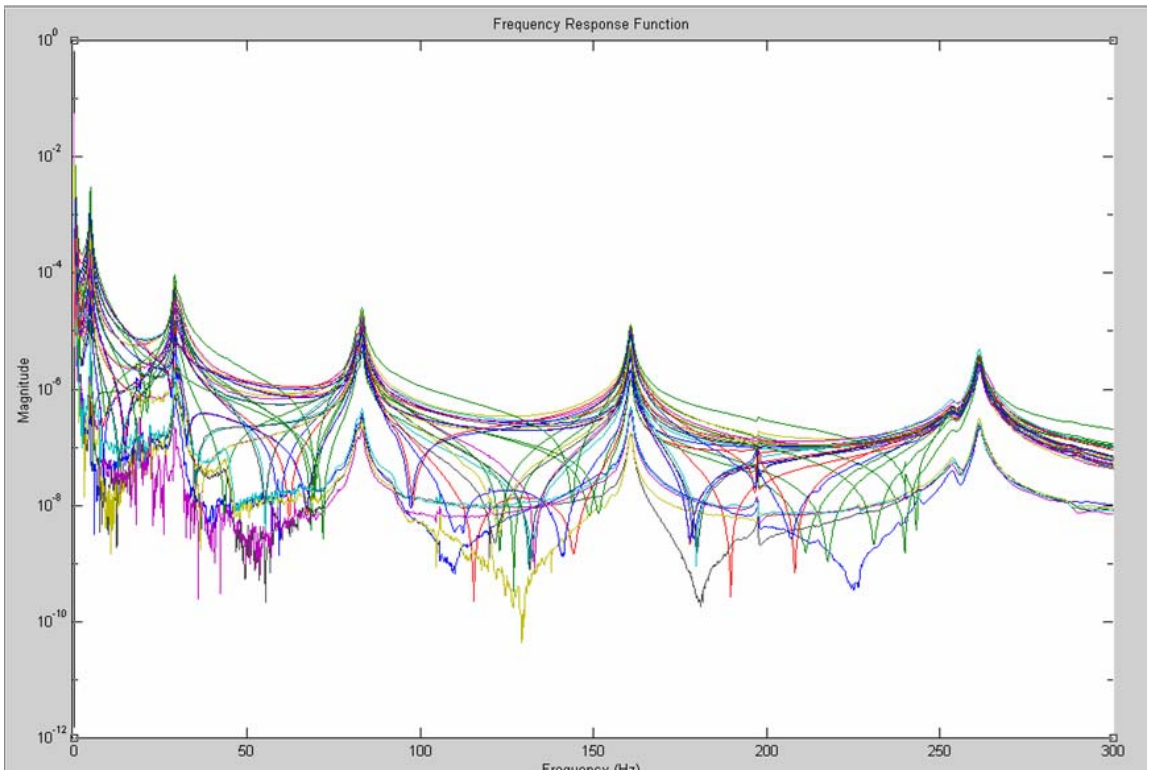

Figure 4-17 FRFs at all input and output stations

All the estimation results from the impact tests of configuration 1 were summarized in Table 4-4 and Table 4-5 and both CMIF and PTD estimates were listed. It could be observed from that variation in the resonant frequencies identified from the three independent impact tests were very

small. We may therefore have high confidence in the frequency estimates. In the contrast, the damping ratio estimates were more uncertain because much greater standard deviation values were associated with them.

Besides, it could be also found that the modal properties identified from the two parameter estimation algorithms – CMIF and PTD – didn't agree with each other. The difference in the estimated natural frequencies was very slight and CMIF method yielded a little bit better estimates than PTD, since there was less standard deviation associated with them. Dramatic discrepancy could be observed in the damping ratio estimates from the two approaches, especially for the second mode. Again the estimated standard deviation in CMIF results was less than that in PTD results.

Compared with that predicted by initial finite element model, the experimentally obtained modal frequencies deviated by around 5% for all the five modes within the measurable frequency band. As to the damping ratios, un-damped system was assumed in the analytical model, since the damping coefficients of steel structures are usually very small and barely had any effects on the resonant frequencies and mode shapes. This assumption was also verified by experimental data from which only the damping ratio for the first mode was over 2%.

The five bending mode shapes were shown side by side with numerical analysis results in Figure 4-18. They were reasonably close to each other, especially the first two modes. It may be due to the simple structural behaviors of a cantilever beam. Mode shapes of higher modes identified from experiments shifted a little toward to the support, compared with their counterparts from initial finite element model.

Table 4-4 Estimated resonant frequencies (Hz) from test configuration 1

Mode #	1	2	3	4	5
Initial FE	4.9099	30.7698	86.1576	168.8423	279.1383
CMIF 1	4.709	29.321	82.913	160.576	260.970
CMIF 2	4.714	29.355	82.965	160.442	261.429
CMIF 3	4.712	29.055	82.789	160.701	260.437
Mean	4.712	29.244	82.889	160.573	260.945
STD	0.003	0.164	0.090	0.130	0.496
Diff (%)	4.037	4.960	3.794	4.898	6.518
95% C. I.	4.712±0.013	29.244±0.705	82.889±0.387	160.573±0.559	260.945±2.133
PTD 1	4.712	29.177	83.230	160.654	261.714
PTD 2	4.724	29.353	83.238	160.523	261.827
PTD 3	4.718	29.004	82.826	160.803	260.699
Mean	4.718	29.178	83.098	160.660	261.413
STD	0.006	0.175	0.236	0.140	0.621
Diff (%)	3.908	5.173	3.551	4.846	6.350
95% C. I.	4.718±0.026	29.178±0.753	83.098±1.015	160.660±0.602	261.413±2.670

Table 4-5 Estimated damping ratios (%) from test configuration 1

Mode #	1	2	3	4	5
CMIF 1	2.106	1.558	0.622	0.288	0.285
CMIF 2	2.087	1.516	0.628	0.271	0.270
CMIF 3	2.086	1.596	0.572	0.211	0.285
Mean	2.093	1.557	0.607	0.257	0.280
STD	0.011	0.040	0.031	0.040	0.009
95% C. I.	2.093±0.047	1.557±0.172	0.607±0.133	0.257±0.172	0.280±0.039
PTD1	2.194	0.618	0.309	0.291	0.503
PTD 2	2.084	0.814	0.398	0.277	0.283
PTD 3	2.394	0.893	0.673	0.226	0.347
Mean	2.224	0.775	0.460	0.265	0.378
STD	0.157	0.142	0.190	0.034	0.113
95% C. I.	2.224±0.675	0.775±0.611	0.460±0.817	0.265±0.146	0.378±0.486

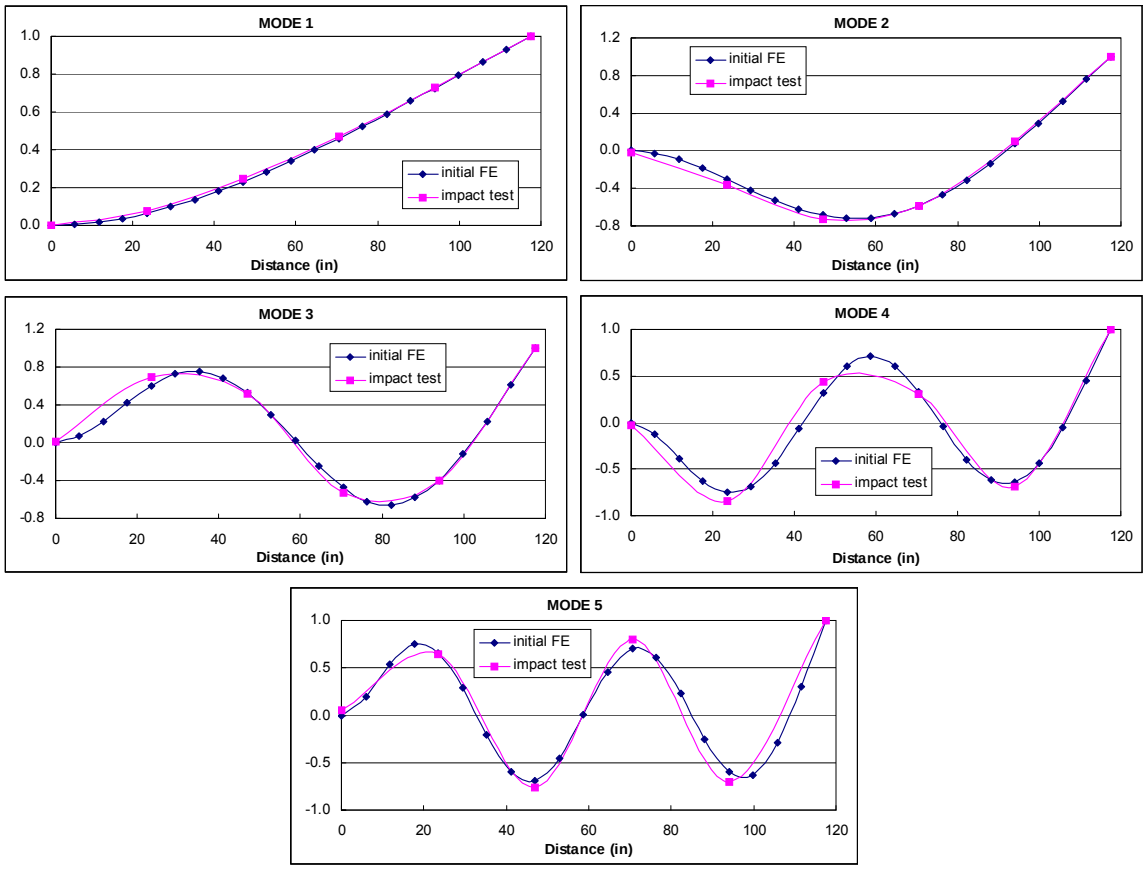

Figure 4-18 Estimated mode shapes from impact test data of test configuration 1

4.3.4 Dynamic Test Results from Test Configuration 2

Similar instrumentation plan were implemented on the test specimen under test configuration 2 and Figure 4-19 showed detailed sensor layout. The magnitude plot of frequency response function at all input and output stations in Figure 4-20 clearly demonstrated that more than five peaks appeared in the frequency band of interest, 0 – 300 Hz. The additional peaks located at the frequency band between 100 and 200 Hz in which only one peak dominated when the beam was tested with configuration 1. Among the four peaks, the first three modes located fairly close with each other and the fourth one separate with them with a distance.

A total of six independent tests were conducted in order to investigate the repeatability of these estimated modal properties. Since the complex boundary assembly added more uncertainties for test setup, the number of independent tests was doubled than previous scenario.

The resonant frequency as well as damping ratio of the modes in the frequency band of interest was identified by CMIF and PTD separately and the results were summarized in Tables 5 through 8. The statistics, mean value, estimated standard deviation and 95% confidence interval, of these estimates were also evaluated.

Both CMIF and PTD algorithms yielded eight modes from impact test data. It could be observed from Table 4-6 and Table 4-7 that variation in resonant frequency estimates from the six independent impact tests was negligible. We may therefore have high confidence in the identified frequency. Although the damping ratios (Table 4-8 and Table 4-9 were more uncertain than modal frequencies, the fluctuation was also very small.

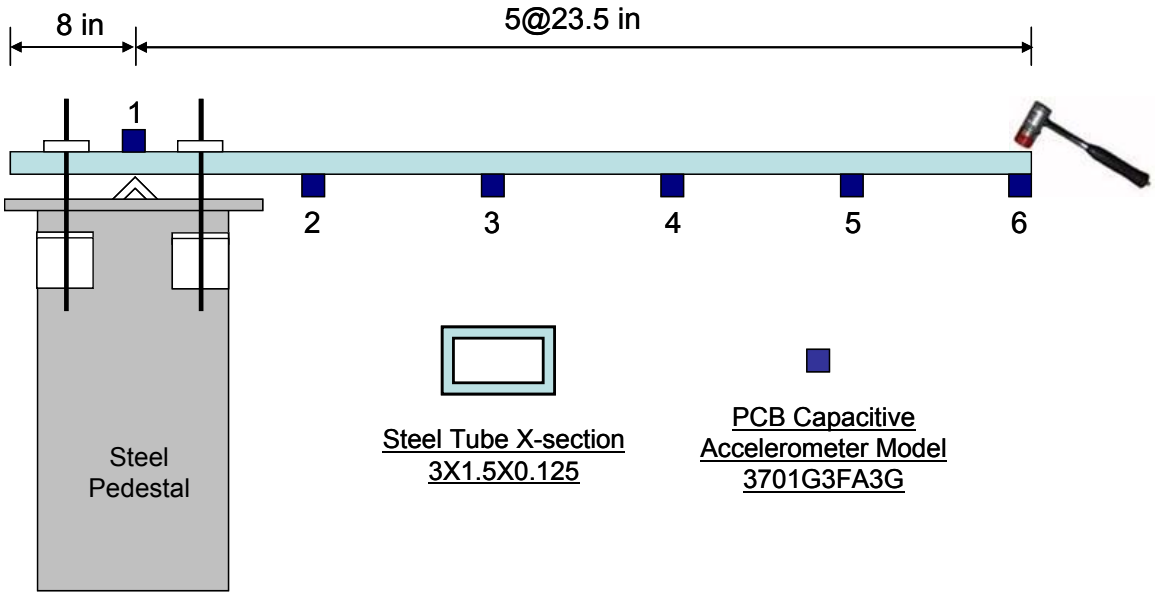

Figure 4-19 Test instrumentation

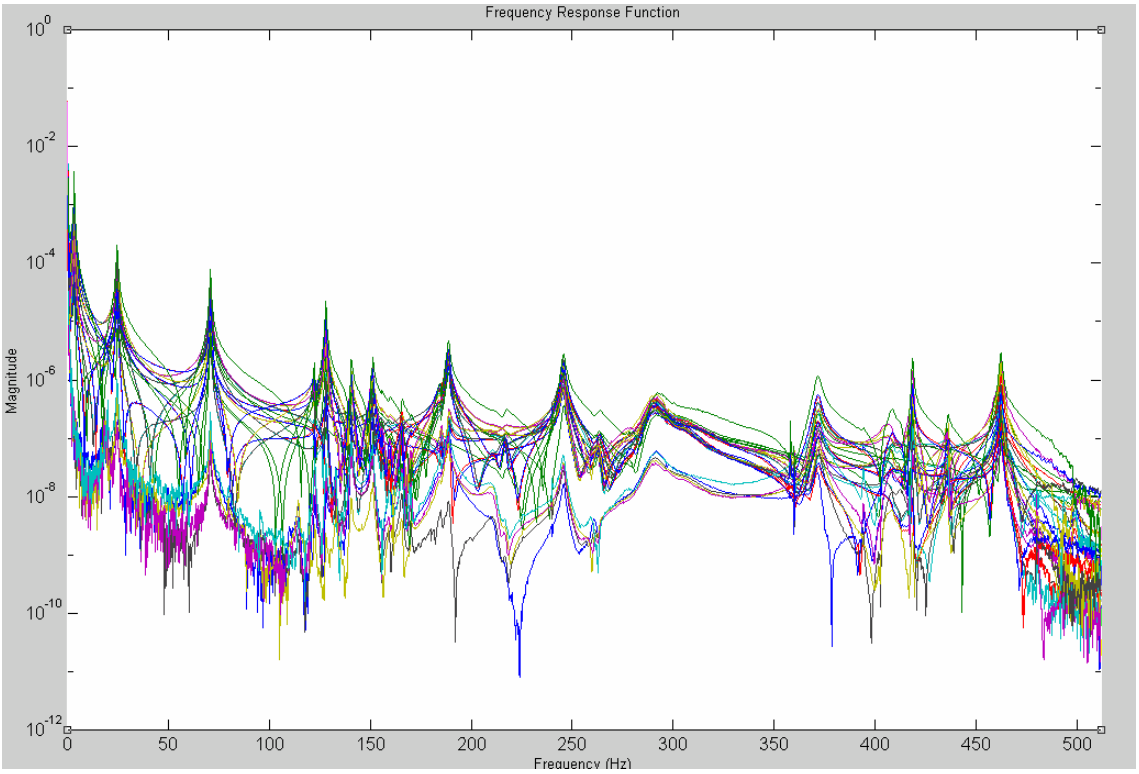

Figure 4-20 FRF and CMIF plots from CMIF algorithm

It could be observed that the natural frequencies estimated from PTD did not exactly agree with that from CMIF and they were slightly greater except the fifth mode frequency. Larger discrepancy existed in the damping ratio estimates from the two algorithms but they were more consistent, compared with the results from tests with configuration 1. Figure 4-21 and Figure 4-22 displayed identified mode shapes from CMIF and PTD respectively. CMIF mode shapes from six independent impact tests almost exactly overlapped with each other. However there was obvious difference in the magnitude of higher modes estimated by PTD.

A quick comparison of the modal information from current test configuration with that from test configuration 1 and initial finite element analysis showed that the first three and eighth modes paired quite well with the first three and fifth modes from analytical prediction, although the values of resonant frequencies were much smaller. The modes 4 through 7, however, all

demonstrated similar modal deflection shapes as the analytical 4th mode and make it difficult to distinguish which should be matched up with the analytical fourth mode.

Table 4-6 Estimated resonant frequencies (Hz) from beam with non-ideal support by CMIF

Mode #	1	2	3	4	5	6	7	8
CMIF 1	3.337	24.606	70.818	127.913	140.516	150.968	188.372	245.359
CMIF 2	3.338	24.608	70.819	127.921	140.527	150.972	188.389	245.372
CMIF 3	3.337	24.611	70.823	127.931	140.537	150.983	188.379	245.397
CMIF 4	3.336	24.616	70.822	127.943	140.548	150.980	188.418	245.362
CMIF 5	3.337	24.614	70.819	127.940	140.543	150.969	188.399	245.399
CMIF 6	3.342	24.618	70.820	127.943	140.541	150.963	188.413	245.406
Mean	3.338	24.612	70.820	127.932	140.535	150.973	188.395	245.381
STD	0.002	0.005	0.002	0.013	0.012	0.008	0.018	0.019
95% C. I.	3.338 ±0.005	24.612 ±0.012	70.820 ±0.005	127.932 ±0.032	140.535 ±0.030	150.973 ±0.020	188.395 ±0.047	245.381 ±0.050

Table 4-7 Estimated resonant frequencies (Hz) from beam with non-ideal support by PTD

Mode #	1	2	3	4	5	6	7	8
PTD 1	3.350	24.660	70.895	127.971	140.515	151.266	188.547	245.631
PTD 2	3.357	24.669	70.874	127.998	140.509	151.282	188.704	245.652
PTD 3	3.353	24.672	70.877	128.007	140.522	151.232	188.558	245.595
PTD 4	3.349	24.668	70.872	127.983	140.594	151.275	188.686	245.445
PTD 5	3.348	24.681	70.880	127.982	140.526	151.310	188.761	245.647
PTD 6	3.353	24.677	70.835	127.968	140.534	151.318	188.767	245.648
Mean	3.352	24.671	70.872	127.985	140.533	151.281	188.671	245.603
STD	0.003	0.007	0.020	0.015	0.031	0.031	0.097	0.080
95% C. I.	3.352 ±0.009	24.671 ±0.019	70.872 ±0.051	127.985 ±0.039	140.533 ±0.080	151.281 ±0.080	188.671 ±0.249	245.640 ±0.206

Table 4-8 Estimated damping ratios (%) from beam with non-ideal support by CMIF

Mode #	1	2	3	4	5	6	7	8
CMIF 1	2.861	1.157	0.298	0.181	0.231	0.291	0.312	0.337
CMIF 2	2.842	1.155	0.293	0.181	0.230	0.287	0.312	0.335
CMIF 3	2.823	1. 155	0.294	0.181	0.239	0.286	0.317	0.339
CMIF 4	2.860	1.132	0.298	0.181	0.236	0.288	0.318	0.344
CMIF 5	2.846	1.113	0.302	0.182	0.236	0.292	0.321	0.353
CMIF 6	2.843	1.101	0.306	0.181	0.235	0.299	0.323	0.349
Mean	2.844	1.136	0.299	0.181	0.235	0.291	0.317	0.343
STD	0.015	0.024	0.005	0.000	0.003	0.005	0.005	0.007
95% C. I.	2.844 ±0.038	1.136 ±0.062	0.299 ±0.013	0.81 ±0.001	0.235 ±0.009	0.291 ±0.012	0.317 ±0.012	0.343 ±0.018

Table 4-9 Estimated damping ratios (%) from beam with non-ideal support by PTD

Mode #	1	2	3	4	5	6	7	8
PTD 1	2.913	1.226	0.281	0.174	0.243	0.252	0.480	0.329
PTD 2	2.903	1.307	0.248	0.183	0.244	0.206	0.208	0.389
PTD 3	2.920	1.332	0.254	0.163	0.261	0.263	0.491	0.319
PTD 4	2.927	1.264	0.277	0.220	0.254	0.254	0.301	0.388
PTD 5	2.917	1.298	0.267	0.181	0.278	0.230	0.268	0.346
PTD 6	2.940	1.259	0.276	0.179	0.261	0.263	0.278	0.335
Mean	2.920	1.281	0.267	0.183	0.257	0.345	0.338	0.351
STD	0.013	0.038	0.013	0.019	0.013	0.022	0.119	0.030
95% C. I.	2.920 ±0.032	1.281 ±0.099	0.267 ±0.035	0.183 ±0.050	0.257 ±0.033	0.245 ±0.058	0.338 ±0.119	0.351 ±0.078

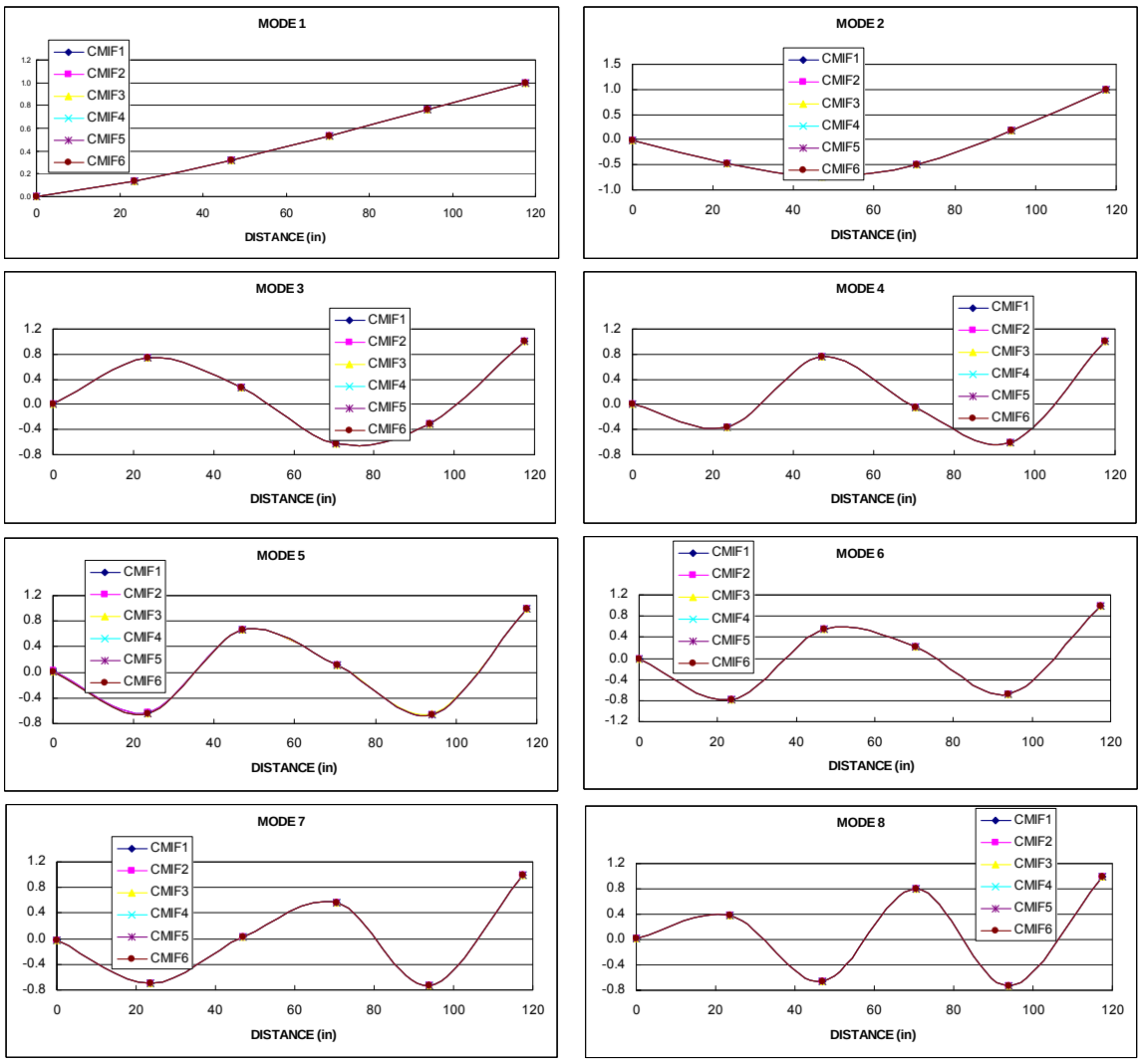

Figure 4-21 Mode shapes from CMIF

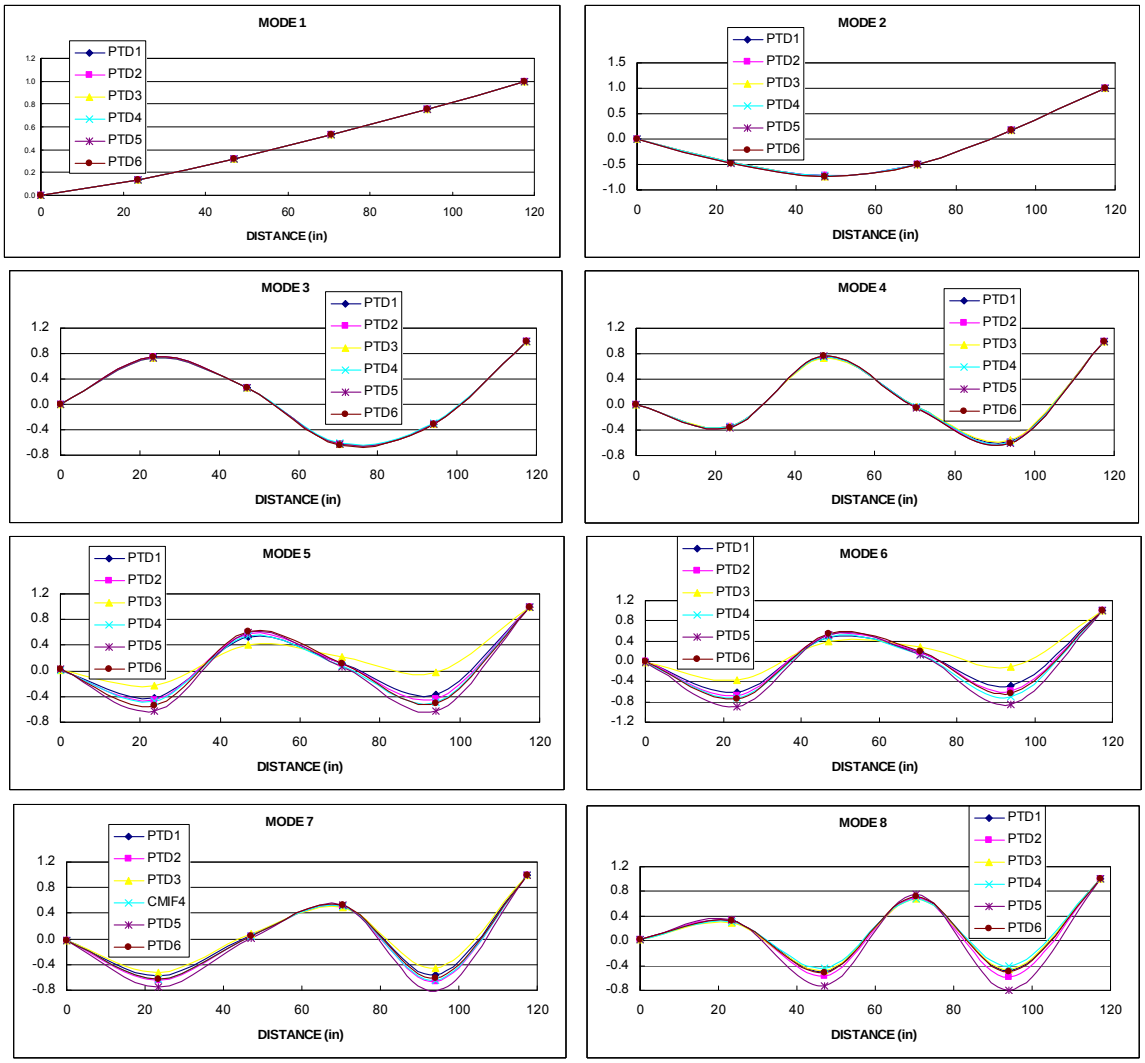

Figure 4-22 Mode shapes from PTD

4.4 Verification of Dynamic Test with Flexibility Index

Flexibility, the inverse of stiffness matrix of the system, was first introduced by Maxwell in 1864. Although physical structural systems are continuous, their behaviors can usually be represented by a parameter model with discretized mass, stiffness and damping of the system. Previous research has shown that flexibility was also of significance for the understanding of structural behaviors and has been proposed as a reliable signature to reflect its existing conditions (Aktan and Toksoy 1994).

Flexibility matrix of a system could not only be generated through static test but also be derived from modal parameters obtained from modal tests. The transformation of resonant frequencies and mode shapes to the system flexibility matrix could be expressed as

$$[f] = [U][\Omega][U]^T$$

or

$$f_{i,j} = \sum_{k=1}^{m} \frac{\phi^k(i)\phi^k(j)}{\omega_k^2}$$

where $\phi^k(i)$ denoted the *i*-th element of the *k*-th mode shape; $f_{i,j}$ was the flexibility coefficient at the *i*-th point under the unit load at point j and ω_k was the *k*-th radian frequency (radian/second). It was worth noting that the formulations above were based on the unit-mass-normalized mode shapes. In this study, the flexibility matrix obtained from static test would serve as an independent measure to verify the results from modal tests.

Since a real-life structure was composed of infinite degrees of freedom, its vibrations were supposed to be the superposition of infinite number of modes. However the number of modes which could be accurately identified from vibration tests was often confined by the number of measurement degrees of freedom and measurable frequency band. In practice, the available amount of accelerometers as well as the capability of data acquisition system was limited. Modal truncation, in terms of temporal and spatial, thus could not be avoided in the construction of modal flexibility. Previous research has shown that lower modes of the system often dominate in flexibility matrix formulation and the resulting modal flexibility would come to convergence with the first several modes.

4.4.1 Static Test

Five Celesco cable-extension displacement sensors (Model PT101) were applied for static test on the beam specimen and the five measurement station were located side by side with the accelerometers along the cantilever span. The displacement transducers were installed on the floor, exactly under each output stations. They were connected with the beam with high-strength strings which barely deformed when subjected to the designed static loading. A high-speed data acquisition system OPTIM would simultaneously collect the voltage signals from all channels and convert to displacement according to the sensitivity of each sensor.

The beam was loaded by a steel cylinder which was placed at each measurement station subsequently. Figure 4-23 displayed the deformation of the beam under a concentrated load at point 5. During the application of static loads, the concentrated load was kept on the structure for a couple of minutes to make sure that the displacement readings settled down around the true values. The vertical deflections of the beam at all the measured locations during all these loading and unloading cycles were recorded simultaneously by OPTIM.

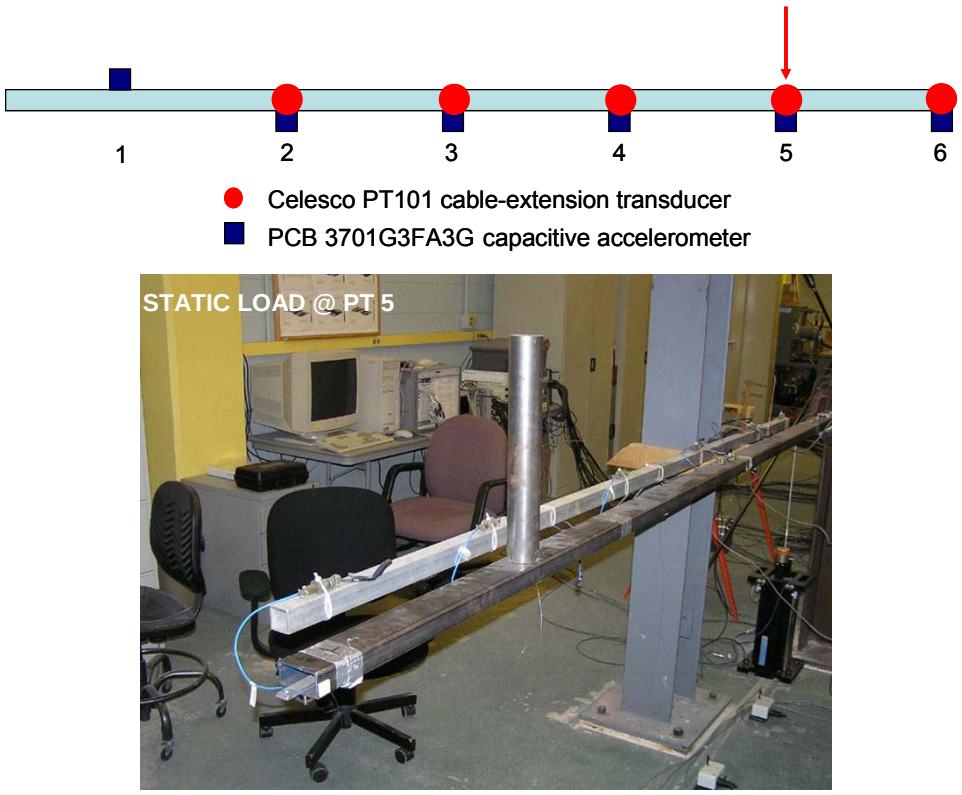

Figure 4-23 Static test on the cantilever beam

4.4.2 Verification for Test Configuration 1

Typical time-history displacement data from static test with configuration 1 were shown in Figure 4-24. The displacements when the 20-lb steel cylinder was concentrated at each measurement station could then be obtained by averaging over the steady segment of the data. These values would later be used to construct the static flexibility matrix. From Figure 4-24, largest vertical displacement took place at the tip of the free end of the beam when the concentrated load was applied at the same location and it was around 1 inch.

As a result of the controlled static load test, a 5x5 static flexibility matrix of the beam was experimentally derived. Virtual loading each measurement point by a unit load (1 lb) will yield the Uniform Loading Surface (ULS) for these selected nodes. Deflected shape of the longitudinal centerline of the beam under ULS loading for the five displacement measurement station was shown in Figure 4-25. Great similarity was found in beam vertical deflections under ULS loading

using the modal flexibility matrices generated with only the first experimental mode and with all five modes. Therefore it could be concluded that the first mode dominated the flexibility space of the cantilever beam.

Figure 4-25 also displayed high correlation between the experimentally obtained flexibility from static test and dynamic test. The reliability of modal properties identified from impact test was thus checked by an independent experimental tool.

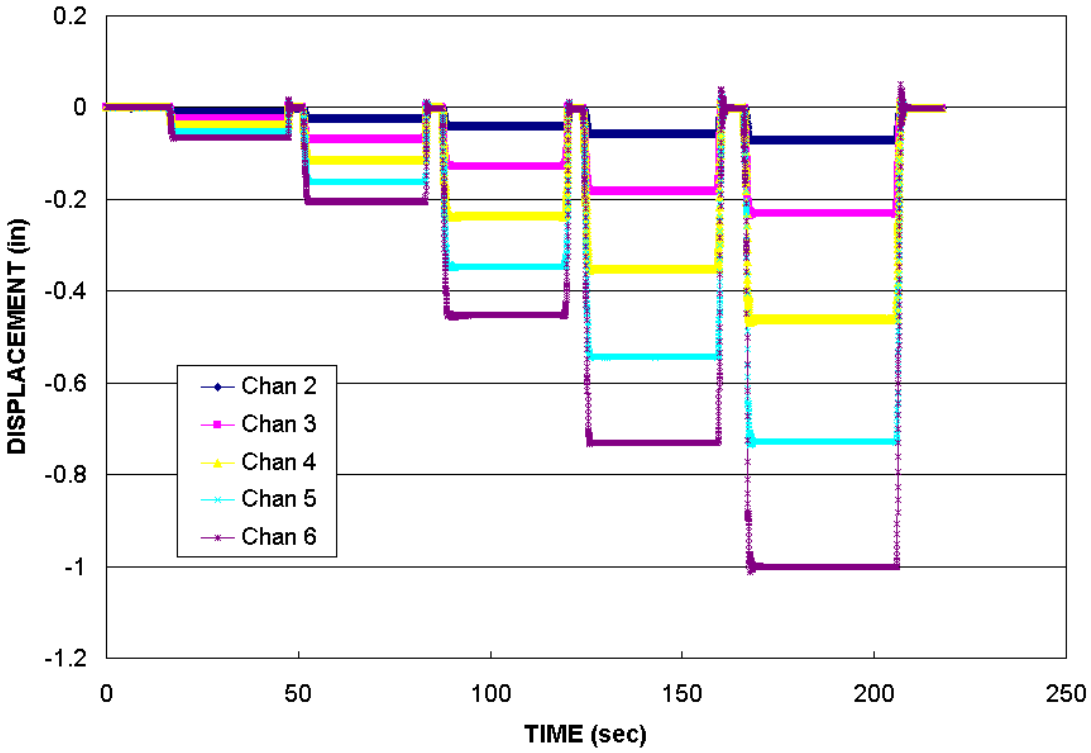

Figure 4-24 Time-history displacement data

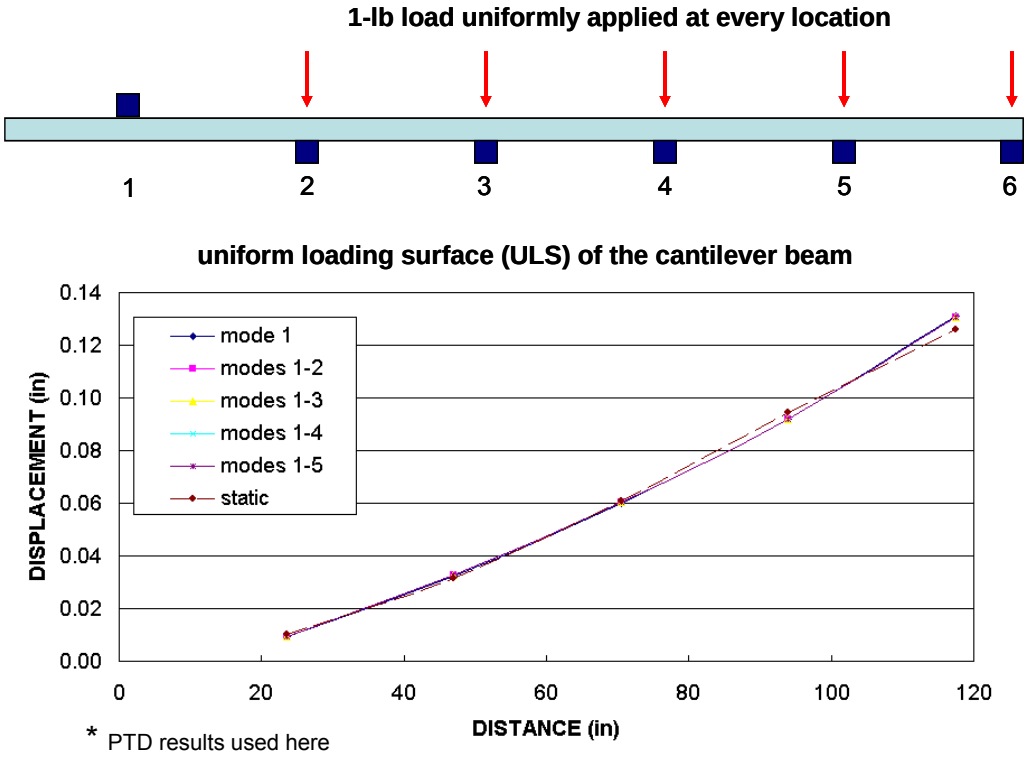

Figure 4-25 Convergence of modal flexibility

4.4.3 Static Test with Configuration 2

Similarly, the time-history displacement data from static test with configuration 2 were shown in Figure 4-26. As the 14-lb steel object was moving from the support end to the free end of the beam, the vertical deflection increased rapidly. Even under a lighter static load of 14 pounds, the maximum displacement at the tip of the beam was about 0.2 inch more. This observation showed that the beam with current configuration was more flexible than that with the previous one.

A 5x5 static flexibility matrix of the beam was generated from the controlled static load test. The deflected shape under virtual unit load (1 lb) at all measurement stations were calculated with the flexibility matrices from static test as well as from impact test. Figure 4-27 demonstrated that the resulting beam deflection using the modal flexibility generated with the first mode was already very close to its counterpart from static test. Again, this could be attributed to the fact that the first modal mode dominated the flexibility space of the cantilever beam.

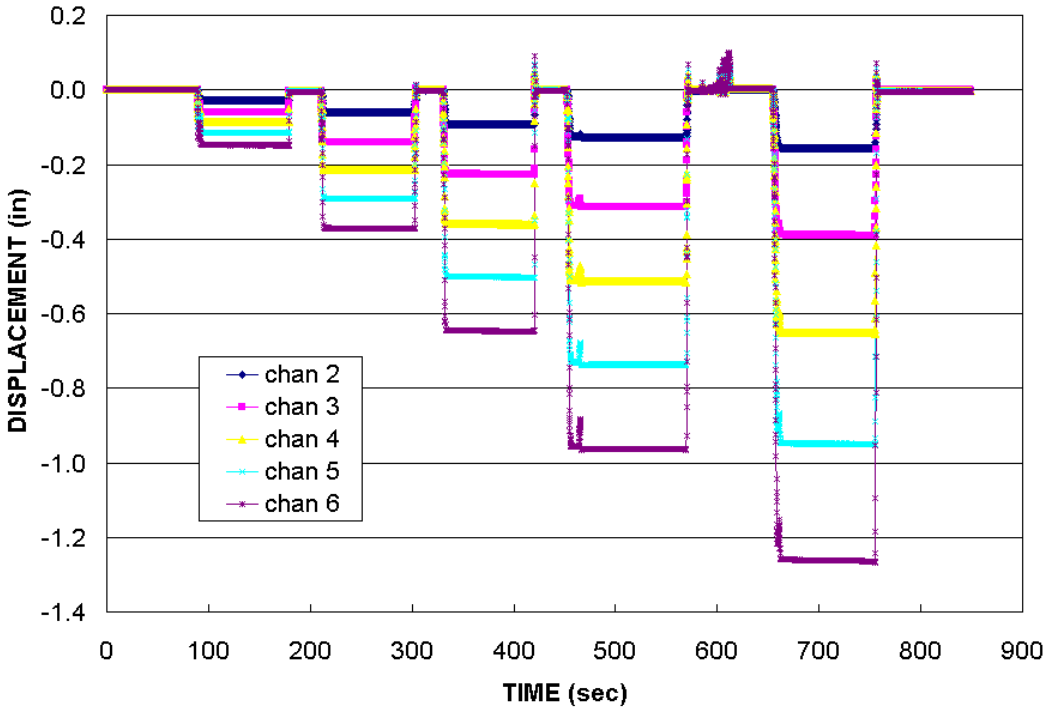

Figure 4-26 Time-history displacement data

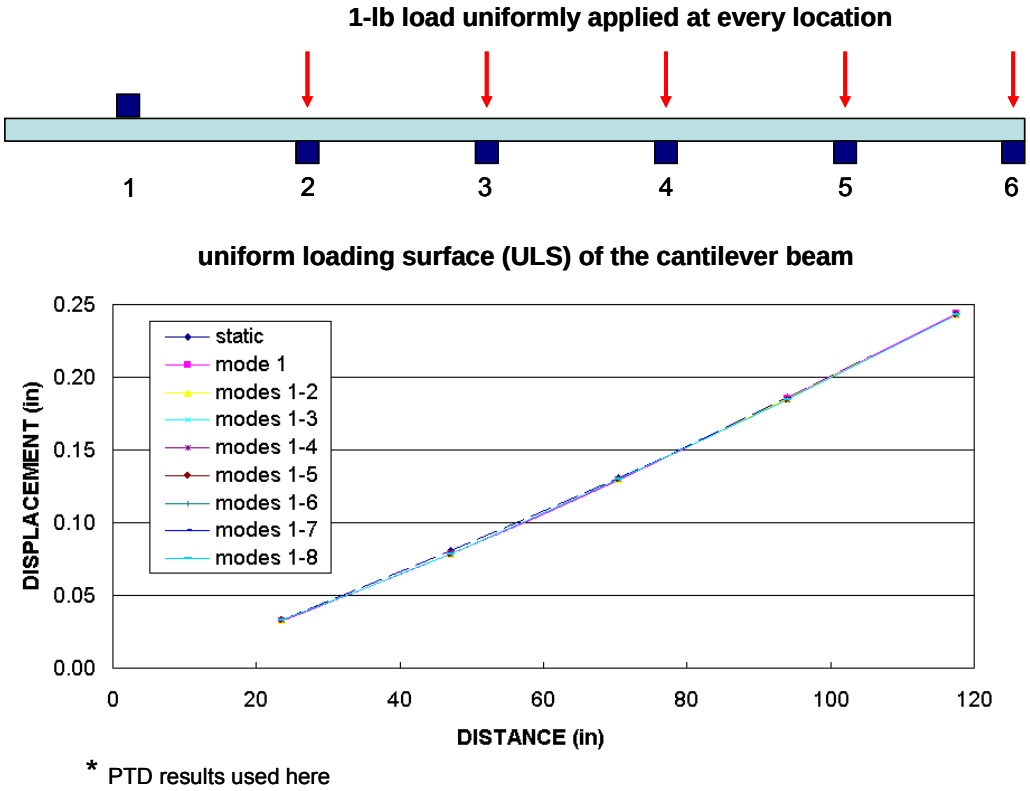

Figure 4-27 Convergence of modal flexibility

4.5 System Identification of the Cantilever Beam – the First Attempt

There is no doubt that good correlation existed between the analytical predictions provided by the initial 20-element FE model and the experimental measurements. All the analytical modes paired up with their experimental counterparts – the frequencies were reasonably close (around 7 percent of difference in the frequency of the fifth mode) and the MAC values of all the five modes were close to 1. From the test data of the configuration 2, a total of eight modes were identified in the same frequency band of 0-300 Hz. The first three modes and the last one were able to match up with the first three and the fifth analytical modes respectively, but four modes between 100-200 Hz demonstrated similar deflection shape and all of them shared similarity with the predicted fourth bending mode. For the four sets of paired modes, the greatest frequency difference rose as high as around 47% but the MAC values for the mode shapes were fairly good (all above 0.94). The decrease in the modal frequencies was expected because of the rotational flexibility allowed by the designed boundary assembly. However, the three additional modes were far beyond the expectation. The following task is to make use of these test observations to improve understanding of the behavior of the structure.

As any other experiments on existing structures, errors associated with data measurement and processing was unavoidable. However, effects of experimentation errors with both random and systematic mechanisms were successfully deactivated in the two test configurations. The modal parameters estimated from multiple impact tests showed good repeatability. They were further verified by using universal loading surface (ULS) index derived from independent static test data. Therefore the main contribution to the noticeable discrepancy observed in test-analysis correlation, especially in test configuration 2, was most likely from the modeling errors inherent in the initial analytical model.

4.5.1 Traditional Error Localization Index

Based on a comparison study on simulated experimental data, Friswell and Mottershead (1995) already demonstrated that error indicators may fail to locate modeling errors in initial FE models when analytical and experimental degrees of freedom don't match up with each other or random noise exist in measurements. Both of the two conditions are always inevitable in engineering practice. In order to further investigate potential applicability of these proposed error localization methods, balancing the eigenvalue equation method and substructure energy function method are applied on the cantilever beam under two different configurations. Since the beam was only instrumented with six accelerometers, the size of experimental degrees of freedom is significantly smaller than that of analytical degrees of freedom and measured mode shapes have to be expanded before any error localization algorithm could be applied. Two expansion techniques– using analytical mass and stiffness and using analytical modal data – are utilized respectively.

For test configuration 1, Figure 4-28 and Figure 4-29 show that the normalized value of the error index q, given by equation (3.11) for the method that balances the eigenvalue equation. If was found that balancing the eigenvalue equation method led to two different error indications, depending on the approaches to expand the measured mode shapes. Figure 4-30 shows the normalized energy function of each beam element. The error indexes developed from the expanded mode shapes obtained by two expansion methods revealed that the most possible erroneous zones of the beam was at elements 1 and 2. Similar observations could be made from the applications of the two error localization indexes in conjunction with two expansion methods, as shown in Figure 4-31, Figure 4-32 and Figure 4-33.

No consistent and solid conclusion could be drawn from the error indicators generated from either balancing the eigenvalue equation method or substructure energy function method. Although these proposed error localization functions may be theoretically sound and even

feasible for cases where simulated experimental data were used, they collapsed easily when applied on real-life systems, even in a simple cantilever. It was most likely due to huge difference in the number of measurement DOFs and that of analytical DOFs.

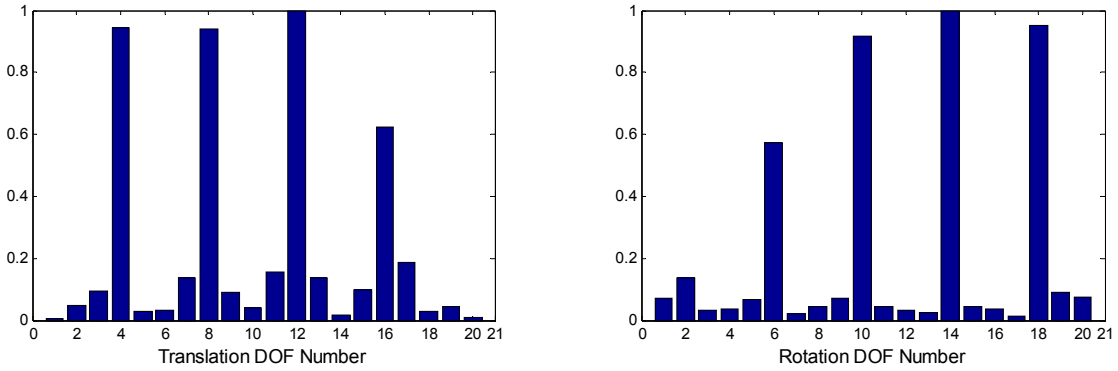

Figure 4-28 Error localization for configuration 1 with balancing the eigenvalue equation method based on expanded experimental mode shapes using analytical mass and stiffness matrices

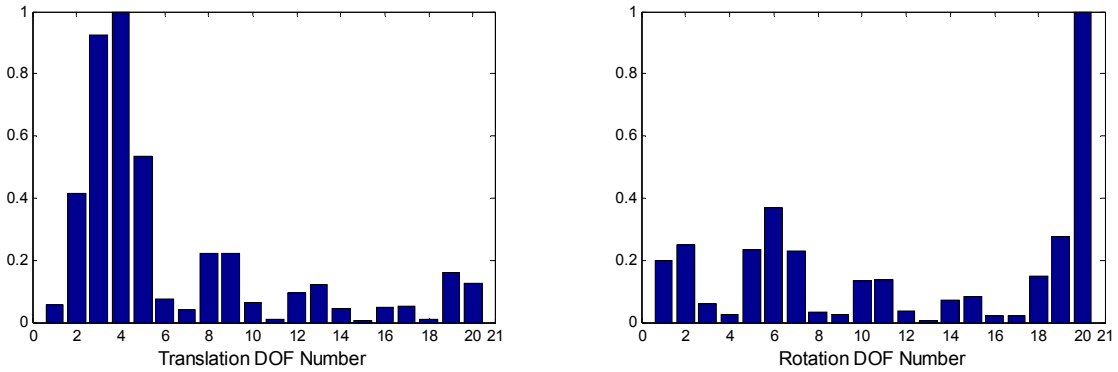

Figure 4-29 Error localization for configuration 1 with balancing the eigenvalue equation method based on expanded experimental mode shapes using analytical modal data

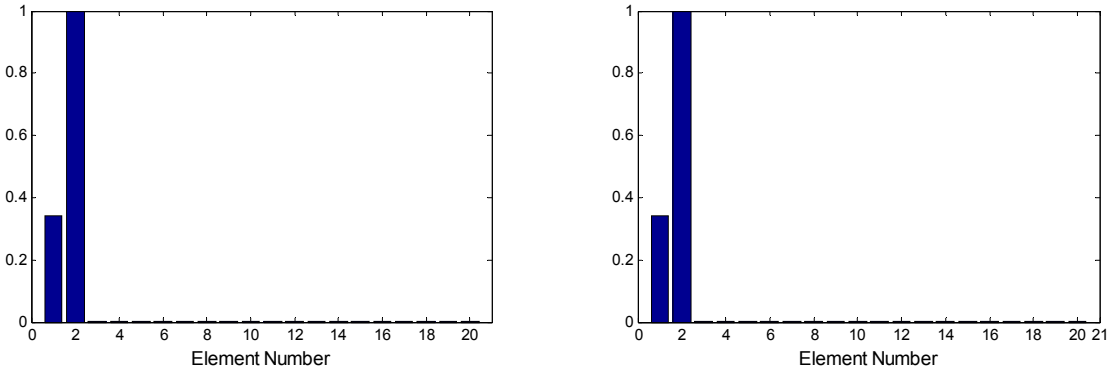

Figure 4-30 Error localization for configuration 1 with substructure energy method based on expanded experimental mode shapes using analytical mass and stiffness matrices (left) and analytical modal data (right)

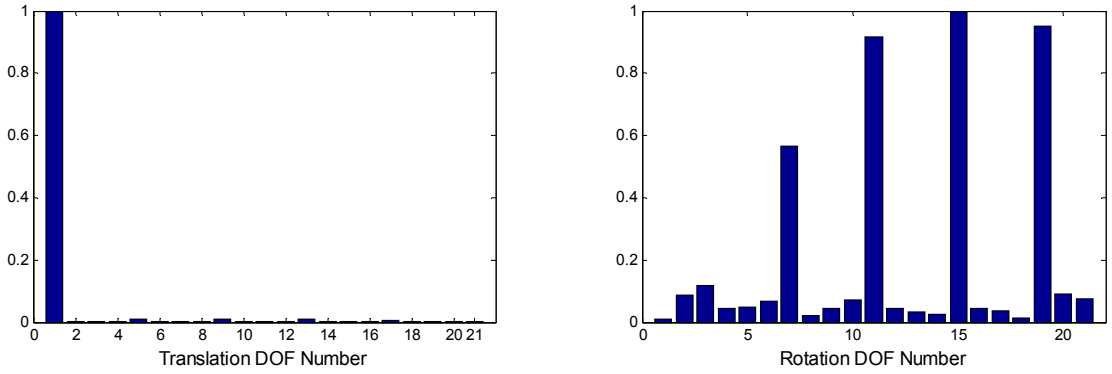

Figure 4-31 Error localization for configuration 2 with balancing the eigenvalue equation method based on expanded experimental mode shapes using analytical mass and stiffness matrices

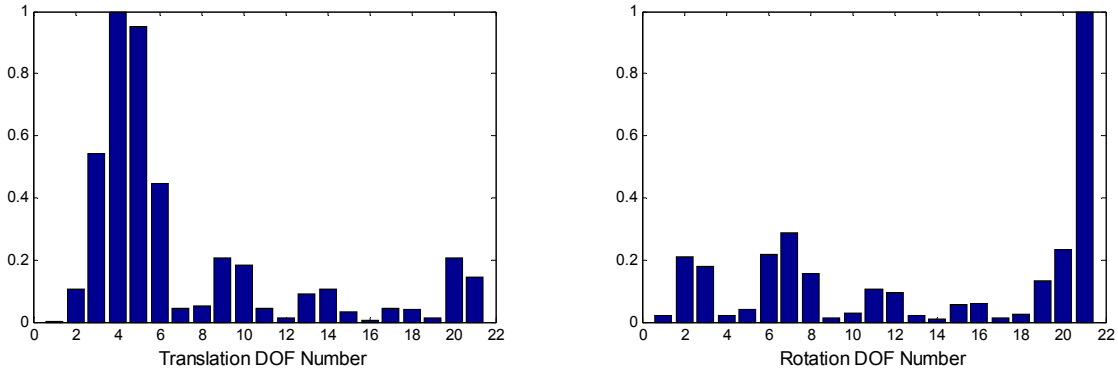

Figure 4-32 Error localization for configuration 2 with balancing the eigenvalue equation method based on expanded experimental mode shapes using analytical modal data

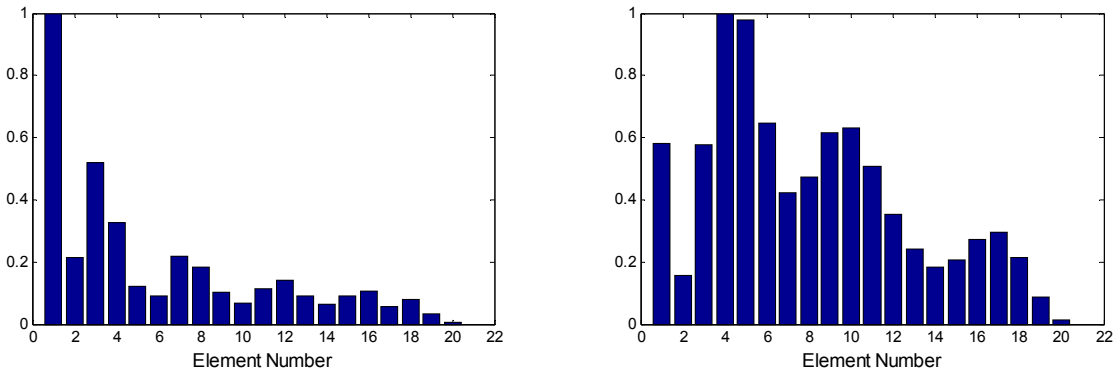

Figure 4-33 Error localization for configuration 2 with substructure energy method based on expanded experimental mode shapes using analytical mass and stiffness matrices (left) and analytical modal data (right)

4.5.2 Model Updating by Inverse Eigen-sensitivity Method

Because of the resemblance of experimental and analytical mode shapes, model updating would be carried out, assuming that the initial 20-element finite element model was adequately correct. This initial model is called as model *A*, for future reference. The material property of the steel beam, modulus of elasticity *E*, was selected as the only parameter to be corrected and it was set as its nominal value of 29,000 ksi in the initial numerical model. The same initial FE model was used in updating runs to reproduce the modal data (frequencies and mode shapes) estimated from impact test with configuration 1 and configuration 2, respectively. The updating process was performed using inverse eigen-sensitivity approach.

The theoretical solution to modal properties of the cantilever beam reveals that any adjustment in the modulus of elasticity will definitely change the resonant frequencies but have on impact on normalized mode shapes. Thus the objective function would include eigenvalue information only. As to the estimated eigenvectors, they were unity normalized to help pair the experimental with the numerical modes correctly in the automatic updating process.

Since eigenvalues from higher modes have greater absolute values, explicit weighting factors were applied on each term in the residual vector in order to equally take into account the

influence of each mode. The updating process was conducted by the nonlinear least square optimization function from MATLAB Optimization toolbox.

A total of three updating runs were conducted. In the first run, frequency residuals were used corresponding to all the five identified modes from impact tests with configuration 1. Four modes in the measurable frequency range from test configuration 2 displayed deflection shapes similar to the theoretical fourth bending mode shape. The residual vector for the 2nd run thus only contained the resonant frequencies of the paired modes from test configuration 2. For consistency, a third run in which the residual vector contained the first three and the last modes from test configuration 1 was also conducted.

The modulus of elasticity *E* after updating for the two test configuration was given in Table 4-10 together with its initial values. About 10 percent change was identified in the updating runs 1 and 3 in order to reduce the difference between experimental and analytical frequencies. The updated value for the Young's modulus in the run 2 was only of two thirds of its nominal value.

Table 4-11 and Table 4-12 listed the initial and updated eigenfrequencies for the three runs. Very similar updated results were found for the 1st and 3rd run, in which the only difference was that only four pairs of eigenvalues were included in the 3rd run. In the updating run 1, a highest relative discrepancy 1.680% appeared in the fifth mode after updating and the values of the rest modes were all below 1.5%. Missing the fourth pair of modes in objective function barely had any influence on updating results. The mode shapes remained the same after updating and Figure 4-39 displayed the comparison between analytical and experimental mode shapes.

For the model updating run 2, the correlation between test and numerical frequencies of the four paired modes was considerably improved. In particular, the frequencies of the 2nd and 3rd mode predicted by updated analytical model were very close to their experimental counterpart. The discrepancy in the frequency of the first mode dropped from 47% to 21%. The four sets of

analytical and experimental modes were compared in Figure 4-40. A graphic comparison of the updated results in run 1 and 3 were also provided in Figure 4-38.

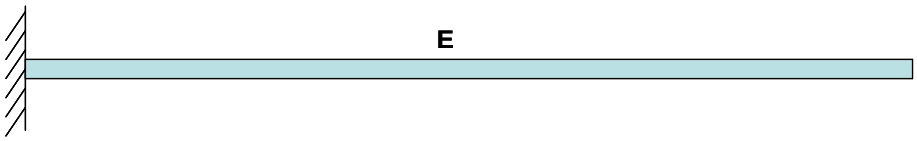

Figure 4-34 Initial Model *A*

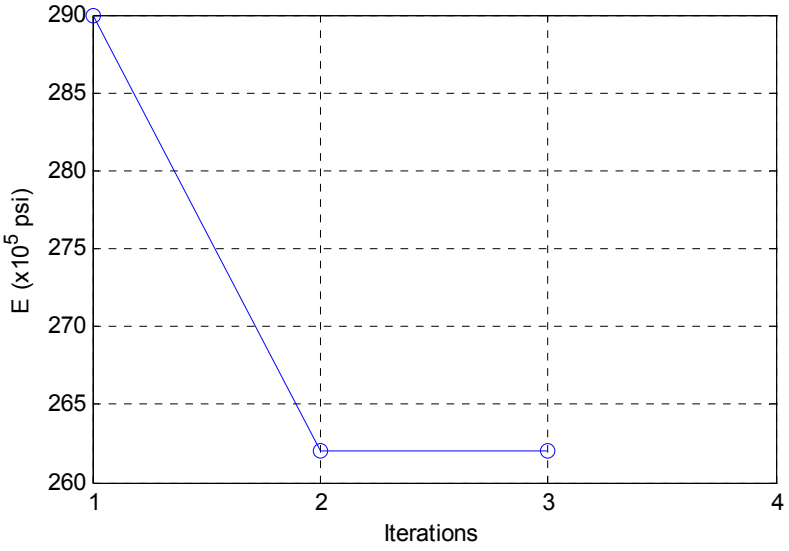

Figure 4-35 Change of the Young's modulus of steel with iteration in Run 1

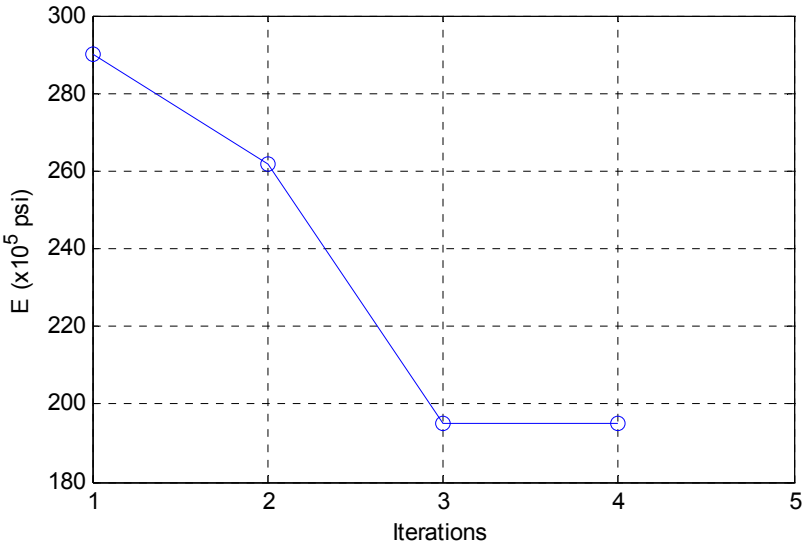

Figure 4-36 Change of the Young's modulus of steel with iteration in Run 2

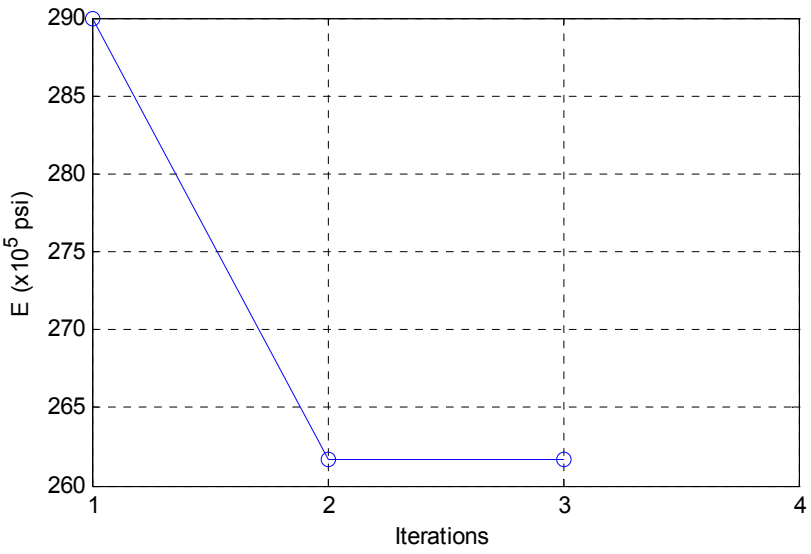

Figure 4-37 Change of the Young's modulus of steel with iteration in Run 3

Table 4-10 Initial and updated parameter with analytical model *A*

Run	Test data source	Updating Para	Initial ($\times 10^5$ psi)	Updated ($\times 10^5$ psi)	Diff (%)
1	**Configuration 1**	*E*	290	262.014	-9.650
2	**Configuration 2**	*E*	290	194.897	-32.499
3	**Configuration 1**	*E*	290	261.724	-9.750

Table 4-11 Correlation between experimental, initial and updated analytical frequencies for runs 1 & 3

Mode #	Test f_T (Hz)	Initial f_I (Hz)	$(f_I-f_T)/f_T$ (%)	Run 1		Run 3	
				Updated f_U (Hz)	$(f_U-f_T)/f_T$ (%)	Updated f_U (Hz)	$(f_U-f_T)/f_T$ (%)
1	4.712	4.910	4.202	4.667	-0.955	4.664	-1.010
2	29.244	30.770	5.218	29.247	0.010	29.231	-0.043
3	82.889	86.158	3.944	81.895	-1.199	81.850	-1.254
4	160.573	168.842	5.150	160.489	-0.052	160.400	-0.108
5	260.945	279.138	6.972	265.328	1.680	265.181	1.623

Table 4-12 Correlation between experimental, initial and updated analytical frequencies for run 2

Mode #	Test f_T (Hz)	Initial f_I (Hz)	$(f_I-f_T)/f_T$·%	Updated f_U (Hz)	$(f_U-f_T)/f_T$·%
1	3.338	4.910	47.094	4.025	20.584
2	24.612	30.770	25.020	25.225	2.490
3	70.820	86.158	21.658	70.631	-0.267
4	127.932				
5	140.535	168.842	-	138.416	-
6	150.973				
7	188.395				
8	245.381	279.138	13.757	228.835	-6.743

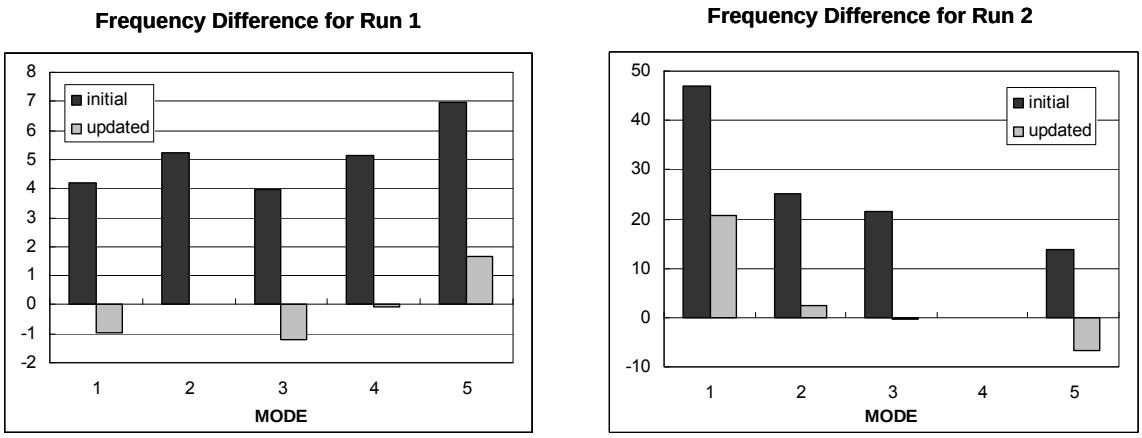

Figure 4-38 Relative frequency differences (%) between experimental and analytical modes

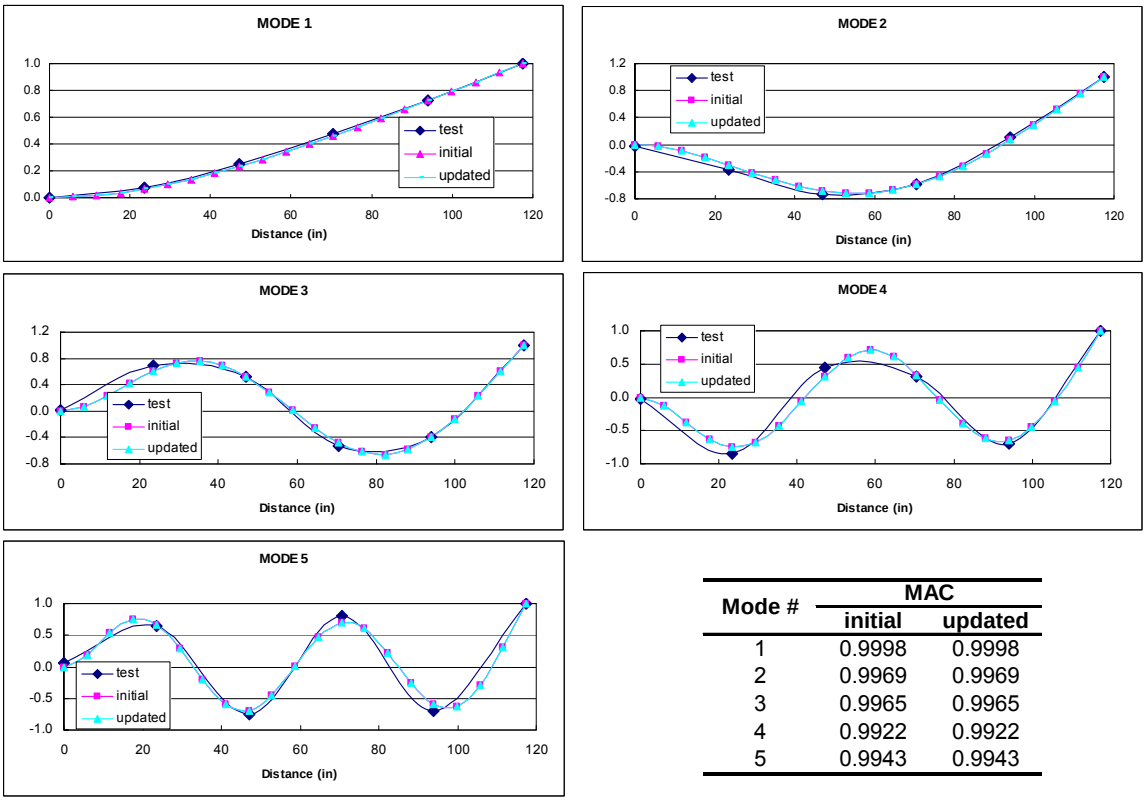

Mode #	MAC	
	initial	updated
1	0.9998	0.9998
2	0.9969	0.9969
3	0.9965	0.9965
4	0.9922	0.9922
5	0.9943	0.9943

Figure 4-39 Correlation of mode shapes from test configuration 1 (Run s 1 and 3)

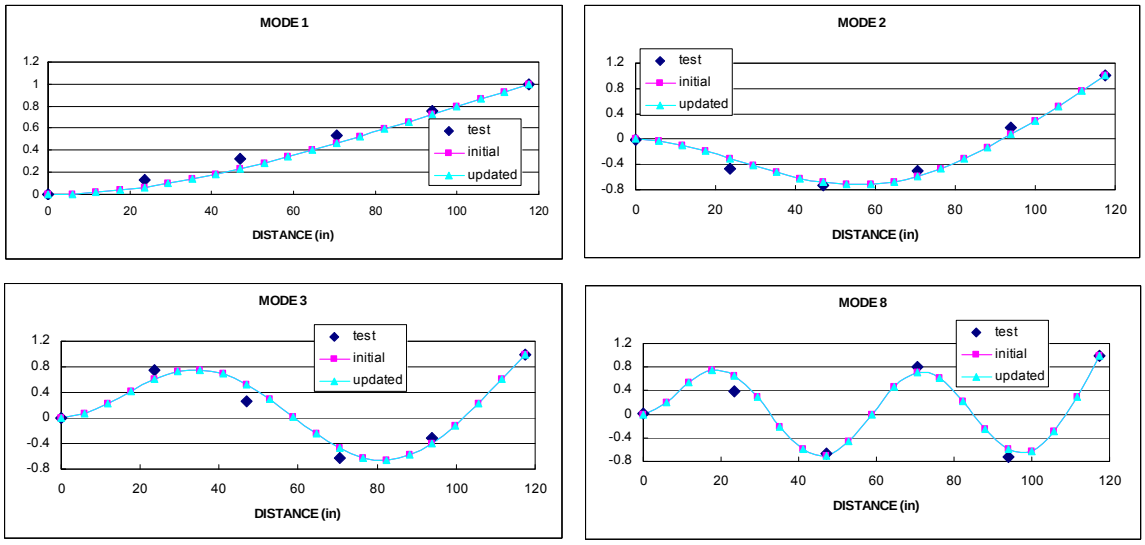

Mode #	MAC	
	initial	updated
1	0.9924	0.9924
2	0.9760	0.9760
3	0.9434	0.9434
4	0.9711	0.9711
5	0.9628	0.9628

Figure 4-40 Correlation of mode shapes from test configuration 2

4.5.3 Discussions about Updating Results

In the first attempt of model updating, a 20-element FE model with fixed boundary condition and erroneous modulus of elasticity was chosen as the initial model for the identification process of the beam under two different configurations. Such a choice was obviously not quite appropriate for the beam under configuration 2, since the flexibility of alumni angle parts in the boundary assembly were designed to permit partial rotation at the support. This situation, however, very much mimic the way how most real-life Sys-Id applications on constructed systems were implemented – set up an initial FE model, take geometry and material properties as the most convenient choices for updating parameters and exclude experimental data which did not have analytical counterparts.

FE model updating showed the strength to reveal actual conditions of a structure by combining numerical analysis and experimental investigation. When an initial FE model is

capable of capturing essential physics of the system of interest and simulating its critical physical behaviors, model updating with a good selection of uncertain parameters is often able to lead to satisfactory updating results. In configuration 1, the test specimen was attached to the steel pedestal with C-shape clamps and hydro-stone and the fixity between the beam and support was approximate to perfectly fixed condition. Therefore the use of an ideally fixed cantilever beam model served as a good start point to simulate the observed physical behaviors. With a decrease of about ten percent in the Young's modulus, the predicted eigen-frequencies in the five modes were all converged to the measured values within two percent of errors.

When the same initial model was applied on the beam under test configuration 2, the modal frequencies yielded from the updated model also considerably improved. However, large different still existed. For instance, the first analytical frequency was still 21 percent less than the experimental counterpart. The cause of the repeated modes remained unknown. Even the improvement in frequency prediction was made possible at a price that the Young's modulus distorted itself by decreasing about 33 percent of its nominal value, which was obviously against the reality. All these evidence showed that current initial model failed to completely and accurately capture the actual physical behaviors of the beam under test configuration 2 and that the modulus of elasticity may not be the dominant factor to control the analysis-test discrepancy. More efforts were in need to discover the controlling epistemic modeling uncertainty associated with it.

Since epistemic type of modeling uncertainty always stems from the lack of the information about the system, additional observations obtained from properly designed, executed and interpreted experiments are the only definitive approach for reducing epistemic uncertainty that clouds constructed system behavior.

4.6 System Identification with Acknowledgement of Epistemic Modeling Uncertainty – the Second Attempt

4.6.1 Dynamic Test to Identify Epistemic Uncertainty

A new dynamic test was designed in order to unveil physical behaviors of the beam with boundary assembly. Seven capacitive accelerometers were utilized in the new instrumentation plan. Two vertical sensors at and close to the tip of the beam remained. One lateral accelerometer was installed at the tip to monitor the lateral vibration of the beam. Since the boundary assembly was designed to be symmetric about the centerline of the beam, the rest four sensors were all located on the same side of the two top steel plates. As shown in Figure 4-41, two of them were to capture vertical movement of the cover plates and two longitudinal ones were for the lateral displacement of the plates ('longitudinal' here was relative to the beam). The elevation view of the test setup was displayed in Figure 4-42.

Hammer impact was applied at every measurement station. The resulting frequency response functions were divided into four groups: (a) vertical sensors on the top plates; (b) vertical sensors on the beam; (c) longitudinal sensors on the top plates and (d) lateral sensor on the beam. As a consequence, four sets of modal frequencies and damping ratios were obtained by processing the grouped FRFs independently. The identified frequencies and damping ratios by CMIF were summarized in Table 4-13 and they were organized in an increasing order of magnitude. From the list, it was observed that some of modes identified from the responses of the plates overlapped with the modes identified from the responses of the beam in the frequency band of interest while some of them were independent on beam vibrations. This observation implied the following facts: (1) the boundary assembly experienced vibrations under the transmitted excitation from the beam; (2) Interactive vibrations existed between the beam and the assembly, which may lead to coupled modes; (3) There are also local vibrations of the plates in both vertical and longitudinal direction. The interactions between the assembly and the beam were believed to be the key factor to

determine the characteristics of repeated modes between 100-200 Hz. It was thus essential to examine the characteristics of each mode observed in the frequency band.

Although all of them demonstrated a deflection shape pattern similar to the 4th bending mode of an ideally fixed cantilever beam, the identified four vertical beam modes actually were different from each other. The mode f = 150.99 Hz was a pure beam mode, with little coupling with the vibrations of the boundary assembly. The f = 128 Hz mode was a global mode – the beam had a vivid vertical vibration and it together with the local vertical movement of top plates dominated this mode while the top plate slightly vibrated laterally. The relatively small peak showed up in the FRF spectra of beam vertical sensors f = 142 Hz mode was a vertical plate mode, coupled with beam vertical mode. For the mode of f = 189 Hz, both the beam and plate vibrated lively with similar level of vibrations and thus it was a global mode of the whole system. The details were shown in Figure 4-43.

The additional dynamic test on the whole structure provided a global view to understand physical behaviors of the system. The original test plan only instrumented the test beam, since the goal of vibration tests was to obtain the dynamic properties of the beam.

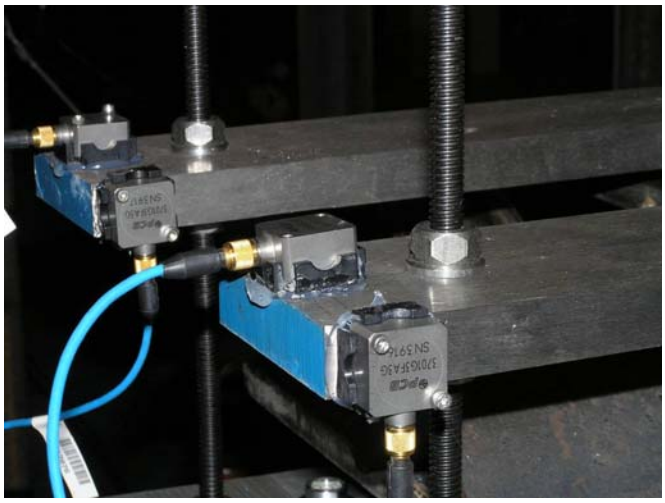

Figure 4-41 Four accelerometers on the boundary assembly

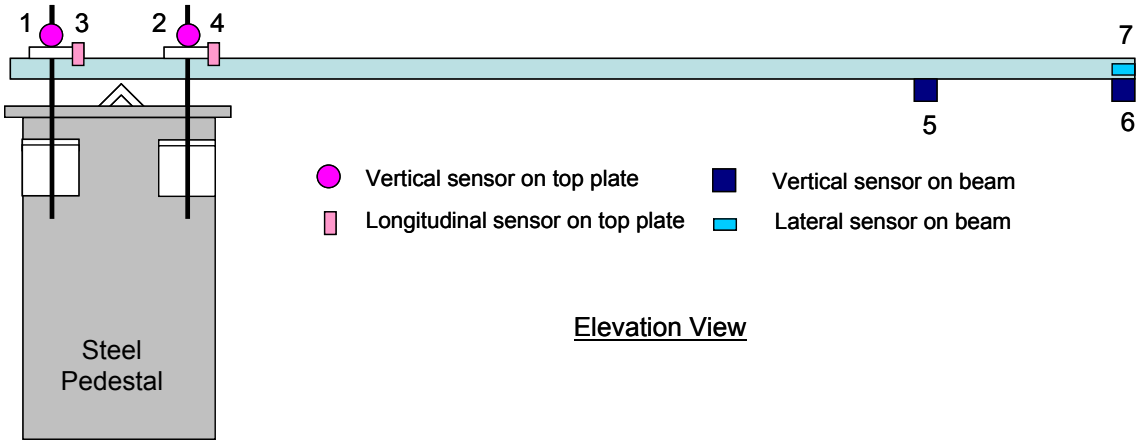

Figure 4-42 Test instrumentation

Table 4-13 Summary of identified modes of beam and top plates between 100-200 Hz

Beam				**Top Plates**			
Vertical		**Lateral**		**Longitudinal**		**Vertical**	
Freq (Hz)	Damping (%)	Freq (Hz)	Damping (%)	Freq (Hz)	Damping (%)	Freq (Hz)	Damping (%)
		114.366	0.599	114.548	0.440		
		118.844	0.361	119.135	0.287	119.204	0.156
		121.750	0.026	121.280	0.092	121.630	0.232
128.320	**0.215**			**128.363**	**0.093**	**128.350**	**0.199**
						132.560	0.232
				136.276	0.056		
142.920	**0.101**					**143.170**	**0.249**
150.99	**0.306**						
		156.532	0.060				
						164.656	0.253
						173.323	0.264
		178.190	0.246	178.499	0.201	178.323	0.105
188.89	**0.536**					**188.870**	**0.395**
						195.935	0.555

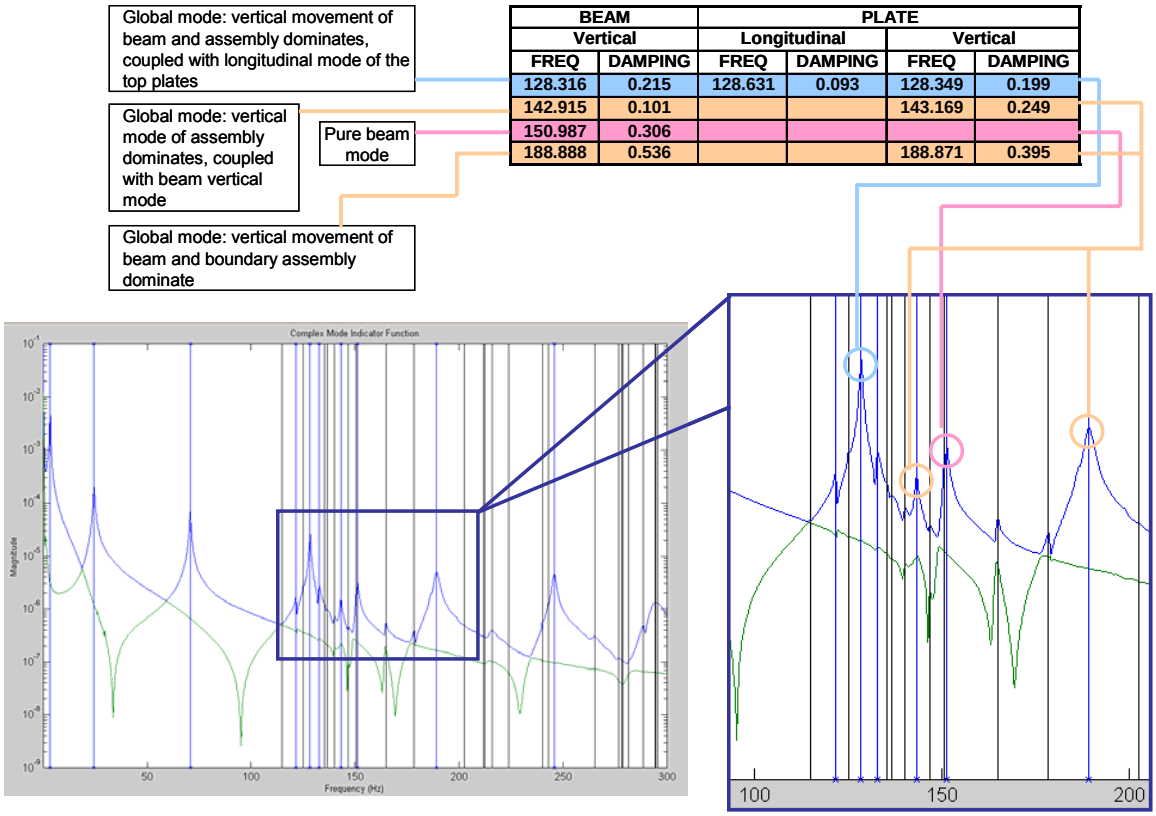

Figure 4-43 Classification of repeated modes of the beam

4.6.2 Model Updating by Inverse Eigen-sensitivity Method – the Second Attempt

In the previous attempt of model updating, a 20-element initial model with fixed boundary condition (referred as model A) was utilized to interpret the experimental results observed from the two test configurations respectively. The updating for the beam under the first configuration yielded reasonably good results. When the same initial model was applied to the beam with the second configuration, considerable test-analysis discrepancy remained and the updated parameter lost its physical significance. Some unknown epistemic modeling uncertainty inherent in the model seriously impaired its capability to simulate the observed structural behaviors.

Thus new initial finite element model was required to properly acknowledge the vivid vibrations the boundary assembly. Ideally a three-dimensional model including the beam as well all the components of the boundary assembly should be the best choice to completely simulate the whole system. However, a 20-element beam model was used, with the vibrations of the boundary

assembly abstracted as two boundary springs, one rotational spring and a vertical translational spring (referred as model B). Although it was obvious that model B would again not able to simulate repeated modes due to the vibration coupling between the beam and the plates, such a choice was based on the following considerations: (1) The effects of the boundary movements were in some degree equivalent to the boundary springs. (2) The resulting model B would be more consistent with model A and therefore it would be easier to compare the updating results; (3) Expanding the model to include the details of every component of the boundary assembly would inevitably to introduce additional uncertainty sources such as connectivity conditions between the rods and top plates. This may not only significantly complicate the identification process but also distract the main focus. Thus it was a compromise which had to be made.

4.6.2.1 Updating Process

To be consistent, the same initial FE model (model B) was also used to update the beam under the first configuration.

Once the initial FE model was determined, a set of candidate model parameters could be selected and they were including the Young's modulus E, the stiffness of the boundary rotational spring K_r and the stiffness of the vertical boundary translational spring K_t. The initial value for E was again set to its nominal value 29000 kpi. The stiffness of springs was initially set to extremely high, which was equivalent to the ideally fixed support conditions.

The residual vector of the updating was comprised of both the eigenvalue information and the unity normalized modal vectors of all paired modes. For the first test configuration, all the five sets of paired modes were included in the residual vector. For the second configuration, besides the four sets of pair modes, the experimental mode f = 150.99 Hz was chosen to match up with the analytical fourth bending mode because it was characterized from additional dynamic test as pure beam vertical mode in which beam vibration had absolute dominance.

4.6.2.2 Sensitivity Analysis

Before model updating computation was carried out, the sensitivities of all updating parameter candidates with respect to the analytical modal data was evaluated with sensitivity analysis in conjunction with factorial experiment design (see details in Chapter 3). A 2-level full factorial experimental design scheme was applied to evaluate the sensitivities of each candidate updating parameters. In order to do so, each factor was numbered and their uncertainty was predefined as the Young's modulus in a range of ±10% of its initial value and the rotational and translational spring stiffness in a range of ±50% of their initial values respectively. The objective function for the sensitivity analysis was defined as the summation of the norm of relative frequency difference and the norm of ULS indexes at each run of the designed tests. Table 4-14 displayed the 2-level 8-run full factorial experiment design.

As shown in Figure 4-44 through Figure 4-46, the effect of rotational spring stiffness controlled the changes in predicted modal data and thus was the dominant factor among the candidates. The interaction effect of the Young's modulus and rotational stiffness of the boundary spring also had considerable impact on the analytical predictions. On the other hand, the vertical spring stiffness was insensitive with modal properties, which implied that including the parameter of the vertical spring stiffness in the updating process may lead to ill-conditioning of the sensitivity matrix at updating iterations. It was thus ignored in the following updating sessions by assuming that the beam was pin-supported with a rotational spring.

Table 4-14 2-level 8-run full factorial design

Run Number	Factor 1: E	Factor 2: K_r	Factor 3: K_t
1	+	+	+
2	+	+	-
3	+	-	+
4	+	-	-
5	-	+	+
6	-	+	-
7	-	-	+
8	-	-	-

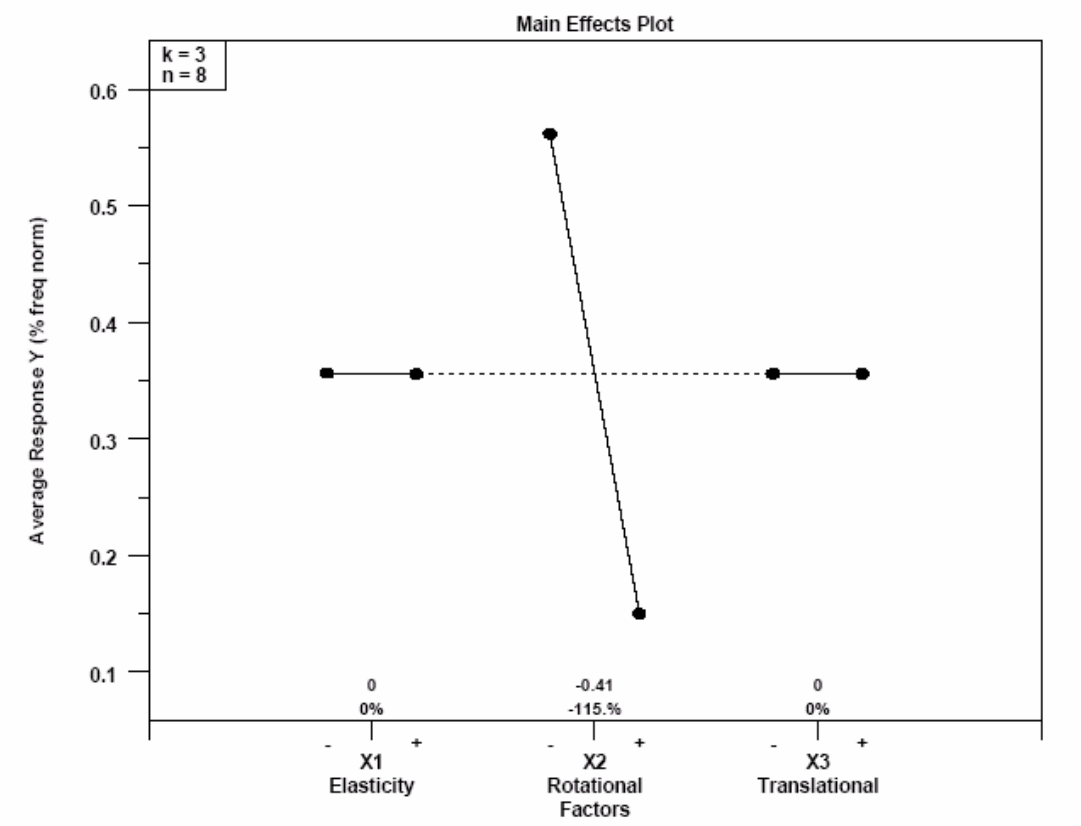

Figure 4-44 Main effect of each factor

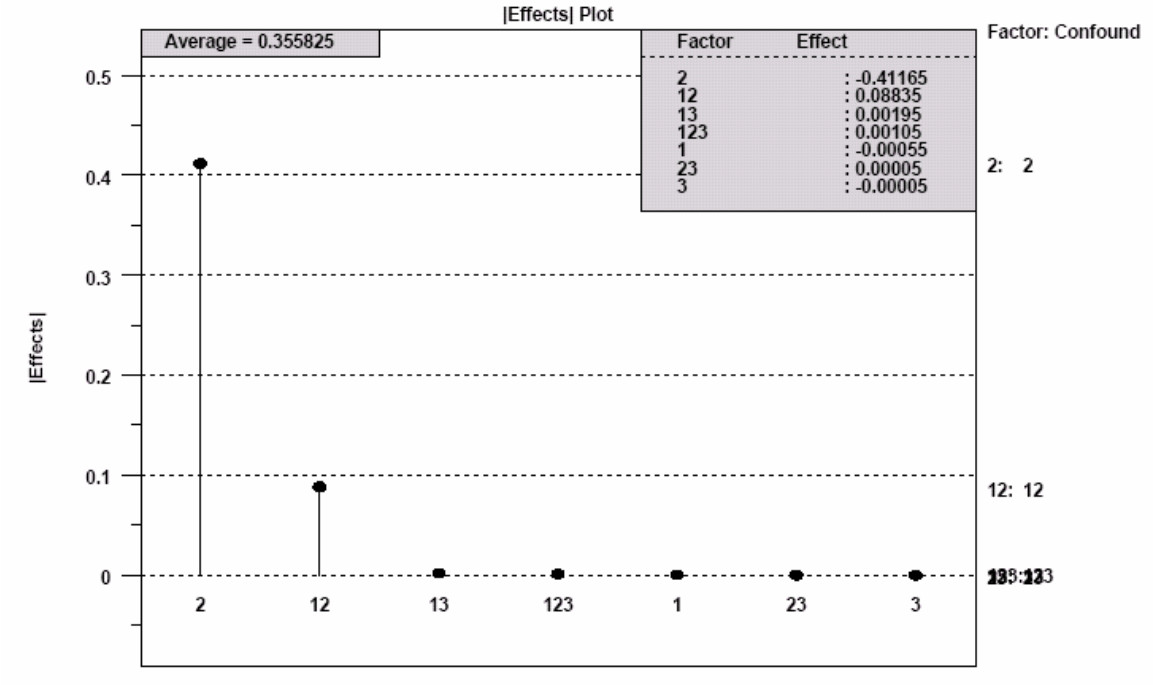

Figure 4-45 |Effect| plot

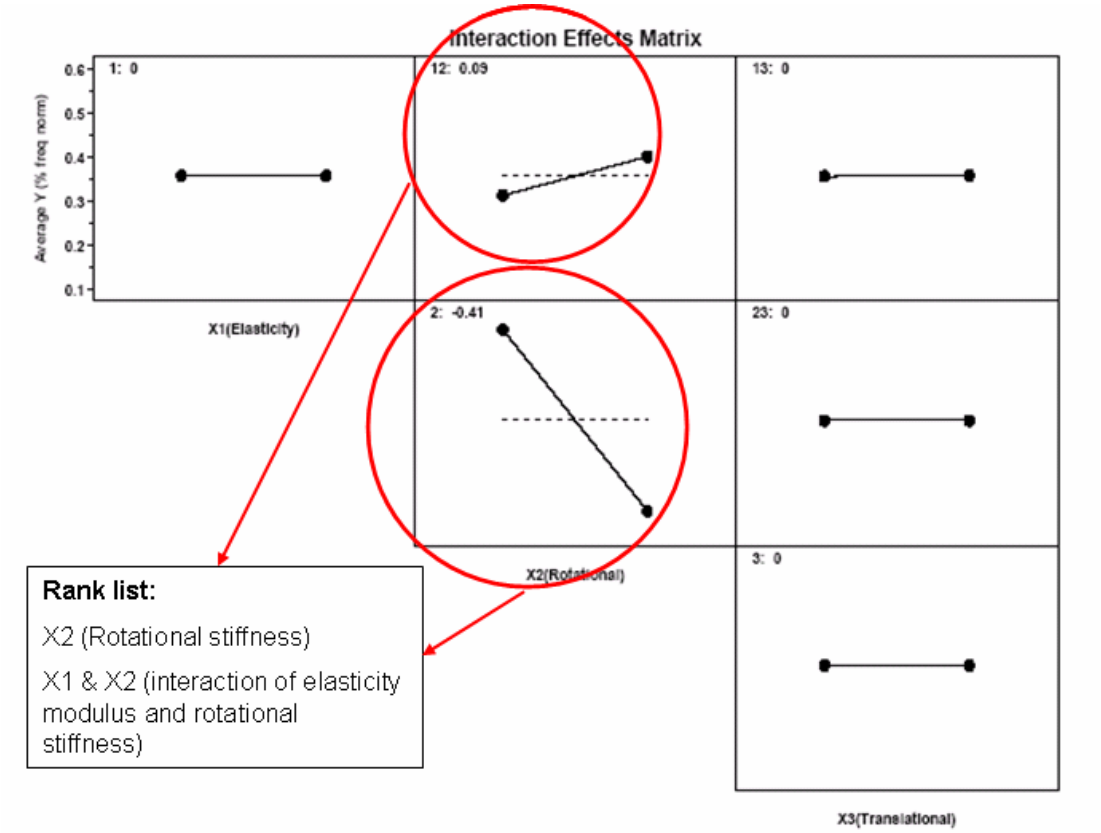

Figure 4-46 Interaction effects

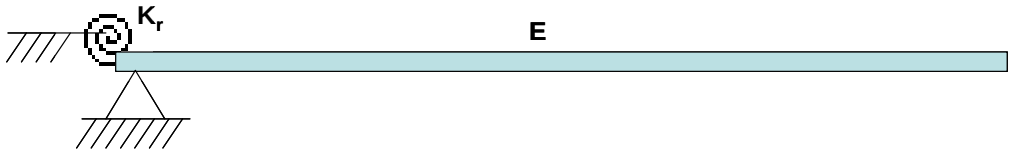

Figure 4-47 Initial model *B*

4.6.2.3 Model Updating & Results

Two updating sessions run 3 through 4 were performed using the initial model *B*. For the beam under configuration 1, the updated model yielded improved predictions on the modal frequencies and the results were very similar to the updated results using the initial model *A*, as shown in Table 4-16. However, by introducing a new variable at the boundary of the beam, the updated Young's modulus was only about 3.6% away from its nominal value. The decrease in the stiffness of the boundary rotational spring implied that the 'ideally fixed' condition was

extremely difficult to simulate even in the more advantageous laboratory environment. Although no significant improvement was observed from the updated mode shapes, both the predictions from the initial and updated model were very close to the experimental observations. The comparison of initial and updated mode shapes was displayed in Figure 4-53.

Table 4-17 illustrated the initial and updated modal frequencies predicted by the initial model *B*. The discrepancy in the frequency of all of the five set of paired modes were successfully reduced within four percent. And the deflection shapes of the modes were also improved considerably as shown in Figure 4-54. As opposed to the results obtained in the first updating attempt using, the improvement in test-analysis correlation was obtained while keeping the physical significance of the model. For instance, the Young's modulus just slightly fluctuated from its nominal value, which agreed with the well accepted fact that the variation range of the modulus of elasticity of steel is often very small. The observed decrease in the rotational spring stiffness represented the flexibility introduced by the boundary assembly at the support.

Since the boundary assembly was not explicitly simulated in the initial model *B*, the interactions between the support and the beam were absent from the analytical predictions, as expected. However, the excellent agreement in the predicted and experimental modal parameters proved that the flexibility at the support controlled the dynamic characteristics of the beam under the configuration 2 and its influence was successfully abstracted by the use of the boundary rotational spring.

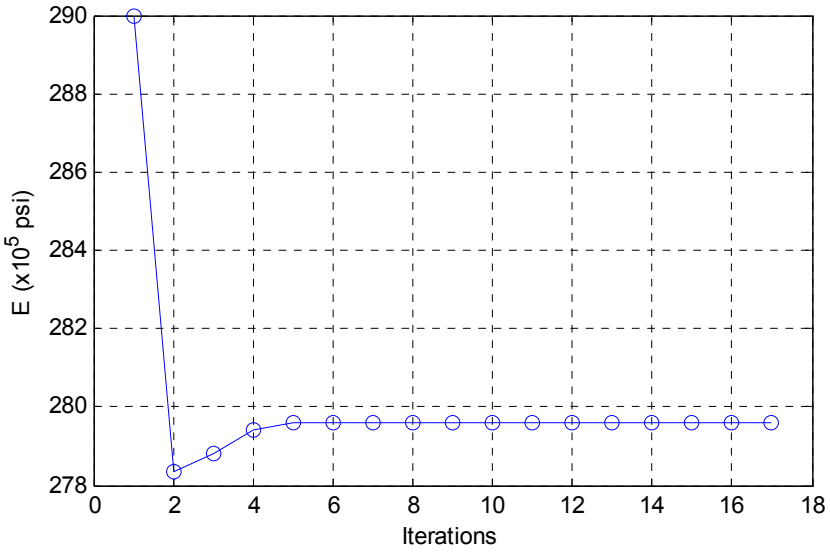

Figure 4-48 Change of the Young's modulus of steel with iteration in Run 4

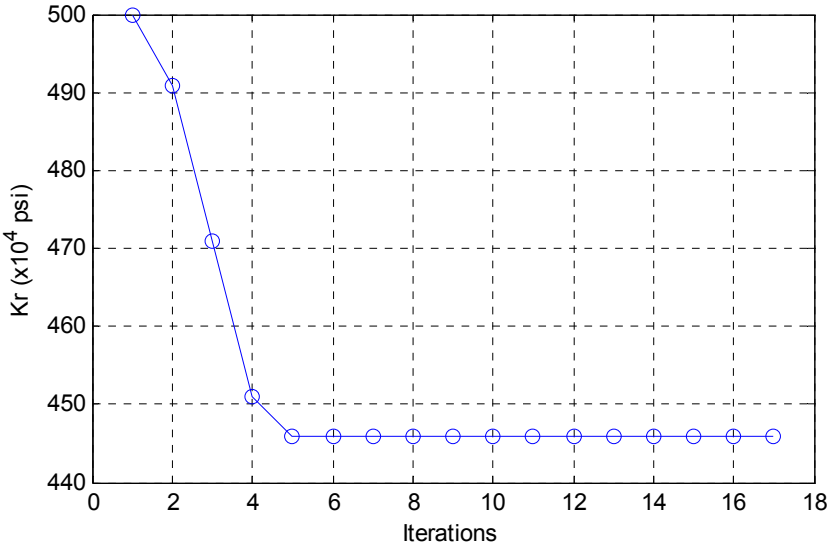

Figure 4-49 Change of the boundary rotary spring stiffness with iteration in Run 4

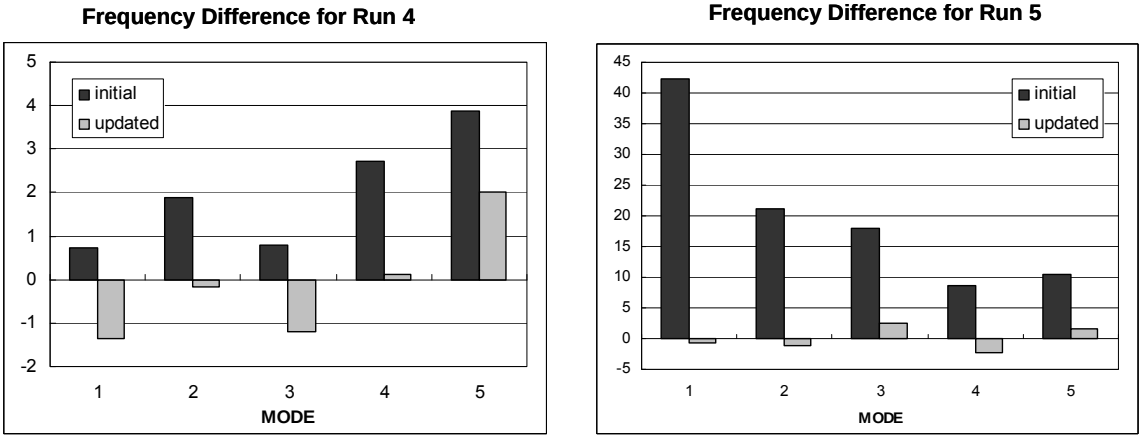

Figure 4-50 Relative frequency differences (%) between experimental and analytical modes

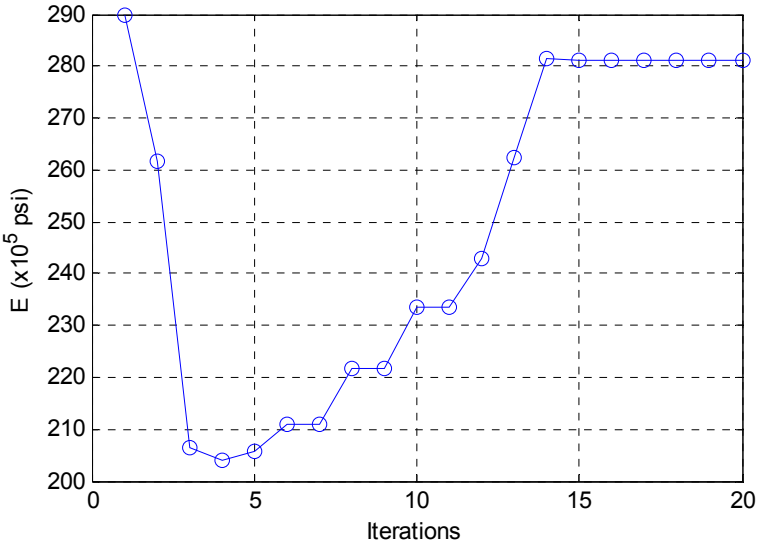

Figure 4-51 of the Young's modulus of steel with iteration in Run 5

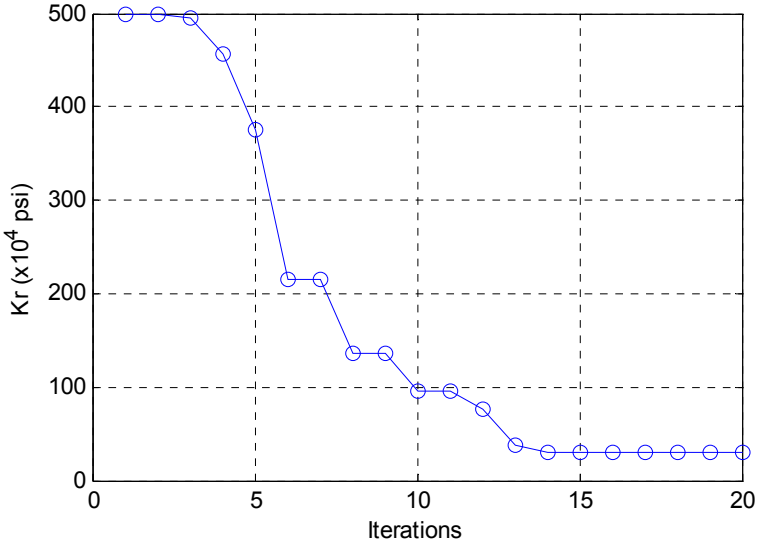

Figure 4-52 Change of the boundary rotary spring stiffness with iteration in Run 5

Table 4-15 Initial and updated parameters with analytical model *B*

Run	Test data source	Updating Para	Initial	Updated	Diff (%)
4	**Configuration 1**	E ($\times 10^5$ psi)	290	279.603	-3.585
	Freq & mode shapes	K_r ($\times 10^4$ psi)	500	445.900	-10.820
5	**Configuration 2**	E ($\times 10^5$ psi)	290	280.983	-3.109
	Freq & mode shapes	K_r ($\times 10^4$ psi)	500	30.740	-93.852

Table 4-16 Updated modal frequencies for the beam under test configuration 1 (run 4)

Mode #	Test f_T (Hz)	Initial f_I (Hz)	$(f_I-f_T)/f_T$ (%)	Run 4	
				Updated f_U (Hz)	$(f_U-f_T)/f_T$ (%)
1	4.712	4.746	0.722	4.648	-1.356
2	29.244	29.798	1.894	29.191	-0.180
3	82.889	83.556	0.805	81.885	-1.212
4	160.573	163.912	2.709	160.743	0.106
5	260.945	271.071	3.881	266.162	1.999

Table 4-17 Updated modal frequencies for the beam under test configuration 2 (run 5)

Mode #	Test f_T (Hz)	Initial f_I (Hz)	$(f_I-f_T)/f_T$ (%)	Run 5	
				Updated f_U (Hz)	$(f_U-f_T)/f_T$ (%)
1	3.338	4.746	42.182	3.317	-0.619
2	24.612	29.799	21.072	24.328	-1.153
3	70.820	83.571	17.983	72.567	2.467
4	150.973	164.016	8.571	147.477	-2.316
5	245.381	271.532	10.470	249.424	1.648

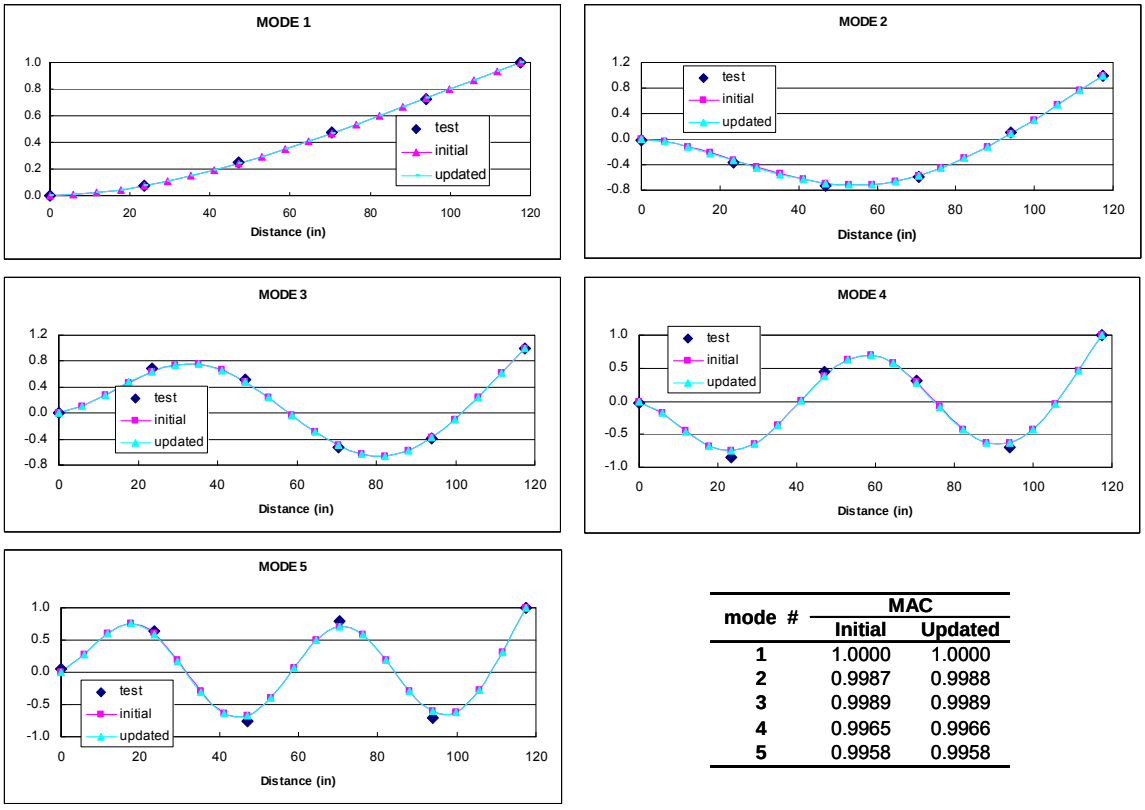

mode #	MAC	
	Initial	Updated
1	1.0000	1.0000
2	0.9987	0.9988
3	0.9989	0.9989
4	0.9965	0.9966
5	0.9958	0.9958

Figure 4-53 Updated mode shapes for the beam under test configuration 1

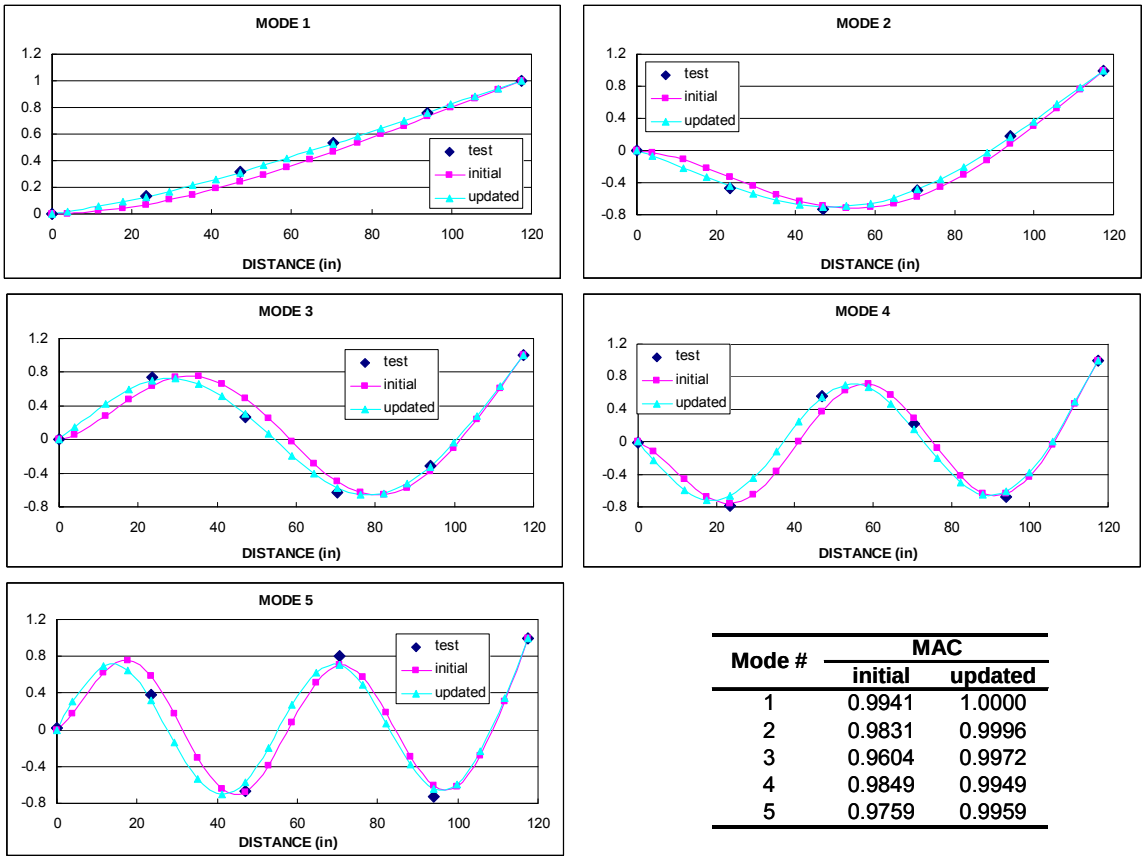

Mode #	MAC	
	initial	updated
1	0.9941	1.0000
2	0.9831	0.9996
3	0.9604	0.9972
4	0.9849	0.9949
5	0.9759	0.9959

Figure 4-54 Updated mode shapes for the beam under test configuration 2

Table 4-18 Comparison of updated parameters

Updating Parameter	Nominal	Run 1: Config 1 with model *A*	Run 2: Config 2 with model *A*	Run 4: Config 1 with model *B*	Run 5: Config 2 with model *B*
E ($\times 10^5$ psi)	290	261.724	194.896	279.603	280.983
Diff (%)		-9.750	-32.795	-3.585	-3.109

4.6.3 Discussion about the Results from the Two Identification Attempts

One common model parameter incorporated in the four updating runs of the two updating attempts was the modulus of elasticity of steel. Theoretically they should converge to the same value after updating. However, significant difference was observed from a side-by-side comparison between the updating results from the four runs, as shown in Table 4-18. When the model *A* was used as the initial model for updating, the value of the updating parameter decreased by one third of it nominal value for the test configuration 2, in contrast with less than 10 percent

of decrease for the test configuration 1. The predictions for the modal properties of the beam under configuration 1 and 2 were both improved but large discrepancy still existed in run 2.

When the updating process started from the initial model *B*, the deviation of the steel modulus of elasticity from its nominal value was very slight in the two updating runs, both within 5 percent. Although they didn't converge to the exact same value, the two updated values were very close. In both cases, the updated model yielded the modal parameters of the beam similar to the experimental results. Good correlation between the updated parameter as well as the modal predictions proved that the initial model *B* efficiently conceptualize the influences of the rotary movement of the boundary assembly on the beam without explicitly incorporating the boundary assembly in the initial model.

Therefore it could be concluded from the observations that the existing of epistemic modeling uncertainty would seriously impair the reliability of the identification results. For the extreme case of the cantilever beam presented here, the updating process (run 2) yielded a model parameter without physical significance and a calibrated model which failed to reproduce the experiment results.

More importantly, the sharp comparison shown in Table 4-18 implied that the selected model parameter for updating would tend to compensate for the influence of epistemic modeling error inherent in the initial model by distorting itself in order to minimize the test-analysis discrepancy. In another word, the unexpected dramatic decrease in the material property of the steel served as a good indicator to remind us of the existence of significant epistemic modeling error in initial analytical model. This could be further generalized as that abnormal change in a dummy updating parameter which was sensitive to the change of modal data and of small variability indicates the existence of epistemic modeling error.

Since modeling error due to epistemic mechanism stemmed from the lack of information about the system under study, most efficient way to mitigate it was additional experiment. In the

cantilever study, the re-designed impact test recognized the interactive movement of the boundary assembly. The epistemic modeling error embedded in the initial model *A* was then successfully mitigated by introducing boundary flexibility in the model *B*. This may be impractical in applications on real-life constructed civil structures.

4.7 Conclusion

By using a cantilever beam set up with two different configurations as a test bed, this chapter investigated the influence of modeling error especially the one with epistemic mechanism on the identification results and proper ways to recognize and mitigate them. The following conclusions could be drawn from this study.

The existence of epistemic modeling error in the initial model for updating often led to unsatisfactory updating results. Although the predictions yielded from the updated model showed considerable improvement in their correlation with test results, the updated model parameters already lost their physical significance. As a result, the reliability of calibrated models would inevitably be in question.

When significant modeling error was not recognized and properly incorporated in the updating process, the selected updating parameters tended to distort themselves to compensate for the influence of the un-acknowledged modeling error. Therefore one or more dummy model parameters, which were sensitive to the change of the modal data and of small variability, could be selected as updating parameters and any unexpected large fluctuation of them indicated the existence of epistemic modeling error.

Additional test data would increase the capability to efficiently mitigate modeling error due to epistemic mechanism. However, ‘additional’ herein meant additional information contained in the re-designed tests, rather than simply repeating the test.

The proposed error localization functions may be theoretically sound and even feasible for cases where simulated experimental data were used, they collapsed easily when applied on real-life systems, even in the simple cantilever beam system. One of the big obstacles for the application of these error indexes is that they often require full set of experimental data. This was impractical because the measurement degrees of freedom were often far less than the analytical degrees or freedom when Sys-Id was applied on constructed civil structures.

Sensitivity analysis based on 2-level factorial experiment design was efficient and capable to identify the interactions of multiple parameters. But the number of designed experiments increased exponentially as the increase in the number of parameters of concerned.

5 System Identification of the Henry Hudson Bridge

5.1 Introduction

This chapter presented the Sys-Id investigation conducted on a real-life long-span steel arch bridge – the Henry Hudson Bridge. It was part of a project led by the Parsons Transportation Group at New York City, of which the primary goal was seismic evaluation and retrofit investigation of the seventy-year bridge in order to protect it from any future seismic event. The output of the Sys-Id was thus expected to be an accurate and complete analytical model that was capable of predicting the performances of the bridge under various critical loading patterns.

It was shown that a reasonable level of confidence could be achieved on the calibrated analytical model by interactively combining element-level three-dimensional a-priori model and ambient vibration monitoring technique. This study demonstrated the strength of integrative Sys-Id in providing in-depth understanding of true state of large-size constructed civil engineering structures. In the meanwhile, the limitations of Sys-Id and the challenges posed for its widespread on real-life systems were also discussed. In the cantilever beam case presented in the previous chapter, the well established beam theory as well as the ideal experiment environment made it possible to successfully localize the controlling epistemic modeling error which dominated the modal properties of the beam. The recognition and mitigation was further achieved through additional dynamic tests. For large-scale real-life civil structures, however, significant sources of uncertainty especial the ones with epistemic mechanisms often occur and propagate at each stage of Sys-Id paradigm. They may arise due to the lack of as-built geometry and material properties, geometric complexity, obscure boundary and connectivity conditions, varying loading environment, intrinsic force distribution and etc. And the combinations of various sources of uncertainty may accumulate or cancel out as the process of system identification and further complicate the recognition and mitigation of uncertainty.

With a deep appreciation about the strength and weakness of Sys-Id applications on constructed systems, the completeness of the calibrated model was evaluated with a global index – the modulus of elasticity of steel, as in the cantilever beam case. The idea behind it lies in the fact that the material property of steel E is a global model parameter with little variability and sensitive to the change of modal data. When significant epistemic modeling uncertainty still existed in the calibrated model, it would distort itself to compensate the test-analysis discrepancy. Therefore if the calibrated model would converge at a value of E other than its nominal value, the change of E could be considered as the compensation made for the existence of epistemic modeling error; otherwise, the calibrated model was the most admissible model with available data, if it may not be valid to conclude that the calibrated model is free of modeling error. Similar idea could be generalized to most of steel structures. For concrete structures, the modulus of elasticity of concrete usually has large variability and some other global model parameters which are with known little variability but sensitive to the change of structural responses could be used.

5.2 Bridge Description

The Henry Hudson Bridge is a major long-span steel arch bridge located in New York City. The bridge spans the Harlem River and connects northern Manhattan to Bronx. The bridge was designed by David Steinman and was opened in 1936. The Henry Hudson Bridge is a toll structure and is owned and operated by the MTA Bridge and Tunnel Authority.

The total length of the bridge and approaches is 2209 feet. The main span of the bridge, which is shown in Figure 5-1, consists of an 840 feet long fixed plate girder arch that provides a vertical clearance of 44 m. The arch span is flanked at its northern end by a steel tower structure, a 200 feet long viaduct and a 270 feet long approach. The arch span is flanked at its southern end by a steel tower structure, a 300 feet long viaduct, and a 409 feet long approach. The viaducts at the northern and southern ends are supported by steel bent structure of various heights at every 18 m. The width of the bridge measured from center-to-center of the vertical columns is 15 m.

The bridge normally carries a total of seven lanes of traffic on two levels, with three lanes devoted to northbound traffic on the upper level and four lanes devoted to southbound traffic on the lower level. The traffic using the bridge consists mainly of light vehicles since commercial truck traffic is prohibited. The bridge was in the process of being re-painted while the ambient vibration testing was being performed, and the contractor periodically had temporary lane closures on the upper and lower levels and heavy equipment on the spans.

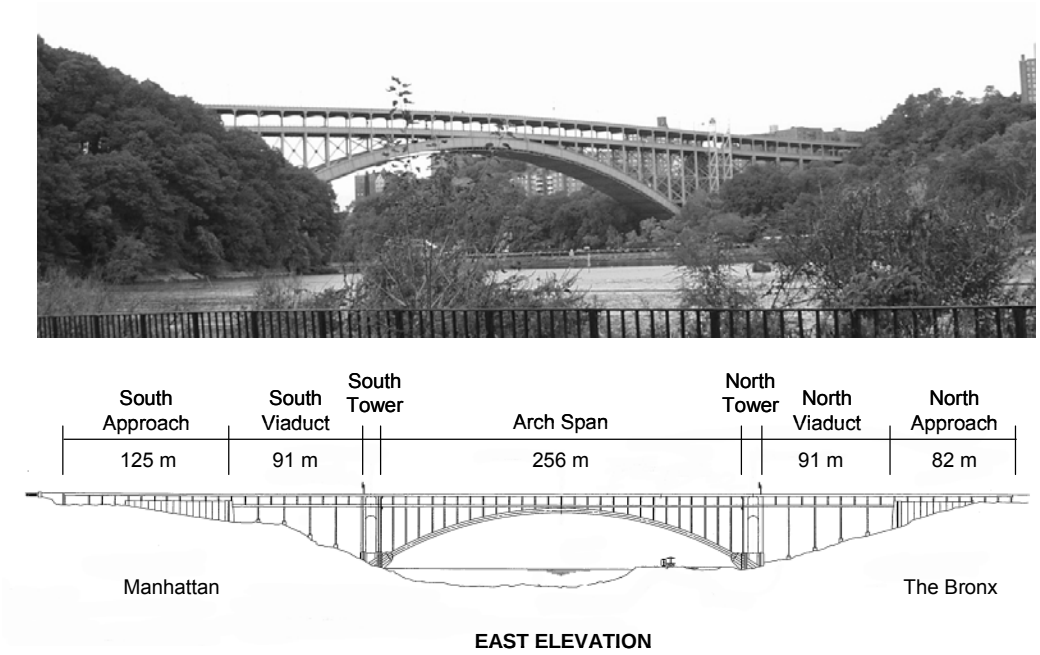

Figure 5-1 Henry Hudson Bridge

5.3 Finite Element Modeling of the Bridge

The same engineering system can usually be simulated with different level of abstraction of the physics in the system. The choice of an analytical model represents a delicate balancing act. The model must be able to capture the essential physics while deliberately ignoring aspects irrelevant to engineering decisions. Hence the first major task for St-Id of the Henry Hudson Bridge was to construct a-priori analytical model. This is not only essential to fulfill the primary goal of this project as seismic performance evaluation and retrofit investigation, but also required to determine important experimentation parameters such as the amount and position of sensors

and critical frequency band of interest. The initial finite element model was constructed by Parsons based on the design and construction documents, maintenance and inspection records. Usually the site observations and material sampling test will permit the analyst to attain firsthand information on current condition of the bridge and identify any anomalies caused by construction or any post-construction events such as traffic accident and retrofit. Consequently the a-priori analytical model was supposed to be a best effort at modeling the three dimensional geometry, support and continuity conditions of the existing structure. However, the accuracy in such a simulation of mass and stiffness distribution as well as damping mechanism of the structure could only be verified by field testing on the bridge.

An element-level FE model was constructed in SAP2000 to idealize the dimensional characteristics and geometric details of the bridge, as shown in Figure 5-2. The model excluded the two approach spans, containing only the main arch span and two viaduct spans. Each real structural element was modeled with at least one analytical element. The important issue was to represent structural members with properly selected element type. The upper and lower decks were discretized into shell elements with six degrees of freedom at each node in order to capture in-plane and out-of-plane deformations of the deck slab. The stringers under the deck were not explicitly simulated and instead their contribution to the floor system was smeared in the model. Three-dimensional beam elements were used to represent the floor beams, verticals, arch ribs, and bents while the bracing and tower truss members were modeled with bar elements to mimic actual end connections. The dimensions of the members were defined based on the design documents. All elements were carefully grouped according to their locations and functions so that it was easy to check whether the local axis orientation of elements in the model conformed to the actual orientation of the members of the bridge.

The main arch, towers as well as bents on the south and north viaduct spans were all rested on massive concrete blocks which then connected with the foundations of the bridge. Taking into

account the superstructure of the bridge only, the initial FE model ignored the structure-foundation interaction and simply utilized pinned or fixed restraints to simulate the support conditions. The expansion joints were located at the interface between the deck and tower at both the deck levels and they were movement system designed to accommodate the longitudinal deformation of the structure under temperature change. The three layers in the lateral direction of the bridge – upper deck, lower deck and arch ribs – were connected with vertical members. In order to ensure the integrity of the structure under vibration, joint constraints were assigned at these interfaces. Weightless rigid links were utilized to simulate connections between the deck and exterior roadway girders and between the deck and floor beams. This was due to the fact that elements in SAP2000 were generally orientated by their centerline. Wind linkage mechanisms were simulated with appropriate releases.

For the deck slab, the unit weight of the deck concrete was assumed to be 150 lb/ft^2. The Young's modulus was assumed to be 3,000 ksi and the shear modulus was 1,250 ksi. For the steel components, the Young's modulus was assumed to be 29,000 ksi and the corresponding shear modulus was taken as 11,154 ksi. These values were the nominal values for material properties utilized in the initial FE model of the bridge.

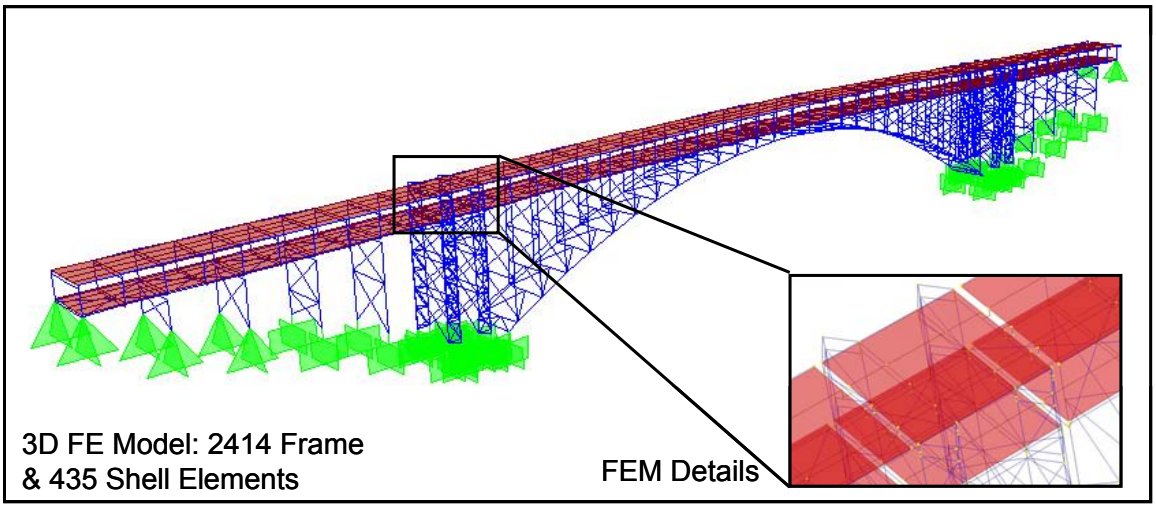

Figure 5-2 Initial Finite element model of the bridge

5.3.1 Sensitivity Analysis Based on the Initial FE Model

After the initial FE model was completed, reviewing some preliminary analysis results through graphical interface and spreadsheet is usually an effective tool to exclude any blatant errors during the model construction, such as geometry and orientation of various elements. However it is yet insufficient for an accurate and complete model. Sensitivity analysis of a selected set of critical model parameters with respect to dynamic responses is frequently utilized to provide insights on physical behaviors and interactions of different components of the structure, although the development of analytical model was still at its infant stage. The primary benefit of sensitivity analysis at this point is to reveal relative importance of each parameter and establish critical ones, since different parameters are not expected to have equal influence on the model response. It should also be noted that sensitive parameters are not necessarily the most uncertain ones and thus they may be not the factors which dominate discrepancy between test and analysis. The interested parameters may include the geometry of the structure (3D idealizations, positions of the nodes and analytical elements), the constitutive properties (material properties, mass and stiffness), and boundary and continuity conditions.

In the sensitivity study, a selected set of parameters from the initial FE model were incrementally adjusted in a predefined bounds and only one parameter was examined each time while the others were set as their nominal values. Although the “one factor each time” strategy was unable to yield information about possible interactions between multiple parameters, it would still provide some insight on the critical parameters which controlled the variation of the modal properties of the structure. Due to the large scale of the model, the influence of each considered parameter was not evaluated at element level and the alteration of the parameter would affect all related elements.

Research experience on long-span bridges indicated that the most sensitive parameters can be material properties, boundary and continuity conditions (Aktan et al 1998). For the bridge under study, the model parameters which were selected for sensitivity analysis included:

(1) The Young's modulus of the steel;

(2) The Young's modulus of the deck concrete;

(3) Variations in boundary conditions;

(4) The constraints between viaduct-deck-arch interface at both the upper and lower decks;

(5) The stiffness of the lateral translational springs located at each end of the two viaduct spans;

The first step of sensitivity analysis was to establish the uncertainty bounds of the selected parameters based on their nominal values. It was always a good rule of thumb to maintain the physical meaning of each parameter. First of all, properties of the two main materials steel and concrete were taken into account. The upper and lower bounds of the Young's modulus of steel members of the bridge were assumed to be 15 percent greater and less than the nominal value given in AISC manual. The variability in the material properties of concrete, both initially and due to deterioration over time, were often much higher than that of steel. The bounds of the Young's modulus were set to be ±30 percent away from its nominal value.

Since only superstructure of the bridge was simulated in the model, boundary conditions representing the structure-foundation interface were was also a critical issue. Previous study on the cantilever beam indicated that prevailing uncertainty about flexibility and displacement kinematics may exist in these regions. In the preliminary bridge model, fixed restraints were utilized to simulate the support conditions of the arch ends, tower and most of viaduct bents, while the southernmost three bents and the northernmost one were modeled using pinned

supports. In sensitivity study, the rotational degrees of freedom in the pinned supports were modified to be fully fixed.

Expansion joints were located at the interface between the viaduct span, tower and the arch span at the two deck levels and thus the continuity conditions between these members determined the behaviors of the movement system of the structure.

The two lateral translational springs were located at the two extreme ends of the south and north viaduct spans of the bridge. They were introduced to take into account the confinement by the approach spans which were excluded from the model. In the initial model, the value of the two spring stiffness was assumed to be 1089 kip/ft. The impact of two lateral springs with translational stiffness would be examined by adjusting the value of spring stiffness from 0 to infinity.

In the initial model, the concrete deck was discretized with a rather coarse mesh size. Each panel of the deck was simulated with only four shell elements. Therefore the convergence of existing deck shell in the initial model was refined by a factor of 2, which meant each shell element was divided in four in the refined model. As a result, there were 16 shell elements in each bridge panel in stead of the original 4. The mesh convergence study was done to make sure that converged global response could be achieved with current discretization. After finer mesh of the deck slab was set up, the floor beams were refined accordingly and joint constraints similar to the ones defined for shell nodes and the corresponding floor beam nodes in initial FE model were assigned to newly created nodes to simulate composite action of the floor system.

5.3.2 Results of Sensitivity Analysis

Modal analysis was performed on the nominal FE model and all the modified models with variation of parameters. The changes in the resulting eigenfrequencies, mode shapes and modal density (i.e. spacing of frequencies) with respective to the fluctuation of one specific parameter

was examined to evaluate the relative importance of each parameter. Specifically, the variation in the modal parameters (frequencies and order of modes) of the first 15 modes was plotted. In addition, the predicted modal results from FE models also served as a guide to determine important parameters of modal testing, such as the frequency band of interest and sensor locations and etc.

When the elasticity modulus of the deck concrete varied between 70 and 130 percent of its nominal value of 3900 ksi, it was observed from Figure 5-3 that there was a slight monotonic increase in the modal frequencies. The change in the frequencies of all the modes was bounded by ±5 percent. The order of appearance of the first fifteen modes remained almost the same. But the first vertical and lateral modes (the 1st and 2nd mode in Figure 5-3) switched when the modulus of elasticity was only 70 percent of its nominal value. The shapes of the 11th, 12th and 13th mode of the revised models were somehow different from their counterparts from the nominal model and therefore some of them were not shown in the figure.

The predicted modal frequencies of the bridge also changed monotonically with the value of the steel modulus, as expected. However, they were much more sensitive to the change of the material property of steel than that of deck concrete. A 15 percent fluctuation in the value of the steel modulus led to over 10 percent change of modal frequencies. No shift in the order of the first fifteen modes was found (see Figure 5-4).

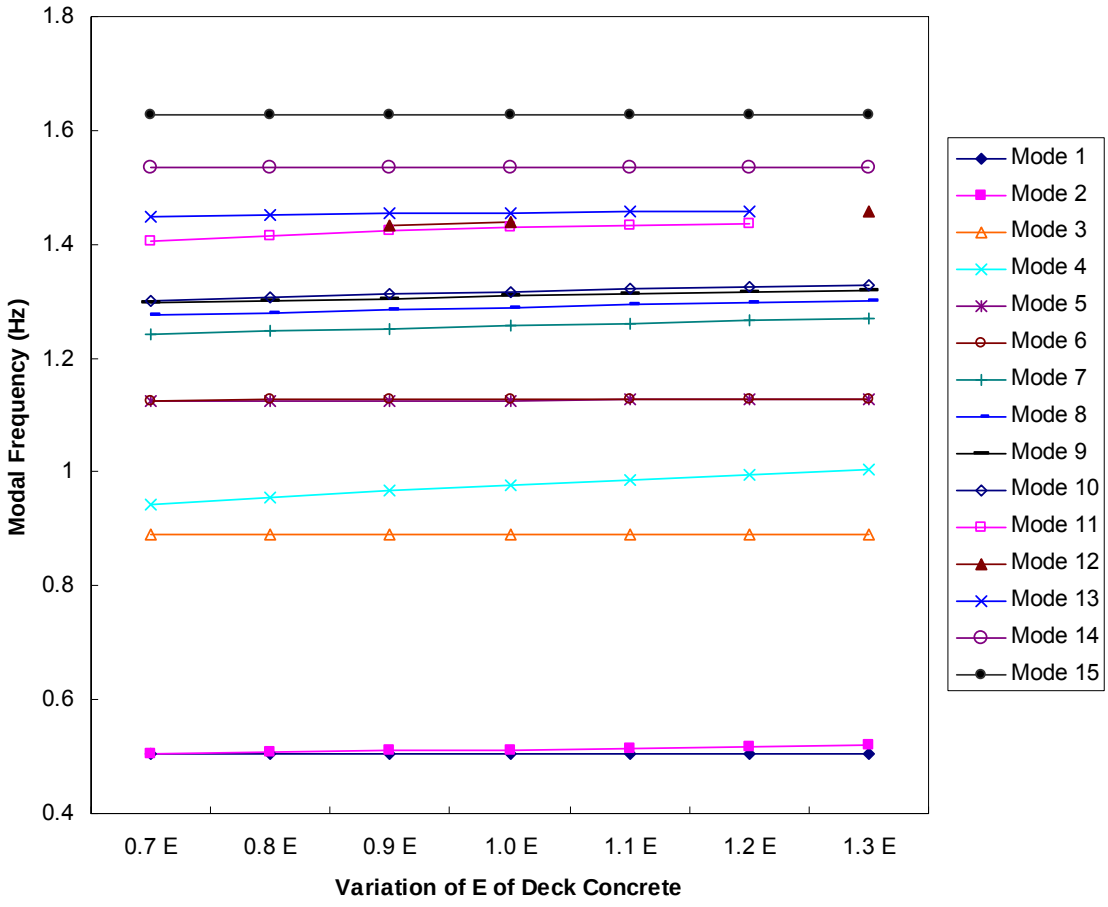

Figure 5-3 Modes versus variation of the Young's modulus of deck concrete

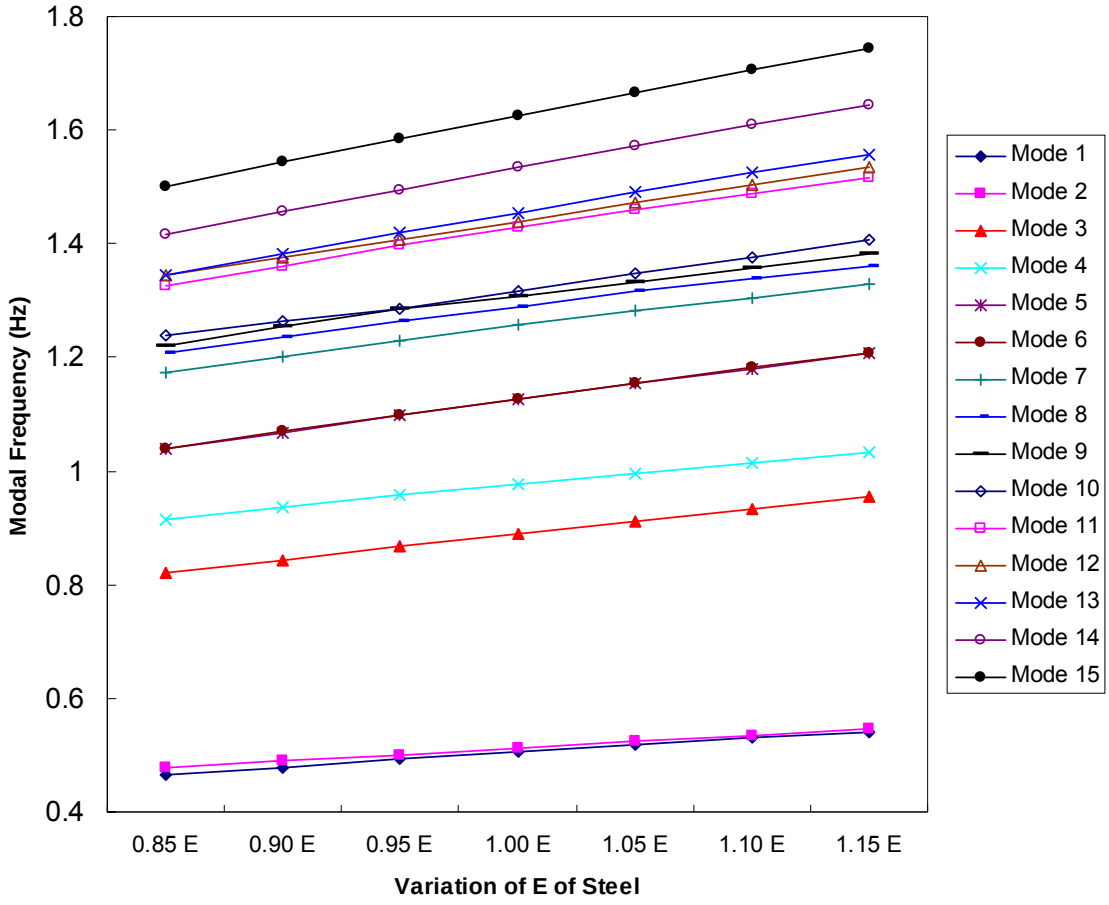

Figure 5-4 Modes versus variation of the Young's modulus of steel

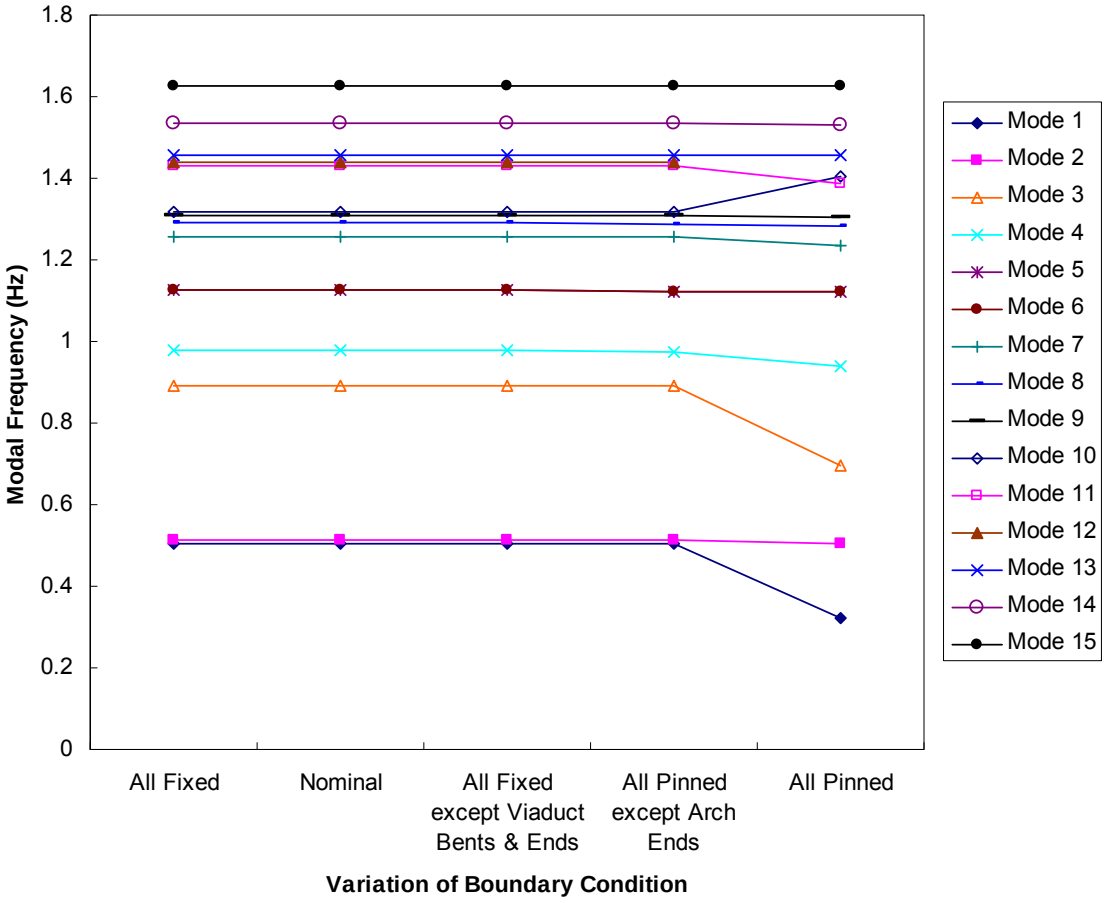

Figure 5-5 Modes versus variation of boundary condition

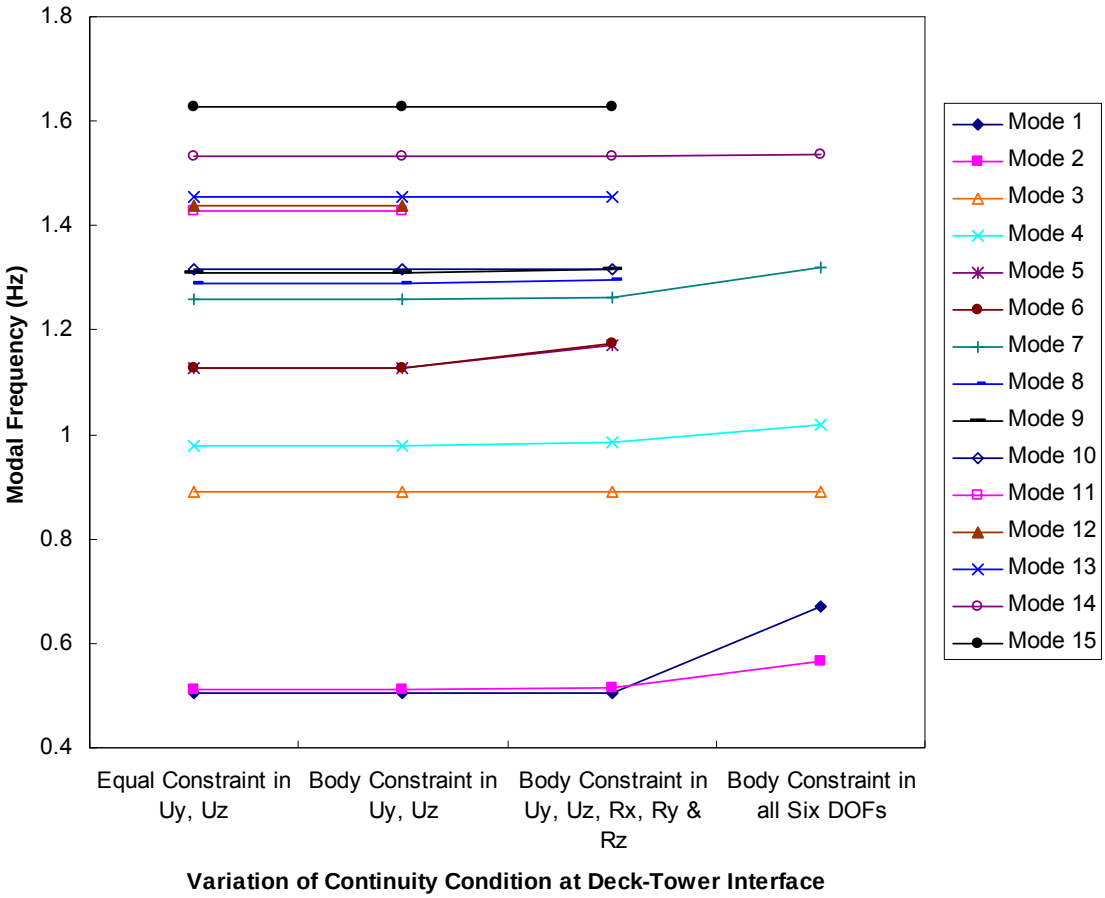

Figure 5-6 Modes versus variation of continuity condition

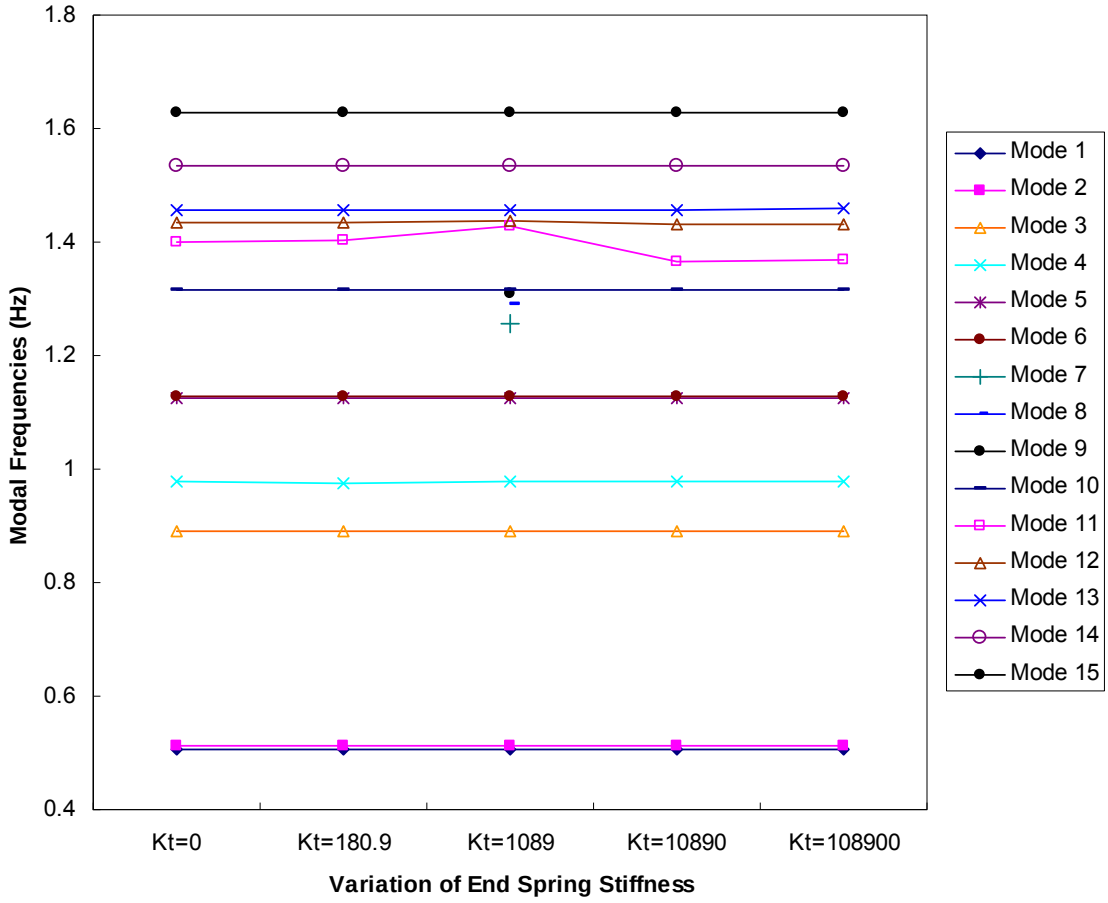

Figure 5-7 Modes versus variation of the stiffness of end springs

In the nominal model, the translational and rotational degrees of freedom at the arch ends and tower supports were fully restrained. The two extreme ends of viaduct spans were assumed to be pinned supported. For the viaduct bents from panel points (PP) 9 through 12 and 17 through 20, they were assumed to be fixed except that PP9 and PP10 were pinned. Because only the superstructure of the bridge was simulated in the model, the assumed boundary conditions represented the effects of the substructure and soil condition on the bridge which was absent in the nominal model. Four cases with different boundary conditions were examined: (1) All supports were fully restrained; (2) All supports except viaduct bents and ends were fully restrained; (3) All supports except arch ends were pinned; (4) All supports were pinned. Compared modal analysis results obtained from the nominal model, no obvious changes were

observed from the aforementioned first three cases. Dramatic changes occurred when the rotational restraints at the arch ends were released. Some of modal frequencies decreased considerably and the order of some modes switched, as shown in Figure 5-5. It could thus be concluded that the rigidity of supports at arch ends was essential for the global stiffness of the bridge. For example, the frequency of the first vertical mode of the bridge dropped as high as about 36.5 percent from the value predicted by the nominal model. But the influence of support conditions of arch ends on each vibration mode was uneven and the discrepancy in the frequency of higher order modes was less significant. Another interesting finding is that the influence on the anti-symmetric modes of the arch span was greater than the symmetric modes. The appearance sequence of the modes was also shifted up and down respectively. However, the lateral motions of the bridge were comparatively much less sensitive to the change in the support conditions of towers and arch ends, since the sequence of the modes was almost the same and the eigenvalues were slightly different.

At the expansion joints which were located at the viaduct-tower-arch interface at the upper and lower deck levels, joint constraints were assigned to the nodes along the fascia girders at the both sides of the bridge. In the nominal model, 'Equal' constraints were used on the translational degrees of freedom in the longitudinal and lateral direction, i.e., Uy and Uz. Three different continuity conditions at these interface nodes were considered in the sensitivity analysis: (1) 'Body' constraints in Uy and Uz; (2) 'Body' constraints in Uy and Uz as well as all rotational degrees of freedom, i.e., Rx, Ry and Rz; (3) 'Body' constraints in all degrees of freedom. In SAP2000 software, an 'Equal Constraint' causes all of its constrained joints to move together with the same or opposite displacements for each selected degree of freedom and it differs from the rigid-body type of constraints in that there is no coupling in rotations and translations. As shown in Figure 5-6, there was no difference between the predicted modal parameters whether the continuity condition at the interface was defined by the use of 'Equal' or 'Body' constraints.

When the rotational degrees of freedom of these joints were constrained, slight change in modal frequencies was observed and two modes in the first fifteen modes could not correlate with any mode from the nominal model. Once the axial degrees of freedom were frozen to force the joints located at expansion joints to displace with each other, the resulting modal analysis results were significantly different from those from the nominal model. First of all, fewer modes appeared in the same frequency band. The order of the first two modes switched, i.e., the first fundamental mode was the first lateral mode because the longitudinal modes of towers and/or spans disappeared. Secondly, the values of the first several modes increased compared with their counterparts from the nominal model. Thirdly, the shapes of lateral modes changed because the discontinuity caused by the relative longitudinal displacement between the nodes at the expansion joints was excluded after body constraints in Ux were assigned.

Two lateral translational springs with a stiffness of 1089 kip/ft were assigned to the extreme ends of two viaduct spans at the upper deck. In the sensitivity analysis, models with spring stiffness which varied between 0 and infinity (108900 kip/ft) were analyzed to compare with the nominal model. Figure 5-7 displayed the first fifteen modes obtained from the nominal model with the spring stiffness as 1089 kip/ft, together with their counterparts identified from the other models with varying spring stiffness. Due to the variation of end spring stiffness, the density and order of the resulting modes from the five models shown in Figure 5-7 were slightly different. Frequencies of vertical modes were independent on the value of spring stiffness, as expected. For the rest of the modes, they were all unavoidably influenced by the restraints of the lateral springs, except the first lateral mode which was dominated by lateral vibration of the main arch span. It could be observed that there were a total of 12 sets of correlated modes and their modal frequencies barely changed with the end spring stiffness except the 11^{th} mode. Three lateral modes from the nominal model, the 7^{th}, 8^{th} and 9^{th} modes, demonstrated unique deflection shapes and they were absent from the modes identified from other modes. Accordingly, each model with

different value of end spring stiffness also generated some modes unique from others. For instance, when the end spring stiffness was equal to 0, the lateral mode of the south viaduct and the north viaduct showed up respectively. In addition, one lateral mode which was dominated by the lower deck and arch rib appeared all the other four models except the nominal model. Good correlation was found in the two models with the spring stiffness equal to 10890 kip/ft and 108900 kip/ft respectively.

5.4 Ambient Vibration Testing of the Bridge

5.4.1 Test Outlines

The scope of the testing included measuring the vibrations of the arch span, the towers and the viaducts due random ambient excitation sources. The primary sources of ambient excitation for this bridge were the relatively light vehicles crossing the spans and wind. Both the north and south viaducts were included in the ambient vibration testing scope since they are supported on bents of different heights. The ambient vibration testing was conducted over a period of about one month.

The bridge was tested in two stages. In the first test stage, a total of 36 accelerometers were installed on the north-half of the arch span, the north tower and the north viaduct. The south-half of the arch span, the south tower and the south viaduct were tested in the second test stage using a total of 40 accelerometers. A total of seven accelerometers were installed at locations on the bridge spans that were common to both test stages in order to permit the measurements from the two test stages to be combined during post-processing.

Multiple data sets were recorded during each test stage. The vibration measurements were recorded during each test stage using a number of different sampling frequencies. The sampling rates used ranged fro 20 Hz to 800 Hz, but the majority of the measurements were sampled at 200 Hz for intervals of 900 seconds. The multiple sample rates were used to permit the effect of bandwidth on identified frequencies to be evaluated.

In order to avoid spatial aliasing, roving instrumentation scheme has more often been used for the ambient vibration tests of many long-span bridges to obtain a greater number of measurement degrees of freedom. But a stationary instrumentation also has its advantage to be able to capture vibrations of all measurement stations simultaneously. Generally it is also easier to collect multiple data records over a longer period of time and under of wider variety of environmental and ambient excitation conditions with a stationary instrumentation scheme. These advantages can be particularly important if the ambient excitation or the structural responses are non-stationary. In this project, with a sufficient number of accelerometers to minimize the potential for spatial aliasing, the locations of the accelerometers on the bridge remained constant for the entire duration of each test stage, that is, the ambient testing was performed using a stationary instrumentation scheme.

The instrumentation scheme developed for the bridge included accelerometers for measuring the vertical, torsion, lateral, and longitudinal vibrations at different locations on the structure. The accelerometers were installed in the following general locations of the bridge: (1) upper and lower level decks, and arch rib of the arch span; (2) upper and lower level decks of the viaduct spans; (3) upper and lower level decks, and approximately mid-height level of the towers.

Figure 5-8 shows the locations on the arch span where vertical vibration responses were measured in each test stage. The locations on the spans where transverse (lateral) vibrations were measured in each test stage are shown in Figure 5-9. The vertical and transverse accelerometers that were placed at lower level bent locations were located along the west side of the bridge and adjacent to the pedestrian sidewalk on the lower level that could be used to access these locations. The vertical and transverse accelerometers placed at upper level bent locations were located along the east side of the bridge and adjacent to a maintenance walkway. The torsional vibration responses are identified by taking the difference between the responses from the vertical accelerometers located on the upper and lower levels at a given bent location. Transverse

accelerometers were placed on the upper level, lower level, and on the arch girder in the arch span, and on the upper and lower levels of the towers and viaducts to measure the relative lateral vibrations at these locations.

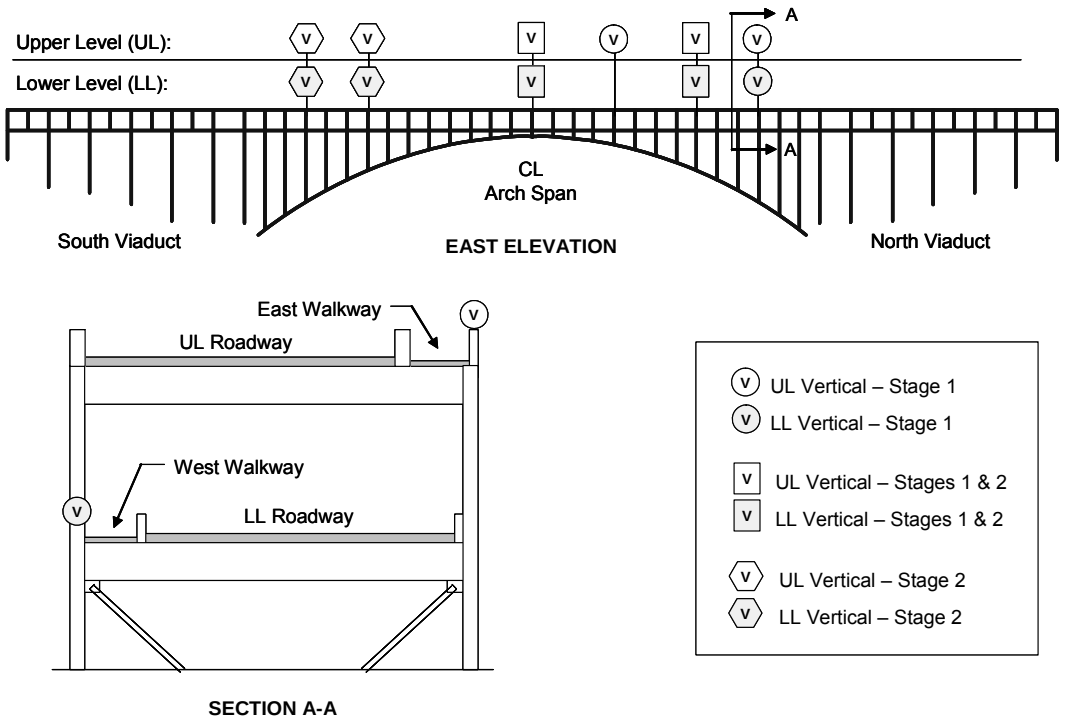

Figure 5-8 Accelerometer locations for measuring vertical and torsional vibrations

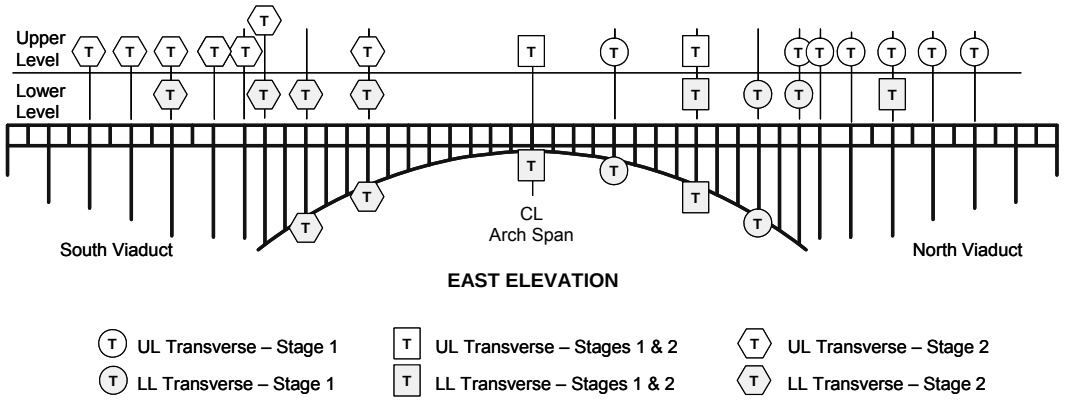

Figure 5-9 Accelerometer locations for measuring transverse (lateral) vibrations

5.4.2 Test Equipment

The data acquisition system was comprised of: (1) uni-axial seismic accelerometers (Model 393C, PCB Piezoelectronics) which have a nominal sensitivity of around 1 Volt/g, a peak measurement range of 2.5 g, a frequency range of 0.025 to 800 Hz, and a broad band resolution of 0.0001 g.; (2) data acquisition station – a Hewlett Packard Model 8401A VXI mainframe with Model 1432A input modules; (3) several Model 481 signal conditioners from PCB Piezoelectronics; (4)a laptop computer. The data acquisition station was setup and removed daily during the conduct of the ambient vibration testing.

A separate cable was run from each accelerometer location to the data acquisition station, which was located under the north viaduct during the first test stage and under the south viaduct during the second test stage. Approximately 25,000 linear feet of coaxial cable was used in conjunction with each test stage. The cable connections and field splices were sealed to protect against any ingress of moisture during the ambient vibration testing.

In order to minimize the potential systematic errors in measurement, the factory supplied calibration value for each accelerometer was verified in the laboratory using the back-to-back calibration method and a shaker device before the accelerometers were deployed in the field. The data acquisition station was also calibrated in the DI3 lab ahead of the field tests.

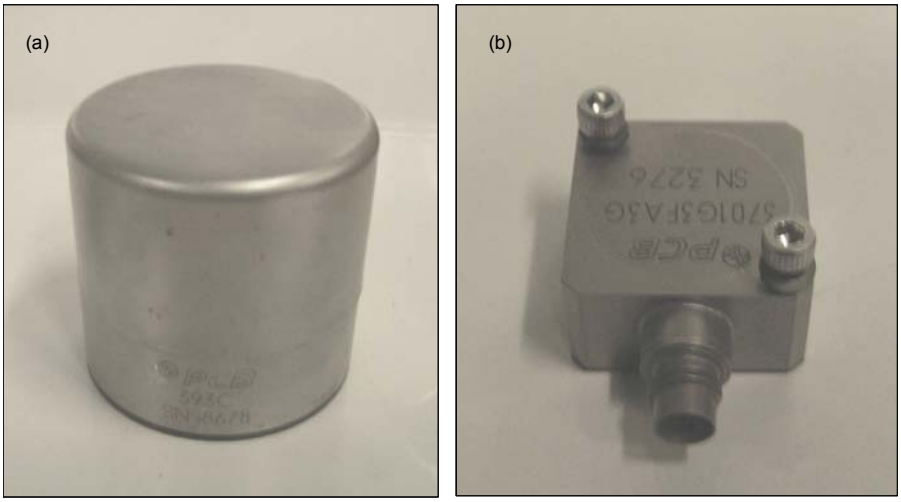

Figure 5-10 (a) Model 393C piezoelectric accelerometer and; (b) Model 3701G3FA3G capacitive accelerometer

Figure 5-11 Vertical and transverse on the lower deck level of the arch span (left); Transverse and longitudinal sensors on the tower (Rigth)

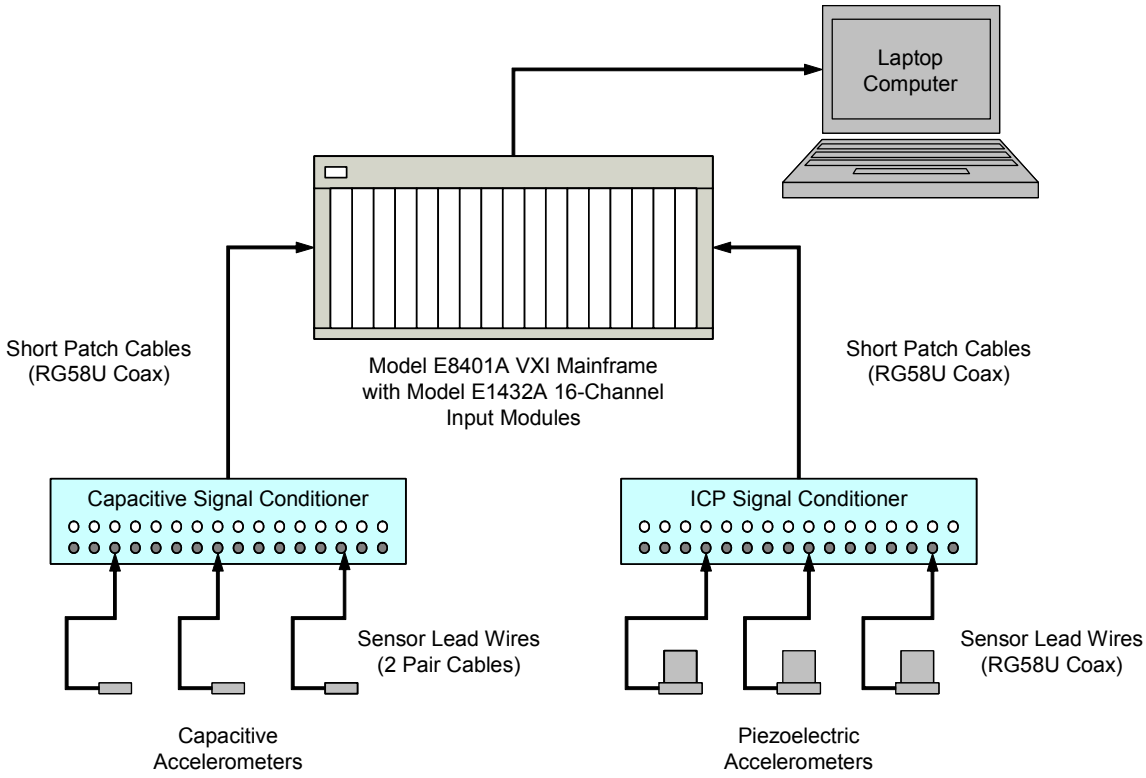

Figure 5-12 Data acquisition hardware components

Figure 5-13 Data acquisition system at the Henry Hudson Bridge

5.4.3 Data Analysis

The data acquisition system was typically operated during daytime hours during both the first and second test stages. During the first test stage (monitoring of the north half of the bridge), the acceleration measurements were typically recorded at 200 Hz (samples per second) for 15 minute

intervals and a total of 57 data sets were collected between September 23 and 29, 2004. The acceleration measurements were recorded at 20 Hz for primarily 30 minute intervals in the second test stage (monitoring of the south half of the bridge) and a total of 7 test sets were obtained.

Although it is generally assumed that sample records of vibration data represent all properties for the process of interest, the justification of stationarity assumption was verified at the beginning of data analysis. Since an infinite number of possible statistics exist, such verifications are often not feasible in engineering applications. Some practical tests for stationarity were developed and summarized by Bendat and Piersol (2000).

It was frequently reported in recent years that structural dynamic properties can be fluctuating with the change of temperature, humidity and the magnitude of traffic load. Another concern about the recorded data was thus whether observable variation of modal parameters of the bridge took place within one-day cycle and within one-week cycle respectively.

The Nyquist Criterion dictates that the sampling rate must be at least twice as fast as the maximum frequency that is to be measured (i.e. the maximum measurable frequency is equal to half the sampling frequency) to prevent aliasing, which is a phenomenon that leads to erroneous frequency estimation. Therefore, the 200 Hz sampling rate used in the first test stage permits a maximum frequency of 100 Hz to be measured and the 20 Hz sampling rate used in the second stage permits a maximum frequency of 10 Hz to be measured. Post-processing of the measurements recorded during the first test stage indicated that most of modes of interest fell in the interval of 0-5 Hz and thus a 20 Hz sampling rate was adequate to identify the natural frequencies of the bridge. To evaluate the influences of test sampling frequency on identified dynamic properties, test data sets with a variety of sampling frequency 20 Hz, 100 Hz, 200 Hz, 400 Hz and 800 Hz were measured during the second test stage, besides the data with 20 Hz sampling frequency.

5.4.3.1 Test of Stationarity

The data measured in an ambient vibration test is generally assumed to be stationary, Gaussian random data without periodic components. The methods used to analyze and interpret the vibration data are directly influenced by these characteristics. Various statistical analysis methods can be used to test whether these assumptions are valid. If the stationarity of measurement data is to be tested based on individual sample records, two assumptions are required (Bendat and Piersol, 2000): (1) any sample record will properly reflect the nonstationary character of the random process in question and (2) any sample record is long enough compared to the lowest frequency component in the data, excluding a nonstationary mean.

If the above assumptions are made, the stationarity of the random data can be tested for a single time domain record using the following procedure which is outlined by Bendat and Piersol (2000) for random data in general, and was utilized by Kijewski and Kareem (1999) for ambient vibration measurements from a tall building: (1) divide the data record for each channel into a number of equal length segments (N), each of which can be regarded as independent; (2) compute RMS values (mean values, mean square values, standard deviations or other similar parameter estimates also work equally well) for each segment and align these values in a time sequence; (3) test the sequence of RMS values for a nonstationary trend. The reverse arrangements test is a widely-used method to test for a nonstationary trend. After the total number of reverse arrangements in the sequence is found, a hypothesis can be made that the data is stationary. This hypothesis would be accepted at a certain level (α %) of significance if the reverse arrangements (A) produced by the sequence of N measurements fall between $A_{N;1-0.5\alpha}$ and $A_{N;0.5\alpha}$. Otherwise, the hypothesis of stationarity is rejected at the α % of significance, and the data are identified as being nonstationary.

One set of acceleration measurement with a sampling frequency of 200 Hz and duration of 3600 seconds was randomly selected for stationarity test, according the procedure outlined

previously. The 720000 data points contained in this record for each accelerometer channel were divided into thirty segments of 24000 data points. Each of these thirty segments corresponded to a 2 minute interval. The RMS accelerations were computed for the 30 segments from the 18 channels of arch span accelerations. The reverse arrangements test revealed that only 3 channels failed to pass the stationarity test for a 1% level of significance. The three channels that did not pass the stationarity test included a vertical accelerometer that was located on the lower level at midspan, a transverse accelerometer that was located on the arch girder at midspan, and a transverse accelerometer located on the upper level at close to midspan. This analysis indicates that the stationarity assumption for the acceleration data measured on the arch span is generally valid.

5.4.3.2 Variability Analysis

Variability in the identified dynamic properties can lead to uncertainty in the interpretation of the results. A previous study from Farrar and Doebling (1997) concluded based on ambient vibration data of a medium-span bridge that significant variability can be observed in the identified dynamic properties due to changes in environmental, service conditions, and the data reduction method used for the measurements.

The variability of the identified frequencies as a function of the level of traffic on the bridge and as a function of the amount of data considered for the analysis was evaluated using discrete data sets collected over a period of several days and at a constant sampling rate of 200 Hz. The data was decimated to 50 Hz for this analysis, and the duration of each discrete data set was 900 seconds. The frequency resolution of the analysis was 0.012 Hz.

The level of traffic crossing the bridge was considered as a parameter for this analysis since it was generally moderate when the measurements were recorded before 15:00 hours (excluding the morning rush hour period) and was much heavier when measurements were recorded after 15:00 hours. The amount of data utilized for the modal parameter estimation was also considered as

another possible source of variability since the random traffic and wind which provide the ambient excitation may not excite all of the frequencies all of the time. This is especially true if the excitation is not broad-banded as is usually assumed. Although ambient temperature was not recorded in conjunction with the ambient vibration testing, its effects are indirectly included in this analysis since the ambient temperature at the site also varied over the course of each day.

The following three cases were considered in this analysis: (1) vertical and transverse frequencies identified from a single data set recorded during periods of either moderate traffic levels (before 15:00 hours) or heavy traffic levels (after 15:00 hours) over a period of several days, (2) vertical and transverse frequencies identified from multiple data sets recorded during periods of either moderate or heavy traffic levels within a single day, and (3) vertical and transverse natural frequencies identified from the combination of all data sets (moderate and heavy traffic levels) collected during a given day. Combinations of discrete data sets are considered in the second and third cases. These data sets were combined in the frequency domain by calculating the mean PSD from the collection of data sets being considered. This method of combining the data sets was found to yield frequency results which were essentially equivalent to the frequency results obtained when discrete data sets are combined end-to-end in the time domain for the combination of 3 records of 900 seconds each.

The identified vertical and transverse frequencies identified from single data sets sampled during moderate and heavy traffic, over a five day period are summarized in Table 5-1and Table 5-2, respectively. It is clear from these results that there was very little variation in the frequencies identified from single 900 seconds long data records collected before 15:00 hours or collected after 15:00 hours for different days of the week.

The percent differences between the vertical natural frequencies identified from single data records collected before and after 15:00 hours on September 24 are summarized in Table 5-3. The vertical frequencies identified from the combination of all data sets for September 24 and the

percent difference between these values and those identified in Table 3 are summarized in Table 5-4. These results indicated a maximum of 1% difference between the identified frequencies for the cases considered.

The percent differences between the transverse natural frequencies identified from single data record collected before and after 15:00 hours on September 24 are summarized in Table 5-5. The transverse frequencies identified from the combination of all data sets for September 24 and the percent difference between these values and those identified in Table 5-5 are summarized in Table 5-6. These results indicate a maximum of 2% difference between the identified frequencies for the cases considered.

Table 5-1 Vertical natural frequencies identified from single data sets sampled before and after 15:00 hours on different days of the week

Date	**20-Sep**	**21-Sep**	**22-Sep**	**23-Sep**	**24-Sep**	**27-Sep**	**29-Sep**	**Mean**	**STD**
Time		**12:39**	**12:20**	**13:19**	**13:44**	**13:48**	**13:19**		
Frequencies (Hz) before 15:00		0.732	0.745	0.745	0.732	0.745	0.732	0.739	0.007
		0.940	0.940	0.940	0.940	0.940	0.940	0.940	0.000
		1.477	1.477	1.477	1.477	1.489	1.465	1.477	0.008
		1.697	1.697	1.697	1.685	1.697	1.697	1.695	0.005
		2.490	2.466	2.466	2.441	2.478	2.502	2.474	0.021
		3.235	3.271	3.235	3.271	3.247	3.235	3.249	0.018
Date	**20-Sep**	**21-Sep**	**22-Sep**	**23-Sep**	**24-Sep**	**27-Sep**	**29-Sep**	**Mean**	**STD**
Time	**17:54**	**17:03**	**17:30**	**17:26**	**15:22**	**17:30**			
Frequencies (Hz) after 15:00	0.732	0.732	0.745	0.745	0.732	0.732		0.736	0.006
	0.940	0.940	0.940	0.928	0.928	0.940		0.936	0.006
	1.489	1.477	1.477	1.465	1.477	1.477		1.477	0.008
	1.697	1.697	1.697	1.685	1.685	1.697		1.693	0.006
	2.478	2.490	2.454	2.478	2.454	2.441		2.466	0.019
	3.223	3.223	3.235	3.223	3.259	3.271		3.239	0.021

Table 5-2 Transverse natural frequencies identified from single data sets recorded before and after 15:00 hours on different days of the week

Date	20-Sep	21-Sep	22-Sep	23-Sep	24-Sep	27-Sep	29-Sep	Mean	STD
Time		12:39	12:20	13:19	13:44	13:48	13:19		
Frequencies (Hz) before 15:00		0.598	0.610	0.610	0.598	0.610	0.598	0.604	0.007
		1.123	1.111	1.184	1.160	1.160	1.172	1.152	0.029
		1.587	1.575	1.550	1.575	1.575	1.575	1.573	0.012
		1.807	1.855	1.904	1.868	1.855	1.831	1.853	0.033
		2.344	2.295	2.319	2.307	2.307	2.307	2.313	0.017
		2.466	2.478	2.466	2.466	2.454	2.478	2.468	0.009
Date	**20-Sep**	**21-Sep**	**22-Sep**	**23-Sep**	**24-Sep**	**27-Sep**	**29-Sep**	**Mean**	**STD**
Time	**17:54**	**17:03**	**17:30**	**17:26**	**15:22**	**17:30**			
Frequencies (Hz) after 15:00	0.598	0.610	0.610	0.610	0.598	0.598		0.604	0.007
	1.196	1.135	1.135	1.172	1.160	1.160		1.160	0.023
	1.563	1.587	1.587	1.587	1.563	1.563		1.575	0.013
	1.855	1.831	1.831	1.904	1.868	1.892		1.864	0.031
	2.307	2.271	2.271	2.332	2.344	2.344		2.311	0.034
	2.466	2.466	2.466	2.478	2.478	2.454		2.468	0.009

Table 5-3 Comparison of vertical natural frequencies identified from single and multiple data records collected on September 24

Single record			Multiple records			% Diff from single record	
Freq (Hz)		% Diff from Pre 15:00 record	Freq (Hz)		% Diff from Pre 15:00 records		
Pre 15:00 record	Post 15:00 record		Pre 15:00	Post 15:00		Pre 15:00 records	Post 15:00 records
0.732	0.732	0	0.732	0.732	0	0	0
0.940	0.928	-1	0.940	0.928	-1	0	0
1.477	1.477	0	1.477	1.477	0	0	0
1.685	1.685	0	1.685	1.685	0	0	0
2.441	2.454	0	2.441	2.466	1	0	0
3.271	3.259	0	3.235	3.247	0	1	0

Table 5-4 Comparison of vertical natural frequencies identified from the combination of all data records with the single and multiple data records collected on September 24

Full-day combination of records	% Diff from single record		% Diff from multiple records	
Freq (Hz)	Pre 15:00 record	Post 15:00 record	Pre 15:00 records	Post 15:00 records
0.732	0	0	0	0
0.940	0	-1	0	-1
1.477	0	0	0	0
1.685	0	0	0	0
2.441	0	0	0	1
3.247	1	0	0	0

Table 5-5 Comparison of transverse natural frequencies identified from single and multiple data records collected on September 24

Single record			Multiple records			% Diff from single record	
Freq (Hz)		% Diff from Pre 15:00 record	Freq (Hz)		% Diff from Pre 15:00 records		
Pre 15:00 record	Post 15:00 record		Pre 15:00	Post 15:00		Pre 15:00 records	Post 15:00 records
0.598	0.598	0	0.598	0.598	0	0	0
1.160	1.160	0	1.160	1.160	0	0	0
1.575	1.563	-1	1.563	1.563	0	1	0
1.868	1.868	0	1.855	1.855	0	1	1
2.307	2.344	2	2.332	2.344	1	-1	0
2.466	2.478	0	2.466	2.478	0	0	0

Table 5-6 Comparison of transverse natural frequencies identified from the combination of all data records with the single and multiple data records collected on September 24

Full-day combination of records	% Diff from single record		% Diff from multiple records	
Freq (Hz)	Pre 15:00 record	Post 15:00 record	Pre 15:00 records	Post 15:00 records
0.732	0	0	0	0
0.940	0	0	0	0
1.477	1	0	0	0
1.685	1	1	0	0
2.441	-2	0	-1	0
3.247	0	0	0	0

5.4.3.3 Frequency Bandwidth Analysis

The objective of this analysis was to evaluate if the frequency bandwidth had any significant effect on the frequencies identified from the acceleration data when using the methods described in the previous section. The frequency bandwidth for the data is theoretically defined as equal to one-half the sampling frequency. To perform this analysis, discrete time domain records that were collected on the same day using sampling rates of 100 Hz, 200 Hz, 400 Hz and 800 Hz were processed and the natural frequencies were identified. The length of the data segments contained within these records for which the DFT was computed was defined such that the same frequency resolution was obtained for each set. Because the size of the segments used to compute the DFT in the 800 Hz sampled data set must be large to obtain the same frequency resolution as the 100 Hz sampled data set, the number of averages used to generate each PSD is much smaller for the 800 Hz sampled data than for the 100 Hz sampled data.

The vertical and transverse frequencies identified from the discrete time domain data records measured using different sampling frequencies are summarized in Table 5-7 and Table 5-8, respectively. The results indicate that the variations observed in the identified vertical and transverse frequencies are very small, and that for many frequencies no variation was observed. Furthermore, the very small variation that is observed for two vertical frequencies and two transverse frequencies is not significant enough that this difference can be directly attributed to the frequency bandwidth. The observed variation also does not appear to be directly related to the number of averages that were used to compute the PSDs from which the natural frequencies were identified.

Table 5-7 Vertical natural frequencies identified from single data records sampled at different frequencies

Sampling frequency (Hz)	**100**	**200**	**400**	**800**	**Mean**	**STD**
No. of averages	**97**	**49**	**21**	**13**		
Frequency resolution (Hz)	**0.024**	**0.024**	**0.024**	**0.024**		
Frequencies (Hz)	0.732	0.732	0.732	0.732	0.732	0.000
	0.928	0.928	0.928	0.928	0.928	0.000
	1.465	1.465	1.465	1.465	1.465	0.000
	1.685	1.685	1.685	1.685	1.685	0.000
	2.441	2.441	2.466	2.466	2.454	0.014
	3.271	3.247	3.271	3.223	3.253	0.023

Table 5-8 Transverse natural frequencies identified from single data records sampled at different frequencies

Sampling frequency (Hz)	**100**	**200**	**400**	**800**	**Mean**	**STD**
No. of averages	**97**	**49**	**21**	**13**		
Frequency resolution (Hz)	**0.024**	**0.024**	**0.024**	**0.024**		
Frequencies (Hz)	0.610	0.610	0.610	0.610	0.610	0.000
	1.172	1.172	1.172	1.147	1.166	0.012
	1.563	1.563	1.563	1.563	1.563	0.000
	1.904	1.880	1.880	1.880	1.886	0.012
	2.344	2.344	2.344	2.344	2.344	0.000
	2.466	2.466	2.466	2.466	2.466	0.000

5.4.3.4 Conclusion for Data Analysis

Measurement errors and uncertainties related to ambient vibration testing of a real-life structural system always is unavoidable. In addition to the structural responses to physical stimuli

at desired locations of the structure, test measurement may also contain contributions from unknown phenomena such as electronic noise, malfunction of the sensors and etc. And they can have significant influence on the data quality and the subsequent analysis and interpretation of the results. This is particularly true in the case of ambient vibration testing of a long-span bridge since the measured accelerations generally are very small and therefore have very low signal-to-noise ratios.

According to the data analysis shown above, several conclusions can be drawn:

(1) The hypothesis of stationarity for the vibration measurements was tested by a reverse arrangements test, and only a small subset of accelerometer channels were unable to pass this test. The accelerations recorded from ambient vibration testing performed on this bridge could be considered to be stationary.

(2) For this particular structure, very insignificant change in the estimated modal parameters was observed due to the amount of traffic flow on the bridge, the time of day the testing performed and the amount of measurement data considered in the parameter estimation process. The apparent lack of any significant ambient temperature related effects on the variability of the identified frequencies seems to contradict the findings from ambient vibration tests of many short to medium span bridges. It could be that natural frequencies of some long-span bridges are not as sensitive to such influences as their short to medium span counterparts because of their size or structural configuration; however, analyses of vibration measurements conducted over a longer term than was done for this bridge would be required to verify this.

(3) Frequency bandwidth of the measurements was not found to have any significant influence on the identified frequencies, provided that the bandwidth used was more than adequate to identify the frequencies in the band of interest for the structure. This is an important consideration since the sampling rate defines the frequency bandwidth. If data is sampled at a rate far in excess of what is necessary to reliably identify the dynamic properties, the duration of the

measurements needs to be large in order to obtain an adequate frequency resolution. A long measurement duration coupled with a very fast sampling rate will lead to difficulties in data processing and storage.

(4) Although the above data analysis was based on measurements obtained from the north half of the bridge, the results were actually representative of the data sets collected either on the north half or the south half of the bridge. The main reason to carry out the data analysis using data from the north half of the bridge was that acceleration measurements with different test parameters were only available for the first test stage.

5.4.4 Modal Parameter Estimation & Results

5.4.4.1 Overview of Modal Parameter Estimation Methods for Ambient Vibration Data

Most of experimentation on mechanical system was conducted by using forced vibration techniques in which the input(s) of the system are generated from a controlled source, such as impulse hammer, shaker and falling weight device, which are measured with the system outputs simultaneously. Frequency response functions or impulse response functions can thus be constructed and they are usually the workbench of most modal parameter estimation algorithms. Ambient vibration testing takes advantage of excitations induced by traffic and wind loads as its input can measure structural responses only and the unknown excitation is generally assumed to have characteristics of Gaussian white noise.

The most fundamental identification method for ambient vibration signals is the so-called peak-picking method. The method is named after its key step – pick the peaks from the auto-power spectral density (PSD) plots of the output channels. Since the input was assumed to be broad-band noise, the peaks in the PSD plots are supposed to correspond to the resonant frequencies of the system under consideration. The relative magnitude and phase information of modal vectors can be extracted from cross power spectral density (CSD) plots. And damping ratios are often obtained using half-power bandwidth method which quantifies the sharpness of

the resonant peaks, although the accuracy of damping estimation is often questionable. Averaging and windowing is crucial to the quality of the generation of power spectral density plots. Coherence functions are often used to enhance robustness of peak-picking procedure.

Although advanced algorithms directly using random vibration signals exist, such as PEM-ARMAV which manipulates the data with multivariate moving average (ARMA) models, many approaches were adapted from the existing algorithms for forced vibration signals. The primary concern is how to construct the impulse response function (IRF) or frequency response function (FRF) with output-only data. In fact, this difficulty can be overcome by making use of estimated auto- and cross-spectrums from recorded random signals. Two common techniques are random decrement and spectrum estimation. A brief description of them will be addressed as below and details about these two methods and their impacts on modal parameter estimation results were provided by Ciloglu (2006).

Random Decrement (RD) technique was proposed by H.A. Cole at NASA during the late 1960's (Cole) and further developed by Ibrahim in 1977 to cover multiple channel measurements. The technique is based on selection of trigger points in time domain signals and averaging signal blocks that are generated every time when the trigger conditions are met. This process transforms random time series into a free decay of the structure that is measured. Four different triggering conditions are used in practice (Asmussen): (1) Level Crossing; (2) Local Extremum; (3) Positive point; (4) Zero crossing with positive slope triggering. Generally, the response of a structural at the time t0+t is comprised of three parts, step response due to the initial displacements at t0, impulse response due to initial velocity at t0 and response due to random loads between t0 and t0+t. By taking averages of time segments every time the response has an initial displacement, the random part of the signal will eventually average out and become negligible. Furthermore, the sign of the initial velocity is expected to vary randomly with time, so the resulting initial velocity will be zero and the only part left in the averaged data will be the free decay response from the

initial displacement. If a reference channel *x(t)* is selected from available data, the RD function of the same channel RD_{XX} and the RD function of another channel *y(t)* based on triggering condition selected from *x(t)* RD_{YX} can be written in the following equations.

$$RD_{XX}(\tau) = \frac{1}{N}\sum_{i-1}^{N} x(t_i + \tau) | \{\text{when } x \text{ satisfies triggering conditions}\}$$

$$RD_{YX}(\tau) = \frac{1}{N}\sum_{i-1}^{N} y(t_i + \tau) | \{\text{when } x \text{ satisfies triggering conditions}\}$$

Spectrum estimation is taking advantage of the fact that the cross correlation functions display decay function resembling impulse response functions if the input is assumed to have white noise characteristics. Hence estimated cross-spectral density functions can serve as equivalent frequency response functions in the absence of physical inputs. In the engineering practice, two non-parametric spectrum estimation techniques were available for the calculation of cross-spectral density (CSD) functions. The first one is often referred as correlogram method. It was developed by estimating cross-correlation functions from raw or modified (windowed) random signals and the resulting cross-correlation functions were transformed into frequency domain with FFT.

$$R_{XX}(\tau) = \frac{1}{N-\tau}\sum_{i=1}^{N-\tau} x(t_i)x(t_i + \tau)$$

$$R_{XY}(\tau) = \frac{1}{N-\tau}\sum_{i=1}^{N-\tau} x(t_i)y(t_i + \tau)$$

The other approach returned power spectral density (PSD) estimates directly from the raw or modified (windowed) data and it is often named as the periodogram method. Detailed discussion is given by Bendat and Piersol (2000).

If time domain data is pursued, either by random decrement or correlogram method, exponential windows may be applied before DFT operation in order to reduce leakage.

After auto- and cross-spectrums of recorded random signals become available, they can be utilized as equivalent frequency response functions. The rest steps are very similar with the procedures for forced vibration signals. Previously mentioned CMIF and PTD algorithms are both applicable and they may lead to estimated modal parameters such as frequencies, damping ratios and mode shapes. However the scaling factors of each identified modal vector will be missing due to the lack of input information. The relatively long duration of recording time was inspired by frequency resolution and spectrum averaging considerations.

5.4.4.2 Data Processing

As indicated by the data analysis in the previous sections, the impact of the amplitude of traffic loading, ambient temperature as well as the sampling frequency on the acceleration responses of the Henry Hudson Bridge was negligible and could be considered as stationary data. In addition, the preliminary modal analysis results obtained from the initial finite element model revealed that the critical frequency bandwidth of the test was actually below 5 Hz. Therefore, seven data sets measured on the south half of the bridge with the sampling frequency as 20 Hz were selected to extract the modal parameters of the bridge. The selection of test data for modal parameter estimation was primarily based on the following considerations: (1) pre-conditioning such as decimation can be skipped and this will help to prevent possible distortion unavoidably induced by filtering. (2) Contamination caused by high frequency components in responses was mitigated. The detailed information about the seven data sets was provided in Table 5-9. A typical data set had a length of 30 minutes and contained 36000 data points, given a sampling frequency of 20 Hz. With a total number of 40 channels, a large amount of information (40 channels × 36000 samples) was available from each data set.

The general data processing procedure applied to each test data file were the following:

(1) Visually inspect each data set channel by channel to exclude noisy or bad ones;

(2) Apply a low-pass Butterworth digital filter to remove any DC bias or drift, and to minimize the influence of high frequency components out of the frequency band of interest;

(3) Cleanse data by removing spurious noise spikes manually;

(4) Cluster the time-domain data according to transverse, vertical, and torsion responses;

(5) Generate pseudo FRF;

(6) Apply parameter estimation algorithms such as complex mode indication function (CMIF) and polyreference time domain (PTD) method.

Each data set was processed independently using the same procedure and these yielded seven sets of modal data (modal frequencies, damping ratios and mode shapes).

Due to the limited number of accelerometers, vertical sensors were installed either at the east side of the upper level and the west side of the lower level of the bridge and were both very close to the vertical truss members connecting the upper and lower levels. Thus the torsion acceleration response for a given bent number was determined by taking one-half of the difference between the two vertical accelerometers at the same location. The resulting acceleration represents the rotation about the longitudinal centerline of the bridge.

Figure 5-14 demonstrated a sample of ambient vibration signal measured on the Henry Hudson Bridge. The flow chart of modal parameter estimation applied on the test measurements was shown in Figure 5-15. Steps 1 through 5 mentioned above were condensed in the ‘preprocessing’ block. The resulting pseudo FRFs were post-processed with both PTD and CMIF approaches respectively.

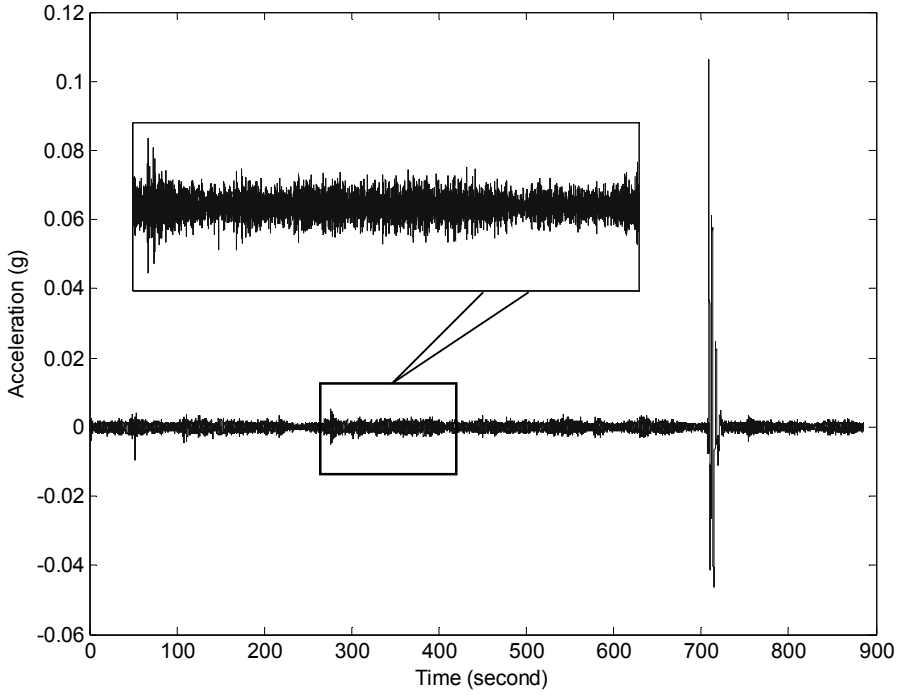

Figure 5-14 Spurious spikes in the time domain acceleration response

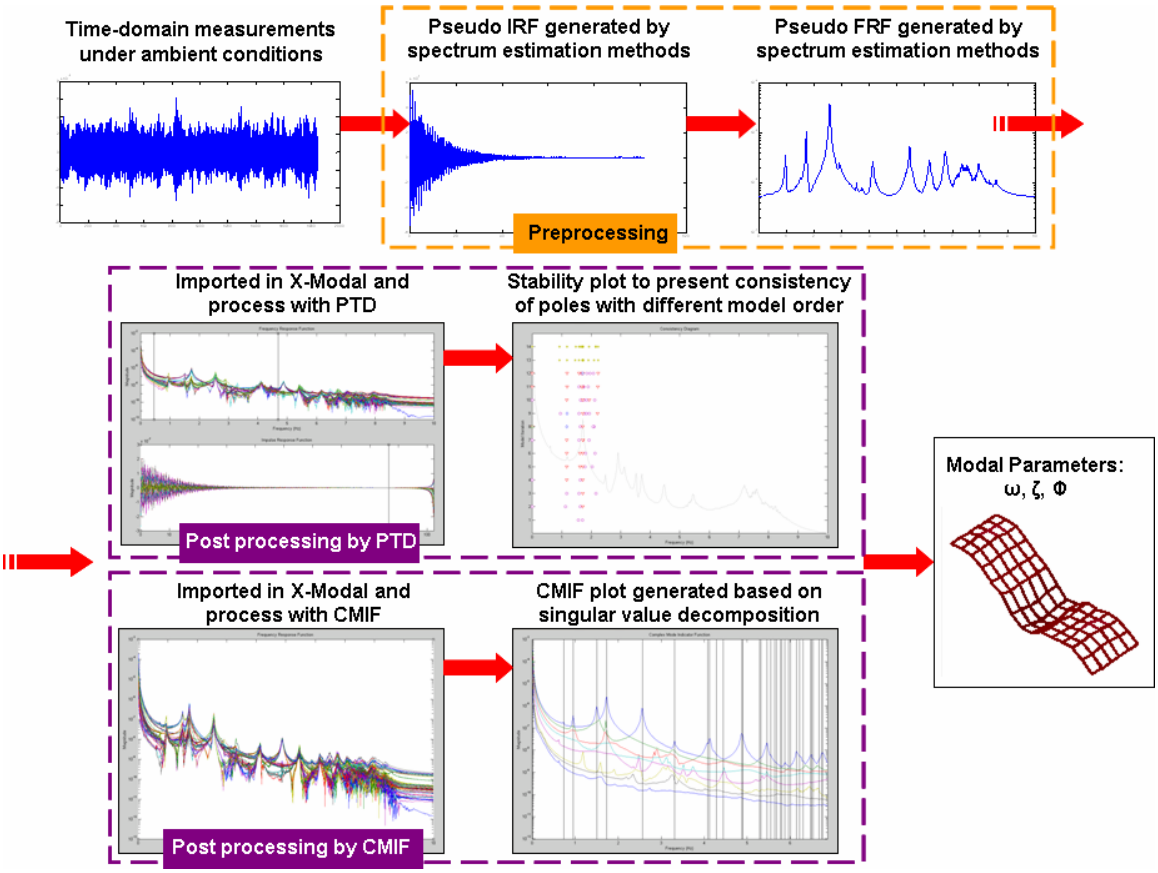

Figure 5-15 Flow chart of modal parameter estimation of ambient vibration data

5.4.4.3 Estimation Results

The final results obtained the data recorded from second stage of the ambient vibration test (the south half of the bridge) are shown in Table 7. The frequencies identified from the two different test stages were generally very close to each other, but most of the frequencies identified from the test on the south half of the bridge were slightly higher than those found from the test on the north half of the bridge. This difference is likely due to the removal of painting contractor's heavy equipment from the bridge before the second test stage.

A total of seven data sets (Table 5-9) were collected on October 13th 2004 with most the accelerometers located on the south half of the bridge. By consequence seven independent samples are available to estimate the modal parameters (frequencies, damping ratios and mode shapes). Table 5-10 presented the mean values of frequency and damping ratio $\bar{f}$, $\overline{\xi}$ and estimated standard deviations $\hat{\sigma}_f$, $\hat{\sigma}_\xi$ of the vertical, lateral and torsional modes that could be identified in the range of 0 – 4.5 Hz. The corresponding mode shapes were shown in Figure. From the mean value and estimated standard deviation, the $100(1-\alpha)\%$ confidence interval on the true value could be evaluated. Assume $\alpha = 0.05$, the resulting 95% confidence interval for the observed frequency and damping ratio were also calculated and listed in Table 5-10. It could be observed that the standard deviations of the identified natural frequencies were very low and as usual the damping ratio estimates were more uncertain. Thus a reasonably high confidence could be assigned to the experimentally identified modal properties.

Although up to several tens of accelerometers were installed on the bridge during ambient vibration monitoring, the number of measurement stations is far from adequacy considering the massive scale of the structure which is over 2,200 feet long and three levels – upper deck, lower deck and arch rib – in lateral direction. This fact made it difficult to view and interpret

experimental observations directly. Therefore the measured mode shapes would be illustrated with initial analytical results in the following section.

Table 5-9 Test statistics for data sets sampled at 20 Hz in the south part of test

Filename	Starting Time	Record Duration (min)
HH80_101304_1226_20Hz.sdf	12:26 PM, 10/13/2004	30
HH80_101304_1305_20Hz.sdf	13:05 PM, 10/13/2004	30
HH80_101304_1439_20Hz.sdf	14:39 PM, 10/13/2004	30
HH80_101304_1554_20Hz.sdf	15:54 PM, 10/13/2004	60
HH80_101304_1629_20Hz.sdf	16:29 PM, 10/13/2004	30
HH80_101304_1703_20Hz.sdf	17:03 PM, 10/13/2004	30
HH80_101304_1741_20Hz.sdf	17:41 PM, 10/13/2004	15

Table 5-10 Experimental Frequencies from PTD methods (Hz)

Mode #	Frequency (Hz)			Damping (%)			Description
	$\bar{f}$	$\hat{\sigma}_f$	95% CI	$\bar{\xi}$	$\hat{\sigma}_\xi$	95% CI	
1	0.739	0.004	0.739 ± 0.010	3.993	4.332	3.993 ± 10.600	vertical
2	0.952	0.002	0.952 ± 0.005	1.432	0.242	1.432 ± 0.593	
3	1.506	0.002	1.506 ± 0.006	1.134	0.144	1.134 ± 0.352	
4	1.732	0.003	1.732 ± 0.007	0.862	0.110	0.862 ± 0.270	
5	2.556	0.002	2.556 ± 0.004	0.570	0.069	0.570 ± 0.170	
6	3.300	0.007	3.300 ± 0.016	0.670	0.067	0.670 ± 0.163	
7	4.110	0.006	4.110 ± 0.016	0.616	0.330	0.616 ± 0.808	
1	0.616	0.002	0.616 ± 0.004	1.606	0.233	1.606 ± 0.570	lateral
2	1.182	0.002	1.182 ± 0.006	1.040	0.119	1.040 ± 0.291	
3	1.587	0.004	1.587 ± 0.010	1.010	0.163	1.010 ± 0.398	
4	1.709	0.001	1.709 ± 0.002	0.644	0.098	0.644 ± 0.240	
5	1.914	0.005	1.914 ± 0.012	1.152	0.160	1.152 ± 0.391	
6	2.362	0.010	2.362 ± 0.023	1.156	0.086	1.156 ± 0.210	
7	2.484	0.002	2.484 ± 0.006	0.622	0.070	0.622 ± 0.171	
8	2.739	0.004	2.739 ± 0.010	1.163	0.125	1.163 ± 0.305	
9	2.901	0.006	2.901 ± 0.016	0.697	0.163	0.697 ± 0.399	
10	3.120	0.012	3.120 ± 0.029	0.742	0.163	0.742 ± 0.399	
11	3.520	0.004	3.520 ± 0.009	0.516	0.074	0.516 ± 0.182	
12	4.446	0.016	4.446 ± 0.040	0.521	0.123	0.521 ± 0.301	

5.5 Calibration of FE model with Experimental Data

After an ensemble of modal properties of the structure including eigenfrequencies, damping ratios and mode shapes was established from test measurements, global calibration was to be performed on the a-priori analytical model to ensure that the critical mechanisms of the bridge were completely and accurately represented. The calibration process would not confine itself to just tuning a set of model parameters so that the resulting model was able to reproduce the observed structural responses. Instead, the following calibration process was to aim to identify the

causes of the measured responses. In this way, not only the discrepancy between the analysis and experiment could be minimized, but also the adjustments made on the initial model would have a sound physical justification.

The initial analytical model of the Henry Hudson Bridge incorporated comprehensive three-dimensional geometry and material properties, involved with a large number of degrees of freedom and model parameters. Modeling errors such as conceptualization error and parameter error could smear into every individual element through the model construction. The strategy for the system identification of such a large-scale and complicated structural system probably would start from the localization of modeling errors which controlled the test-analysis discrepancy, especially the ones with epistemic mechanism. This step was achieved by combining test-analysis correlation, sensitivity analysis and engineering judgment. Then it was followed by tuning the model manually by trial and error. Automatic updating approach such as the one utilized in the previous chapter was not implemented at this stage and might be conducted to polish the calibration results in the future work. This decision was based on the following considerations. First of all, modeling errors with epistemic mechanisms were usually involved with the selected model form, element types and connectivity conditions. They were often difficult to be parameterized as a set of variables and hence it was beyond the capability of automatic inverse eigensensitivity method to correct them. In addition, the finite element model created for the bridge was fairly detailed and comprehensive. This resulted in thousands of analytical degrees of freedom, compared with tens of measurement degrees of freedom. The dramatic difference in the number of analytical and experimental DOFs required either reducing analytical modes or expanding experiment modes. The associated reduction or expansion errors could not be distinguished from modeling errors. Another constraint is from the SAP2000 program which prevented users from automatically accessing to the analytical system matrices. This fact posed great challenge to develop an interface to communicate between finite element program and

available updating algorithms based on MATLAB (used in the cantilever beam case). It should be noted that there existed commercial software package such as FEMTools (Dynamic Design Solutions) which could interface with FEA programs such as ABAQUS and ANSYS.

5.5.1 Test-Analysis Correlation

As opposed to manufactured systems such as automobiles and machineries, constructed civil engineering structures which are usually of massive size and difficult to access seldom have the luxury to be extensively instrumented. The number of measurement degrees of freedom which is in hundreds at most is often far less than that of analytical degrees of freedom which may be in thousands. Additionally, the low-amplitude nature of ambient vibration implied that it may not contain sufficient energy to excite all modes in the frequency band of interest. For higher order vibration modes, it is also difficult to have them well stimulated. The resulting incompatibility between experimental and analytical results in both frequency and spatial sense poses as a major challenge to the test-analysis correlation. As a consequence, current modal testing of large-scale constructed structures as well as interpretation of the test results is more of an art with expert guidance and adaptive processing than a well-defined experimental procedure.

The a-priori analytical model was constructed on the basis of nominal values of material and geometry properties and ideal representation of the movement and floor system of the bridge. Although it had not been calibrated, the nominal model should provide rational predictions as long as all stiffness and geometry were included. However, it is well known that large finite element models tend to generate some numerical or spurious vibration modes which do not necessarily exist in real life. The simulated vibration modes could thus be grouped into three categories when compared with the experimental results: (1) actual vibration mode of the structure which has an experimental counterpart; (2) actual vibration mode of the structure which has not been excited by ambient input from traffic and wind loads; (3) spurious numerical

vibration modes. A preliminary modal analysis conducted on the initial finite element model of the Henry Hudson Bridge revealed that over sixty modes fell into the frequency band below 5 Hz.

The following task would be to conduct an initial correlation between experimental and analytical results. The primary benefit of such a correlation was to assess the degree of success of nominal FE model in simulating the dynamic properties of the bridge. Generally it is appropriate to make as many different types or levels of comparison as possible to obtain a global view of the difference between analysis and experiment, not to rely on one. Comparisons of modal parameters are usually the most common way of test-analysis correlation, since they can be predicted individually and comparisons can be confined to specific frequency ranges with greater facility for the analyst. In this specific case, it was reasonable to screen all analytical vibration modes and pair up with the experimentally obtained modal vectors.

5.5.1.1 Comparison of Natural Frequencies

Natural frequencies were the easiest and most obvious comparison to perform. Since SAP2000 does not provide damping values in modal analysis, only measured and predicted eigenfrequencies were compared. However, it should be noted that such a direct comparison should be carried out between paired vibration modes because frequency order (sequence) predicted by the analytical model may not necessarily agree with that of experimental modes. Actually the order by which vibration modes appeared in the frequency range of interest revealed important information of relative mass and stiffness distribution of the structure.

Table 5-11displayed the two sets of eigenfrequencies obtained from analytical prediction and test measurement respectively and relative difference between each other was also calculated. It could be found that seven experimentally identified modes matched up with but were consistently greater than their analytical counterparts. The largest discrepancy existed in the first vertical mode and the experimental frequency was more than 30% greater than the analytical value, while the difference in other modes were reasonably small (below 7%). More importantly, bending

mode in vertical direction came first in the analytical results while the lowest experimental mode corresponded to lateral vibration of the bridge. Because longitudinally the bridge was comprised of the south viaduct span, main arch span and the north viaduct span and vertically there were three components, i.e., the arch rib, lower deck and upper deck, the lateral vibration of the bridge were determined by the relative amplitude and phase of each component and therefore was much complicated. Only the first three predicted lateral modes which had a fairly good correlation with the experimental observation were listed in the table.

A more useful format was obtained by plotting the identified frequencies against each other for each mode included in comparison. If the two sets of values were in a good agreement, the points should lie on or close to a straight line with a slope of 1. This plot made it possible to visualize not only the degree of test-analysis correlation of eigenfrequencies but also the nature and trend of the discrepancy, from which possible cause may be identified. Figure 5-16 showed that all points were above the line which denoted a perfect test-analysis correlation, which indicated that the actual bridge was stiffer in vertical direction than analytical prediction.

Table 5-11 Comparison of modal frequency

Mode	Analytical		Experimental		Diff (%)
	Freq (Hz)	Description	Freq (Hz)	Description	
1	0.505	2nd vertical bending	0.739	2nd vertical bending	-31.664
2	0.512	1st lateral bending (arch)	0.616	1st lateral bending (arch)	-16.883
3	0.890	3rd vertical bending	0.952	3rd vertical bending	-6.513
4	0.977	2nd lateral bending (arch)	1.182	2nd lateral bending (arch)	-17.343
5	1.257	1st lateral bending (global)	1.587	1st lateral bending (global)	-20.794
6	1.535	1st vertical bending	1.506	1st vertical bending	1.926
7	1.651	4th vertical bending	1.732	4th vertical bending	-4.677
8	2.393	5th vertical bending	2.556	5th vertical bending	-6.377
9	3.137	6th vertical bending	3.300	6th vertical bending	-4.939
10	3.955	7th vertical bending	4.110	7th vertical bending	-3.771

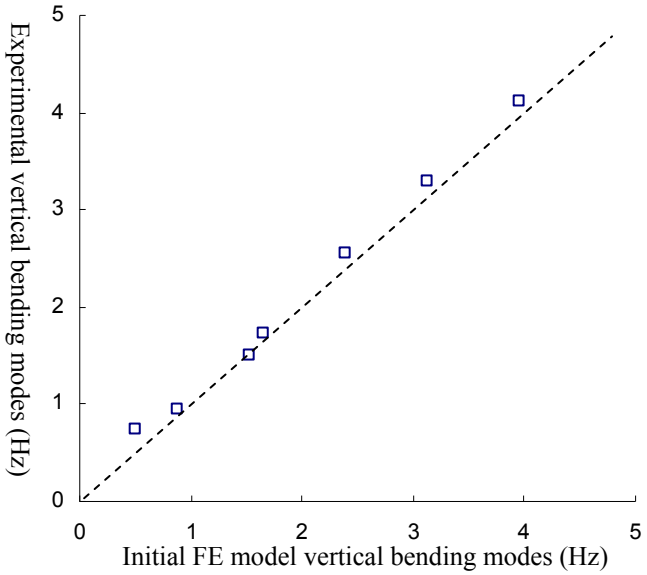

Figure 5-16 Comparison of eigenfrequencies of experiment and initial FE model

5.5.1.2 Graphical Comparison of Mode Shapes

Most of complex structures tend to have vibration modes which are not well separated. Hence it is important to ensure that the analytical and experimental modes are correctly matched up to represent the same vibration mode before any comparison can be performed. One of the most direct and effective way is to overlay the one plot on the other for visual inspection. In this case, proper scaling information was missing in the experimentally obtained mode shapes because no input measurements were available in ambient vibration monitoring. Hence each measured mode shape was scaled to be consistent with its analytical counterpart when all analytical modes were screened to pair up with experimental results.

For the vertical response of the bridge, the measured deflection shapes on the arch span agreed reasonably well with those predicted by initial FE model. The vertical movement of the south and north viaduct spans was not measured, since only the arch span of the bridge was instrumented with accelerometers. Such a test plan was determined according to observations from initial FE analysis that the two viaduct spans were relatively stiff in vertical direction with closely-spaced bridge bents.

The first two lateral modes obtained from the test measurements were dominated by the main arch span and all the three components – the arch rib, lower and upper decks – moved in phase. And from the third lateral mode up, more global vibration which consisted of the coupling between viaduct spans and arch span were observed. As a consequence of the graphic comparison, only the three analytical lateral modes were paired up with their experimental counterparts.

Another important observation was that significant vibrations occurred on the two towers when reviewing the analytical results. Several tower dominated mode shapes appeared in rather low frequency range. For example, considerable tower motion in the longitudinal direction of the bridge was observed in the fifth and sixth analytical mode respectively, immediately after the first two vertical modes and two lateral modes. In the two tower modes, the tower moved vividly with little correlation with the viaduct span and arch span which it connected with. Quite a few span modes were also coupled with active bending or torsion motion of one or both of the towers. These observations indicated that continuity conditions may not be appropriately assumed in initial FE model at tower-deck interfaces at the lower and upper levels where expansion joints were located.

The disadvantage of three-dimensional plotting was that the differences may be easily seen but difficult to interpret. Sometimes it was even confusing because so much information was included. A convenient solution is to project the 3D plots into 2D plane and the pattern of any deviation between the two mode shapes could then be exemplified in the resulting 2D profiles. However, cautions should be paid when trying to interpret difference between two mode shapes with their 2D profiles, since considerable discrepancies in space could be smeared into the plane plot and then became negligible. Figure 5-17 through Figure 5-23 displayed the comparison between the vertical deflection shapes from experiment and initial analysis, while the first three pairs of lateral modes were shown in Figure 5-24 through Figure 5-26.

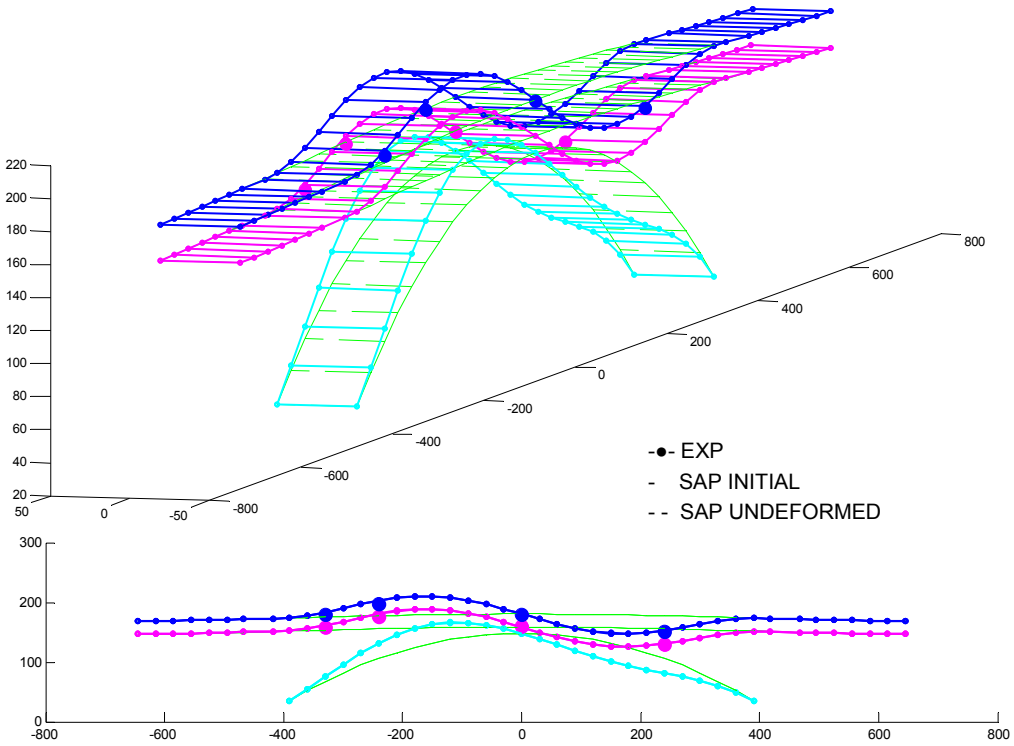

Figure 5-17 Experimental and initial analytical vertical mode 1

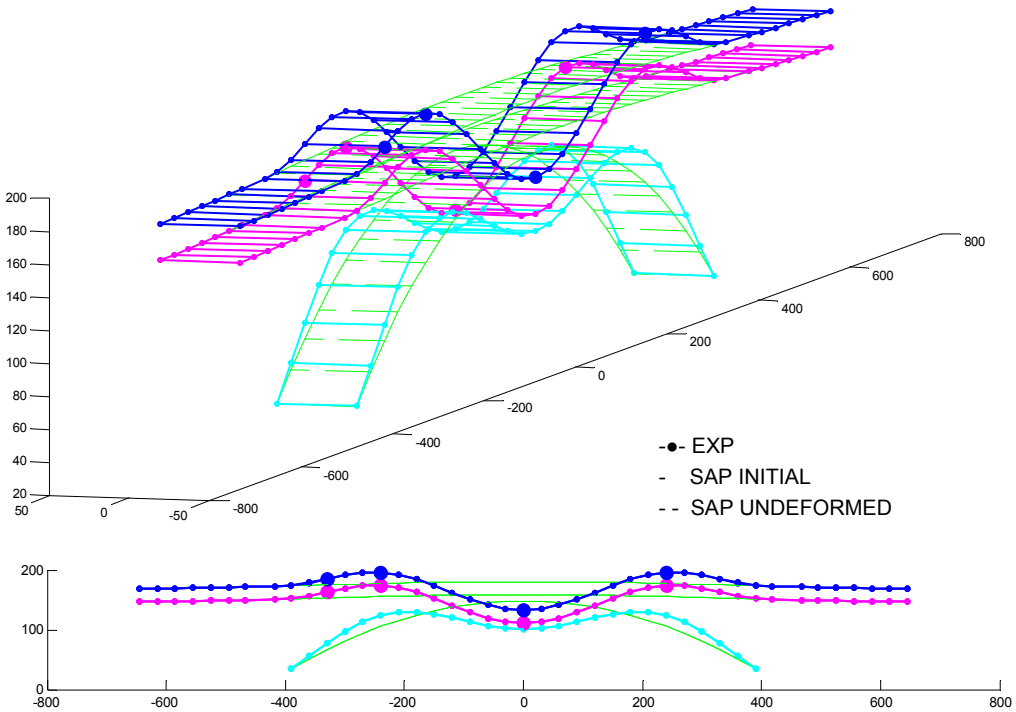

Figure 5-18 Experimental and initial analytical vertical mode 2

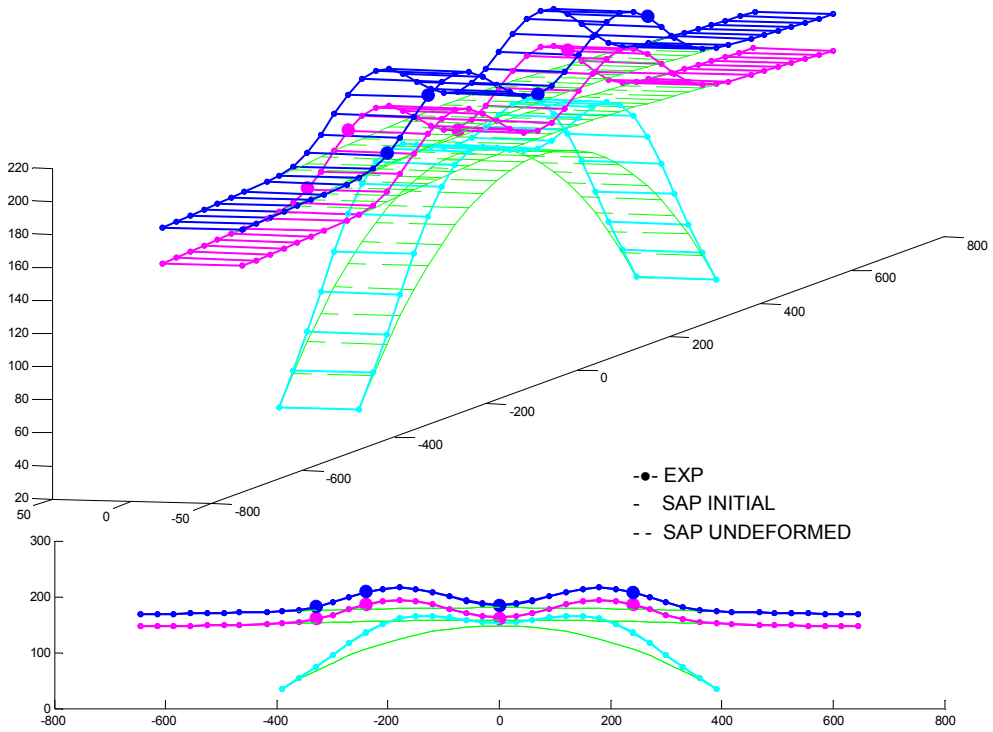

Figure 5-19 Experimental and initial analytical vertical mode 3

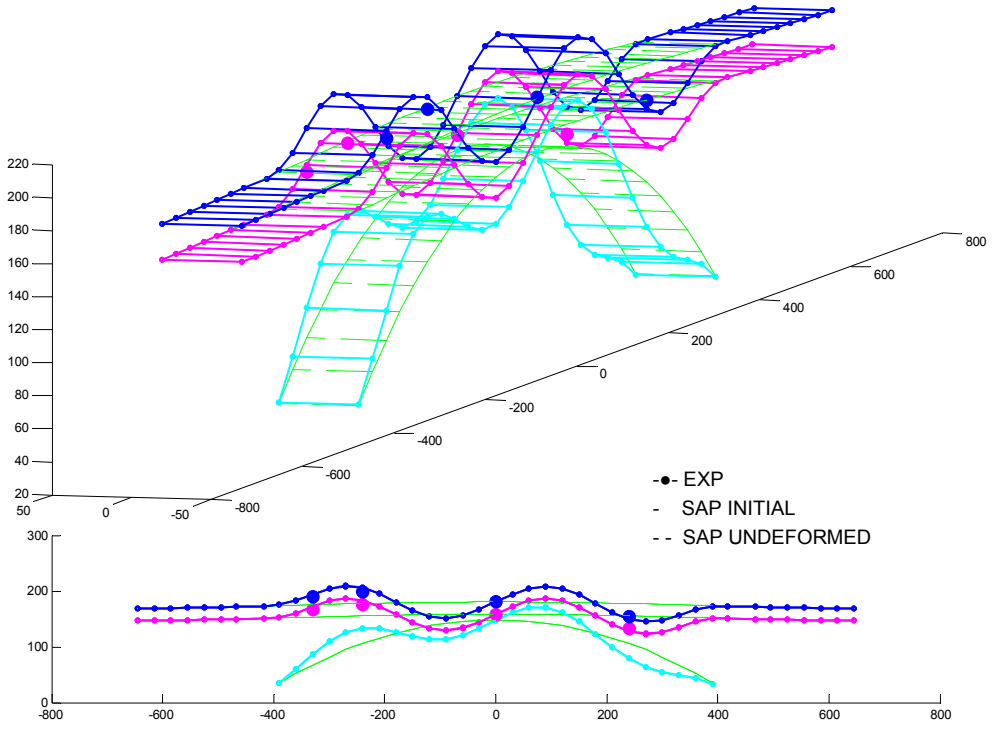

Figure 5-20 Experimental and initial analytical vertical mode 4

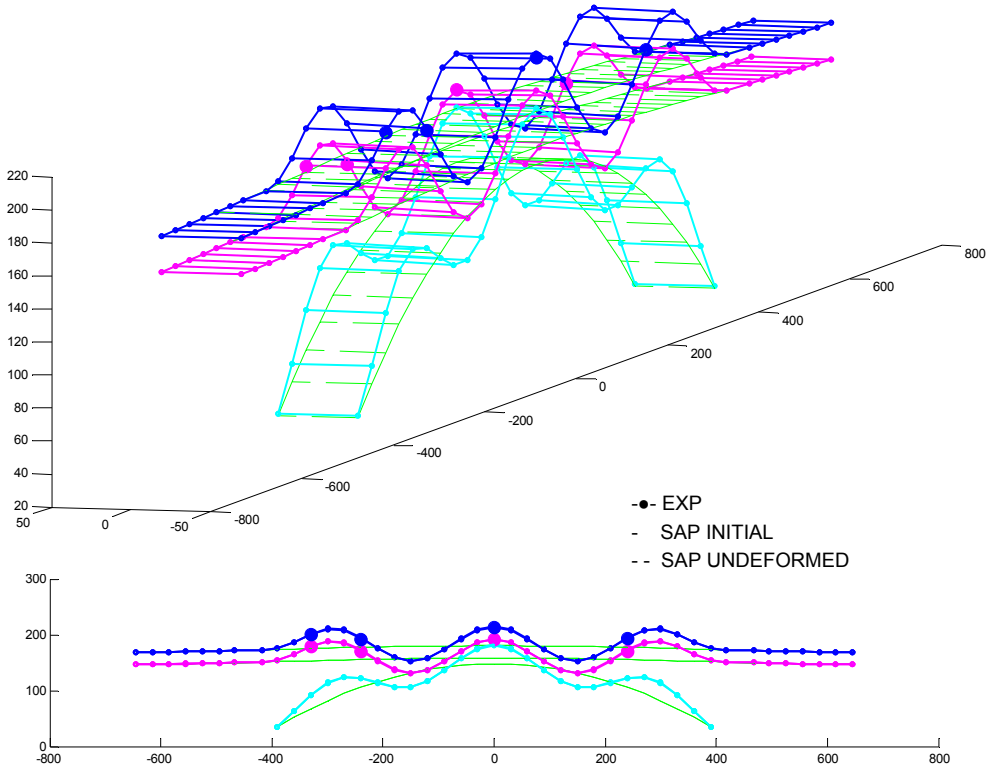

Figure 5-21 Experimental and initial analytical vertical mode 5

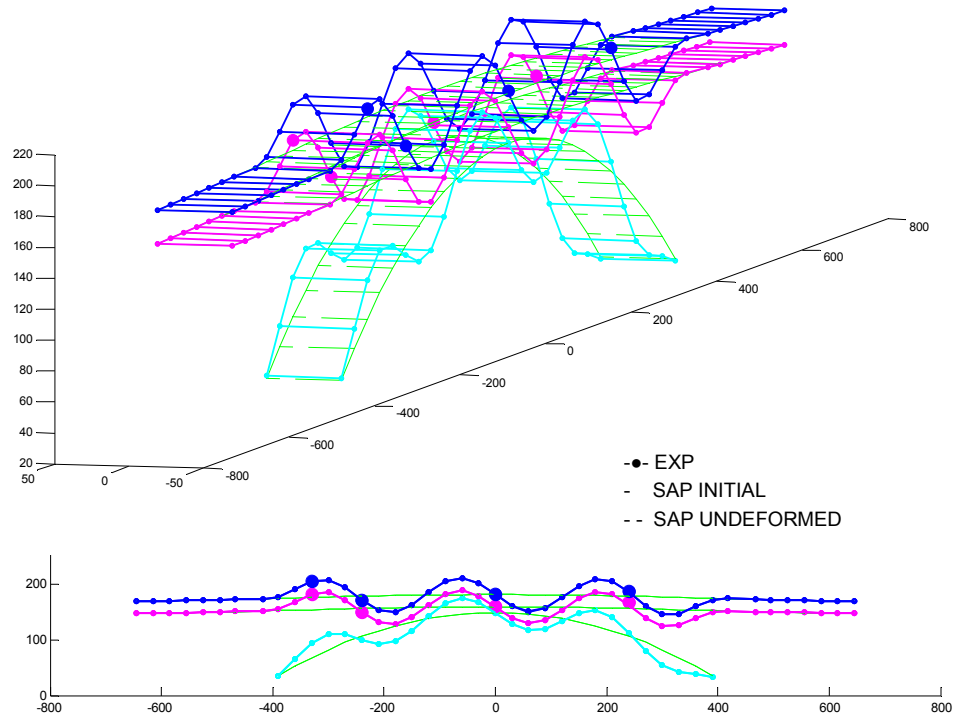

Figure 5-22 Experimental and initial analytical vertical mode 6

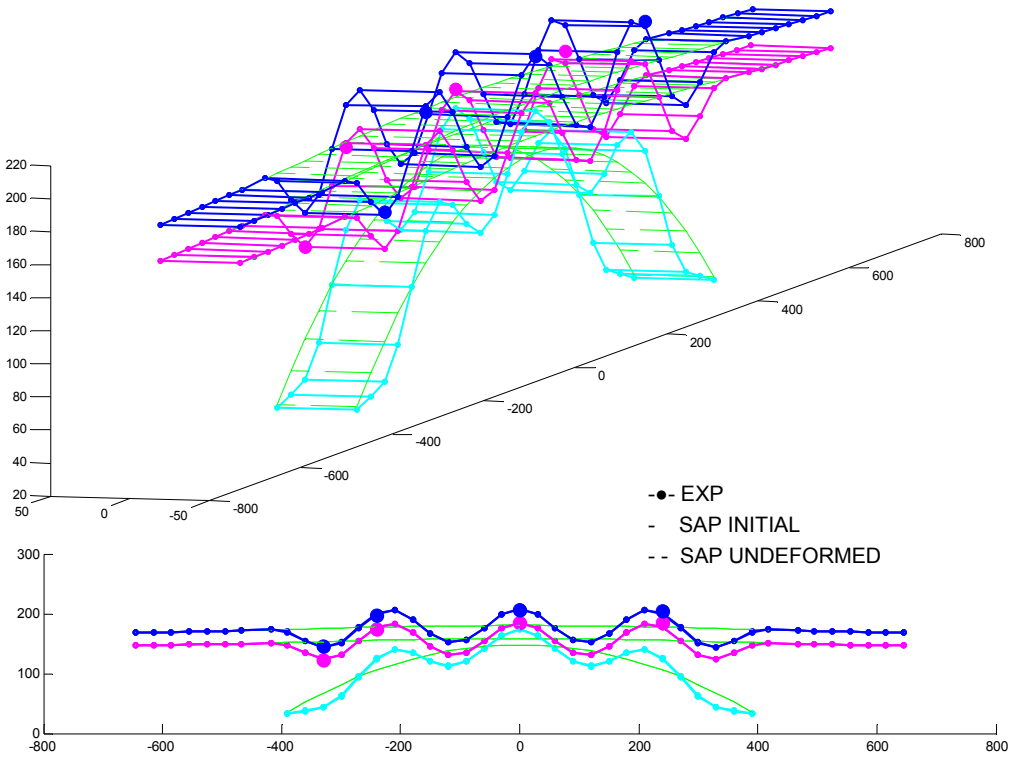

Figure 5-23 Experimental and initial analytical vertical mode 7

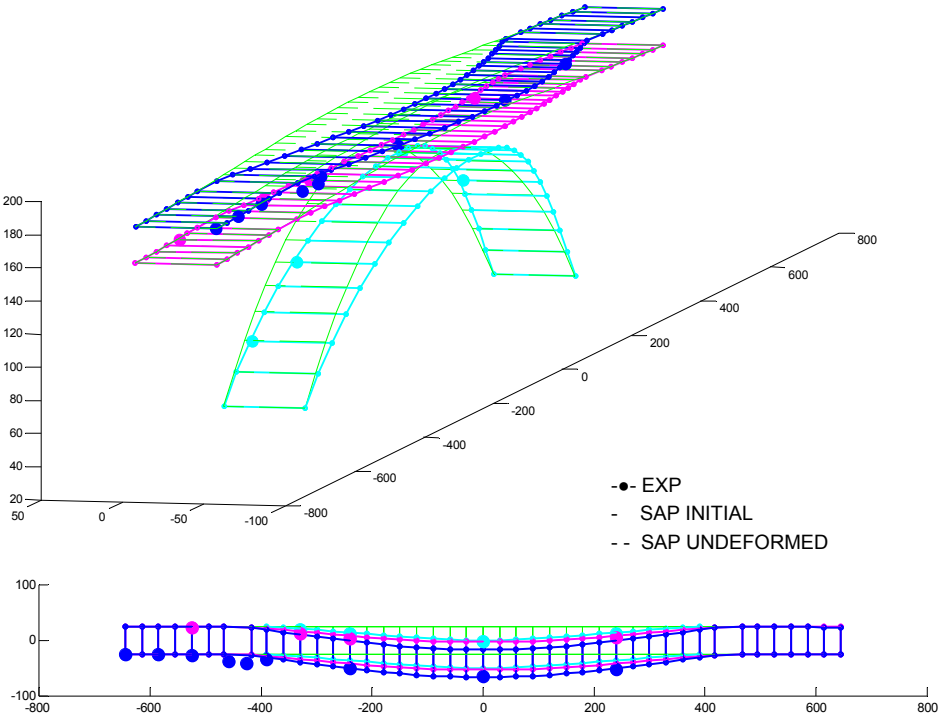

Figure 5-24 Experimental and initial analytical lateral mode 1

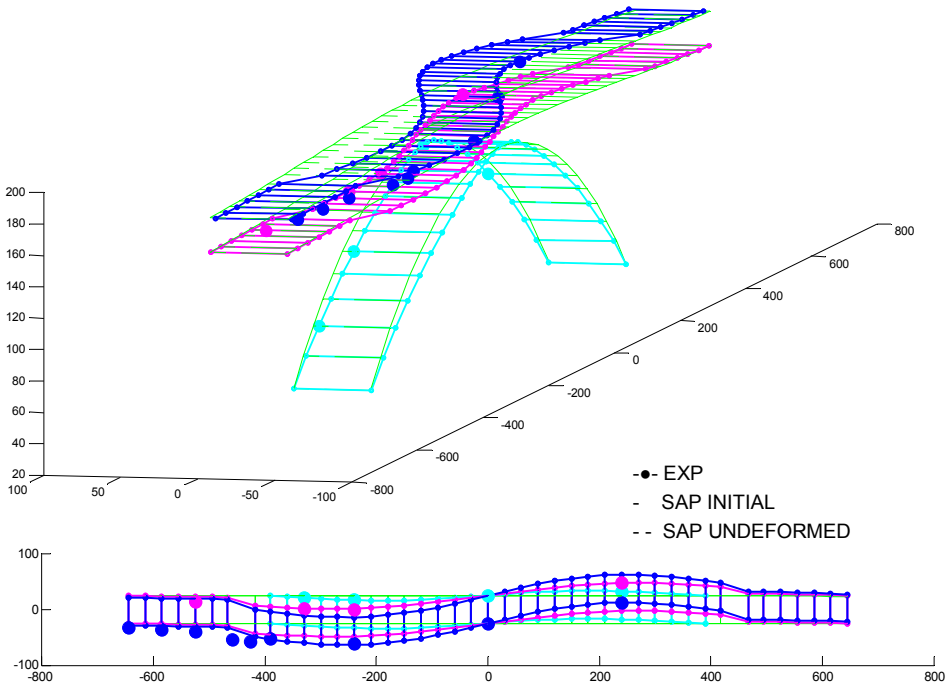

Figure 5-25 Experimental and initial analytical lateral mode 2

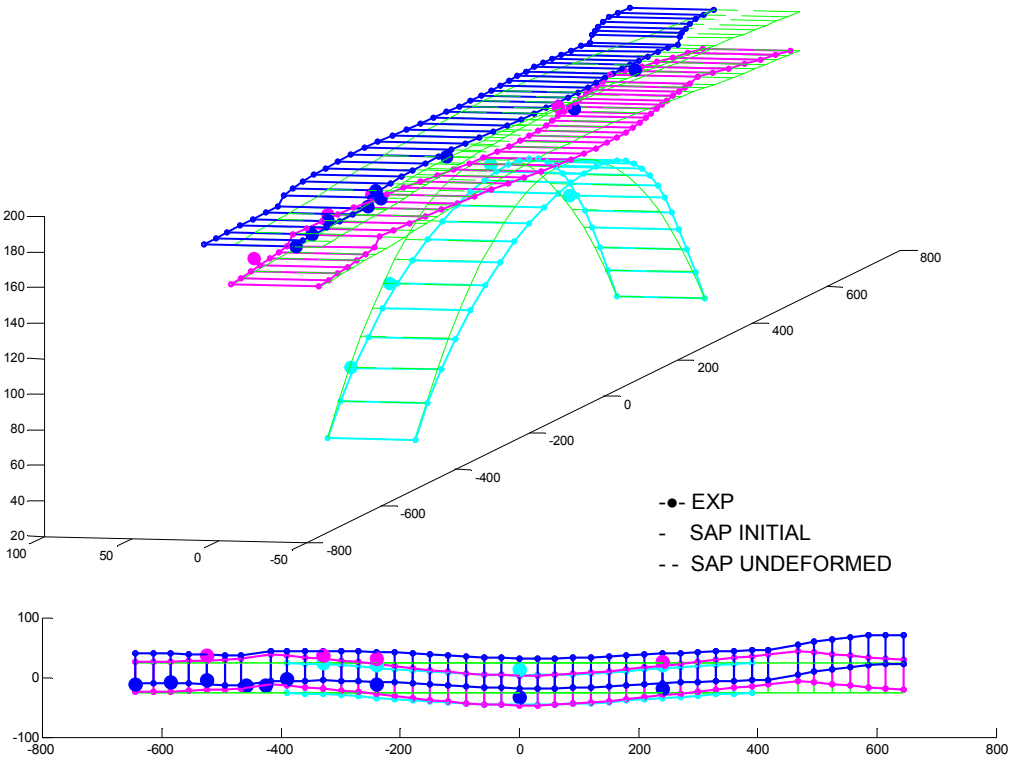

Figure 5-26 Experimental and initial analytical lateral mode 3

5.5.1.3 Numerical Comparison of Mode Shapes

As an alternative to graphic comparison of mode shapes, indexes such as Modal Scale Factor (MSF) and Modal Assurance Criterion (MAC) for pairs of mode shapes under scrutiny can be computed to evaluate the degree of their correlation.

The MAC matrix of the first seven pairs of vertical analytical and experimental modes was shown in Figure 5-27 and it revealed that good correlation existed between them. The large value of the off-diaganal member between modes 1 and 4 stemed from the coarse measurement grid, which was obvious when compared with analytical mode shape in Figure 5-17 and Figure 5-20. Figure 5-25 illustrated the correlation between the first four pairs of predicted and observed lateral modes. Although the MAC values for the first two lateral modes were above 0.9, as shown in Figure 5-28, the degree of correlation dramatically decreased in the third and fourth mode which might be attributed to the lack of good excitation in lateral direction under normal operation condition of the bridge.

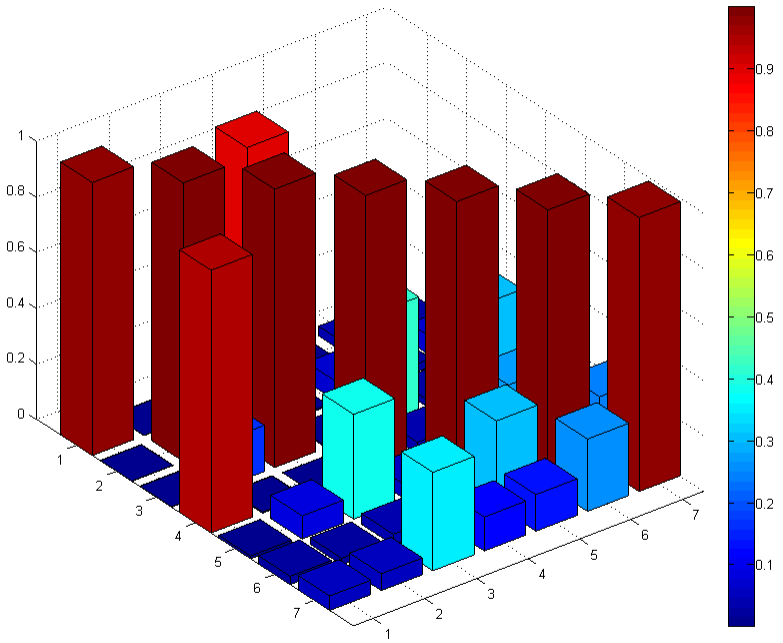

Figure 5-27 MAC of experimental and initial analytical vertical modes

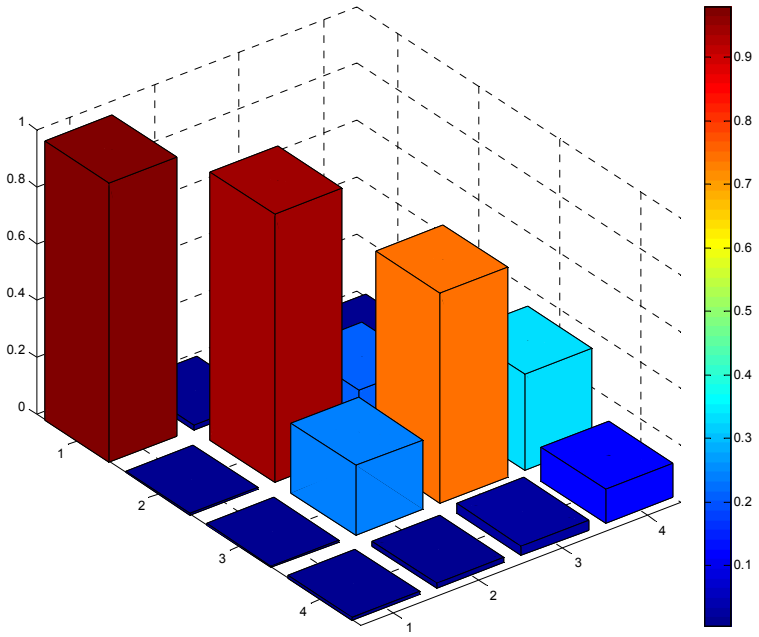

Figure 5-28 MAC of experimental and initial analytical lateral modes

5.5.1.4 Conclusion for Test-Analysis Correlation

The correlation between experiment and preliminary analysis revealed that considerable discrepancy existed in terms of simulation of mechanisms of flexibility, inertia, and support and continuity condition of the bridge. Calibration of the initial FE model was essential to improve its capability to represent the global structural dynamic behaviors.

A total of 10 modes identified from the test measurements were paired up with their analytical modes. Seven of them were vertical modes and the rest of them were lateral modes. Both the graphic comparison and the values (close to 1) of the diagonal elements in the calculated MAC index matrix showed that good correlation existed in the vertical modes of the initial model and experiment. This indicated that the stiffness distribution of the main arch span of the bridge was properly conceptualized by the initial model. But as shown in Table 5-11, the predicted modal frequencies for almost all vertical modes were consistently lower than the experimental ones. Possible reason would be that either the mass and/or the stiffness in the vertical direction were not properly simulated. Unlike the arch span, the south and north viaduct spans were

supported at every other panel point by the bridge bents. Thus the vertical motions of viaduct spans would only affect higher vibration modes. This was proved in eigenvalue analysis of the preliminary model in which two viaducts did not participate in the vibrations of the first several modes. It should be noted that the first two vertical modes displayed a curvature of second and third bending in the arch span respectively. And they were followed by a mode shape which demonstrated a similar curvature as the third bending but had no zero-crossing points. Hence it may be inappropriate to define it either the first or third bending mode.

For the lateral vibrations of the bridge, the first two lateral modes predicted by the nominal model matched up well with the corresponding experimental results in terms of deflection shapes while the eigenfrequencies were lower by more than 15 percent. The arch rib, lower and upper decks of the arch span moved together to form a lateral bending shape while the deflection of the deck levels at viaduct spans had comparatively lower amplitude especially the first mode. In the meanwhile both the modes were also slightly coupled with torsion motions since slight vertical displacements were observed from the mode shapes. From the third mode and up, however, one-to-one correspondence was difficult to be determined between the higher-order frequencies and deflection shapes of the a-priori model and those obtained through modal testing.

For example, the movement of upper deck in the analytical eighth mode shared some similarity with that of the third experimental lateral mode while the lower deck deflected differently because of the opposite phase in analytical and test results. Hence it was extremely difficult to have the amplitude, curvature and phase of the relative movements of the arch, lower and upper decks at arch span and viaduct spans displayed in simulated modes completely agree with those of test measurements. In another word, there was a lack of global lateral vibration of the whole bridge in the finite element simulation. One explanation for this phenomenon could be the connectivity conditions between viaduct and tower and between tower and arch at the lower and upper deck levels. Most of the observed higher-order lateral mode shapes were involved with

combinations of movement from the viaduct spans and arch span and they were different from the analytical lateral mode shapes by the relative amplitude and/or phase of one or more structural components. Therefore the boundary conditions at the end of viaduct spans as well as the continuity condition at the viaduct-tower-arch interface were critical areas for the structural behaviors in lateral direction.

The sequence of appearance of the first vertical and lateral models reversed in test measurement, compared with the predictions from the preliminary modal analysis. This implied that the resistance provided by vertical members of the bridge was greater than estimated. As a result, the relative stiffness in vertical and lateral direction simulated by the initial FE model was against the reality. It should be noted that the first two vertical modes displayed a curvature of second and third bending in the arch span respectively. And they were followed by a mode shape which demonstrated a similar curvature as the third bending but had no zero-crossing points. Hence it may be inappropriate to define it either the first or third bending mode.

5.5.2 Global Calibration

5.5.2.1 Procedure of Global Calibration

Global calibration of the initial FE model can usually be performed both in modal and flexibility (geometric) spaces. In modal space, the correlation between analytical and experimental frequencies and mode shapes was achieved by adjusting the stiffness or the mass or a combination of both. In flexibility space, changes in mass of the structure may have little impact on the structural flexibility (inverse of stiffness). However, the calibrated analytical model was supposed to match experimental results in both modal and flexibility spaces.

The global calibration process on the a-priori analytical model of the Henry Hudson Bridge was conducted primarily in the modal space. In order to systematically carry out the calibration, some necessary procedures were proposed, as shown in the flowchart below. The adjustments

made on were based on the test-analysis correlation, sensitivity analysis and engineering heuristics.

The first step of the global calibration attempted to increase the vertical bending stiffness of the structure because the modal frequencies predicted from the initial model was observed to be less than their experimental counterparts. This could be achieved by either adjusting the material and geometric properties (such as *EI*) of all members which contributed to the vertical bending stiffness of the bridge or strengthening the connectivity between the upper and lower decks and the lower deck and the arch rib so that the arch action of the main arch span could be reinforced.

The poor correlation in the lateral vibration between analysis and experiment could be attributed to several sources. First of all, under normal operation conditions, the responses of the bridge were mainly from the traffic induced excitations. Therefore many lateral modes in the frequency range of interest may not be well excited. Secondly, the sensitivity analysis revealed that the translational spring stiffness at the two extreme ends of the viaduct spans and the continuity condition at the viaduct-tower-arch interface had significant influence on the lateral movement of the bridge (the modal frequencies, the sequence of modes and mode shapes). Hence, the second step of the global calibration would aim to improve the test-analysis correlation in the lateral direction.

The final step was to check the completeness of the updated model. The completeness of a FE model may be defined as the state of the model in which all of the critical mechanisms of the structure were properly conceptualized. The reason behind the model completeness check was to ensure significant modeling error with epistemic mechanism embedded in the initial model were acknowledged and parameterized as much as possible.

Table 5-12 Procedure of global calibration

Calibration Process	Purpose
Global calibration in modal space (by adjusting parameters and/or continuity conditions in vertical direction of the bridge	To make the frequency values of analytical model have minimum discrepancy with those of experiment and to make the mode order of analysis consistent with that of experiment
Further global calibration in modal space (by adjusting parameters, and/or, boundary and continuity conditions in lateral direction of the bridge)	To improve test-analysis correlation in the lateral movement of the bridge, including the modal frequencies, mode order and mode shapes
Check the completeness of the analytical model	To assure that the analytical model is complete so that all critical global stiffness and force distribution mechanisms are simulated

5.5.2.2 Calibration Results

For the main arch span, there were three layers vertically to carry the loads – the arch rib, the lower and upper decks, which were connected by vertical members at the fascia girders at each level. In the initial analytical model, the relative displacement between the top joints of the columns between the arch rib and the lower deck and the corresponding joints along the fascia girder of the lower deck were constrained with 'Equal Constraints' in all three translational degrees of freedom. These constraints were replaced by 'Body Constraints' in all six degrees of freedom in the updated model. Similarly the moment releases of the same columns were deleted at their bottom joints where they directly connected with the arch ribs. For all vertical members between the lower and upper decks, on both the arch span and two viaduct spans, rigid offsets were defined at the top joints of these members to reinforce the connections. By applying these adjustments, the arch action of the arch span was strengthened. This led to a shift up in all of the modal frequencies, not only in vertical direction. However, the influence on the vertical modes was obviously much more significant so that the order of the first vertical and lateral mode was reversed. As a result, the sequence of modes was consistent with those of experimental modes.

Although the vertical vibrations of the main span was very sensitive to the support conditions of the arch ends, as indicated in the sensitivity analysis, the boundary conditions of the updated

analytical model remained the same after the global calibration. The fully fixed restraints were considered as a reasonable idealization for the massive concrete blocks at the arch ends and no experimental data were available to justify any modification. The sensitivity analysis also revealed that the boundary conditions of the viaduct bents had far less impact on the global dynamic properties of the bridge (frequency, sequence of mode and mode shape) and therefore they were all unchanged.

The sensitivity analysis on the nominal model revealed that the dynamic characteristics relied heavily on the continuity conditions of the viaduct-tower-arch interface where the expansion joints were located. In the initial model, the discontinuity at the lower deck was represented by two separate floor beams and the joints along the fascia girders at each side of expansion joint was constrained by 'Equal Constraint' in vertical direction. And rigid links with proper releases as well as 'Equal' joint constraints in both lateral and vertical direction were used to simulate the movement of the upper deck at each side of expansion joint. As a result, the towers were completely free from restraint in the longitudinal direction except that they were fixed at the bottom. This could explain why in the nominal model pure tower modes appeared just after the first two vertical and lateral modes of the bridge. However, from the responses of the accelerometers installed at the mid-height of the tower, no significant peaks showed up before 4 Hz. This observation indicated that the viaduct-tower-arch interface was stiffer than what was expected. Consequently the relative movement in the longitudinal direction was frozen by additional joint constraint at the corresponding node points at both the lower and upper deck levels. Besides, the shear and torsion releases in the rigid links at the tower and upper interface were deleted. The aforementioned modification strengthened the bridge in both lateral and vertical direction.

Table 5-13 Comparison of modal frequencies before and after global calibration

Mode #	Experimental (Hz)	Initial (Hz)	Diff (%)	Updated (Hz)	Diff (%)	Description
1	0.616	0.512	-16.883	0.588	-4.545	1st lateral bending (arch)
2	0.739	0.505	-31.664	0.721	-2.436	2nd vertical bending
3	0.952	0.890	-6.513	0.973	2.206	3rd vertical bending
4	1.182	0.977	-17.343	1.054	-10.829	2nd lateral bending (arch)
5	1.506	1.257	-16.534	1.404	-6.773	1st lateral bending (global)
6	1.587	1.535	-3.277	1.566	-1.323	1st vertical bending
7	1.732	1.651	-4.677	1.714	-1.039	4th vertical bending
8	2.556	2.393	-6.377	2.505	-1.995	5th vertical bending
9	3.300	3.137	-4.939	3.276	-0.727	6th vertical bending
10	4.110	3.955	-3.771	4.061	-1.192	7th vertical bending

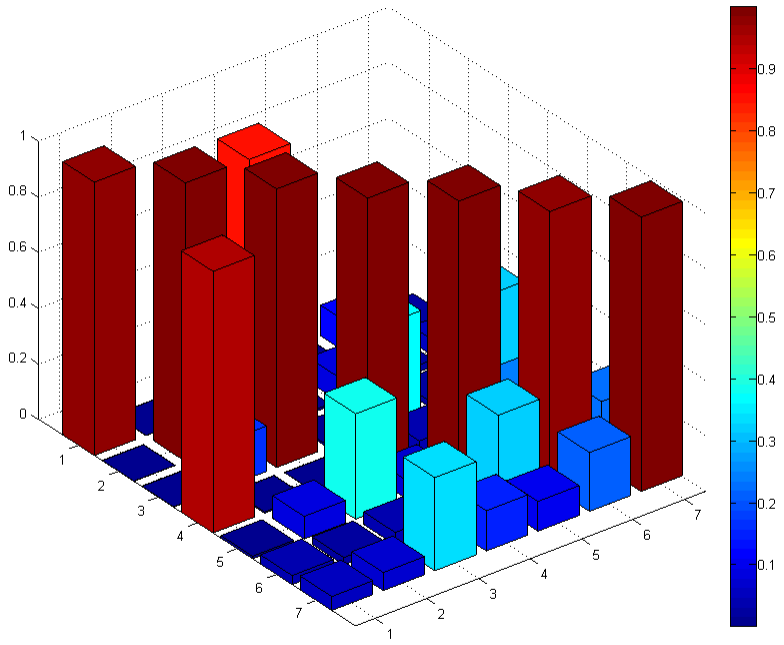

Figure 5-29 MAC of experimental and updated analytical vertical modes

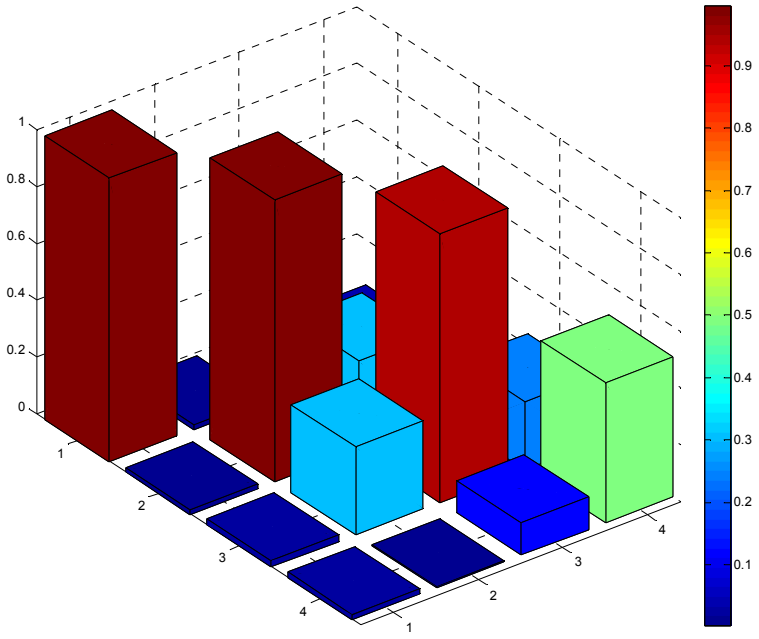

Figure 5-30 MAC of experimental and updated analytical lateral modes

5.5.2.3 Model Completeness Check

The model completeness check is an essential step for the integrative paradigm of Sys-Id. As discussed before, the system identification of large-scale constructed system is usually a highly under-determinate inverse problem. If more than one initial model is constructed at the early stage, model completeness check will serve to select the best model which represents the actual structure with most accuracy and completeness; If only one a-priori model is simulated, this check will judge whether the critical mechanisms which control the physical behaviors are appropriately conceptualized. However, it should be noted that the complete model is typically very difficult to obtain because of the limited amount of test data and inadequate heuristics information. In such case, the completeness check will lead to the most admissible model with available information; otherwise, additional experiments may be needed.

The evaluation tool obtained through the cantilever beam study in the previous chapter was extended to be applied on the Henry Hudson Bridge. The study on the cantilever showed that

global model parameter with little variability such as the steel modulus of elasticity *E* tended to distort itself to compensate unacknowledged modeling error in order to minimize the test-analysis discrepancy. This could serve as an excellent tool to recognize the existence of epistemic modeling error. In the Henry Hudson Bridge case, the modulus of elasticity of steel E was utilized to check the model completeness of the calibrated analytical model. The material property of steel *E* was a global model parameter. And as indicated from the sensitivity analysis, it was sensitive to the change of the modal data. The following figures displayed the fluctuation of a predefined error index which is comprised of the modal data with the perturbation of the *E* around its nominal value. For the initial analytical model, the predicted modal data converged when *E* was over 15 percent of its nominal value and the corresponding error index was still as high as 0.289. After the global calibration, the analytical modal data converged around the nominal value of *E* with the error index far less than that from the nominal model. Although it may not be valid to conclude that the calibrated model is free of modeling error, it was the most admissible model with the available data.

The error index was defined as

$$NORM = \sqrt{\sum_{i=1}^{7}\left(\frac{FREQ_{Ai} - FREQ_{Xi}}{FREQ_{Xi}}\right)^2}$$

where $FREQ_{Ai}$ and $FREQ_{Xi}$ denote the analytical and experimental modal frequencies respectively.

MODE #	0.85 *E*	0.90 *E*	0.95 *E*	1.00 *E*	1.05 *E*	1.10 *E*	1.15*E*	1.20 *E*	1.25 *E*	EXP
1	0.4660	0.4795	0.4925	0.5053	0.5177	0.5298	0.5416	0.5532	0.5645	0.739
2	0.8204	0.8441	0.8671	0.8895	0.9114	0.9328	0.9537	0.9741	0.9941	0.952
3	1.4152	1.4561	1.4958	1.5345	1.5723	1.6091	1.6451	1.6804	1.7149	1.506
4	1.5234	1.5671	1.6096	1.6510	1.6913	1.7307	1.7692	1.8068	1.8437	1.732
5	2.2083	2.2716	2.3332	2.3931	2.4515	2.5086	2.5643	2.6182	2.6724	2.556
6	2.8965	2.9789	3.0589	3.1369	3.2128	3.2868	3.3592	3.4298	3.4989	3.300
7	3.6551	3.7579	3.8578	3.9549	4.0495	4.1416	4.2303	4.3151	4.4086	4.110
NORM	0.4684	0.4190	0.3754	0.3389	0.3108	0.2927	0.2855	0.2893	0.3034	

DIVERGENCE ◄——————————————————► DIVERGENCE

Figure 5-31 Sensitivity of the initial model with respect to elasticity modulus of steel *E*

MODE #	0.85 *E*	0.90 *E*	0.95 *E*	1.00 *E*	1.05 *E*	1.10 *E*	1.15*E*	EXP
1	0.6723	0.6889	0.7050	0.7207	0.7360	0.7510	0.7656	0.739
2	0.8981	0.9237	0.9486	0.9729	0.9966	1.0196	1.0422	0.952
3	1.4445	1.4862	1.5268	1.5663	1.6048	1.6424	1.6792	1.506
4	1.5852	1.6294	1.6723	1.7141	1.7556	1.7949	1.8337	1.732
5	2.3128	2.3787	2.4428	2.5052	2.5659	2.6252	2.6832	2.556
6	3.0259	3.1114	3.1945	3.2755	3.3543	3.4312	3.5064	3.300
7	3.7531	3.8587	3.9612	4.0610	4.1582	4.2531	4.3457	4.110
NORM	0.2091	0.1449	0.0883	0.0583	0.0844	0.1355	0.1914	

DIVERGENCE DIVERGENCE

Figure 5-32 Sensitivity of the updated model with respect to elasticity modulus of steel *E*

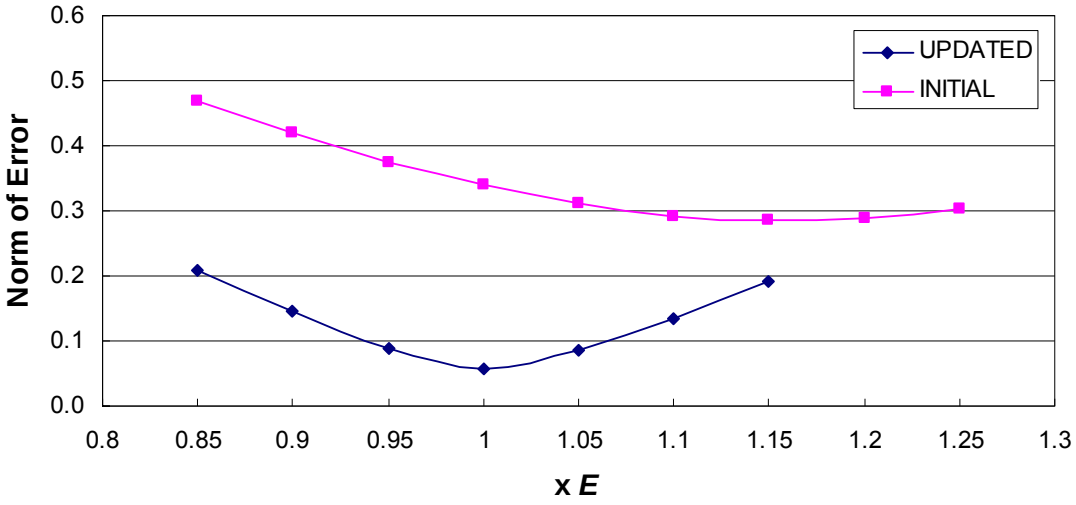

Figure 5-33 Comparison of sensitivity of the initial and updated model with respect to elasticity modulus of steel *E*

5.6 Conclusion & Discussion

An integrative application of Sys-Id on a long-span steel arch bridge was presented in this chapter. By taking advantage of an element-level three-dimensional finite element model and ambient vibration technique, this application demonstrated the strength of Sys-Id to provide in-depth understanding of the physical behaviors of large-scale constructed systems. As the identification progressed, it was obvious that each step of the process were interwoven together. The a-priori analytical model assisted not only in the design of ambient vibration testing but also for the interpretation of the modal parameters extracted from the test measurements. On the hand, the large amount of test data was carefully manipulated to examine the stationarity, variability and the effects of sampling bandwidth. And the parameter estimation results were then used for

the global calibration of the bridge so that the accuracy and completeness of the analytical model could better reflect the actual structural behaviors.

The global calibration of the analytical model of the bridge was accomplished on the basis of correlation analysis, sensitivity analysis as well as engineering heuristics. With the available dynamic test data, the global attributes of the bridge in the vertical direction was identified with a reasonable level of confidence. Relatively less reliability was obtained in the modal properties in lateral direction which were predicted by the calibrated model, primarily because the lateral modes of the bridge was unable to be well excited under normal operational conditions. Although this was a common problem associated with ambient monitoring, the lateral vibration attributes of the bridge is critical in this case, since the calibrated model would ultimately serve as a baseline to seismic performance of the bridge.

For large-scale complicated constructed systems, the identification process was always involved with various sources and levels of uncertainty, especially uncertainty due to epistemic mechanism. For the experiment aspect, proper data analysis and post-processing techniques were useful to recognize and mitigate the uncertainty associated with experimental data. For the analytical aspect, the model completeness check was essential to ensure that all critical mechanisms of the structure were appropriately conceptualized in the calibrated model. The idea behind was that one or more global model parameters which were sensitive to the change of updating and had small variability tended to distort themselves to compensate the test-analysis discrepancy if significant modeling errors were not acknowledged. By making use of the modulus of elasticity of steel E as a global index, a comparison of sensitivity of E with respect to a predefined error index between the initial model and the calibrated model revealed that the calibrated model was an admissible model with available test data.

6 Conclusions & Future Work

6.1 General Remarks

The use of system identification for characterization of constructed systems has gained increasing interest over the last decade. However, tremendous difficulties remain for civil engineering in the transition toward the integrative framework of modeling and simulation, modal testing and analysis, and model calibration and validation. Those difficulties primarily stem from a lack of reliability in the outcome of system identification, especially for large-scale complex constructed civil structures. Gradually our inability to accurately simulate, measure, interpret and predict actual physical behaviors to influence the followed decision making shapes up the skepticism towards system identification held by the owners/stewards of constructed systems. It is believed that the more significant barriers for more widespread implementations of system identification lie in fundamental gaps in knowledge of unique attributes associated with civil systems, rather than technological barriers such as practical sensing and networking techniques. As opposed to mass-produced manufactured mechanical systems, civil structures are generally constructed as one of a kind. Each individual structure distinguishes itself by the as-built characteristics of material and geometry, intrinsic force distribution, soil-foundation interface and possible mechanisms leading to nonlinear and nonstationary behaviors and so on. There is sufficient evidence that current knowledge about the loading, behavior and performance of constructed systems is greatly incomplete. The incompleteness and inaccuracy smear into identification process through model construction, test design and execution, data processing interpretation as well as model updating, and gives rise to epistemic uncertainty.

The research presented herein attempted to establish a better understanding about this most critical and pervasive challenge facing civil engineers today, with particular focus on epistemic uncertainty which is commonly encountered in a priori model construction during the process of identifying an existing civil engineering structure. The thesis was designed to reveal the impact of

epistemic modeling uncertainty on the reliability of field calibrated finite element model of a constructed system. Since conceptualizing and simulating of a constructed system is more or less involved with simplification and abstraction, feasible techniques were developed to recognize and mitigate epistemic modeling uncertainty when these unacknowledged uncertainties played a control role on the test-analysis discrepancy. In applications of system identification on large-size complex structures, the mismatch between the level information in detailed finite element model and test measurements often produced an ill-conditioned and non-unique inverse problem. In order to reduce uncertainties and the degree of non-uniqueness, the thesis also demonstrated an integrative system identification of a long-span bridge structure and approaches to evaluate the adequacy of calibrated analytical model were investigated.

6.2 Conclusions

6.2.1 Impact of Epistemic Modeling Uncertainty

As the summary about modeling uncertainties encountered in real-life applications of system identification (Chapter 2) illustrated, epistemic modeling uncertainty associated with one specific model of a constructed system may originate from a large amount of different mechanisms, in terms of geometry, kinematics of deformation, material properties and their variation, boundary and continuity conditions, any nonlinearity and non-stationary structural properties and loads. Their influence on the dynamic properties of a structure (natural frequencies, damping ratios and mode shapes) also varies in different cases. Furthermore, epistemic modeling uncertainty was usually closely related to the choice of model form, element type, idealization of boundary and continuity conditions and etc and parameterization of them was often difficult. In this thesis, the challenging epistemic modeling uncertainty was approached through a test bed in the laboratory – a steel cantilever beam with two test configurations. The integrative paradigm of system identification was applied on the different beam setups and the impact of epistemic modeling

uncertainty on the reliability of characterization of constructed systems was evaluated by comparing the results of different identification cases.

In the first identification attempt, a 20-element beam model with ideally fixed support was generated as the initial analytical model for the two beam setups, pretending not to know that the boundary assembly in the configuration 2 would inevitably introduce partial fixity. All five predicted modes from the initial model were paired up with the experimental results from test configuration 1. The test-analysis correlation was further improved by adjusting the only updating parameter, i.e., the Young's modulus of steel. In contrast, the initial model failed to simulate the repeated vibration modes which were observed from the beam under configuration 2. Only the first three and the fifth analytical modes were matched up with their experiment counterparts. Since four of the experiment modes demonstrated deflection shapes similar with the theoretical fourth bending mode, there was immense uncertainty associated with the correlation between the measured and simulated fourth mode. Although the gap in natural frequency from the analytical model and experiment observation narrowed considerably after updating, relatively large difference remained especially in the natural frequency of the first mode. The updating forced the pre-selected model parameter lost almost one third of its initial (nominal) value.

As shown in the difference in the estimated values of the same updating parameter, epistemic modeling uncertainty had a significant impact on the reliability of calibrated analytical model. The two updated parameter values obtained from two identification cases were supposed to converge to the exactly same number, since they stood for the material property of the same beam under two different test configurations. However, the Young's modulus of steel was adjusted to be around 90 percent and 67 percent of its nominal value respectively. Especially for the beam under second configuration, such a dramatic decrease in the material property was obviously against the reality, and the updating parameter could be considered physically meaningless. The only reasonable explanation for it was that the selected updating parameter was not the

controlling factor for the poor test-analysis correlation and significant epistemic uncertainty was still embedded in the calibrated analytical model.

Therefore, it could be concluded that complete and accurate localization of modeling uncertainty in an initial analytical model was crucial for the success of identification. When significant epistemic modeling uncertainty due to imperfect knowledge about the system existed, the selected updating parameters, although they might be not the dominate uncertainty sources, they tended to distort themselves during the updating procedure in order to compensate for the test-analysis discrepancy. As a result, either the updating parameters lost their physical significance, or the identification could not converge, or both.

6.2.2 Recognition and Mitigation of Modeling Uncertainty

The abnormality in the updated value of the elasticity modulus for the beam under test configuration 2 accurately indicated the existence of epistemic modeling uncertainty. Since epistemic uncertainty, as defined, was due to a lack of information about the structure under study, most effective approach to mitigate it was often involved with additional test data. For the beam under the second test configuration, supplementary impact tests were designed and executed to provide an overview of the global attributes of the system. The test observations revealed that the boundary assembly experienced considerable vibrations when the system was excited at the overhang span of the beam. As a result of coupling between the different subcomponents of the system, more than one mode in the frequency band between 100-200 Hz displayed similar vibration shapes. However, all of the vibration shapes were associated with different characteristics; some were dominated by the beam while others were dominated by local vibrations of the top assembly.

Another initial analytical model was therefore constructed to account for the identified interaction between the beam and the assembly. In order to be consistent with previous identification case, only the beam was explicitly simulated and the effect of vivid boundary

movement was idealized as support spring, although the new model was still unable to simulate the repeated experiment modes. Consequently the analytical fourth bending mode was matched up with one of the four repeated experiment modes, in which the vibration of the beam was significantly greater than the assembly. The identification results obtained for the two test configurations using the new initial analytical model showed that the discrepancy in the frequency of all of the five set of paired modes were successfully reduced within four percent in both cases. As opposed to the results obtained in the previous a priori model, the improvement in test-analysis correlation was achieved without sacrificing the physical significance of the model. The updated values for the Young's modulus just slightly fluctuated from its nominal value and they were reasonably close to each other.

Therefore a feasible and effective indicator for the presence of epistemic modeling uncertainty associated with the a priori model of a constructed system was to incorporate into updating procedure one or more dummy global model parameters which are sensitive to the change of dynamic properties of a structure and of little known variability. Any excessive change in these global model parameters after calibration often implied that they distorted themselves to compensate the effects of unacknowledged modeling uncertainties. Additional test data could greatly increase our capability to efficiently localize and mitigate modeling uncertainty due to epistemic mechanism. It should be noted that 'additional' herein actually meant additional information contained in the supplementary tests, rather than simply repetition of previous experiments.

6.2.3 Model Adequacy Evaluation

Model construction for a large-scale complex constructed system such as long-span bridges was a process of simplification and abstraction. The resulting analytical model was often inherent with various sources of modeling uncertainty caused by misrepresentation and incomplete representation of the structure. However, the incomplete and inaccurate information from test

measurements obtained with sparse test grid made it impossible to pinpoint the effects of all uncertainty sources in the a priori model. Therefore, model adequacy evaluation played an essential part during in identification of a constructed system to ensure all critical physical mechanisms were appropriately conceptualized.

The proposed integrative Sys-Id paradigm was applied on a long-span steel arch bridge, the Henry Hudson Bridge, by taking advantage of an element-level three-dimensional finite element model and ambient vibration technique. This application demonstrated the strength of Sys-Id to provide in-depth understanding of physical behaviors of large-scale constructed systems. As the identification progressed, it was obvious that each step of the process were interwoven together. The a-priori analytical model assisted not only in the design of ambient vibration testing but also for the interpretation of the modal parameters extracted from the test measurements. In the meanwhile, experimentally obtained dynamic properties of the bridge were used for global calibration of the bridge. In order to eliminate possible misinterpretation of the test data, the statinarity, variability and effects of sampling bandwidth were examined before modal parameter estimation.

The global calibration of the bridge was carried out on the basis of correlation analysis, sensitivity analysis and engineering heuristics, using experimental modal parameters (natural frequencies and mode shapes). As a result, the global attributes of the bridge in the vertical direction were identified with reasonable accuracy. Relatively less confidence was on the predicted modal properties in lateral direction, primarily because the lateral modes were unable to be well excited under normal operational conditions. Although this was a common problem associated with ambient monitoring, the lateral vibration attributes of the bridge was often critical when the calibrated model would ultimately serve as a baseline to seismic performance of the bridge.

The finding from the cantilever test bed was extended as an efficient tool to examine the adequacy of the globally calibrated bridge model. The idea behind was that one or more global model parameters which were sensitive to the change of updating and had small variability tended to distort themselves to compensate the test-analysis discrepancy if significant modeling uncertainties were not acknowledged. Since the main material of the bridge was steel, the modulus of elasticity of steel was again utilized to assess adequacy of the globally calibrated bridge model. The value of a predefined error index indicated that the calibrated model converged when the elasticity modulus was around its nominal value and any perturbation of it led to diverged analytical prediction. In contrast, the initial model converged at the value of the elasticity modulus over 15 percent over its nominal value and the norm of the test-analysis difference was much greater. It demonstrated that with available information the epistemic modeling uncertainties associated with the a priori bridge model were significantly reduced. The globally calibrated model could be considered the most admissible model for the bridge.

As a conclusion, integrative system identification paradigm was a powerful tool to characterize the actual behaviors of a constructed system and it is feasible to be used on large-scale complex civil engineering structures. In real-life applications, systematical utilization of engineering heuristics often played a critical role in reducing modeling uncertainty and epistemic modeling uncertainty in particular embedded in the a priori model of the structure. The resulting model could be further examined to ensure all critical physical behaviors of the structure were completely and accurately simulated. One effective model adequacy evaluation tool proposed here was developed based on the finding from the cantilever study. Any observed divergence of predicted modal properties with respect to the perturbation of model parameters which were sensitive and of little variance indicated significant epistemic uncertainty remained in the model. Otherwise, further improvement in the calibrated model required additional information about the structure.

6.2.4 Others

Preparatory procedures such as correlation analysis, error localization, sensitivity analysis and test data informativeness quantification were essential for the following actual updating computation. Correlation analysis made it possible to determine the correlated mode pairs (a pre-requisite of most model updating methods) and also provided early indication for the localization of modeling uncertainty.

Sensitivity analysis was a conventional tool to assist analyst to identify the most sensitive parameters from a pool of candidates with respect to the available structural responses. In addition to the traditional sensitivity analysis which change one factor at a time, the improved approach which was based on 2-level factorial experiment design attempted to provide a clear picture of how these candidate parameters behave separately and together. This was proved in the cantilever case. But the number of designed experiments increased exponentially as the increase in the number of parameters of concerned.

A good number of error localization indexes were summarized and they may be theoretically sound and even feasible for cases when simulated experimental data were used. However they collapsed easily when applied on real-life systems, even in the simple cantilever beam system. One of the big obstacles for the application of these error indexes is that they often require a full set of experimental data. This was impractical because the measurement degrees of freedom were often far less than the analytical degrees or freedom when Sys-Id was applied on constructed civil structures. Consequently numerical errors associated with mode expansion techniques seriously hamper the accuracy of the error localization indexes.

6.3 Future Work

For the future research, the following suggestions were provided:

(1) The thesis proposed a feasible approach to recognize the existence of epistemic modeling error in the initial analytical model for updating process. However, methods to provide indications about the exact localization of errors required additional research efforts.

(2) In both the lab and the real-life applications, various sources of experimental uncertainties were lumped as one random process. Their effects on the following model calibration were acknowledged by using the average values of the estimated modal parameters from several sets of independent test data. In future study, a stochastic framework of model updating can be investigated to incorporate aleatory and epistemic experiment and modeling errors.

(3) When model calibration was conducted using modal data of the structure, the influence from the change of mass and stiffness could not be distinguished. In this thesis, the mass was assumed known and remained unchanged. However, modal data could be transformed into the modal flexibility and thus used as reference data for the updating. Under such circumstances, the stiffness of the structure could be exclusively calibrated. Another alternative was to make use of static data such as static displacement and strain measurement. Besides, analytical model calibrated by static data was likely able to yield predictions of strain and stress at the critical areas of interest with more accuracy, which may be more desirable for applications such as fatigue monitoring and control.

REFERENCE

1. Abdel-Ghaffar, A.M. and Scanlan, R.H. (1985). "Ambient Vibration Studies of Golden Gate Bridge: I. Suspended Structure." Journal of Engineering Mechanics, 111(4): 463-482.

2. Ang, A. H.-S. & De Leon, D. (2005). Modeling and analysis of uncertainties for risk-informed decision in infrastructures engineering, Structure and Infrastructure Engineering, 1(1): 19-31.

3. Abe, M. (1998), Vibration control of structures with closely spaced frequencies by a single actuator, *Journal of Vibration and Acoustics,* Transactions of the American Society of Mechanical Engineers, **120**, 117–24.

4. Aktan, A.E., Daniel, N.F., Brown, D.L., Dalal, V., Helmicki, A.J., Hunt, V.J. and Shelley, S.J. (1996). "Condition assessment for bridge management." Journal of Infrastructure Systems, 2(3), 108-117.

5. Aktan, A.E., Farhey, D.N., Helmicki, A.J., Brown, D.L., Hunt, V.J., Lee, K.L. and Levi, A. (1997). Structural Identification for condition assessment: experimental arts. Journal of Structural Engineering, 123(12), 1674-1684.

6. Aktan, A.E., Catbas, F.N., Turer, A. and Zhang, Z. Structural identification: analytical aspects. Journal of Structural Engineering, 124(7), 817-829.

7. Aktan, A.E., Catbas, F.N., Grimmelsman, K.A. and Tsikos, C.J. (2000). "Issues in infrastructure health monitoring for management." Journal of Engineering Mechanics, 126(7), 711-724.

8. Aktan, A.E. and Faust, D. (2003). "A holistic integrated systems approach to assure the mobility, efficiency, safety and integrity of highway transportation." Proc. Of the 1st International Conference on Structural health Monitoring and Intelligent Infrastructure, Tokyo, Japan, November 13-15, 2003.

9. Aktan, A.E., Ellingwood, Bruce, and Kehoe, Brian, "Performance-Based Engineering of Constructed Systems, Forum Paper, Journal of Structural Engineering, 311-323, March 2007.

10. Alampalli, S. (1998). Influence of in-service environment on modal parameters, Proc. Of IMAC 1998, 111-116.

11. Alaylioglu, H. and Alaylioglu, A. (1999). "Finite element and experimental bases of a practical bridge management and maintenance system." *Computers and Structures*, 73, 281-293.

12. Andersen, P. (1999). Aalborg University, Identification of civil engineering structures using vector ARMA models. PhD thesis, Aalborg, Denmark

13. Askegaard, V. and Mossing, P. (1988). Long term observation of RC bridge using changes in natural frequencies. Nordic Concrete Research, 7, 20-27.

14. Avitabile, P. (2000). "Model updating – endless possibilities." Proc. Of IMAC 2000, 562-570.

15. Baker, T.A. and Marsh, E.R. (1996). "Error localization for machine tool structures." IMAC 96, 761-768.

16. Banan, M. R., Banan, M. R. & Hjelmstad, K. D. (1994a), Parameter estimation of structures from static response. Part 1: Computational aspects, *Journal of Structural Engineering, ASCE*, 120(11), 3243–58.

17. Banan, M. R., Banan, M. R. & Hjelmstad, K. D. (1994b), Parameter estimation of structures from static response. Part 2: Numerical simulation studies, *Journal of Structural Engineering, ASCE*, 120(11), 3243–58.

18. Beck, J. L. & Katafygiotis, L. S. (1998), Updating models and their uncertainties. I: Bayesian statistical framework, *Journal of Engineering Mechanics*, 124, 455–61.

19. Beck, J.L., Guest Ed. (2004). Journal of Engineering Mechanics: Special issue on the structural health monitoring benchmark problem. 130(1).

20. Beolchini, G.C. and Vestroni, F. (1997). "Experimental and analytical study of dynamic behavior of a bridge." Journal of Structural Engineering, 123(11), 1506-1511.

21. Berman, A. (1998). "Validity of improved mathematical models – a commentary." Proc. Of IMAC 1998, 681-691.

22. Bijaya Jaishi and Wei-Xin Ren (2005). "Structural finite element model updating using ambient vibration test results." Journal of Structural Engineering, 131(4), 617-628.

23. Black, C.J. and Ventura, C.E. (1999). "Analytical and experimental study of a three span bridge in Alberta, Canada." IMAC 1999, 1737-1743.

24. Box, G.E.P., Hunter, W.G., Hunter, J.S. (2005). Statistics for experimenters: design, innovation and discovery. 2nd Ed., Wiley-Interscience, Hoboken, NJ.

25. Brownjohn, J.M.W., Dumanoglu, A.A, Severn, R.T. and Taylor, C.A. (1987). Ambient vibration measurement of the Humber Suspension Bridge and comparison with calculated characteristics. Proc. Of the Institution of Civil Engineers (London), 83 (2), 561-600.

26. Brownjohn, J.M.W., Dumanoglu, A.A., Severn, R.T, Blakeborough, A. (1989). Ambient vibration survey of the Bosporus Suspension Bridge. Earthquake Engineering & Structural Dynamics, 18(2), 263-283.

27. Brownjohn, J.M.W., Dumanoglu, A.A., Severn, R.T (1992). Full-scale dynamic testing of the second Bosporus Suspension Bridge. Proc. Of the World Conference on Earthquake Engineering, 2695

28. Brownjohn, James M. W. and Pin-Qi Xia (2000). "Dynamic assessment of curved cable-stayed bridge by model updating." Journal of Structural Engineering, 126(2), 252-260.

29. Brownjohn, J.M.W., Moyo, Pilate, Omenzetter, Piotr and Lu, Yong (2003). "Assessment of highway bridge upgrading by dynamic testing and finite-element model updating." Journal of Bridge Engineering, ASCE, 8(3), 162-172.

30. Brownjohn, J. M. W., Moyo, P., Omenzetter, P. & Lu, Y. (2003), Assessment of highway bridge upgrading by testing and finite-element model updating, *Journal of Bridge Engineering, ASCE*, **37**, 162–172.

31. Bradley, E., Easley, M. & Stolle, R. (2001), Reasoning about nonlinear system identification, *Artificial Intelligence*, 133, 139–88.

32. Buckland, P.G., Hooley, R., Morgenstern, B.D., Rainer, J.H. and van Selst, A.M., Suspension bridge vibrations: computed and measured, ASCE Journal of Structural Division 105 (1979) (ST5), pp. 859–874.

33. Burdet, O. (1993), Load testing and monitoring of Swiss bridges, Comité Européen du Béton, safety and performance concepts, bulletin d'information n°219, Lausanne, Suisse.

34. Burdet, O. & Badoux, M. (1999), Long-term deflection monitoring of prestressed concrete bridges retrofitted by external post-tensioning—examples from Switzerland, IABSE symposium "Structures for the Future—The Search for Quality," *Rio de Janeiro Report*, **83**, 112–4.

35. Burdet, O. & Fleury, B. (1997), Pont sur la Lutrive aval (VD)- Rapport d'essai de charge statique complémentaire, EPFL-IBAP.

36. Burdet, O. & Zanella, J.-L. (2000), *Automatic Monitoring of Bridges using Electronic Inclinometers*, IABSE, Lucerne Congress Structural Engineering for Meeting Urban Transportation Challenges, Zürich, Switzerland, pp. 398–9, September.

37. Cantieni, R. (1984). “Dynamic load testing of highway bridges.” Transportation Research Record, 950, 141-148.

38. Casas, J.R. (1998) Dynamic testing and model updating of cable-stayed bridges. IMAC, 1360-1366.

39. Castello, D. A., Stutz, L. T. & Rochinha, F. A. (2002), A structural defect identification approach based on a continuum damage model, *Computers and Structures*, **80**, 417–36.

40. Catbas, F.N., Lenett, M. Aktan, A.E., Brown, D.L., Helmicki, A.J. and Hunt, V. (1998). “Damage detection and condition assessment of Seymour Bridge.” IMAC 1998, 1694-1702.

41. Catbas, F.N. and Aktan, A.E. (2002). Condition and damage assessment: issues and some promising indices. Journal of Structural Engineering, 128 (8). 1026-10236.

42. Catbas, F.N., Ciloglu, S.K., Hasancebi, O., Grimmelsman, K. and Aktan, A.E. (2007). “Limitations in structural identification of large constructed structures.” Journal of Structural Engineering, 133(8), 1051-1066.

43. Chang, T. Y. P. (1998). "Field ambient vibration measurement on Kap Shui Mun Cable-Stayed Bridge: Phase II measurement." Rep. Prepared for Lantau Fixed Crossing Proj. Mgmt. Ofc., Hwy. Dept. of the Hong Kong SAR Govt., Hong Kong University of Science and Technology, Clear Water Bay, Kowloon.

44. Chase, S.B. (2005). "The Role of Sensing and Measurement in Achieving FHWA's Strategic Vision for Highway Infrastructure." Sensing Issues in Civil Structural Health Monitoring, pp.23-32, Springer, Netherlands, December 06, 2005

45. Chaudhary, M. T. A., Abe, M., Fujino, Y. & Yoshida, J. (2000), Performance evaluation of two base-isolated bridges using seismic data, *Journal of Structural Engineering, ASCE*, **116**(10), 1187–95.

46. Chen, G. (2001). FE model validation for structural dynamics. PhD thesis, University of London, London, UK.

47. Chen, G., Ewins, D.J. (2004). FE model verification for structural dynamics with vector projection. Mechanical Systems and Signal Processing, 18, 739-757.

48. Chen, J.C. and Garba, J.A. (1980). Analytical model improvement using modal test results. AIAA J., 18, 684-690.

49. Christian, J. T. (2004). "Geotechnical engineering reliability: how well do we know what we are doing?" *Journal of Geotechnical and Geoenvironmental Engineering*, ASCE, 130(10), 985-1003.

50. Ciloglu, K. (2006). "The impact of uncertainty in operational modal analysis for structural identification of constructed systems." PhD thesis, Drexel University, Philadelphia, PA.

51. Clough, R.W. and Wilson, E.L. (1999). "Early finite element research at Berkeley." Presented at the Fifth U.S. National Conference on Computational Mechanics, Univ. of Colorado at Boulder, Aug. 4-6, 1999

52. Cornwell, P.J., Farrar, C.R., Doebling, S.W. and Sohn, H. (1999). "Environmental variability of modal properties." Experimental Techniques, Nov/Dec, 45-58?

53. Cunha, J., Cogan, S. & Berthod, C. (1999), Application of genetic algorithms for the identification of elastic constants of composite materials from dynamic tests, *International Journal for Numerical Methods in Engineering*, **45**(7), 891–900.

54. Cunha, A., Caetano, E. and Delgado, R. (1999). "Dynamic tests on large cable-stayed bridge." Journal of Bridge Engineering, 6(1), 54-62.

55. Daverio, R. (1995), Mesures des déformations des ponts par un système d'inclinométrie, Rapport de maîtrise EPFL-IBAP, Lausanne, Switzerland

56. Dunn, S. A. (1998), The use of genetic algorithms and stochastic hill-climbing in dynamic finite element model identification, *Computers & Structures*, **66**(4), 489–97.

57. Farrar, C.R., Doebling, S.W., Cornwell, P.J. and Straser, E.G. (1997). Variability of modal parameters measured on Alamosa Canyon Bridge. Proc. Of IMAC 1997.

58. Farrar, C.R., Cornwell, P.J., Doebling, S.W. and Prime, M.B. (2000). "Structural health monitoring studies of the Alamosa Canyon and I-40 bridges." Los Alamos National Laboratory Report LA-13635-MS.

59. Favre, R., Burdet, O., Charif, H., Hassan, M. & Markey, I. F. (1995), Enseignements tirés d'essais de charge et d'observations à long terme pour l'évaluation des ponts en béton et le choix de la précontrainte, Office Fédéral des Routes, recherche 83/90, Suisse.

60. Feng, M.Q., Kim, D.K., Yi, J.-H. and Chen, Y. (2004). "Baseline models for bridge performance monitoring." Journal of Engineering Mechanics, 130(5), 562-569.

61. Fest, E. (1997), *Système de mesure par inclinométrie: Développement d'un algorithme de calcul des flèches*, DEA Ecole Normale supérieur de Cachan, France

62. Fissette, E. and Ibrahim, S. (1988). "Error localization and updating of analytical dynamic models using a force balance method." IMAC 1988, 1063-1070.

63. Friswell, M.I. and Penny, J.C.T. (1992). "The effect of close or repeated eigenvalues on the updating of model parameters from FRF data." Transactions of the ASME, Journal of Vibration and Acoustics, 114(4): 514-520.

64. Friswell, M. I. & Mottershead, J. E. (1995), *Finite Element Model Updating in Structural Dynamics*, Kluwer, Dordrecht

65. Fritzen, C.P. and Zhu, S. (1991). Updating of finite-element models by means of measured information. Computers and Structures, 40, 475-486.

66. Fritzen, C.-P., Kiefer, Th. (1992). "Localization and correlation of errors in analytical models." IMAC92, 1064-1071.

67. Fu, Y. and DeWolf, J.T. (2001). Monitoring and analysis of a bridge with partially restrained bearings. Journal of Bridge Engineering, 6(1), 23-29.

68. Fujino, Y. and Abe, M. (2002). "Structural health monitoring in civil infrastructures and research on SHM of Bridges at University of Tokyo." SIME Report 2002-02, Society for Infrastructure Maintenance Engineering, Tokyo, Japan.

69. Gloth, G. (2000). "Using mode shape expansion techniques for pretest analysis and correlation." IMAC 2000, 1237-1243.

70. Goldberg, D. E. (1989), Genetic Algorithms in Search, Optimization, and Machine Learning, Addison-Wesley, Reading, MA.

71. Golinval, J.-C. and Link, M. (2003). "Cost action F3 'structural dynamics' (1997-2001) – an European cooperation in the field of science and technology." Mechanical Systems and Signal Processing, 17(1), 3-7.

72. Grimmelsman, K.A. and Aktan, A.E. (2005). "Impacts and mitigation of uncertainty for improving reliability of field measurements." The 2nd International Conference on Structural Health Monitoring of Intelligent Infrastructure, Shenzhen, China, November 16-18, 2005.

73. Grimmelsman, K.A. (2006). "Experimental characterization of towers in cable-supported bridges by ambient vibration testing." PhD thesis, Drexel University, Philadelphia, PA.

74. Gysin, H. (1990). “Comparison of expansion methods for FE modeling error localization.” IMAC 1990, 195-204.

75. Hajela, P. & Soeiro, F. J. (1990), Structural damage detection based on static and modal analysis, *AIAA Journal*, **28**(6), 1110–5.

76. Harik, I.E., Allen, D.L., Street, R..L., Guo, M., Graves, R.C., Harison, J. and Gawry, M.J. (1997). “Free and ambient vibration of Brent-Spence Bridge.” Journal of Structural Engineering, 123(9), 1262-1268.

77. Harik, I.E., Allen, D.L., Street, R..L., Guo, M., Graves, R.C., Harison, J. and Gawry, M.J. (1997). “Seismic evaluation of Brent-Spence Bridge.” Journal of Structural Engineering, 123(9), 1269-1275.

78. Hart, G.C. and Yao, J.T.P. (1977). “System Identification in structural dynamics.” Journal of Engineering Mechanics, Division ASCE, 103(EM6), 1089-1104.

79. Hemez, F.M. and Farhat, C. (1994). “Comparing mode shape expansion methods for test-analysis correlation.” IMAC 1994, 1560-1567.

80. Hemez, F. M. & Doebling, S. W. (2001), Review and assessment of model updating for non-linear, transient dynamics, *Mechanical Systems and Signal Processing*, **15**(1), 45–74.

81. Hjemlstad, K.D., Wood, S.L. and Clark, S.J. (1992). Mutual residual energy method for parameter estimation in structures. Journal of Structural Engineering, 118(1), 223-242.

82. Hjelmstad, K. D. & Shin, S. (1997), Damage detection and assessment of structures from static response, *Journal of Engineering Mechanics*, **123**(6), 568–76.

83. Holland, J. (1975), *Adaptation in Natural Artificial Systems*, University of Michigan Press, MI

84. Housner, G. W., Bergman, L. A., Caughey, T. K., Chassiakos, A. G., Claus, R. O., Masri, S. F., Skeleton, R. E., Soong, T. T., Spencer, B. F. & Yao, J. T. P. (1997), Structural control: Past, present, and future, *Journal of Engineering Mechanics, ASCE*, **123**(9), 897–972.

85. Hu, N., Wang, X., Fukunaga, H., Yao, Z. H., Zhang, H. X. & Wu, Z. S. (2001), Damage assessment of structures using modal test data, *International Journal of Solids and Structures*, **38**, 3111–26.

86. Hudson, W.R. (1971). Serviceability performance and design consideration. Highway Research Board, Spec Rep 126, p140-9.

87. Ibanez, P., Matthiesen, R.B., Miller, W.R. and Smith, C.B. (1972). Experimental vibration tests at nuclear power plants. ISA Transations, 11(3), 289-296.

88. Imregun, M. and Visser, W.J. (1991). A review of model updating techniques. Shock and Vibration Digest, 23, 9-20.

89. Imregun, M. and Ewins, D.J. (1993). “An investigation into mode shape expansion techniques.” IMAC 1993, 168-175.

90. Imregun, M., Visser, W.J. and Ewins, D.J. (1995). "Finite element model updating using frequency response function data. I. theory and initial investigation." Mechanical Systems and Signal Processing, 9(2): 187-202.

91. Imregun, M., Sanliturk, K.Y. and Ewins, D.J. (1995). "Finite element model updating using frequency response function data. II. Case study on medium-size finite element model." Mechanical Systems and Signal Processing, 9(2): 203-213.

92. Inaudi, D., Elamarib, A., Pflug, L., Gisinb, N., Breguetb, J. & Vurpillot, S. (1994), Low-coherence deformation sensors for the monitoring of civil-engineering structures, *Sensors and Actuators*, **A44**, 125–30.

93. Ivanovic, S.S., Trifunac, M.D. and Todorovska, M.I. (2000). "Ambient vibration tests of structures – a review." Bulletin of Indian Society of Earthquake Technology, Special Issue on Experimental Methods, December, 2000.

94. Jaishi, Bijaya and Ren, W.-X. (2005). "Structural finite element model updating using ambient vibration test results." Journal of Structural Engineering, 131(4), 617-628.

95. Katafygiotis, L. S. & Beck, J. L. (1998), Updating models and their uncertainties. II: Model identifiability, *Journal of Engineering Mechanics*, **124**, 463–67.

96. Kay, H., Rinner, B. & Kuipers, B. (2000), Semi-quantitative system identification, *Artificial Intelligence*, **119**, 103–40.

97. Kirkpatrick, S., Gelatt, C. & Vecchi, M. (1983), Optimization by simulated annealing, *Science*, **673**, 220.

98. Koh, C. G., Chen, Y. F. & Liaw, C.-Y. (2003), A hybrid computational strategy for identification of structural parameters, *Computers and Structures*, **81**, 107–17.

99. Kramer, C., De Smet, C.A.M. and Peeters, B. (1999). Comparison of ambient and forced vibration testing of civil engineering structures. Proc. Of IMAC 1999. 1030-1034.

100. www.kuleuven.ac.be/bwm/SIMCES.htm

101. Lallement, G. and Piranda, J. (1990). Localization methods for parametric updating of finite element models. Proc. Of IMAC 1990, 579-585.

102. Law, S.S., Chan, T.H.T. and Wu, D. (2001). "Efficient numerical model for the damage detection of large scale ?" Engineering Structure, 23, 436-451.

103. Lewis, R. M., Torczon, V. & Trosset, M. W. (2000), Direct search methods: Then and now, *Journal of Computational and Applied Mathematics*, **124**, 191–207.

104. Lin, J.-W, Betti, R., Smyth, A.W., Longman, R.W. (2003). On-line identification of non-linear hysteretic structural systems using a variable trace approach. Earthquake Engineering and Structural Dynamics, 30(9), 1279-1303.

105. Lin, R.M. and Ewins, D.J. (1994). "Analytical model improvement using frequency response functions." Mechanical Systems and Signal Processing, 8(4), 437-458

106. Linderholt, A. and Abrahamsson, T. (2001). “Informative data for model parameter updating.” IMAC 2001(?), 581-586.

107. Linderholt, A. and Abrahamsson, T. (2005). “Optimizing the informativeness of test data used for computational model updating.” Mechanical Systems and Signal Processing, 19, 736-750.

108. Link, M. (1991). Comparison of procedures for localizing and correcting errors in computational models using test data. Proc. Of IMAC 1991, 479-485.

109. Link, M. and Conic, M. (2000). Combining adaptive FE mesh refinement and model parameter updating. Proc. Of IMAC 2000, 584-588.

110. Liu, P. & Chian, C. (1997), Parametric identification of truss structures using static strains, *ASCE Journal of Structural Engineering*, **123**(7), 927–33.

111. Liu, S.C. and Yao, J.T.P. (1978). “Structural identification concept.” Journal Structural Division, ASCE, 104(12), 1845-1858.

112. Ljung, L. (1999), *System Identification—Theory for the User*, Prentice Hall, Englewood Cliffs, NJ

113. Luco, J.E., Trifunac, M.D. and Wong, H.L. (1988). Isolation of soil-structure interaction effects by full-scale forced vibration tests. Earthquake Engineering and Structural Dynamics, 16(1), 1-21.

114. Macdonald, J.H.G. and Daniell, W.E. (2005). “Vibration of modal parameters of a cable-stayed bridge identified from ambient vibration measurements and FE modeling.” Engineering Structures, 27, 1916-1930.

115. Maia, N.M.M., Reynier, M. and Ladeveze, P. (1994). “Error localization for updating finite element models using frequency response functions.” IMAC 1994, 1299-1308.

116. Mares, C. & Surace, C. (1996), Application of genetic algorithms to identify damage in elastic structures, *Journal of Sound and Vibration*, **195**(2), 195–215.

117. Martin, O. & Otto, S. W. (1996), Combining simulated annealing with local search heuristics, *Annals of Operations Research*, **63**, 57–75.

118. Mayes, R.L. (1997). “A tool to identify parameter errors in finite element models.” IMAC 97, 825-831.

119. McLamore, V.R., Hart, G.C. and Stubbs, I.R. (1971). Ambient vibration of two suspension bridges. Journal of the Structural Division, 97, pp2567-2582.

120. Modak, S. V., Kundra, T. K. & Nakra, B. C. (2002), Comparative study of model updating studies using simulated experimental data, *Computers and Structures*, **80**, 437–47.

121. Moon, F.L. and Aktan, A.E. (2006). Impacts of epistemic (bias) uncertainty on structural identification of constructed (civil) systems. Shock Vibration Digest, 38(5), 399-420.

122. Mottershead, J.E. and Friswell, M.I. (1993). Model updating in structural dynamics: a survey. Journal of Sound and Vibration, 167(2), 347-375.

123. Mottershead, J.E., Friswell, M.I. and Zhang, Y. (1995). "On discretization error estimates for finite element model updating." IMAC 1995, 1289-1296.

124. Mottershead, J.E., Mares, C., James, S. and Friswell, M.I. (2006). Stochastic model updating: Part 2 – application to a set of physical structures. Mechanical Systems and Signal Processing, 20(8), 2171-2185.

125. Natke, H.G. (1988). Updating computational models in the frequency domain based on measured data: a survey. Probabilistic Engineering Mechanics, Essex, U.K., 8, 28-35.

126. Oberkampf, W.L., Helton, J.C., Joslyn, C.A., Wojtkiewicz, S.F and Ferson, S. (2004) Challenge problems: uncertainty in system response given uncertain parameters. Reliability Engineering and System Safety, 85, 1-3, 11-19.

127. Park, K. C. & Felippa, C. A. (2001), A flexibility-based inverse algorithm for identification of structural joint properties, in *Proceedings of ASME Symposium on Computational Methods on Inverse Problems*, 15–20 November 1998, Anaheim, CA

128. Pavic, A. and Reynolds, P. (2003). Modal testing and dynamic FE model correlation and updating of a prototype high-strength concrete floor. Cement and Concrete Composites, 25, 787-799.

129. Peeters, B. and De Roeck, G. (1998). Stochastic subspace system identification of a steel transmitter mast. Proc. Of IMAC 1998, 130-136.

130. Peeters, B. (2000). System identification and damage detection in civil engineering. PhD thesis, Katholieke University, Leuven, Belgium.

131. Peeters, B. Maeck, J. and De Roeck, G. (2001). Vibration-based damage detection in civil engineering: excitation sources and temperature effects. Smart Materials and Structures, 10(3), 518-527.

132. Perregeaux, N. (1998), Pont de la Lutrive-N9, Equipement et analyse du comportement au moyen du système de mesure à fibre optique SOFO, Diploma thesis, EPF-Lausanne.

133. Perregaux, N., Vurpillot, S., Tosco, J-S., Inaudi, D. & Burdet, O. (1998), Vertical displacement of bridges using the SOFO system: A fiber optic monitoring method for structures, in *ASCE-12th Engineering Mechanics. Conference Proceedings: A force for the 21st Century*, San Diego, USA, 791–4.

134. Raphael, B. & Smith, I. F. C. (2003a), *Fundamentals of Computer Aided Engineering*, John Wiley, UK

135. Raphael, B. & Smith, I. F. C. (2003b), A direct stochastic algorithm for global search, *Journal of Applied Mathematics and Computation*, **146**(2–3), 729–58.

136. Reich, G. W. & Park, K. C. (2001), A theory for strain-based structural system identification, *Journal of Applied Mechanics*, **68**(4), 521–27.

137. Ren, W.-X., Blandford, G.E. and Harik, I.E. (2004). "Roebling Suspension Bridge. I: Finite-Element Model and Free Vibration Response." Journal of Bridge Engineering, 9(2): 110-118.

138. Ren, W.-X., Harik, I.E., Blandford, G.E., Lenett, M. and Baseheart, T.M. (2004). "Roebling Suspension Bridge. II: Ambient Testing and Live-Load Response." Journal of Bridge Engineering, 9(2): 119-126.

139. Ren, W.-X., Zhao, T. and Harik, I.E. (2004). "Experimental and analytical modal analysis of steel arch bridge." Journal of Structural Engineering, 130(7), 1022-1031.

140. Ren, W.-X., Peng, X.-L. and Lin, Y.-Q. (2005). "Experimental and analytical studies on dynamic characteristics of a large span cable-stayed bridge." Engineering Structures, 27, 535-548.

141. Robert-Nicoud, Y., Raphael, B., Burdet, O., Smith, I. F. C. (2005). Model Identification of bridges using measurement data, *Computer-Aided Civil and Infrastructure Engineering*, 20(2), 118-131.

142. Salawu, O.S. and Williams, C. (1995). "Review of full-scale dynamic testing of bridge structures." *Engineering Structures*, 17(2), 113-121.

143. Sanayei, M. & Onipede, O. (1991), Damage assessment of structures using static test data, *AIAA Journal*, **29**(7), 1174–79.

144. Sanayei, M. & Saletnik, M. J. (1996a), Parameter estimation of structures from static strain measurements. I: formulation, *Journal of Structural Engineering, ASCE*, **122**(5), 555–62.

145. Sanayei, M. & Saletnik, M. J. (1996b), Parameter estimation of structures from static strain measurements. II: error sensitivity analysis, *Journal of Structural Engineering, ASCE*, **122**(5), 563–72.

146. Sanayei, M. & Scampoli, S. (1991), Structural element stiffness identification from static test data, *Journal of Engineering Mechanics, ASCE*, **117**, 1021–36.

147. Sanayei, M., Wadia-Fascetti, S., Arya, B. and Santini, E.M. (2001). Significance of modeling error in structural parameter estimation. Computer-Aided Civil and Infrastructure Engineering, 16, 12-27.

148. Sestieri, A. and D'Ambrogio, W. (1989). "Why be modal: how to avoid the use of modes in the modification of vibration systems." International Journal of Analytical and Experimental Modal Analysis, 4(1), 25-30.

149. Sharman, K. C. & Esparcia-Alcazer, A. I. (1993), Genetic evolution of symbolic signal models, in *Proceedings of the 2d IEE/IEEE International Workshop on Natural Algorithms in Signal Processing*, University of Essex, Nov. 1993, vol. 2, paper 29, pp. 1–11.

150. Sinha, J.K., Friswell, M.I. (2003). The use of model updating for reliable finite element modeling and fault diagnosis of structural components used in nuclear plants. Nuclear Engineering and Design, 223(1), 11-23.

151. Sohn, H. & Law, K. H. (1997), A Bayesian probabilistic approach for structural damage detection, *Earthquake Engineering and Structural Dynamics*, **26**, 1259–81.

152. Sohn, H. & Law, K. H. (2001), Damage diagnosis using experimental ritz vectors, *Journal of Engineering Mechanics, ASCE*, **127**(11), 1184–93.

153. Teughels, A., Maeck, J. & Roeck, G. (2002), Damage assessment by FE model updating using damage functions, *Computers and Structures*, **80**, 1869–79.

154. Teughels, A. and De Roeck, G. (2004). "Structural damage identification of the highway bridge Z24 by FE model updating. " Journal of Sound and Vibration 278, 589-610.

155. Torkamani, M.A.M. and Ahmadi, A.K. (1988). Stiffness identification of two- and three-dimensional frames. Earthquake Engineering and Structural Dynamics, 16, 1157-1176.

156. Turner, M.J., Clough, R.W., Martin, H.C. and Topp, L.J. (1956). "Stiffness and deflection analysis of complex structures." Journal of Aerospace Science, 23, 805-824.

157. Udwadia, F.E. (1994). "Methodology for optimum sensor locations for parameter Id in dynamic systems." Journal of Engineering Mechanics, 120(2), 368-390.

158. Vanik, M.W., Beck, J.L. and Au, S.K. (2000). "Bayesian probabilistic approach to structural health monitoring." Journal of Engineering Mechanics, 126(7), 738-745.

159. Varney, R.F. and Galambos, C.F. (1966). "Field dynamic loading studies of highway bridges in the US, 1948-1965." Transportation Research Record, 99-105.

160. Ventura, C.E., Felber, A.J. and Stiemer, S.F. (1995). "Experimental investigations of dynamics of Queensborough Bridge." Journal of Performance of Constructed Facilities, 9(2), 146-155.

161. Ventura, C.E., Brincker, R., Dascotte, E. and Andersen, P. (2001). "FEM updating of the heritage court building structure." Proceeding of the International Modal Analysis Conference, Kissimmee, FL, Feb5-8 2001.

162. Vurpillot, S., Krueger, G., Benouaich, D., Clément, D. & Inaudi, D. (1998), Vertical deflection of a pre-stressed concrete bridge obtained using deformation sensors and inclinometer measurements, *ACI Structural Journal*, **95**(5), 518–26.

163. Wang, M.L., Heo, G. and Satipathi, D. (1998). A health monitoring system for large structural systems. Smart Materials and Structures, 7, 606-616.

164. Wenzel, H. and Pichler D. (2005). Ambient vibration monitoring. John Wiley & Sons, England.

165. Wilson, J.C. and Liu, T. (1991). Ambient vibration measurements on a cable-stayed bridge. Earthquake Engineering and Structural Dynamics, 20(8), 723-747.

166. Worden, K. (2003). Cost action F3 on structural dynamics: benchmarks for working group 2 – structural health monitoring. Mechanical Systems and Signal Processing, 17(1), 73-75.

167. Wu, J.R. and Li, Q.S. (2004). Finite element model updating for a high-rise structure based on ambient vibration measurements. Engineering Structures, 26, 979-990

168. Xu, Y.L., Ko, J.M. and Zhang, W.S. (1997). Vibration Studies of Tsing Ma Suspension Bridge. Journal of Bridge Engineering, 2(4), 149-156.

169. Yang, M.M. and Brown, D.L. (1997). "SVQ/QR based model error indicator function." IMAC 97, 572-578.

170. Yu, L., Law, S. S., Link, M. & Zhang, L. M. (1999), Damage detection in bolted joint structures using element contribution to modal strain energy, in M. I. Friswell, J. E. Mottershead, and A. W. Lees (eds.), *Proceedings of the Second International Conference on Identification in Engineering Systems,* Swansea, pp. 516–26.

171. Zapico, J.L., Gonzalez, M.P., Friswell, M.I., Taylor, C.A. and Crewe, A.J. (2003). "Finite element model updating of a small scale bridge." Journal of Sound and Vibration, 268, 993-1012.

172. Zhang, Q.W, Chang, T.Y.P. and Chang, C.C. (2001). Finite-element Model Updating for the Kap Shui Mun cable-stayed bridge. Journal of Bridge Engineering, ASCE, 6(4), 285-293.